



UNIVERSITÀ
DEGLI STUDI
DI PADOVA

Sede Amministrativa: Università degli Studi di Padova
Dipartimento di Salute della Donna e del Bambino - SDB

CORSO DI DOTTORATO DI RICERCA IN:

MEDICINA DELLO SVILUPPO E SCIENZE DELLA PROGRAMMAZIONE SANITARIA

CURRICOLO: Emato-oncologia, genetica, malattie rare e medicina predittiva

CICLO XXXII

**AML BLASTS SUPPORT A LEUKEMIA-PERMISSIVE
MICROENVIRONMENT REVEALING THE STROMAL
CONTRIBUTION ELIGIBLE FOR INNOVATIVE
3D TARGETING**

Coordinatore: Ch.mo Prof. Carlo Giaquinto

Supervisore: Dott.ssa Martina Pigazzi

Dottoranda: Dott.ssa Giulia Borella

Index

Summary.....	1
Introduction.....	4
Acute Myeloid Leukemia.....	4
Pediatric AML classification.....	6
AML diagnosis, treatment and outcome.....	9
The bone marrow niche.....	13
Pivotal cellular components players in the BM niche.....	14
Leukemia bone marrow niche.....	18
Modelling of human myeloid leukemia.....	26
<i>In vitro</i> AML models.....	26
<i>In vivo</i> AML models.....	32
Aim of study.....	38
Materials and Methods.....	39
Results.....	52
MSCs characterization AML-MSCs vs. h-MSCs.....	52
AML-MSCs display the same morphology and immunophenotype of h-MSCs.....	52
AML-MSCs increase growth kinetics and osteogenic differentiation potential.....	53
AML-MSCs exert an aberrant anti-inflammatory potential.....	55
AML-MSCs support hematopoietic stem cell proliferation.....	56
Specific gene expression profile of AML-MSCs.....	60
LOPAC ^{®1280} high throughput drug screening on MSCs.....	69
3D-AML long term cultures set up.....	77
3D-AML scaffold mimics the leukemia bone marrow niche <i>in vitro</i>	77
3D-AML cultures secretome.....	82
Drug screening in 3D-AML cultures.....	87
Use of the humanized 3D-AML niche to improve AML dissemination and engraftment <i>in vivo</i>	90
3D-humanized AML niche implantation in NSG mice.....	90
Humanized 3D-AML model for a local drug testing <i>in vivo</i>	93
Discussion and Conclusion.....	95
References.....	104
Secondary projects.....	120
About the author.....	148

List of abbreviations

3D	Three Dimensional
AIEOP	Associazione Italiana Ematologia e Oncologia Pediatrica
ALL	Acute Lymphoblastic Leukemia
AML	Acute Myeloid Leukemia
ANG	Angiopoietin
ANGPT1	Angiopoietin 1
AraC	Cytarabine
BM	Bone Marrow
BM-MSCs	Bone Marrow-Mesenchymal Stromal Cells
BMPs	Bone Morphogenetic Proteins
CAM-DR	Cell Adhesion-Mediated Drug Resistance
CFU-F	Colony Forming Unit-Fibroblast
CI	Combination Index
CLL	Chronic Lymphoblastic Leukemia
CM	Conditional Medium
CML	Chronic Myeloid Leukemia
CR	Complete Remission
CXCL12	C-X-C Motif Chemokine Ligand 12
DAMP	Damage Associated Molecular Pattern
ECs	Endothelial Cells
ECM	Extracellular Matrix
EFS	Event Free Survival
FAB	French American British
FDR	False Discovery Rate
GEMM	Genetically Engineered Mouse Models
GEP	Gene Expression Profiling

GO	Gene Ontology
GVHD	Graft Versus Host Disease
HA	Hydroxiapatite
HR	High Risk
HSCs	Hematopoietic Stem Cells
HSCT	Hematopoietic Stem Cell Transplantation
HSPCs	Hematopoietic Stem Progenitor Cells
HTS	High Throughput Screening
HUVEC	Human Umbilical Vein Endothelial cell
IC₅₀	Half maximal Inhibitory Concentration
i.p.	Intraperitoneal
iPSCs	Induced Pluripotent Stem Cells
IR	Intermediate Risk
ISCT	International Society for Cellular Therapy
JMML	Juvenile Myelomonocytic Leukemia
LTC-IC	Long Term Culture-Initiating Cell
Lep-R	Leptin Receptor
LSCs	Leukemic Stem Cells
LOPAC	Library Of Pharmacologically Active Compounds
MDS	Myelodysplastic Syndrome
MFI	Mean Fluorescence Intensity
MgHA/Coll	Collagen matrix with Magnesium-doped Hydroxyapatite nanophase
MM	Multiple Myeloma
MPN	Myeloproliferative Neoplasm
MRD	Minimal Residual Disease
MSCs	Mesenchymal Stromal Cells
ncRNAs	non coding RNA
Nes	Nestin
OPN	Osteopontin

OS	Overall Survival
PCA	Principal Component Analysis
PCL	Poly ϵ -caprolactone
PDGFRA	Platelet Derived Growth Factor Receptor Alpha
PDX	Patient Derived Xenograft
PEG	Polyethylene Glycol derivatives
PLA	Polylactic Acid
PLG	Polylatide-co-glucolide
p.o.	Oral administration
PU	Polyurethane
RARγ	Retinoic Acid Receptor gamma
RLU	Relative Luminescent Unit
R-MSCs	Mesenchymal stromal cells derived at remission
SCF	Stem Cell Factor
SDF1	Stromal cell-Derived Factor 1
SEM	Scanning Electron Microscopy
SF	Stroma Free
SILAC	Stable Isotope Labeling by/with Amino acids in cell culture
SM-DR	Soluble Factor-mediated Drug Resistance
SR	Standard Risk
TCP	Tricalcium Phosphate
TGF-β	Transforming Growth Factor beta
TPO	Thrombopoietin
VCAM-1	Vascular Cell Adhesion Molecule 1
VEGF-C	Vascular Endothelial Growth Factor C
WES	Whole Exome Sequencing
WHO	World Health Organization

Summary

Acute myeloid leukemia (AML) is a biologically and genetically heterogeneous disorder characterized by the rapid expansion of immature myeloid blasts in the bone marrow (BM). AML represents around 20% of all the cases of acute leukemia in childhood, and its outcome has significantly improved over the past 20 years, with a complete remission rate of 88%; although this disease still represents a challenges due to the considerable occurrence of relapse, which is the main cause of treatment failure, impacting also on the survival of the more favorable AML subgroups. One of the main challenges in pediatric leukemia is the discovery of new therapies that ameliorate the effect of the chemotherapy currently in use, or reduce toxicity and severe side effects. To date, new targeted drugs currently under investigation in clinical trial for AML, such as FLT3 inhibitors, show poor or no efficacy in patients with respect to the surprising results obtained in the *in vitro* testing. This failure could be explain by pediatric AML as a rare disease with a sophisticated genetic characterization at diagnosis that subdivides patients into small groups with low number of children eligible for early phase clinical trials as well as to the inadequate *in vitro* and *in vivo* models currently available for drug testing. The existing models in fact, do not recapitulate physiological leukemia context, including inter- and intra-tumor genetic heterogeneity, cell-cell and cell-stroma interactions, as well as the BM microenvironment. The BM microenvironment consists in stromal cells, such as mesenchymal stromal cells (MSCs), osteoblasts, endothelial cells, macrophages, adipocytes, and fibroblasts that have an indispensable role in the regulation and support of hematopoietic stem and progenitors cells (HSPCs) through cell-cell interaction and paracrine secretion of cytokines and extracellular matrix molecules, thereby helping to ensure the life-long supply of mature blood cells. Several evidences suggested that BM stromal cells contribute also to cancer progression and relapse by favoring growth and clonal evolution of malignant cells supporting chemo-resistance. By the way, this issue still remain mostly uncertain and unknown with few mechanistic data exploring MSCs role in pediatric AML.

During my PhD program I focused my research on studying the role played by the BM niche components in leukemia, and at the development of a three dimensional (3D) culture system to mimic the leukemia BM microenvironment. The final aim of studying leukemia primary cells in an exogenous humanized niche would be performing more predictive drug screenings *in vitro* and then *in vivo* to boost new front-line drugs into clinical trial in order to improve children outcome.

A large part of this PhD project was committed to dissect the characteristic of MSCs derived from a large cohort of pediatric AML patients (AML-MSCs), compared with MSCs derived from healthy donors (h-MSCs). In this context I reported that AML-MSCs exhibited altered growth properties and osteogenic differentiation potential with respect to h-MSCs. Additionally AML-MSCs did not exert anti-inflammatory activity *in vitro*, normally sustained by h-MSCs, with a significantly altered ability to support healthy hematopoietic cell differentiation. Finally, I demonstrated that AML-MSCs had a different gene expression profile with respect to h-MSCs, mostly related to IL 17 signaling pathway, response to hypoxia, cell differentiation, as well as cytokines production, finally revealing that AML-MSCs are altered stromal cells that, together with leukemia blasts, could create a leukemic BM niche responsible for disease onset or progression. Thus, a categorical question about whether AML derived from primary defects of HSCs and the AML-MSCs observed changes represented an adaptation induced by leukemia itself arose. Indeed, I examined the AML-MSCs and MSC derived from BM at remission after chemotherapy (R-MSCs). Interestingly, the comparative analysis of gene expression profile, proliferative rate and transforming ability suggested a direct causal relationship between the presence of leukemic cells and MSCs features, with important stromal functions restored in the R-MSCs as soon as leukemic cells were therapeutically eradicated as previously found in h-MSCs. These results suggested that AML-MSCs might be a novel potential target to treat AML if combined with conventional strategy or innovative targeted therapy, as new therapeutic opportunity for AML patients in order to achieve the remission with less doses of chemotherapy. Thus, during the second year of my PhD, I performed a high throughput drug screening of 480 compounds from a commercial Library of Pharmacologically Active Compounds (LOPAC[®]), in order to discover drugs active on the AML-MSCs. This screening uncovered 17 compounds able to reduce AML-MSCs viability, without toxicity over h-MSCs and AML blasts. Furthermore, I performed the validation step on one of these niche-targeted drugs, Lercanidipine-HCl, in order to use it in drug testing in combination with chemotherapy. So, I next moved to treatment with the necessity to have a physiological 3D context where both, AML-MSCs and AML would grow and targeted together. I took into consideration the use of a bioengineered 3D culture system, with a porous scaffold of collagen and hydroxyapatite where to seed AML cells *in vitro* with the possibility to add BM stromal components, such as MSCs, osteoblasts, and endothelial cells up to 21 days. This 3D system was confirmed to allow the growth of all cells types and AML to maintain the characteristics of the original leukemia diagnosis. I improved knowledge for 3D-secretome of this system by using mass spectrometry revealing different factors being secreted by AML-MSCs and not by h-MSCs, thus confirming the AML-MSCs being reprogrammed to sustain AML.

I then use of this innovative 3D model to test chemotherapies and new drugs, such as Quizartinib, I- BET151, and Dasatinib in order to determine more reliable effective doses in AML, since the 3D model recapitulate a more physiological condition, and revealing a synergistic activity of treatments when combined with the previously selected drug, Lercanidipine-HCl, targeting AML-MSCs. These findings of AML treatment in 3D showed that niche-targeted therapy exerted an overall reduction in tumor proliferation and sustain an active crosstalk between AML blasts and microenvironment during pharmacological activity.

Finally, during the last part of my PhD program, I tried to use this 3D model *in vivo*, with the aim to recreate a humanized niche in mice and introduce a rapid platform for drug testing of those drugs previously identified *in vitro*. I documented a well-organized BM niche that permitted AML cell proliferation in the 3D system up to 12 months from the implantation in mice. I finally, set up a novel useful *in loco* screening where drugs previously tested in 3D-AML cultures *in vitro*, should be refined before the prioritization of the best candidates to advance the preclinical setting in patient' derived xenograft models in phase II-like trials.

In conclusion this project rises with important results for future investigations on the pathogenesis of AML, its microenvironment and new treatment approaches. We highlight that leukemia stromal cells have aberrant activity within the niche by contributing to AML proliferation and maintenance. Further integrative and functional studies are under investigation to solve the paradigm of the role of the microenvironment in tumor onset. Moreover, we provide evidences that targeting the stromal microenvironment and, working in synergy with current or new front-line therapies, could face the residual disease in AML and the occurrence of relapse. The use of this 3D-model for primary AML long-term cultures represents a new tool for dissecting leukemia microenvironment role in the progression of disease, as well as a new platform for rapid drug testing analyses, to determine more predictable efficacy of combination approaches, both *in vitro* and *in vivo* and will be useful in the definition of individualized treatment modalities for AML patients.

Introduction

Acute Myeloid Leukemia

Hematopoiesis is a sophisticated process of cell differentiation. The hematopoietic hierarchy begins from the pluripotent hematopoietic stem cells (HSCs) which, thanks to its stem potential, give rise to both the hematopoietic *lineages*, lymphoid and myeloid, that are able to self-renewal and differentiate through maturation, producing the mature and specialized blood cell types. This process is achieved by an intrinsic differentiation program of cells and with the interaction with microenvironment, where cell-cell contacts, cytokines, grow factors and ligands cooperate in the regulation of this process². Ineffective hematopoiesis, resulting in homeostatic imbalance in the production of blood cells, leads to a series of haematological disorders, including leukemia. Acute leukemia is the most common haematological malignancy occurring during childhood. Its origin depends on which progenitor that are corrupted in differentiation and proliferation capabilities leading to lymphoblastic leukemia, when the progenitor is lymphoid, or myeloid leukemia, when is from the myeloid *lineage*³ (Figure 1).

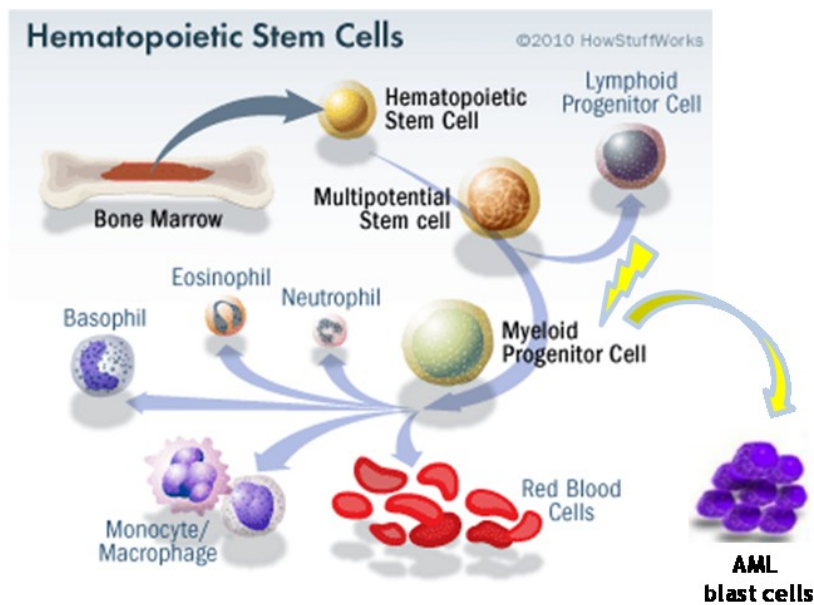


Figure 1. Cellular origin of blood cells show the differentiation process occurring for the myeloid *lineage* from the hematopoietic stem cell. Yellow arrow points the mutational event contributing to an abnormal undifferentiated leukemic cell which expands and produce the AML blasts cells (modified from How stem cell work 2010, S. Watson).

Pediatric AML is relatively rare (represents the 15-20% of overall leukemia in the childhood) with an incidence of 7-8 cases per million per year in Italy⁴. AML incidence is higher in infants (newborn, until one year of life) and in adolescents (>10 years) and is caused by the clonal transformation of a myeloid cell precursor characterized by the block of its differentiation an uncontrolled proliferation and survival. The neoplastic myeloblasts can be arrested in a variety of differentiation stages, supporting the loss of the normal hematopoietic functions. These abnormalities are the results of somatic genetic alterations that cooperate to establish the leukemic clone. These cells, called blast cells, accumulate in the bone marrow (BM) and other organs originating the onset of acute leukemia. To be called acute, these abnormal immature leukemic cells must be present in BM for a percentage greater than 20%^{3,5}. Clinical symptoms are heterogeneous and can be fatigue, bleeding, fever, pain in joints and bones, enlarged lymphnodes, liver and spleen, cutaneous manifestations, recurrent infections, anaemia or thrombocytopenia.

AML represents a heterogeneous disease in terms of immunophenotype and genetic abnormalities. The current hypothesis of the AML development identifies one or more driver mutations occurring within the context of a HSCs^{6,7} conferring a proliferative advantage to clonal expansion, then other concomitant mutations, namely passengers^{8,9}, occur creating the leukemic “founding” clone detected at the diagnosis with other subclones leading to a significant intra- and inter-tumor heterogeneity^{6,8}. This complex clonal architecture of pediatric AML is reflected in a functional heterogeneity of each clone documented as different AML cells ability to engraft in mice, to grow *in vitro*, or to evade therapy and mediate a disease relapse⁸⁻¹⁰.

Historically, there are two main types of genetic aberrations namely class I mutations (occurring in genes as *c-KIT* and *FLT3*) that confer proliferative and survival advantages to cells, and type II mutations that lead to impaired hematopoietic differentiation and apoptosis process (mutation in *MLL*, *CBF* genes or fusion genes like *RUNXI-RUNXITI*)¹¹. Accordingly to the “two hits model” of cancer, the mutations conferring pro-survival/proliferative advantage (class I) need to be associated with the mutations that complete outset of acute myeloid leukemia (class II). More recently a new model of AML pathogenesis has been described, which includes three additional categories of mutations, demonstrated to cooperate in the onset of AML: class III mutations lead to defects in genes involved in epigenetic modification and regulation, class IV mutations affect genes of cellular adhesion and genes regulating migration pathways and finally, class V mutations alter genes that regulate DNA repair and splicing^{12,13}. In this new scenario AML constitutes an exceptional biological model of cooperative genetic and epigenetic alterations that initiates the myeloid

transformation and sustain its progression. A schematic representation of this complex mutational AML landscape is shown in Figure 2.

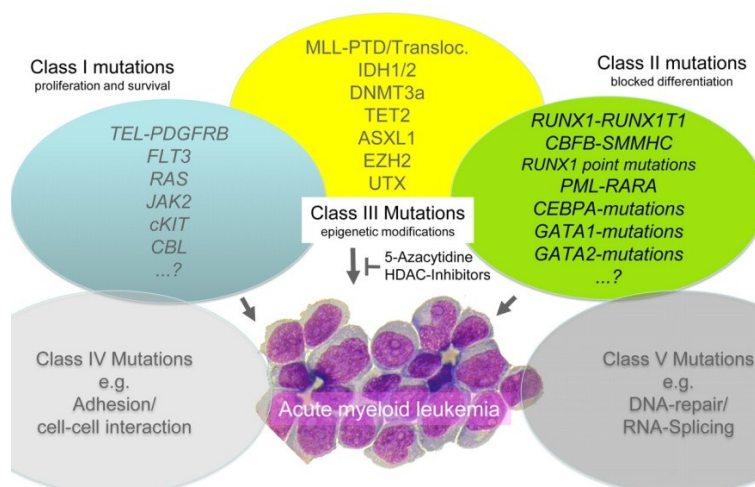


Figure 2. Schematic view of the genetic AML pathogenesis; by this theory AML derives from mutations of five different classes for affecting genes involved in different pathways (from Blood 2012, C. Thiede).

Pediatric AML classification

Prognosis of childhood AML has improved significantly over the past decades and the probability of cure is approximately 60-70% in most of the developed countries¹⁴. This results have been achieved thanks not only to the use of more effective anti-leukemic agents and significant improvements in supportive care, but also to progresses made in the risk stratification of patients at diagnosis, shown in Table 1, with a consequent risk-directed therapy^{15,16}.

Risk Group	Prognostic Markers
Standard Risk (SR)	CBF anomalies (t(8;21)(q22;q22), inv(16)(p13q22), t(16;16)(p13;q22)), MRD <0,1% at TP1. Normal karyotype, NPM1 mutation and MRD <0,1% at TP1.
Intermediate Risk (IR)	Normal karyotype t(9;11)(p22;q23) without any other cytogenetic abnormalities t(1;11)(p32;q23) t(11;19)(p13;q23) t(16;21)(p11;q22)FUS-ERG, t(3;5)(q25;q34) other cytogenetic abnormalities M7 t(1;22), independent from patient's age patients not SR or HR MRD at TP1 >0,1% but <1% and with MRD at TP2 <0,1%.
High Risk (HR)	Cytogenetic anomalies associated with poor outcome: -complex karyotype (>3 anomalies), -monosomy (-7, -5, others), -t(9;11)(p22;q23) associated with other anomalies, -cytogenetic anomalies, 11q23 non included in IR: t(11;17)(q23;q21), t(10;11)(p12;q23), t(4;11)(q21;q23), t(6;11)(q27;q23), t(x;11) -rare cytogenetic anomalies: t(6;9)(p23;q34), t(8;16)(p11;p13), t(9;22)(q34;q11), t(5;11)NUP98/NSD1, t(4;11)MLL/ArgBP2 FLT3-ITD Normal cytogenetic + CBFA2T3-GLIS2 FAB M0, M6, M7 without t(1;22) Infants (excluded LAM M7 with t(1;22)) Patients with uncomplete morphological remission at the end of the first induction cycle MRD >1% at TP1 or >0,1% at TP2 Patients not SR and WBC >100x10 ⁹ /Liter.

Table 1. AML Risk groups stratification, according to AIEOP AML 2013 trial.

In 1970 the first classification of AML nominated “French-American-British (FAB) classification” that categorized AML into 7 subtypes, namely from M0 to M7, was provided. The FAB classification was based on the morphological and histological characteristics of the leukemic cell, as well as the stage of differentiation of leukemic blasts¹⁷ (Table 2). This first FAB classification system was used to group AML into different morphological subtypes, but it had limited power in reflecting the biological, genetic and clinical characteristics, resulting in limited prognostic significance.

FAB classification of Acute Myeloid Leukemia (AML)

FAB Subtype	Name
M0	Undifferentiated myeloblastic leukemia
M1	Acute myeloblastic leukemia with minimal maturation
M2	Acute myeloblastic leukemia with maturation
M3	Acute promyelocytic leukemia
M3h	Acute promyelocytic leukemia, hypergranular variant
M3v	Acute promyelocytic leukemia, microgranular variant
M4	Acute myelomonocytic leukemia
M4eos	Acute myelomonocytic leukemia with eosinophilia
M5	Acute monoblastic leukemia
M5a	Acute monoblastic leukemia, poorly differentiated
M5b	Acute monoblastic leukemia, differentiated
M6	Acute erythroid leukemia
M7	Acute megakaryoblastic leukemia

Table 2. Different morphological AML subtypes according to the first FAB classification.

For these reason FAB classification was replaced by the World Health Organization (WHO) classification published in 2001, with karyotype and molecular aberrations took into account¹⁸. However, FAB classification remained relevant as it formed the basis of the WHO's subcategory of AML "not otherwise specified". In the WHO classification, patients with t(8;21), inv(16), or *KMT2A (MLL)* translocations, which collectively constituted nearly half of the cases of childhood AML, were classified as AML with "recurrent cytogenetic abnormalities". In this classification system the bone marrow percentage of leukemic blast requirement for the diagnosis of AML decreased from 30% to 20%. Moreover, an additional clarification was made so that patients with recurrent genetic anomalies did not need to meet the minimal blast requirement to be considered an AML at diagnosis. In 2008 in fact, the WHO expanded the number of cytogenetic abnormalities linked to AML classification and, for the first time, included specific gene mutations, such as *CEBPA* and *NPM1*, in its classification system. The 2016 WHO classification revision divided AML into 6 groups summarized in Table 3.

2016 WHO classification of Acute Myeloid Leukemia (AML)

AML with recurrent genetic abnormalities

AML with t(8;21)(q22;q22); *RUNX1-RUNX1T1*
 AML with inv(16)(p13.1;q22) or t(16;16)(p13.1;q22); *CBFB-MYH11*
 APL with *PML-RARA*
 AML with t(9;11)(p21.3;q23.3); *MLLT3-KMT2A*
 AML with t(6;9)(p23;q34.1); *DEK-NUP214*
 AML with inv(3)(q21.3q26.2) or t(3;3)(q21.3;q26.2); *GATA2, MECOM*
 AML (megakaryoblastic) with t(1;22)(p13.3;q13.3); *RBM15-MKLI*
 AML with *BCR-ABL1* (provisional entity)
 AML with mutated *NPM1*
 AML with biallelic mutations of *CEBPA*
 AML with mutated: *RUNX1* (provisional entity)

AML with myelodysplasia-related features

AML related to previous chemotherapy or radiation

AML not otherwise specified

AML with minimal differentiation (M0)
 AML without maturation (M1)
 AML with maturation (M2)
 Acute myelomonocytic leukemia (M4)
 Acute monoblastic/monocytic leukemia (M5)
 Pure erythroid leukemia (M6)
 Acute megakaryoblastic leukemia (M7)
 Acute basophilic leukemia
 Acute panmyelosis with fibrosis

Myeloid proliferations related to Down syndrome

Transient abnormal myelopoiesis (TAM)
 Myeloid leukemia associated with Down syndrome

Myeloid sarcoma

Table 3. The 2016 World Health Organization (WHO) revision and classification of myeloid neoplasm and acute leukemia (from Blood 2009, J.W. Vardiman).

This latter findings revealed that recurrent abnormalities are markers of AML, but even if several efforts have been spent to identify if these structural alterations, intra-chromosomal rearrangements, and genetic mutations were sufficient to reconstitute an acute leukemia *in vivo*, all of them were unable, as single mutation, to mimic an acute disease suggesting that other mutations or events might concur to the leukemia burden onset. Therefore increasing the knowledge of AML clonal heterogeneity is necessary to explain the evolutionary process that leads to leukemogenesis^{9,19}.

AML diagnosis, treatment and outcome

AML diagnostic procedure involves the characterization of the pathology, for prognostic purpose and for the evaluation of the appropriate therapy. According to the guidelines of the Associazione

Italiana di Ematologia e Oncologia Pediatrica (AIEOP), this characterization is based on several analyses of the BM aspirates. At first the diagnosis of AML is given when 20% of myeloid blasts are identified by cell morphology analysis of the BM by cytochemistry staining to determinate the FAB subtype (Table 4; WHO criteria 2006)²⁰.

Cytochemical Reaction	Cellular Element stained	Blasts identified
Myeloperoxidase (MPO)	Neutrophil primary granules	Myeloblasts strong positive; monoblasts faint positive; Lymphoblasts negative.
Sudan Black B (SBB)	Phospholipids	Myeloblasts strong positive; monoblasts faint positive; Lymphoblasts negative.
Specific esterase	Cellular enzyme	Promyelocyte stage positive.
Nonspecific esterase (NSE)	Cellular enzyme	Monoblasts strong positive; Others negative.
Periodic acid-Schiff	Glcogen and related substances	Lymphoblasts's and pronormoblasts negative to positive; Myeloblasts usually negative; Metamyelocyte & PMN strong +ve.

Table 4. Cytochemical reactions useful to classify the acute leukemias.

Then, immunophenotypic analysis for the characterization of the cellular *lineage* and maturation level of the neoplastic cells and, together with cytogenetic and molecular biology investigations for reveal the presence of known prognostic genetic abnormalities is performed. Nowadays in 95% of pediatric AML patients at diagnosis at least one genetic lesion identified, for whom a risk adopted therapy can be pursued¹⁴.

The prognosis of Italian children affected by AML has significantly improved over the last two decades, with current 8 years Event-Free Survival (EFS) and Overall Survival (OS) of 55% and 68%, respectively, achieved in the multicenter AIEOP AML 2002/01 protocol⁴. This improvement was largely due to a stratification of patients in risk classes with a consequent risk-directed therapy, to the optimization in induction and post remission treatment strategies (high-dose of Cytarabine), to increased supportive therapy and mainly to the introduction of hematopoietic stem cell transplantation (HSCT)⁴. Conventional AML therapy is based on intensive use of Cytarabine (AraC) and/or Idarubicin, Cytarabine and Etoposide (ICE) being frequently used in pediatric AML. All standard risk (SR) patients achieved complete remission (CR) after chemotherapy alone, whereas for children allocated at intermediate and high risk categories, an intensive chemotherapy consisting of 4-5 cycles typically including Cytarabine combined with Idarubicin is provided.

Moreover, for high risk patients beside chemotherapy, the use of HSCT is desirable in the Italian but also in international pediatric AML trials²¹⁻²³. In particular, HSCT in first CR is used only for the high risk (HR) group in the AIEOP AML 2002/01 protocol, and in a more selected subsets of high risk cases for others international groups²⁴. This latter option is sustained by AIEOP-Italian studies that revealed the use of auto- or allo-HSCT in HR patients resulted in lower incidence of leukemic recurrence, with an acceptable treatment-related mortality²⁵.

Despite these improvements and an increased AML patients' outcome, around 30% of children still relapse, and after disease recurrence, the risk to die is extremely high (>50%)^{5,14}. Notably, the outcome in the Italian cohort of SR patients is inferior than expected for a large proportion of patients carrying either t(8;21) or inv(16) who relapsed^{4,15}. Furthermore, risk of organ toxicity with severe late-effects is often derived from the current cytotoxic treatments (5-10%)²⁶⁻³⁰. This latter is an extremely important point in children care since cytotoxicity includes cardio-toxicity, gastrointestinal toxicity and neurotoxicity, moreover neutropenia and disruption of skin and mucosal barriers and other complications that often lead to bacterial and fungal infections that can be extremely severe in compromised children with cancer^{5,30}. Besides, the increase use of HSCT confers a risk of graft versus host disease (GVHD) and death. The consequence of these adverse effects is that 5% of pediatric AML patients die, as result of treatment-related complications^{4,5}. These findings emphasize that new therapeutic strategies are urgently needed in pediatric AML. Many compounds with novel and diverse mechanisms of action and therapeutic strategies are actively being under evaluation in clinical trials, including monoclonal antibodies, immunotherapy (e.g. anti-PD1 monoclonal antibody)³¹, and epigenetic therapy (e.g. Azacitidine)^{32,33} (Figure 3). Nevertheless, even if many efforts have been spent in drug discovery for more targeted therapies to cure pediatric AML or at least to reduce toxicity and side effects, no innovative drugs were included in clinical trials up to now^{5,34,35}. Furthermore, in the last years the role of the microenvironment is increasingly recognized as being tumor-protective, considered a "sanctuary" for tumor cells allowing leukemic cells to survive the effect of therapy, and new treatment strategies directed at reversing this protective effect are also under investigation^{36,37}.

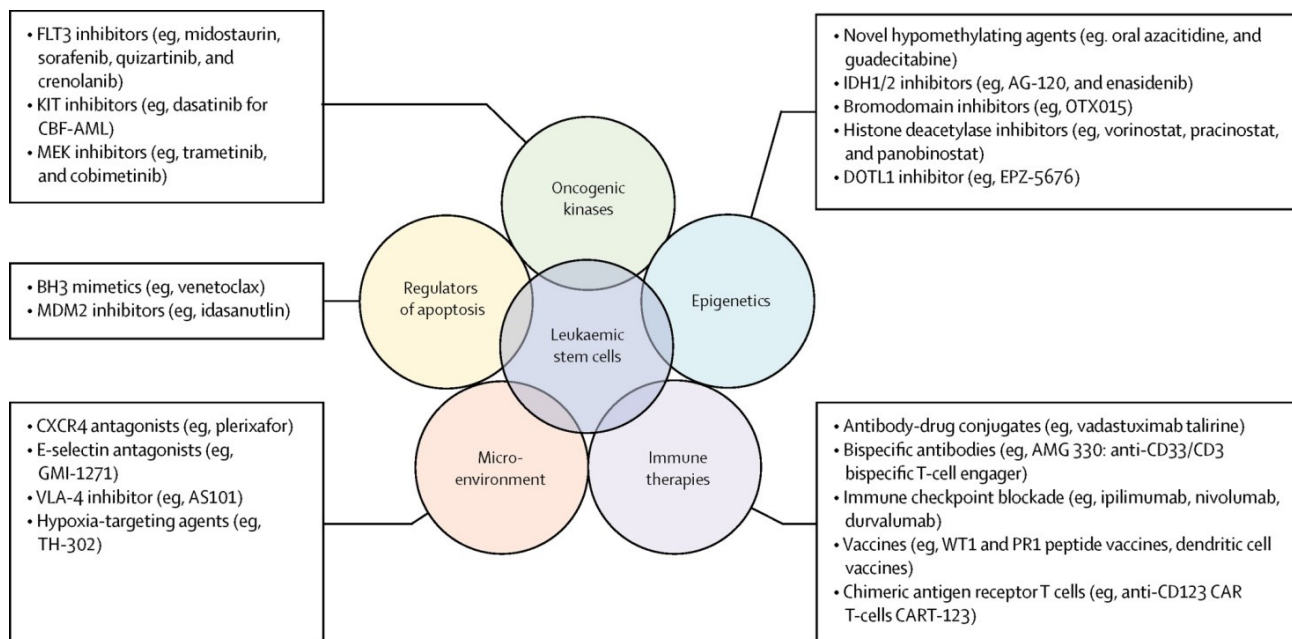


Figure 3. Examples of selected novel therapeutic strategies in AML (from Lancet 2018, N.J. Short).

The bone marrow niche

A niche is defined as local microenvironment within a tissue that allows the maintenance of stem or progenitor cells and regulates cellular fate³⁸. The physiological equilibrium in blood tissue, that ensure the life-long supply and regeneration of mature blood cells, is not achieved by HSCs or hematopoietic stem progenitors cells (HSPCs) autonomously, but rather it is due to fundamental communications with surrounding hematopoietic environment, namely the bone marrow microenvironment, which harbours different stem cell niche³⁹.

Knowledge bases regarding the architecture of the human BM, the HSCs distribution in the niche, and the function of its different cellular constituents have markedly improved in the past few years. The BM microenvironment consists of non-cellular components like extracellular matrix (ECM) proteins, including collagen, fibronectin, laminin and hyaluronic acid. On the other hand, the biology of HSCs is thought to be regulated by a complex array of cell populations, mainly represented by arteriolar⁴⁰ and sinusoidal⁴¹ endothelial cells, mesenchymal stem cells (MSCs)⁴², osteoblasts⁴³, sympathetic neurons⁴⁴, non-myelinating Schwann cells⁴⁵, adipocytes⁴⁶, megakaryocytes⁴⁷, macrophages, neutrophils, and regulatory T cells⁴⁸.

Human HSCs have been found preferentially located at the trabecular areas of the BM (Figure 4)⁴⁹. In detail, within the hematopoietic niche it is possible to recognize two distinct specialized areas: the endosteal niche (also called osteoblastic niche) and the perivascular niche. The endosteal niche is the interface between the bone and the BM and it is mainly composed of osteoblasts and osteoclasts at the trabecular bone, and sinusoids which are fenestrated vessels allowing the passage of cells in and out of the blood circulation and carrying the oxygen, growth factors, and nutrients. In this region, usually reside the long-term HSCs that find a suitable microenvironment for the maintenance of a quiescent state or slow-cycling cells⁵⁰. In the perivascular niche there are a lot of vessels and hematopoietic progenitor cells (short-term HSCs) ready to migrate into peripheral circulation and to differentiate into mature blood cells^{2,51-53}. In reality a separation of the two microenvironments is difficult and HSCs interact with numerous and simultaneous cell-extrinsic signalling settings (Figure 5).

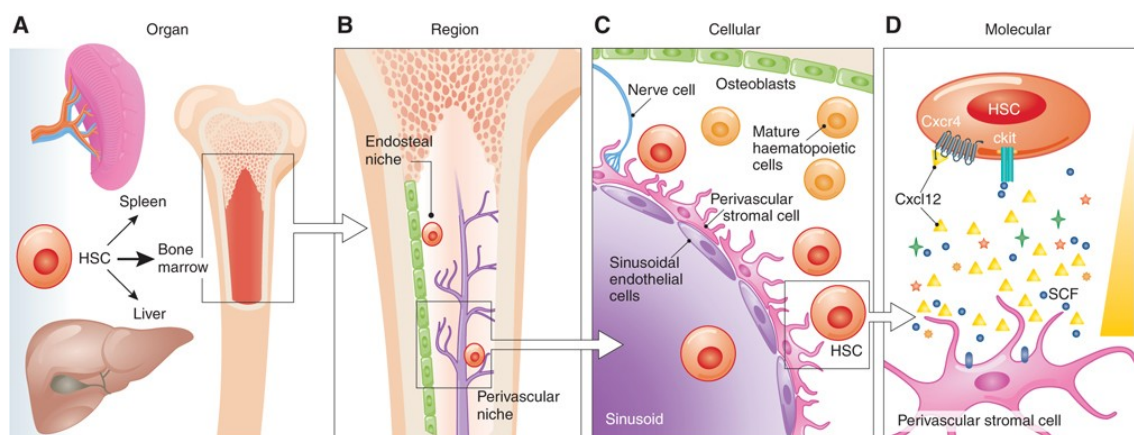


Figure 4. BM niche. (a) HSCs can circulate temporarily in organs, such as spleen and liver, but (b) the majority of HSCs reside in the BM at perivascular or endosteal niche, (c) interacting with different cells types, such as osteoblasts, endothelial cells and nerve cells. In the BM niche, cells secrete factors involved in hematopoietic homeostasis regulating quiescence, self-renewal and differentiation processes, such as SCF and CXCL12 (from EMBO J 2013, F. Urgate & E.C. Forsberg).

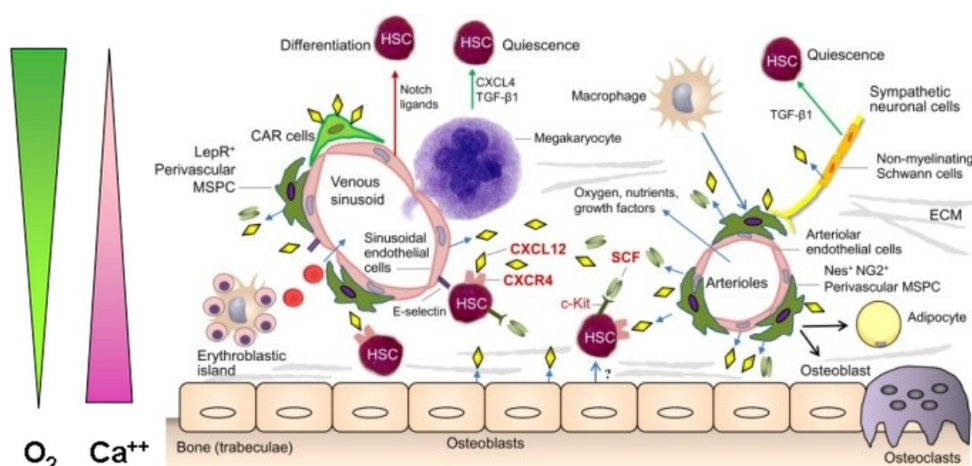


Figure 5. The BM niche is composed of stromal cells derived from MSCs which are able to differentiate in osteoblasts/osteocytes, adipocytes, and osteoclasts; endothelial cells derived from endothelial stem cells (ESCs). Regulatory signals include cell-intrinsic regulatory mechanisms, adhesion molecule interactions, extracellular matrices (ECMs), and environmental components such as calcium (Ca^{++}), oxygen (O_2), proteases, as well as humoral factors including cytokines and chemokines (modified from Blood 2008, J.J. Lataillade and from Blood Research 2016, T. Schroeder).

Pivotal cellular components players in the BM niche

Osteoblasts

The close physical interaction between HSCs and osteoblasts, supposed a crucial role of the osteo-*lineage* cells in the BM niche⁵² (Figure 6). Indeed, the skeleton is absolutely necessary for

mammalian haematopoiesis, as demonstrated by genetic studies where the absence of osteoblastic differentiation was shown to block the haematopoietic process⁵⁴. It has been demonstrated that osteo-*lineage* cells support HSCs expansion *in vitro*, producing important factors implicated in HSCs regulation, including Interleukin 6 (IL 6), Transforming Growth Factor β (TGF- β), Granulocyte Colony-Stimulating Factor (G-CSF), thrombopoietin (TPO), angiopoietin 1 (ANGPT1), and CXCL12 (also called SDF-1)⁵⁵ (Table 5). Furthermore, during osteoblastic differentiation various functions have been demonstrated at different stages, such as long-term reconstitution activity, adhesion/homing and production of pro-HSCs cytokines. Evidences that during the early phase of osteoblastic differentiation, osteoprogenitors cells maintain and enhance HSCs production triggering their migration towards vascular niche has been also observed; whereas in their terminal and mature stage, osteoblasts seem to be detrimental for HSCs retention at the endosteum region⁵².

Endothelial cells

In human BM, comparable to mice, endothelial cells (ECs) reside both in the endosteal and in vascular regions (Figure 6). These compartments are highly vascularised and produce angiocrine factors and cytokines that enhance HSCs proliferation but also produce specific cell adhesion molecules, as E-selectin, VCAM-1, and ICAM-1, all factors with a fundamental role in the mobilization of HSCs from BM to blood stream^{2,52}. Expression of stem cell factor (SCF), CXCL12, and E-selectin by ECs contribute to HSCs maintenance, and regeneration of sinusoidal endothelial cells that are required for hematopoietic recovery from myeloablation (Table 5). Finally, it has been demonstrated that the conditional depletion of CXCL12 in NG2⁺ pericytes induces the mobilization of quiescent BM HSCs into circulation and results in a reduction of BM HSCs⁴².

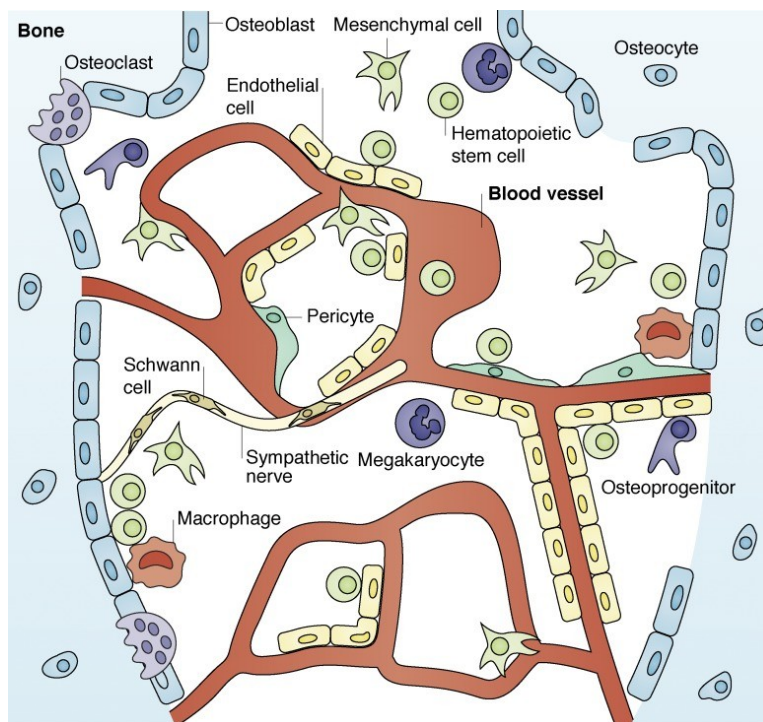


Figure 6. The hematopoietic BM niche. The BM is a heterogeneous environment composed of different cell types. The two main architectural components of the blood tissue are the bone and the vessels, integrated in a complex network connected to nerve fibers. Associated with these structures there are different cell types, as depicted in the figure, regulating the tissue homeostasis and the normal HSCs fate in healthy and disease conditions (from JEM 2018, A. Abarrategi).

Mesenchymal stromal cells (MSCs)

While there has been a long history of research and debates about the contribution of bone and endothelial cells to healthy hematopoiesis, the indispensable role of MSCs for the regulation of normal HSPCs has been unrevealed during the last years. MSCs occupy endosteal and vascular niche and are often spatially associated to HSCs, supporting a strong interaction between these two types of cells^{52,56}. The first description of mesenchymal precursor cells in the BM derived from studies of Friedenstein *et al.*, who identified colony-forming units of fibroblasts (CFU-F) obtained from BM in suspensions⁵⁷. Besides the stem cell-defining propriety of self-renewal these mesenchymal precursor cells exhibit the potential to differentiate into different mesodermal *lineages* such as bone, cartilage, and fat cells, as well as communicate with HSCs via secreted factors involved in the HSCs maintenance, such as the c-KIT, TPO, ANGPT1, and Interleukin 7 (IL 7)⁵⁶. Of note, MSCs produce niche factor CXCL12², necessary for the activation of CXCR4 receptor (expressed by immature hematopoietic cells) and the CXCL12-CXCR4 axis that regulates homing, retention and migration of HSCs in BM, as well as HSCs quiescence (Table 5). In addition of these soluble factors, the cross-talk between surrounding cells and HSCs is also

mediated by cell-bound molecules, such as adhesion molecules and Notch ligands. Furthermore, the dynamic nature of MSCs accounts for their role in diverse biological processes such as tissue regeneration and repair, anti-fibrosis, angiogenesis, survival and maintenance of other cell populations in the niche, and immune-modulation^{58,59}. Indeed, in this regard, one of the most noteworthy propriety of MSCs is their role in immune suppression and modulation, both reported to aid in tumor development. MSCs inhibit the response of allo-reactive T lymphocytes⁶⁰, the proliferation and cytotoxicity of NK cells⁶¹, the generation and maturation of dendritic cells and B cells⁶². MSCs are also known to preserve neutrophil viability and function, induce macrophage M1/M2 phenotype transformation, and promote generation and induction of CD4⁺CD25⁺ or CD8⁺ T regulatory cells.

Molecules	Actions	References
Angiopoietin (ANG)	Maintains HSC non-proliferation state	Arai <i>et al.</i>
Bone morphogenetic proteins (BMPs)	Induces bone and cartilage formation; support growth and differentiation of HSCs	An <i>et al.</i>
Chemokine ligand 12 (CXCL12) (SDF-1)	Maintains HSCs by binding to CXCR4 on HSCs	Sugiyama <i>et al.</i>
Fibroblasts growth factor (FGF)	Maintain MSCs self-renewal	Di Maggio <i>et al.</i>
Osteopontin (OPN)	Regulates HSCs proliferation	Stier <i>et al.</i>
Stem cell factor (SCF)	Regulates HSCs self-renewal	Kent <i>et al.</i>
Thrombopoietin (TPO)	Maintains HSCs proliferation	Yoshihara <i>et al.</i>
Vascular cell adhesion molecule 1 (VCAM1)	Facilitate cell homing via cell-cell interaction	Mercier <i>et al.</i>
Wnt	Regulates HSCs self-renewal	Kim <i>et al.</i>

Table 5. Essential molecules that regulates the bone marrow niche function.

In mice, several MSCs subsets have been identified based on the expression of specific markers with regard to their localization within the BM cavity and their function proprieties^{63–65}. In detail, MSCs can express specific marker including Nestin (Nes), NG2, platelet-derived growth factor receptor α (PDGFRA), CD51, Sca-1 and Leptin receptor (Lep-R)⁶⁶. In contrast, to this advanced understanding of MSCs in mice, the knowledge about human MSCs is more limited due to technical limitations in tracking and visualizing these cells *in vivo*. To cope with these restrictions and to facilitate as much as possible the comparability of results retrieved from differentially generated cells, the International Society for Cellular Therapy (ISCT) has proposed minimal definition criteria for MSCs which are based on surface marker expression, plastic adherence and *in vitro* differentiation potential (Table 6)⁶⁷.

1. Adherence to plastic in standard culture conditions;		
2. Phenotype	Positive ($\geq 95\%$ +)	Negative ($\leq 2\%$ +)
	CD105	CD45
	CD73	CD34
	CD90	CD14 or CD11b
		CD79 α or CD19
		HLA-DR
3. <i>In vitro</i> differentiation: osteoblasts, adipocytes, chondroblasts (demonstrated by staining of <i>in vitro</i> cell culture).		

Table 6. Summary of criteria to identify the MSCs.

Leukemia bone marrow niche

The role of the hematopoietic niche in maintaining or inducing physiologic and pathological conditions is documented². During leukemogenesis, blasts compete with healthy hematopoietic cells for niche resources, modifying the BM microenvironment and transforming it in a “leukemic BM niche”. Several studies documented that different cellular components and signals in leukemic microenvironment are able to regulate malignant cells dormancy and to enhance evasion from chemotherapy, suggesting that the interaction between stromal non-hematopoietic cells and malignant clones could be responsible of drug resistance⁶⁸. Moreover, BM microenvironment has been reported to have not only a supportive role for leukemic cells, but also to have primary events favouring abnormalities occurring in the normal hematopoietic process, which can lead to disease (Figure 7).

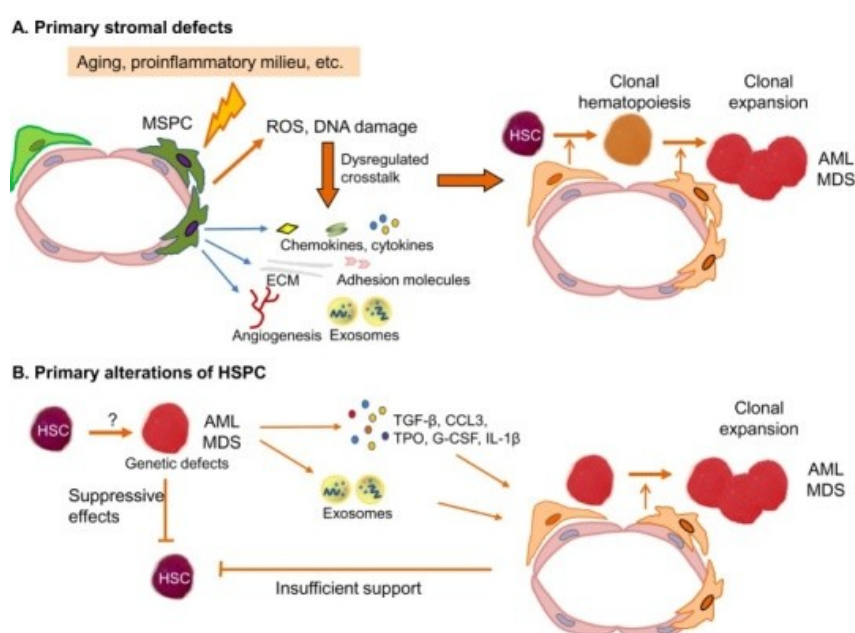


Figure 7. Patho-physiological models of AML. (A) AML originates from a primary stromal defect. Functional alterations of MSCs results in genotoxic stress and dysregulation crosstalk with HSCs favouring the acquisition of genetic and molecular aberrations, supporting the establishment and expansion of clonal hematopoiesis. (B) AML originates from primary alterations of HSCs, together with a second step where these clonal hematopoietic cells induce phenotypic and functional changes in the BM microenvironment turning it into a self-reinforcing niche, which supports malignant cells limiting healthy hematopoiesis (from Blood Research 2016, T. Schroeder).

Malignant myeloid progenitor cells modulate the BM microenvironment

There are several examples illustrating the major concept that malignant HSCs can remodel the BM microenvironment and tilt the competitive balance by reducing or expanding the number of leukemia-inhibiting or leukemia-supportive cells to advance disease toward malignancy. In a murine model of terminal phase of Chronic Myeloid Leukemia (CML), CML-osteoblasts were significantly reduced and functionally inhibited by leukemic cells⁶⁹. Furthermore, two other studies demonstrated how leukemic cells directly affected surrounding niche cells. They explained that secretion of G-CSF by leukemic cells resulted in decreased expression of CXCL12 by BM stromal cells and hereby impaired HSPCs maintenance⁷⁰. In the second similar model, a separate group demonstrated that the malignant CML cells stimulated MSCs to overproduce functionally altered osteoblasts, which accumulate in the BM cavity as inflammatory myelofibrotic cells; they also identified a role for TPO and CCL3 (also known as macrophage inflammatory protein 1 α , MIP-1 α), and direct cell-cell interaction in driving osteoblasts expansion and remodelling. These CML-osteoblasts exhibited impaired capacity to support normal hematopoiesis by reducing the expression of hematopoietic-retention factors⁷¹. Evidences also in acute leukemia have been produced, in a mouse model of AML with the t(9;11)*MLL-AF9* rearrangement. Authors observed a significant reduction in osteoblasts in the mice BM with a resulting reduced and impaired normal haematopoiesis^{72,73}. At the same time, when mice were treated with factors that enhanced osteoblasts production, prolonged survival and decreased leukemia infiltration in *MLL-AF9* mice were observed^{72,73}. These results showed a rescue of the niche modulatory effects acting as a potential therapeutic strategy. Taken together, all of these data support that the leukemia-induced manipulation of niche elements serves as a self-reinforcing mechanism to leukemia instead of normal hematopoiesis, to enhance competitiveness, tumorigenic angiogenesis, and treatment resistance.

In addition to the change of osteoblasts, genetic aberration in MSCs, different from those acquired by the hematopoietic cells, have been largely discussed. In particular, discordant data of structural chromosomal changes were described in BM-MSCs of 25% of Myelodysplastic Syndrome (MDS) and also in AML-derived MSCs⁷⁴, these latter findings being extended in other paper where 44% of

patients with MDS and 54% of those with AML⁷⁵ were included harbouring genetic aberrations in the BM microenvironment. Other conflicting results have been also reported with regards to the biological behaviour of MSCs derived from AML, such as their clonogenic potential and hematopoietic support capacities were shown to be reduced in some AML patients^{76–80}, or proliferative advantages towards the hematopoietic support by AML-derived MSCs^{81,82}. These controversies were probably related to a limited number of samples, as well as to different experimental settings. Anyway, recently increasing findings indicate that MSCs from *de novo* AML are structurally, epigenetically and functionally altered and that this impaired stromal support substantially contributes to hematopoietic insufficiency in AML⁸³.

Communication between AML cells and BM microenvironment is an important hallmark of hematopoietic malignant transformation which is either guided by cell-cell contacts or by the extracellular secretory molecules which could include circulating extra-vesicles which include nucleic acid, proteins, metabolites or lipids⁸⁴. Several critical transcription factors, adhesion molecules, cytokines and pathways, such as the Notch1, Wnt, Shh, BMP, and TGF- β have been involved in the cross-talk between MSCs and HSCs and described altered in AML-derived MSCs (Figure 8). However, whether and how these abnormalities influence the pathogenesis of AML is currently under discussion^{70,71}. Finally, immunologic characterization of BM-MSCs from AML patients, respect to MSCs derived from healthy donors, showed an increased immunosuppressive mechanisms with increased IL 10 expression correlating to disease outcome⁸⁰. Several data supported that an altered production of pro-inflammatory cytokines from the BM microenvironment could aid in the initiation and maintenance of haematological malignancies and favour the growth of leukemic cells^{85,86}.

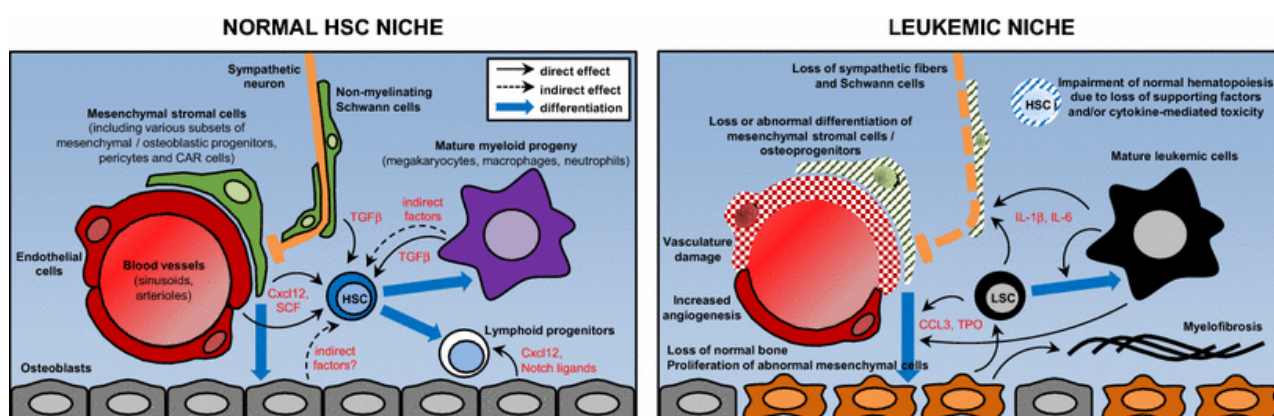


Figure 8. Overview of the main components of the BM-HSCs niche and their alterations in leukemia. Simplified scheme of the healthy hematopoietic niche (left) and in the context of malignancy (right). The right panel summarizes niche abnormalities observed in various experimental settings (from Cellular and Molecular Life Sciences 2017, A. Sanchez-Aguilera & S. Méndez-Ferrer).

Niche-induced myeloid malignancies in mice

Taking into account the physiological relevance of the BM microenvironment, several investigators have tested the hypothesis in which genetic alterations of non-hematopoietic niche cells are capable of inducing myeloid malignancies debating the concept of AML originating exclusively from HSCs-intrinsic genetic defects (Figure 9). The initial evidence on the role of genetically transformed stromal cells in the genesis of MDS come from Rupec *et al.* who established that deletion of *Ikbα* from the stromal cells of mice led to MDS⁸⁷. Further evidences about niche-driven myeloid disorders came from murine models with deletion of Retinoic acid receptor gamma (*RARγ*) gene from the microenvironment, exhibiting a myeloproliferative neoplasm (MPN)-like phenotype upon transplantation of bone marrow or spleen cells from *RARγ*^{-/-} mice to wild type mice, but not in *RARγ*^{-/-} mice⁸⁸. This finding exemplified that a defective microenvironment might initiate neoplasms. Another interesting study demonstrated a link between deletion of *RB* (Retinoblastoma) gene in HSCs, as well as stromal cells able to establish a myeloproliferative-like disorder resulting in subsequent mobilization and loss of HSCs⁸⁹. Similarly, the Notch ligand endocytosis regulator *Mib1* (Mind bomb) deletion in MSCs resulted in constitutional activation of Notch signalling in microenvironment, leading to a myeloproliferative disease characterized by leukocytosis, extramedullary hematopoiesis and splenomegaly⁹⁰. Collectively, these studies highlighted that genetic changes or alteration of non-hematopoietic elements of the BM microenvironment might induce hematopoietic dysfunction that could directly contribute to disease initiation or a pre-leukemic condition (analogous to an oncogenic “first hit”). However, these models are able to demonstrate a hyperproliferation of HSCs but not a true malignancy, suggesting that additional mutations are required in the hematopoietic cells to induce acute leukemia onset. Two subsequent studies refined this concept and by the manipulation of specific stromal cell subsets, a pivotal role of MSCs and osteoblasts cells for the pathogenesis of AML was shown. Briefly, one sophisticated model by Raaijmakers *et al.* reported that deletion of RNAse III endonuclease *Dicer1* with reduced levels of SBDS (Shwachman-Bodian-Diamond Syndrome) protein in mesenchymal osteo-progenitors (but not in mature osteoblasts) resulted in MDS phenotype associated with acquisition of genetic alterations and a propensity to develop AML⁹¹. In a recent study by Zambetti *et al.*, there was a further support that the deletion of *SBDS* gene in mesenchymal progenitor cells induced mitochondrial dysfunction, oxidative and genomic stress in HSCs and that the damaged associated molecular pattern (DAMP) molecules (s100a8 and s100a9) secreted by MSCs drive tissue failure and malignant hematopoietic transformation⁹². In one more model, constitutively active β-catenin and subsequent Wnt signalling in osteoblasts cells caused a transplantable AML phenotype⁴⁷. These changes were induced by the expression of *Jagged1* in niche-cells and consequentially activation of

Notch signalling in hematopoietic cells. These findings recently demonstrated that specific gene deletion within MSCs is associated with human hematological malignancy and can be considered playing a role as primary drivers of disease.

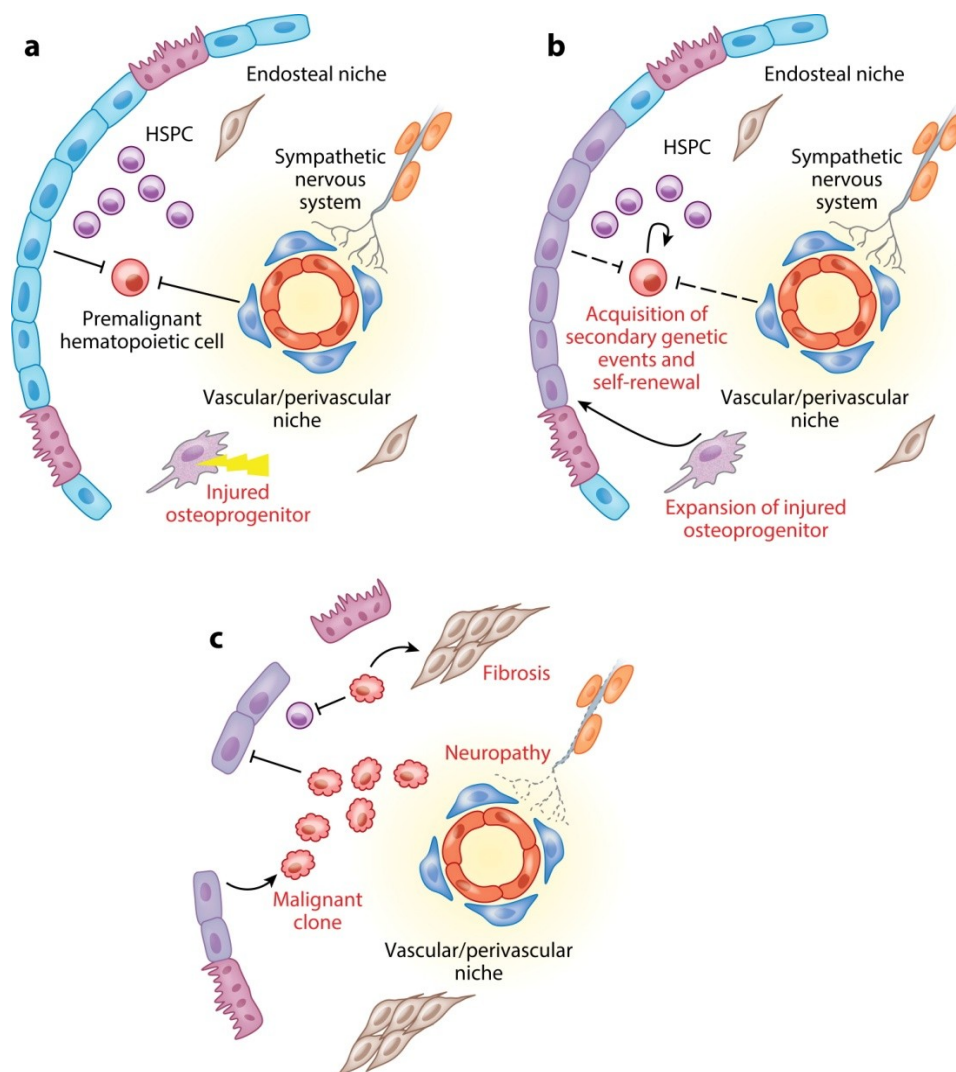


Figure 9. Schematic view of BM niche modifications putatively causing leukemia onset. HSPCs fate is regulated by intrinsic and extrinsic stimuli in the BM microenvironment. (a) pre-malignant clones are not advantaged in normal conditions so they don't survive; (b) if an injury happens to BM stromal cell (e.g. osteo-progenitors), they could expand and replace normal osteoblasts present in endosteal niche that are co-responsible for the block of pre-malignant cells; (c) pre-malignant cell is now able to proliferate and to acquire other mutations lead to malignant clone expansion and to further modification of BM niche, advantaging tumor cells and, at the same time, impairing normal HSPCs (from Annual Review of Pathology: Mechanisms of Disease 2016, J. Hoggatt).

It is still uncertain whether similar changes in the microenvironment alone are causative of human leukemia. An additional clinical setting where the interaction between an abnormal microenvironment and hematopoietic cells has been shown is that of transplantation. Albeit rare, there are multiple reports of donor cell-derived neoplasia that occurred after a BM transplant from a

healthy donor⁹³. Although it is possible that some of these cases were the result of undetected malignant clones in the donor, the data are also consistent with niche-induced haematological malignancies in human. In this context of donor-cell-leukemia, abnormalities of the recipient microenvironment might be an inherent features or could results from damaging effect of previous treatment. Indeed, the intensive chemical and radiation exposure experienced by the recipient BM microenvironment might trigger comparable inflammatory activation within stroma, resulting in increased ROS production and elevated leukemogenic potential^{94,95}.

The role of microenvironment in resistance to chemotherapy

In the last years, the tumor microenvironment is increasingly being recognized as a critical factor in mediating drug resistance. Resistance may occur through the soluble release of growth factors, secreted by osteoblasts, ECs, and stromal cells and by contact-dependent mechanisms via cell-cell and cell-extracellular matrix interactions. The term, soluble factor-mediated drug resistance (SM-DR) or cell adhesion-mediated drug resistance (CAM-DR) has been used to describe the phenotype in which interaction of malignant cells with small molecules or stroma confers resistance to chemotherapy. SM-DR and CAM-DR has been described *in vitro* for both primary tumours and cell lines derived from several hematologic malignancies⁹⁶⁻⁹⁸. As noted above, CXCL12, VEGF, IL 6, FGF, G-CSF, and other soluble molecules mediate chemotherapy resistance via different mechanism. Vascular endothelial growth factor C (VEGF-C) facilitates leukemia progression with a higher *ratio* of BCL-2 to BAX, which suggest suppressive effects on cell apoptosis and it has also been shown to rescue leukemia cells from chemotherapy-induced cell death⁹⁹. Osteoblasts have been shown to protect AML cells from CXCL12-*induce* cell death trough a soluble factor-mediated mechanism in both CXCL12-expressing AML cell line and clinical patients samples¹⁰⁰. In addition, HSCs and leukemic cells tightly adhere to osteoblasts on the bone surface or stroma through a series of adhesion factors (integrins and cadherins) and extracellular matrix proteins (fibronectin and osteopontin). These cell-to-cell-to-matrix interactions play a critical role in the process of mobilization and homing and in drug resistance and clinical recurrence¹⁰¹. Recent research efforts have uncovered new forms of intercellular communication that include intercellular exchanges of vesicles, plasma-membrane protrusions, lysosomes, and mitochondria¹⁰². In 2016, Moschoi and colleagues have been demonstrated that BM-MSCs transfer functional mitochondria to AML cell *in vitro* and *in vivo* through endocytic pathways, leading to a 1.5-fold increase in energy production and significantly better survival rate of the leukemia cells during chemotherapy^{103,104}.

The leukemic niche as a therapeutic target

By elucidating the role of the BM microenvironment in the pathogenesis of haematological tumours, recent studies have provided the frame-work for identifying and validating novel therapies that target both leukemic cells and cells in their surrounding microenvironment representing a novel therapeutic approach. Hereby, it is possible that by synergistically acting together with conventional therapies targeting the leukemia microenvironment might overcome resistance mechanism. This latter can be achieved through several strategies: i) affecting the key self-renewal pathways in leukemia cells that are promoted by the niche; ii) block of the pro-survival signalling pathways induced by stromal cells to AML cells; iii) affecting homing and adhesion through interference with chemokines and adhesion molecules; iv) targeting the hypoxic milieu of leukemic environment, and v) inhibiting abnormally activated pathways within the cells in the niche (Table 7).

In a first attempt, several investigations, mainly pre-clinical studies, aimed to reverse the resistance to chemotherapy by interfering the adhesion of leukemic cells to stromal cells, which by blocking AML cell homing into the BM niche could act as a protective microenvironment niche. In this context, the CXCR4-CXCL12 axis^{105,106}, VLA-4¹⁰⁷, E-selectin¹⁰⁸ and CD44^{109,110} have been identified as interesting candidates for such approach. Most of the progress in targeting AML-stroma interactions has been made by development of CXCR4 inhibitors (e.g. AMD3100); these agents may also inhibit the pro-survival signals provided to the blasts via CXCR4/CXCL12 signalling. The results of the combination using CXCR4 inhibitor in addition to intensive or less-intensive chemotherapy are encouraging and have demonstrated safety of these agents and synergistic effect in most pre-clinical models of CLL¹¹¹, Acute Lymphoblastic Leukemia (ALL)¹¹², and AML^{105,106}. To note, limited results from studies in human are available yet¹¹³.

The interaction between VLA-4 on AML cells and VCAM-1 on MSCs represent another promising candidate for targeted therapy. VLA-4 inhibitor (e.g. AS101) or humanized VLA-4 monoclonal antibody (e.g. Natalizumab) tested in pre-clinical models prolong the survival in mice after chemotherapy abrogating drug resistance^{114,115}.

Besides anti-homing and anti-cell adhesion approaches, other known BM niche components are under evaluation for targeted therapy. One advanced approach for influencing the leukemia microenvironment is the targeting of angiogenesis. The anti-VEGF monoclonal antibody (e.g. bevacizumab) that neutralize VEGF-A is the first anti-angiogenic agent that has been validated as new cancer therapy. The combination of these compounds with cytarabine, in adult AML patients, has been demonstrated to improve the overall response of 48% in the phase II study¹¹⁶. Although these agents may affect endothelial BM niche, that may, in turn, enforce expansion of hypoxic niches and possibly promote chemo-resistance. In this context, HIF-1 α is being explored not only in

solid tumor models but also in leukemia models. These include a novel antisense oligonucleotide against HIF-1 α and small-molecule HIF-1 α inhibitors¹¹⁷; however, the applicability of these reagents to AML niche biology remains to be established.

In conclusion, recent studies have elucidated multiple intrinsic and extrinsic factors that provide potential opportunities to improve therapeutic targeting of AML cells, even if investigation on the BM microenvironment will be still necessary to understand AML genesis and to design new therapeutic combination strategies. This latter opportunity may be pursued only if *in vitro* models will include the presence of the BM niche components, and if successful *in vivo* pre-clinical AML model will be generated.

Regimen	Phase	ClinicalTrials.gov identifier	Response
CXCR4 inhibitors			
Plerixafor + daunorubicin/cytarabine	I	NCT00990054	CR: 67%
Plerixafor + G-CSF, mitoxantrone/etoposide/cytarabine	I	NCT00906945	
Plerixafor + cytarabine/etoposide	I	NCT01319864	
Plerixafor + mitoxantrone/etoposide/cytarabine	I/II	NCT00512252	CR/CRi: 46%
VLA-4 inhibitor			
AS101 + chemotherapy	II	NCT01010373	
E-selectin inhibitor			
GMI-1271 + mitoxantrone/etoposide/cytarabine	I/II	NCT02306291	
Hypoxia-inducible agents			
TH-302	I	NCT01149915	

Table 7. Clinical studies of agents targeting AML-stroma interactions (modified from Therapeutic Advances in Hematology 2016, A. Rashidi & J.F. DiPersio).

Modelling of human myeloid leukemia

One of the main challenges in pediatric leukemia is the discovery of new therapies that ameliorate the effect of the chemotherapy currently in use, or that reduce toxicity and severe side effects. The new targeted drugs that are under investigation in clinical trial for AML, such as FLT3 inhibitors¹¹⁸, show poor or no efficacy in patients with respect to *in vitro* testing results; these failures could be due to the inadequate *in vitro* and *in vivo* models used for drug screening because no robust pre-clinical models of AML are up to now available^{119,120}. The main limit has been recognized in the idea that the existing models do not recapitulate physiological leukemia context, including inter- and intra-tumor genetic heterogeneity, cell-cell and cell-stroma interactions, as well as the BM microenvironment: all aspects playing important roles in drug treatment response. Another main limit to successfully introduce a new drug in clinic is constituted by the fact that AML is a rare disease, and that the sophisticated genetic characterization at diagnosis divides patients into smaller groups that may guarantee a low number of children eligible for early phase clinical trials. Indeed, the creation of new models and systems to improve the pre-clinical validation of drugs is the main challenge to improve pediatric AML drug portfolio.

In vitro AML models

2D models

In vitro models for studying AML are based on AML immortalized cell lines, most of them harbouring the recurrent genetic abnormalities found in AML patients. These cells, can be expanded for long-term *in vitro*, and during this time they can acquire mutations, changing leukemia immunophenotypic features thus leading to heterogeneity that can cause bias in experiments and in drug screening sensitivity¹²¹. Another strategy could be of using primary pediatric AML bone marrow cells, derived from BM of patients at diagnosis, but the primary cultures can survive *in vitro* for a short time of 24-48 hours and for most of them, after thaw, it would be very difficult to proliferate. This latter finding can mainly depend on the lack of the physiological context, necessary for the AML cells. Moreover, these cultures need to be implemented with high concentration of fetal bovine serum, cytokines, and nutrients for their short-term survival, but they should induce hematopoietic differentiation process, and overall these conditions are poorly recapitulating the BM microenvironment thus influencing cancer cells metabolism and main characteristics¹²¹. Last, but not least, substrates on which cells are cultured (plastic or glass) and their planar surface (2D) are not appropriate to mimic the physiological niche context, far away from the mechanical proprieties

of tissue and from the real three dimensional (3D) BM niche, with a lot of other fundamental factors and diverse cellular subtypes¹²¹.

2D model with feeder layer

Recently many efforts have been spent to establish new methods for culturing of hematopoietic stem cells and leukemic derived cells together with different cell types known to be present in the BM niche¹²²⁻¹²⁴. By the way, one of the first study proposed in 1977, described the first attempt of recreating a BM niche and the author, Dexter, gave the name to its culture model to study the process of hematopoietic differentiation¹²⁵. Dexter performed a stromal cell layer, where MSCs were derived from mouse bone marrow, and then seeded with HSCs derived from mouse and demonstrated that this co-culture prolonged HSCs viability and stemness for a time of 7-12 weeks, especially increased if the culture medium was supplemented with cytokines. This advantage was explained by the direct cell-cell interactions occurring between HSCs and the stromal cells with an additional role played by the stromal-secreted paracrine factors¹²⁵. More recently, in the 2014, a similar layered co-culture system and a drug screening was performed¹²⁶. Briefly, they showed that the drug response of AML cells maintained in co-cultures with MSCs *in vitro* was similar to response of *in vivo* model using an immunodeficient mice, suggesting that these *in vitro* models could be used as an *in vitro* surrogate for xenotransplantation. The authors found that MSCs had a higher potency to support *in vitro* AML cells survival than human umbilical vein endothelial cells or the Osteoblasts derived from osteosarcoma cells, the Soas-2 cells, with a comparable sensitivity profile to Cytarabine as seen in *in vivo* model, emphasising that even a relatively simple and easy *in vitro* model system might be sufficient to recapitulate the real effect of a drug when used in a physiologic leukemic BM microenvironment¹²⁶.

This layered-culture system (2D) has then been applied for many purposes, including for high-throughput drug screenings. In particular, the Golub laboratory screened over 14.700 compounds to identify drugs that could selectively affect leukemia stem cells (LSCs) receiving stromal support using a layered co-culture system. The screen allowed the identification of drugs that eradicated LSCs via a non-cell-autonomous manner by implicating stromal function, as well as drugs that directly targeted LSCs¹²⁷. These models, and many others^{126,128,129}, suggested that mimicking the BM microenvironment *in vitro*, in order to grow primary cells *ex vivo*, was possible, and that MSCs supported AML cell growth maintaining the leukemia immunophenotype and preventing AML cell differentiation. Overall, these layered co-cultured models hold promises as: 1) they allow a very thight control over system components; 2) they are easily manipulated and 3) are perfectly scalable for both high-throughput screening and mechanistic/functional studies. Nevertheless, the layered-

AML co-culture model did not recapitulate the 3D complexity of BM niche, and stromal cells are likely to be polarised on the basal surface of the cells, which receive different signals from their apical side exposed to the culture medium. Due to these drawbacks, the idea to consider the three-dimensionality in cell culturing was pursued. In 3D models AML cells ability to adhere to neighbouring cells of the BM niche or to the extracellular matrix in the endosteal and vascular niche can be studied, and can help to dissect how leukemia cells escape from therapy and can re-emerge to induce relapse.

3D model

The recent advances in the use of a 3D systems with leukemia and stromal cells derived from patients have been shown to improve the development of *ex vivo* disease-model and cell development-model providing accurate picture of *in vivo* interaction in the human niche with a more predictable response to different treatments *in vivo*^{130–133}. 3D cultures models differ each other in mechanical and biochemical environmental factors, in cell-cell and cell-ECM interactions, and in access and physiological gradients of nutrients, oxygen and drugs¹²¹. 3D models have properties comparable with those of the *in vivo* human BM such as pore size, surface area/volume ratio, and surface cell-adhesive features, to allow free penetration of infused cells and establishment of cell-cell and cell-niche associations. Recent advances in cell biology, micro-fabrication techniques, and tissue engineering have enabled the development of a wide range of 3D cell culture technologies. Culture platforms have varied from large porous scaffolds (scaffold with pores large enough for cell penetration that represent truly 3D culture)¹³², to nanofiber scaffolds (cells are not able to penetrate the scaffold), up to hydrogel (a polymeric network that encapsulates cells)¹³⁴ (Figure 10). A list of 3D BM mimicking biomaterial-platforms, with own advantages and disadvantages, using both natural and synthetic biomaterials for HSCs and AML expansion are itemised in Table 8¹³⁵. Furthermore, multiple different bioreactor setups have been used to improve HSCs culture by perfusing the hydroxyapatite scaffold with BM stromal cells to establish a stromal fraction, followed by perfusion with HSCs and maintained *in vitro* by connecting it to a micro fluidic pump¹³⁶. Cultures in rotating wall vessel bioreactors and orbital shake flasks with intermittent shaking both showed a higher multiplication of cells expressing the surface marker CD34⁺ respect to static cultures: the bone marrow-on-a-chip by Torisawa *et al.* despite not being fully synthetic is probably one of the most advanced bone marrow analogous described so far¹³⁶. Natural materials used to create porous scaffolds are typically of the bone: collagen (type I or type II)^{136–138}, fibronectin, laminin, and glycosaminoglycans, such as hyaluronic acid and heparin sulfate¹³⁵, all present in the BM and known to attract HSCs and AML cells. Other natural materials

are often used as scaffolds, in particular matrigel¹³⁹, chitosan¹⁴⁰ and alginate¹⁴¹; these latter materials need to be functionalized being synthetic matrices, with native ECM molecules or inorganic components, such as tricalcium phosphate (TCP) or hydroxyapatite (HA)¹⁴²; by the way all these modifications cannot only affect cells adhesion, but also influence other cellular signalling pathways limiting their use. HA based scaffold is the best model of the ECM and biochemical environment because this component is widely present in the endosteal niche: it contains calcium and might control Ca^{2+} gradients in the culture; Tortelli *et al.* had demonstrated that HA-scaffolds supported stem cell adherence, ECM production, and MSCs differentiation^{143,144}. Moreover, a separate study has recently been shown that HA crystals influence the direction of MSCs differentiation towards osteoblasts *lineage*¹⁴⁵. Other conventional synthetic polymers are used for scaffold, including polyurethane (PU)¹⁴⁶, polyethylene glycol derivatives (PEG)¹⁴⁷, polylactic acid (PLA), poly(lactide-co-glycolide) (PLG)¹⁴⁸, poly ϵ -caprolactone (PCL)¹⁴⁹, and all these materials are used alone or mixed together.

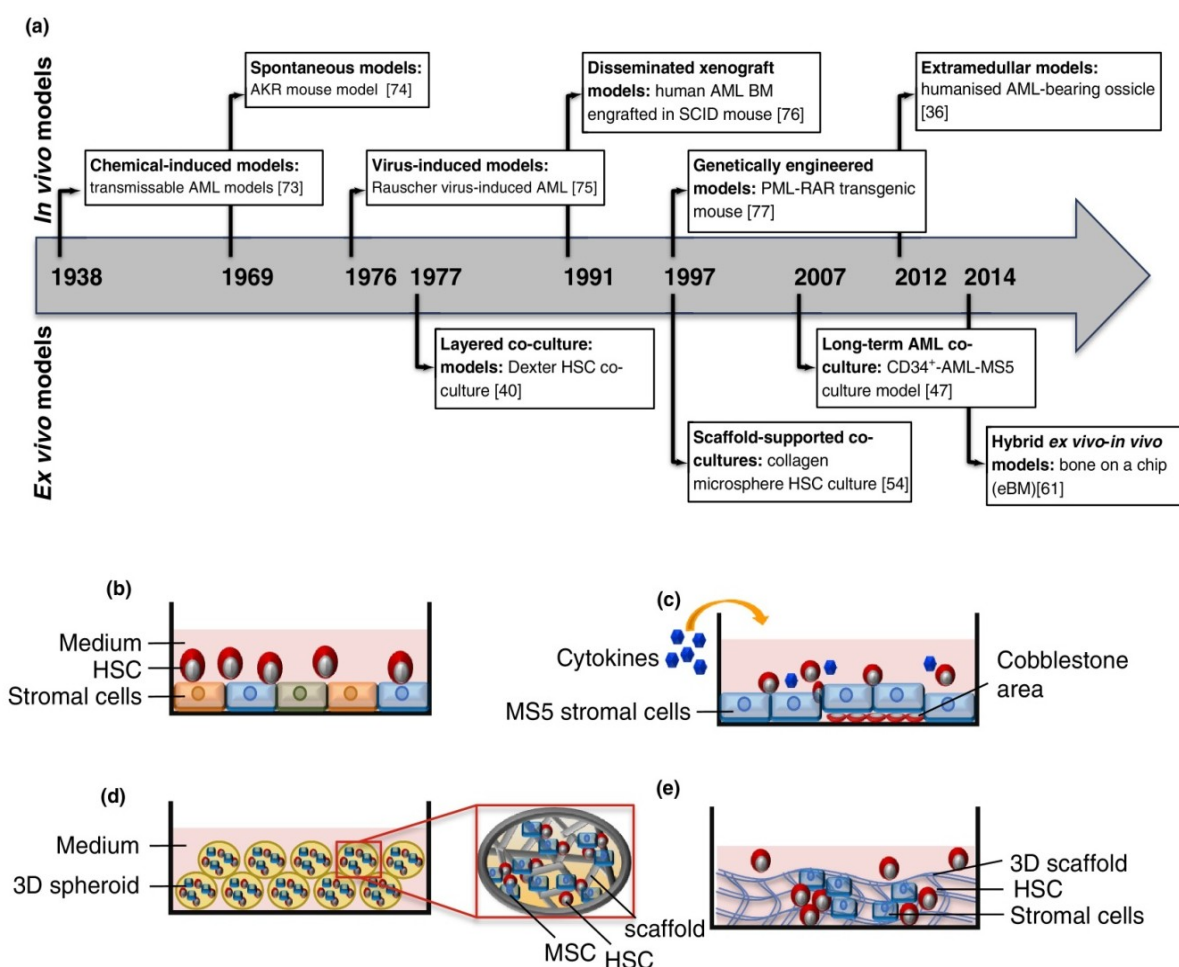


Figure 10. History of the *in vitro* 3D culture models. (a) The timing of *ex vivo* and *in vivo* experimental AML models. The boxes show the year when each model was developed and the first example published. (b-d) The configuration of different *ex vivo* culture models. (b) Dexter culture system where primary HSCs were co-cultured with the adherent cell fraction of primary bone marrow aspirates. (c) Long-term AML/MSCs co-culture developed by Gosliga and colleagues. (d,e) scaffold-supported 3D culture model. The 3D scaffold can derive from decellularized extracellular matrix, collagen, hydrogel, hydroxyapatite-collagen combination, synthetic scaffold, and so on (from Drug Discovery Today 2016, S.P.S. Dhama).

Source of Biomaterial	Scaffold type	BM components	Screening drug sensitivity	Reference
Natural	Collagen scaffold	Isolated MSCs, CD34 ⁺ HSCs	No	133, 131
	Bone-derived/decellularised ECM scaffold	Mouse isolated MSCs and MS5 stromal cell-derived ECM, CD34 ⁺ HSCs	No	
Synthetic	PEG hydrogel	Isolated MSCs, CD34 ⁺ HSCs	No	130, 135, 143
	PGA/PLLA/PLGA/PCL/PU/PET/PVF/PMMA	Isolated MSCs, leukemic cell lines	No	
Chip	Bone-inducing biomaterial	Whole BM	No	128, 132

Table 8. HSCs and AML 3D cell cultures describes and used in literature.

3D systems, where the interaction of cells is established with engineered-biomaterial-based platforms, have also been explored for *ex vivo* HSCs/leukemia cells expansion. One big limitation of current leukemia research is the limited number of primary cells that can be used for research purposes from the BM sample collected at diagnosis. Therefore, their expansion for *in vitro* studies is desirable. The 2D system imposes multiple barriers to this expansion, such as reduction in clonogenicity and differentiation capacity¹³⁷. Papadimitropoulos *et al.* demonstrated a promising 3D system using a porous scaffold for blasts expansion; unlike the case in 2D system, in the 3D system cells proliferated and differentiated maintaining their progenitor properties with a 4.3-fold higher clonogenicity and a higher efficiency of differentiation. Overall, also MSCs were expanded, maintaining their functions¹⁵⁰. Hashemi *et al.*, then, suggested that *ex vivo* expansion of HSCs was possible to increase CD34⁺ cells derived from umbilical cord blood with several implications in further their use¹⁵¹.

Many different 3D culture systems with different complexity were developed and found to support HSCs expansion and maintenance better than when cultured in 2D systems^{152,153}, demonstrating also that scaffold composition, stiffness and topology (geometry) affect HSCs behaviour. Nichols *et al.* described scaffolds fabricated with an inverted colloidal crystal geometry to mimic aspects of the niche¹⁵⁴; the co-cultures of stromal cells and CD34⁺ HSCs in these scaffolds supported cells

expansion and promoted B cells differentiation when compared to the 2D cultures. Similarly, Tan *et al.*, used bio-derived bone to co-culture CD34⁺ HSCs with MSCs in an attempt to replicate the native osteoblastic niche, finding that the 3D scaffold led to a 5- to 7-fold increase in the frequency of long-term-culture-initiating cells (LTC-IC) number (defined as an indicator of primitive HSCs) over two weeks of culture, significantly higher than in 2D cultures¹⁴⁰. Together, these results suggest that the network architecture of porous scaffold can affect HSCs fate decision, and that co-culture with stromal cells is often a requirement for selective expansion. Cukierman *et al.* discovered that BM-fibroblasts had higher motility and divided more rapidly in 3D than in 2D culture conditions¹⁵⁵; moreover, they observed that the asymmetric shape of fibroblasts acquired in 3D cultures clearly represented the original cell shape when in BM. In contrast, the mechanical constraint imposed by the 2D system caused the anchoring receptors to re-distributed from the dorsal to ventral surfaces in adherent cells, creating an imbalance that deviated from the real tissue cell composition¹⁵⁶. Furthermore, other factors, such as stiffness and availability of cytokines, via the production of a gradient 3D biomaterial, have been evaluated as crucial components of the 3D cultures. In a study published by Schneider laboratory, when the HSCs were seeded on a collagen hydrogel embedded with MSCs, different subsets of the HSCs population were identified showing a different distribution associated with a diverse differentiation level¹³⁵, being associated with an unequal cytokines distribution and availability from the MSCs. Thus, in a more recent time several models of haematological disease using 3D bone marrow system have been established with the 3D cultures promising to be a bridge between the 2D culture and the *in vivo* modelling. As mentioned above, several studies demonstrated that in 3D cultures AML cells resulted more resistant to therapy with respect to 2D^{122,123,135}. Aljitalawi *et al.* created a matrigel-based 3D scaffold of MSCs co-cultured with leukemia cell lines where leukemia cells were found more chemo-resistant and proliferative, supporting that 3D cultures might be considered for more reliable drug screenings^{122,157}. These findings confirmed that BM niche might contribute to produce major factors influencing the therapy failure or leukemia progression. Thus, 3D models provide an important *ex vivo* alternative to mouse models, permitting to leukemia cells a long-term proliferation, with the possibility to genetically or pharmacologically manipulate individual hematopoietic cell populations, or to modulate/stimulate stromal components with cytokines in a direct or multimodal manner. Last, but not least, 3D cultures represent the best tool for high-throughput drug screening within the microenvironment context, mimicking closely the patient drug response for a robust drug efficacy prediction.

Despite these *in vitro* models can recapitulate, at least in part, a humanized *in vivo* BM niche, murine models are fundamental and are the actual pre-clinical model for drug discovery and drug

testing process for the subsequent translation of new compounds in clinic^{120,158} and also to understand how AML cells interact with the niche. Whereby, innovative *in vivo* methods have been studied and proposed with the same aim: recapitulate the complexity of human BM niche.

***In vivo* AML models**

Murine animal models are the election model for studying hematopoietic diseases. Inbred strains of mice have been used to study leukemia since the 1930s using either inoculation of human leukemic cells or by mutagen treatments. Several mouse strains, such as AKR, develop spontaneous leukemia over time caused by the murine retrovirus MCF247 transduced. Although these spontaneous models resemble the human disease and have contributed to our understanding of the biology of AML, the inconsistency in time required to disease onset, the low or variable penetrance, and poor response to therapy meant that they were unsuitable for drug discovery studies¹⁵⁹. The landmark technology of genetic engineering (transgenic) using homologous recombination provide the platform for the design, development, and application of an array of mouse model of AML. The genetically engineered mouse models (GEMM) of AML include gene knock-in, traslocator, and invertor-based methods using conditional alleles to investigate chromosomal rearrangements associated with AML were then arrived¹⁶⁰. However, the generation of GEMMs is a labour-intensive, slow process, ultimately produces only a small number of mice model with the required genotype¹⁶¹. In addition, GEMMs often show heterogeneity in disease penetrance and burden, making the interpretation of pre-clinical drug testing very difficult¹⁵⁹. In addition to genetic modelling of cancer, the xenograft model where patient-derived cancer cells are transplanted into recipient mice is a matter of intense investigations. Despite continuous improvements in the creation of new *in vivo* models for the study of leukemia, pediatric AML remains one of the hematologic malignancies with low engraftment performance in Non-obese diabetic mice with severe combined immunodeficiency (NOD/SCID) or NSG mice strain (NOD-SCID^{Prkdc}IL2r^{-/-})^{162,163}. Unfortunately, though the use of cell line is the most successful way to induce AML in mice, but they could not reproduce the patient's tumor biology for several issues: cell lines do not mimic the sophisticated genetic architecture that each AML, nor they cannot acquire new mutations after the onset, producing the clonal evolution and selection that have been recognized during AML progression and therapy of patients^{19,158}. Thus, the necessity to develop Patient Derived Xenograft (PDX) is recently increased. PDX mice models derived from primary tumor cells serially implanted in immunodeficient mice, with the aim to maintain patient's tumor immunophenotype, genetic and genomic features. PDXs have been created for several solid tumors and have been documented to conserve original tumor characteristics, such

as heterogeneous histology, malignant phenotype, genotype and molecular signature¹⁵⁸. These models have been shown to predict clinical outcome of patients, being the best model for pre-clinical testing, identification of biomarkers and personalized therapies¹⁵⁸. Furthermore, for patient's derived cells no intermediate *in vitro* culture passages take place before the implantation of these samples into murine host, avoiding significant known *in vitro* genetic cells transformation or clones selection. Tumor cells can be implanted hetero-topically (generally in subcutaneous site) or ortho-topically in immunodeficient mice. The difference respect the classic xenograft model is about the development of PDX model. PDXs creation consists in four steps and the first generation of engrafted mice are commonly name as P0 (passage zero). While tumor spreads in the P0, the passage of these malignant cells to other mice generations is necessary. Generations thereafter are indicated as P1, P2, and P3. Mice at the P3 generation are suitable to be used for drug screening, after ensuring that during passages the original implanted tumor characteristics (genetic and genomic) were maintained (Figure 11).

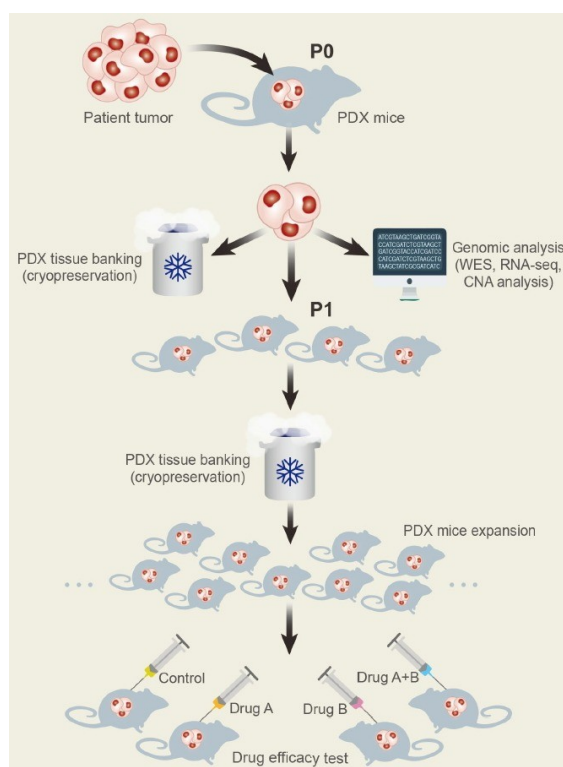


Figure 11. Generation of PDX models. Surgical specimens from cancer patients are divided into small pieces and transplanted into immunodeficient mice (P0). When tumors are grown in P0 mice, xenografts are used for genomic analysis including whole exome sequencing (WES), RNA sequencing (RNA-seq), and copy number alteration (CNA) analysis, and then maintained in cryo-banks for preservation. After expanding tumor xenografts in immunodeficient mice (P1 and more to P3), *in vivo* drug responsiveness is screened in these models with high reproducibility and robustness (from Molecules and Cells 2016, S.Y. Cho).

To date, PDXs are available for most of solid tumors, but pediatric AML ones failed to engraft in mice¹⁶⁴. An important number of studies documented that pediatric AML samples were not able to engraft in immunodeficient mice strains (NSG strains) probably because the majority of myeloid growth factors are species-specific, so murine model is unable to support human leukemic stem cells survival^{120,163}. In the last years new techniques, based on manipulation of mouse and human microenvironment reconstitution in mice, have enhanced human adult AML cell engraftment thanks to the expressing human cytokines or containing cells able to give signals^{133,165,166}. The injections of human cytokines directly into mice produced a transient improvement in engraftment, but this effect was dampen over time¹⁶⁷. Alternatively, the use of transgenic expression of human SCF, GM-CSF, and IL 3 (three human poorly cross-reacting cytokines) into NOD-SCID or NSG mice led to improvements in the expansion of normal myeloid cells. These animals were enabled to engraft AML from samples that have historically been very difficult to study *in vivo*, such as those harbouring standard risk features, the Core Binding Factor (CBF) oncogenes (*AML1-ETO*) or *CBFβ-MYH11*, and samples from Chronic Myelomonocytic Leukemia (CMML) and Juvenile Myelomonocytic Leukemia (JMML) patients^{120,168,169}. The main limitation of this approach consists in the non-physiological levels of human cytokines expressed by these transgenic mice that would eventually lead to myeloid biasness or exhaustion of self-renewal capacity. To circumvent this problem and obtain physiological levels of human cytokines, knock-in mice have been developed, such as the MISTRG; these mice were genetically engineered to express human M-CSF, IL 3, CD172α, TPO, and GM-CSF to allow efficient human cell development¹⁷⁰. MISTRG mice showed higher engraftment of HSPCs derived from peripheral blood than conventional NSG mice¹⁷¹, and also support a robust engraftment of adult AML samples derived from favourable-risk group (e.g. the *CBF* oncogenes)¹⁷². Nevertheless, since human haematopoiesis takes place in specialized niche, in this mice other human niche-specific factors were still missed, thereby excluding important interactions and pushing to novel approaches where a human BM niche could be realized^{133,173–175}.

Nowak Laboratory, using a sophisticated approach, co-injected patient-derived MSCs with MDS cells directly in the BM cavity of NSG-SGM3 mice, a humanized NSG mice¹⁷³, resulting in an increase in leukemia engraftment, and highlighting the role of the niche for MDS. Last, but not least, Waskow Laboratory have recently generated a NSG model expressing a hypomorphic Kit receptor variant (NSGKit^{Wv})¹⁷⁴; Kit mutants weakened the interaction of endogenous-mouse HSCs with Kit ligand (also called SCF) expressed by niche cells, thereby providing a competitive advantage for exogenous-human HSCs expressing wild-type Kit variants. These mice are of particular interest when investigating HSCs-niche or AML-niche interactions¹⁷⁴. Moreover, recent advances in bioengineering have enabled the use of material scaffolds to create a humanized

microenvironment that acts as a frame-work to support cell proliferation and differentiation and study cell–cell interactions with the aim of maintaining implanted cellular phenotypes. Functional human MSCs are used to create a layer of stroma on the carrier material, which provides the “niche” for other cell types to reside in, such as murine hematopoietic and vascular cells, resulting in a human-mouse chimeric tissue useful for hematopoietic studies using primary patients cells^{165,176–179}. The advantages of this model are that (1) it is nearly fully human which enhances the engraftment efficacy of human leukemic cells; and (2) both the stromal cells, as well as the leukemic component can be genetically modified before transplantation. The first study of successful AML engraftment in humanized microenvironment came from Vaiselbuh *et al.*, who developed an ectopic niche by coating polyurethane scaffolds with MSCs. Results showed that 8 weeks after the implantation of these scaffolds into NOD-SCID mice, *de novo* vascularization and osteoblasts, as well as adipocytes development, were demonstrated in an organized human-BM microenvironment¹⁸⁰. Primary AML cells injected directly in pre-implanted scaffolds, or injected by retro-orbital technique, engrafted in the scaffolds and were able to proliferate. Furthermore, CD34⁺ LSCs were observed in scaffolds 5 months after implantation, and these LSCs were found in direct contact with the human stroma, suggesting it as a preferable niche for this subset of leukemic cells¹⁸⁰. A later study, similar scaffolds with genetically engineered human MSCs, which secrete human IL 3 and TPO, showed to allow a better preservation of the myeloid compartment¹⁷⁵. The Schuringa Laboratory, using ceramic scaffolds coated with MSCs, showed positive engraftment (74% of patients engrafted) from adult AML patients. Within 12 weeks, subcutaneously implanted scaffolds formed structures mimicking the human BM niche, including bone formation with embedded mouse vasculature. Interestingly, favourable-risk adult AML patients with inv(16) aberration, which usually do not engraft in the murine BM, were able to engraft in humanized scaffolds in NSG mice and colonized the host murine organs, including BM, spleen, and liver. More importantly, scaffolds allow maintenance of the clonal heterogeneity in injected cells recovered from primary transplants, and their LSCs self-renewal capacity was retained, as demonstrated by serial transplantation assays¹⁸¹. In a similar study using a different technical approach, Reinisch *et al.* demonstrated a comparable retention of sub-clonal architecture in AML patient samples¹³³. Finally, Battula *et al.* developed a different approach for studying human AML niche in mice, by the implant of human bone in mice. This approach used freshly collected human BM biopsies from patients and directly transplanted into NSG mice, using Matrigel as a carrier. The mouse-implanted human BM tissue underwent to vascularization and bone restoration, providing a functional human BM microenvironment capable of supporting the engraftment of human leukemia, a process that authors related to increased osteogenic activity in human bone implant¹⁸².

In summary, the evolution of strategies used over the years to develop pre-clinical *in vitro* and *in vivo* models to study normal and malignant human hematopoiesis aimed to answer a multitude of questions using various tissue engineering approaches (Table 9). Some of these studies have developed innovative protocols where carrier material scaffolds required various periods of *in vitro* culturing and pre-culturing prior to *in vivo* implantation¹⁸³, whereas others used *in vivo* models directly^{184,185}, with varying experimental time frames ranging from 12 weeks to 34 weeks¹³³. Another important aspect to note is the use of stromal cell types for generating the humanized niche; most studies used human mesenchymal cells, whereas others co-injected human ECs, or osteoblasts, or total human BM cells, thereby increasing the humanized nature of the implants^{182,184,186}. Lastly, the use of conditioning regimens in mice (such as irradiation) before the implantation of the cell-seeded biomaterial^{133,177,187} is somewhat controversial, as it may adversely affect the newly formed hematopoietic niche and regress the vasculatures that are derived from ECs. It is worth noting that each of these approaches have specific and sometimes unique scientific values, and all will undeniably play a significant role in various aspects of future pre-clinical studies.

Model	Advantages	Disadvantages
Spontaneous	No/minimal manipulation needed Whole-organism system available to study disease pathogenesis	Many not be accurate/translational to human disease condition Typically arises in older animals-time consuming and more costly
Xenograft (cell-line derived)	Relative simplicity High yield Rapid results Relatively inexpensive Multiple routes of administration Avoid immune rejection with immunocompromised strains Useful as first step investigation Useful as confirmatory for <i>in vitro</i> findings	Lack of organ/system microenvironment (except for orthotopic) Lack of immune system interaction with tumor cells Relative inability to test complex genomic interaction in a single-cell system Cell lines likely differ significantly from parental source (tumor)
Xenograft (patient-derived)	Relative simplicity High yield Rapid results Multiple routes of administration Avoid rejection with immunocompromised strain Useful as first step investigation More true representation of tumor cell biology than above Useful for investigation into efficacy of therapeutics on human tumor cells	Lack of organ/system microenvironment (except for orthotopic) Lack of immune system interaction with tumor cells Relative inability to test complex genomic interaction in a single-cell system
Humanized mice	Competent immune system to model tumor-immune interaction Can engraft cell lines, human tumor tissue, or genetically manipulated cells More true representation of tumor cell biology in a human-like system Useful for investigation of tumor pathobiology	Expensive Time consuming Generally need to establish breeding colony
Germline transgenic	Fidelity alteration of gene of interest Immunocompetent mice Useful for testing tumor development Useful for testing therapeutic approaches Useful for testing chemopreventative techniques	Transgene is universally expressed in every tissue Transgene is expressed throughout embryologic development Genetically not as complex as many human tumors
Conditional transgenic	Fidelity alteration of gene of interest Immunocompetent mice Targeted tissue-specific expression Targeted temporal expression Useful for testing tumor development Useful for testing therapeutic approaches Useful for testing chemopreventative techniques	Challenging technique Expensive Many mice will not carry desired genotype following crossing Genetically not as complex as many human tumors

Table 9. AML murine models advantages and disadvantages (modified from *Frontiers in Oncology* 2017, R. Koknken).

Aim of study

The overall aim of this research project was to discover and to re-assess alternative treatments to improve the portfolio of agents active in childhood AML for identify new drugs for children with AML, to finally reduce and improve outcome.

Most of the recently tested novel anti-leukemia agents have failed the pre-clinical and clinical validation phases, and one main limit in AML field is related to the inappropriateness of current pre-clinical models used to study drug efficacy, that do not consider the three-dimensionality of leukemia microenvironment and the role of this microenvironment in chemo-resistance. Indeed, the first aim of this project was to characterize one crucial component of leukemia niche: the mesenchymal stromal cells (MSCs) when derived from bone marrow of leukemia patient or healthy bone marrow to explore the mechanism trough which MSCs could induce leukemia initiation or sustain its progression. Then, to further deeper this issue I aimed to create an appropriate *in vitro* 3D model, to be then used also *in vivo*, to target AML in its physiological context with the aim to produce robust results on new drugs, new therapeutic combined strategies and predictable drug efficacy ranges in a robust 3D model that mimics the leukemia niche. This latter aim would improve pre-clinical data on AML novel drugs to be entered, in a near future, phase II and III clinical trials.

Materials and Methods

Patients' samples and healthy controls

In this study, bone marrow (BM) or peripheral blood samples of a total of 68 pediatric patients affected by *de novo* AML were provided by the pediatric OncoHematology Lab of the Padua Hospital, being the Associazione Italiana Emato Oncologia Pediatrica (AIEOP) reference center for the pediatric AML diagnosis. Diagnosis of leukemia was established according to standard criteria based on immune-histochemical staining, immune-phenotyping, cytogenetic studies and molecular genetics, as detailed in the AIEOP AML 2002/01 treatment protocol⁴. Samples were obtained at diagnosis (n=62) and/or at various time points during the course of treatment. For 5 patients, paired samples of MSCs at diagnosis and at complete remission (R-MSCs) were available. Patient's characteristics are reported in Table 1 and 2. MSCs derived from 9 healthy donors were used as control sample. Signed informed consent was obtained from all patients and donors, and the study was performed in accordance with the Declaration of Helsinki and approval by our local institutional review board.

Cell lines and primary cells cultures

The leukemic cell lines HL-60 (DMSZ- Germany) and ML-2 (DMSZ) were cultured in RPMI 1640 (Thermo Fisher Scientific, Waltham, MA, USA), while SHI-1 (DMSZ) were maintained in culture with DMEM (Thermo Fisher Scientific, Waltham, MA, USA). All the media were enriched with 10% FBS (Thermo Fisher Scientific), 2mM glutamine (Gibco, Life Technologies, CA, USA) and 100U/mL streptomycin/penicillin (Gibco, Life Technologies). Human Umbilical Vein Endothelial Cells (HUVEC, Lonza, USA) were cultured in M200 culture medium (Gibco, Life Technologies) supplemented with LSGS (Thermo Fischer Scientific) in flasks previously coated with Collagen type I (11,2 µg/mL, BD Biosciences, Franklin Lakes, NJ). Cells were sub-cultured using 0.05% trypsin (Biochrom GmbH, DE) and 0.02% EDTA solution.

Primary cells were cultured at 37°C in RPMI Medium 1640 supplemented with 10% FBS, 2mM glutamine (Gibco, Life Technologies) and 100U/mL streptomycin/penicillin (Gibco, Life Technologies), 50 ng/mL thrombopoietin (TPO), 50 ng/mL stem cell factor (SCF), 50 ng/mL FML-like tyrosine kinase 3 ligand (Flt3L), 20 ng/mL interleukin-3 (IL 3) and 20 ng/mL interleukin-6 (IL 6), all these cytokines purchased from Miltenyi Biotec (Miltenyi Biotec, Bergisch Gladbach, DE).

Isolation and culture of Mesenchymal Stromal Cells

MSCs from patients (AML-MSCs) and healthy donors (h-MSCs) were derived from BM mononuclear cells. Cells were counted and plated at 100.000 cells/cm² in StemMACS MSC Expansion Media (Miltenyi Biotec) supplemented with 100 U/mL penicillin/streptomycin (Gibco, Life Technologies) and 2mM glutamine (Gibco, Life Technologies), incubated at 37°C. After 1 day of culture, the non-adherent cells were removed and fresh medium was added to the adherent ones. The resulting adherent cells were expanded until 90% confluence and then re-plated and expanded in larger flasks. To re-seed MSC cells, they were trypsinized (Trypsin/EDTA Solution, Biochrom GmbH,) at 37°C for 5 min, harvested in medium with FBS to inactivate trypsin, centrifuged and plated at 5.000 cells/cm² in fresh medium. All experiments were carried out using MSCs derived from passage 2-5.

Patient ID	Genetic rearrangement /mutation	Age	Gender	MSCs	Patient ID	Genetic rearrangement /mutation	Age	Gender	MSCs
#1	Cbfb-MYH11	10	M	YES	#32	MLL-AF9	2	M	-
#2	-	7	M	YES	#33	-	16	M	YES
#3	MLL	1	F	YES	#34	-	12	M	YES
#4	NUP98-NSD1, FLT3-pif	4	M	YES	#35	-	2	F	YES
#5	NPM1 ^{MUT} , FLT3	5	F	YES	#36	NPM1 ^{MUT} , FLT3	8	M	YES
#6	MLL-AF10	13	F	YES	#37	DEK, NPM1 ^{MUT}	15	F	-
#7	FLT3-ITD	14	F	YES	#38	AML1-ETO	17	F	YES
#8	MLL-AF6	16	M	YES	#39	-	6	M	YES
#9	Cbfb-MYH11	2	M	YES	#40	Cbfb-MYH11	15	F	YES
#10	Cbfb-MYH11	9	M	-	#41	-	4	F	YES
#11	-	17	M	YES	#42	AML1-ETO	22	M	YES
#12	-	10	F	YES	#43	-	12	F	YES
#13	MLL-MLL (PTD), FLT3-I	13	F	YES	#44	Cbfb-MYH11	12	M	YES
#14	NUP98-NSD1	13	M	YES	#45	-	1	M	YES
#15	NUP98-NSD1, FLT3-ITD	17	M	YES	#46	-	13	M	YES
#16	Cbfb-MYH11	15	M	YES	#47	Cbfb-MYH11	4	M	-
#17	-	2	F	-	#48	Cbfb-MYH11, GLIS	1	F	YES
#18	-	2	F	-	#49	AML1-ETO, C-KIT ^{MUT}	5	F	YES
#19	-	10	M	YES	#50	Cbfb-MYH11, GLIS	1	F	YES
#20	-	13	M	YES	#51	MLL-AF4 mix	9	M	-
#21	MLL-AF10	7	M	-	#52	MLL-AF6	13	M	-
#22	AML1-ETO	9	F	YES	#53	-	7	F	YES
#23	-	10	M	YES	#54	DEK-KAN, FLT3	15	F	YES
#24	MLL-AF9	1	M	YES	#55	Cbfb-MYH11, C-KIT ^{MUT}	1	F	YES
#25	-	15	F	YES	#56	-	17	F	YES
#26	NPM1 ^{MUT} , FLT3	13	M	-	#57	MLL-AF10	14	F	YES
#27	-	17	M	YES	#58	AML1-ETO	7	M	YES
#28	-	1	F	YES	#59	Cbfb-MYH11	18	M	YES
#29	AML1-ETO	7	F	YES	#60	-	15	M	YES
#30	FLT3	18	M	YES	#61	-	3	M	YES
#31	-	4	M	-	#62	-	2	F	YES

Table 1. Main characteristics of the patients with AML used to derived blasts and MSCs. Legend: -, negative, no mutation found by the current screening¹⁸⁸⁻¹⁹⁰, Age in years; M, Male; F, Female.

Patient ID	genetic rearrangement /mutation	Age	Gender	Time between onset and remission	HSCT
R-MSCs#1	Cbfb-MYH11	10	M	595	
R-MSCs#4	NUP98-NSD1, FLT3	4	M	558	YES*
R-MSCs#44	Cbfb-MYH11	12	M	103	
R-MSCs#45	-	1	M	124	
R-MSCs#54	DEK-KAN, FLT3	15	F	89	YES
R-MSCs#63	-	16	F	142	
R-MSCs#64	-	11	M	35	
R-MSCs#65	-	15	F	176	
R-MSCs#66	NUP98-NSD1, FLT3-ITD	15	F	932	YES*
R-MSCs#67	NPM1 ^{MUT}	16	F	1254	
R-MSCs#68	NPM1 ^{MUT}	10	F	511	

Table 2. Molecular characteristics of 11 MSCs derived from AML patients after treatment in complete remission (R-MSCs). -, negative, no mutation found by the current screening; Age in years; M, Male; F, Female; Time between onset and remission in days; HSCT, hematopoietic stem cell transplantation; *R-MSCs#4 HSCT at day 119, *R-MSCs#66 HSCT at day 754.

Flow cytometry

For the detection of the surface markers, the following conjugated antibodies were used: Phycoerythrin (PE)-conjugated human CD73 (Invitrogen, Carlsbad, CA), Fluorescein Isothiocyanate (FITC)-conjugated human CD105 (BD Biosciences, USA), Phycoerythrin-Texas Red (ECD)-conjugated human CD45 (Beckman Coulter, Brea, CA), PE-conjugated human CD11b (Beckman Coulter), Phycoerythrin-Cyanin7 (PC7)-conjugated human CD34 (8G12, BD Biosciences), Phycoerythrin Cyanin5 (PC5)-conjugated human CD38 (BD Biosciences), Allophycocyanin (APC)-conjugated human CD33 (BD Biosciences), PC7-conjugated human HLADR (BD Biosciences), PE-conjugated human CD56 (Beckman Coulter), PC5-conjugated human CD7 (Beckman Coulter, CA, USA), PE-conjugated human CD41 (BioLegend, CA, USA), APC-conjugated human CD42 (Invitrogen). Briefly, cells were stained with the conjugated primary antibody for 30', rinsed in PBS1x and then fluorescence was detected with Cytometer FC 500 Instrument (Beckman Coulter) or CytoFLEX (Beckman Coulter) or FACSCanto (BD Biosciences). Overlay histograms were set up with Cytobank platform. Data are presented as fold change of Median Fluorescence Intensity (MFI) of positive-cells respect to the relative isotypic control, in the live-gated cell population.

For intracellular staining, cells were fixed in 4% formaldehyde for 10', washed in PBS1x, permeabilized in 0.1% Tween20 for 20', washed in PBS1x, blocked with 3% bovine serum albumin (BSA) for 30', incubated with 1:500 primary anti-human CaV1.2 (CACNA1C) antibody (Alomone labs, Jerusalem, Israel) in 3% BSA + 20% FcR Blocking Reagent for 30', washed in PBS1x, incubated with 1:500 Alexa Fluor 488 Goat Anti-Rabbit (IgG) secondary antibody (ThermoFisher) for 30', washed in PBS 1x and finally analyzed with Cytometer FC 500 Instrument (Beckman Coulter).

MSCs differentiation potential

The second criteria for assessing cells to be MSCs was the *tri-lineage* differentiation capacity, which was assessed using hMSC differentiation BulletKit™ (Lonza, Basel, CH) following the manufacturer's instructions, at cell passage 3. Briefly, for adipocytic differentiation, cells were seeded in adipogenic differentiation media (hMSC differentiation BulletKit™ adipogenic, Lonza). Differentiated adipocytes were detected with oil Red stain (Sigma-Aldrich-Meck S.r.l., Milan, IT) after 21 days. All images were captured using an inverted microscopy (Zeiss Axio Imager M1 epifluorescence microscope, Zeiss, Oberkochen, Germany) using a 10x objective. For osteoblastic differentiation of AML-MSCs and h-MSCs, cells were seeded in osteogenic differentiation media (hMSC differentiation BulletKit™ osteogenic, Lonza). Differentiated osteoblasts were detected with Alizarin Red S stain (Sigma-Aldrich-Meck). To have a quantitative measure of the osteogenic differentiation levels, Alizarin Red was quantified as previously described¹⁹¹: briefly, the absorbance of the differentiation media collected from the samples on days 7, 14, and 21 was read at 405 nm using VICTOR3™ multilabel plate reader (1420, Perkin Elmer, Milan, IT). Condrogenic differentiation was performed following the manufacturer's instructions using hMSC differentiation BulletKit™ condrogenic media (Lonza).

Cell viability assay

Cell viability of MSCs or AML cells was evaluated using CellTiter-Glo® assay (Promega Corporation, Fitchburg, WI) following the manufacturer's guidelines. Briefly, 5×10^3 cells in 100 μ L of proper medium were cultured in sterile 96-well plates and incubated at 37°C. Cell viability-ATP production was evaluated at the indicated time points by adding 100 μ L CellTiter-Glo® reagent, incubating for 20' at room temperature (RT) and recording the luminescence with the VICTOR3™ multilabel plate reader (Perikin Elmer).

RNA isolation and quantitative real-time PCR

Total RNA was isolated using Trizol (Invitrogen). One microgram of RNA was reverse-transcribed into cDNA using the SuperScript II system (Invitrogen) according to the manufacturer's instructions. Expression of mRNA were measured by Real Time PCR (RQ-PCR) on an ABI 7900HD platform (Applied Biosystems, Foster City, CA) using the Syber Green PCR master mix (Applied Biosystems) and normalized on *GUS* housekeeping gene using the $2^{-\Delta\Delta C_t}$ method. See Table 3 for primer sequence.

Gene	Forward	Reverse
<i>OPN</i>	TTGCAGCCTTCTCAGCCAA	GGAGGCAAAAGCAAATCACTG
<i>TNAP</i>	CCTCCTCGGAAGACACTCTG	GCAGTGAAGGGCTTCTTGTC
<i>CaV1.2</i>	GGTCCATGGTCAATGAGAATACG	GGCTCCCATAGTTGGAACCTT
<i>CD45</i>	GGAAGTGCTGCAATGTGTCA	CCAGCTTCAACTTCCAAATGGTA
<i>GUS</i>	GAAAATATGTGGTTGGAGAGCTCATT	CCGAGTGAAGATCCCCTTTTTA

Table 3. Primer list for Real Time PCR.

Gene expression analysis of MSCs

We analyzed RNA collected from 6 h-MSCs, 15 AML-MSCs and 6 R-MSCs. Briefly, RNA quality was assessed on an Agilent2100 Bioanalyzer (Agilent Technologies, Santa Clara, CA, USA), and 100 ng of total RNA were labeled and hybridized to GeneChip™ Human Genome U133 Plus 2.0 Array (Affymetrix, Santa Clara, CA, USA) for 16 h at 45°C using a rotational oven and washed according to Affymetrix standard protocols using a GC450 Fluidics Station (Santa Clara, CA, USA). The Genechips were scanned with an Affymetrix 7G scanner and the CEL files generated were analyzed through Affymetrix Expression Console Software (version 1.3) which normalizes array signals using a robust multi-array averaging (RMA) algorithm. Probes were re-annotated using GENECODE v.19 gene annotation database⁵⁵ (www.genecodegenes.org). Transcripts were included if at least the 95% of nucleotides overlapped with probes. Unsupervised analysis was performed using probes set with 90% of variants variability and clustering was performed using Euclidean distance and Wards method.

For gene functional enrichment analysis Gene Ontology Metascape analysis was performed and were identified differentially expressed genes, considering a fold change of 2.5 ($p < 0.05$).

Isolation of CD34⁺ cells

Mononuclear cells (MNCs) were isolated from cord blood samples by density centrifugation using the lymphocyte separation medium Lymphoprep (Nycomed Pharma, Oslo, Norway). CD34⁺ cells

were positively selected from MNCs by immune-magnetic cell separation (Miltenyi Biotec) using CD34 MicroBead Kit (Miltenyi Biotec) and following the manufacturer's instructions.

MSCs-CD34⁺ co-culture

h-MSCs or AML-MSCs were plated at a density of 5.0×10^3 cell/cm² in StemMACSTM MSC Expansion Media (Miltenyi Biotec). 24 h later, MSC media was removed and healthy CD34⁺ cells were seeded onto MSCs at a density of 2.1×10^4 cell/cm² in hematopoietic media (Methocult H5100, StemCell Technologies, Vancouver, CA) in the presence of a cytokines mixture (100ng/mL human SCF; 100ng/mL human Flt3L; 20 ng/mL human IL 3, IL 6, and G-CSF; Miltenyi Biotec) and cultured for up to 10 days. After 5 and 10 days of co-culture, CD34⁺ cells were harvested and human CD45 and CD34 were evaluated by flow cytometry.

MSCs-32D co-culture

h-MSCs or AML-MSCs were plated at a density of 5.0×10^3 cell/cm² in StemMACSTM MSC Expansion Media (Miltenyi Biotec). 24 h later, MSC media was removed and murine IL-3 dependent 32D cells were seeded onto MSCs at a density of 1×10^5 cell/cm² in RPMI 1640 Medium (Gibco, Thermo Fisher Scientific) supplemented with 1mM Sodium Pyruvate, 4,5 g/L of D-glucose, in presence or absence of 10 ng/mL of mouse interleukin-3 (IL 3) (Miltenyi Biotec). Cell density was determined by trypan blue exclusion.

Collection of conditioned medium (CM) of MSCs

h-MSCs or AML-MSCs were plated in StemMACSTM MSC Expansion Media (Miltenyi Biotec), with 2 mM glutamine (Gibco, Life Technologies), and 100 U/mL penicillin/streptomycin (Gibco, Life Technologies) and until confluence in a humidified incubator at 37°C. When MSCs reached confluence, medium was substituted with MEM Alpha (Gibco, Life Technologies) supplemented with 2% FBS, 2 mM glutamine, 100 U/mL penicillin/streptomycin, with (namely stimulated, st) or without (namely unstimulated, unst) a cocktail of pro-inflammatory cytokines composed by 25 ng/mL hIL 1b, 20 ng/mL hIL 6 and 25 ng/mL hTNF α . 24 h later, the medium was removed, cells were washed three times with MEM Alpha (1x) (Gibco, Life Technologies) and medium was replaced with MEM Alpha (1x) (Gibco, Life Technologies) containing 2 mM glutamine (Gibco, Life Technologies) and 100 U/mL penicillin/streptomycin (Gibco, Life Technologies) for the following 18 hours. We collected medium centrifuged at 4.000 rpm for 10' (to discard residual cells), and used to culture HUVEC cell line in Tube Formation Assay.

HUVEC Tube Formation Assay

Matrigel[®] Matrix (Corning B.V.) was thawed overnight at 4°C. The day of the assay, 100 µL of Matrigel were seeded in the 96-well plate and left to polymerize at 37°C for at least 30 min. Then, 2x10⁴ HUVEC were resuspended in 100 µL of h-MSCs-CM or AML-MSCs-CM (conditioned medium with inflammatory cytokines, see above section), supplemented with 10% FBS (Thermo Fisher Scientific), and then seeded on the solidified matrix. The formation of the tube networks was evaluated after 4 h of incubation at 37°C and compared with HUVEC seeded in a standard medium of MEM alpha (1x) (Gibco, Life Technologies) supplemented with 10% FBS (Thermo Fisher Scientific) used as control. At the end of incubation, cell tubes were imaged with a phase contrast inverted microscope at 4x objective magnifications and analysis was performed with ImageJ Angiogenesis Analyzer.

iPSCs Culture

CTRL iPSCs and iPSCs with CBFA2T3-GLIS2 knock-in were kindly donated from lab of “Oncologia ed Ematologia Pediatrica Lalla Seràgnoli” of the “Azienda ospedaliera-Universitaria di Bologna” (Prof. Andrea Pession, Italy). iPSCs were cultured in Essential 8 medium (ThermoFisher) and in vitronectin (Thermofisher) coated wells. iPSCs were passed every 3 days in DPBS/0.5mM EDTA Ultrapure (Thermofisher).

Differentiation of iPSCs into hematological lineage

h-MSCs or AML-MSCs were plated in StemMACS[™] MSC Expansion Media (Miltenyi Biotec), with 2 mM glutamine (Gibco, Life Technologies), and 100 U/mL penicillin/streptomycin (Gibco, Life Technologies) and let grow until confluence in a humidified incubator at 37°C. When MSCs reached confluence, iPSCs CBFA2T3-GLIS2 and iPSCs CTRL were induced to differentiate into hematological *lineage*¹⁹². Briefly 4-5 colonies from each iPSCs after being cultured for 4 days were picked and put into MSCs previously coated wells and let co-culturing in Essential 8 medium. After 1 day, in order to induce iPSCs differentiation, the medium changed in StemPro34 (Thermofisher) enriched with 100U/mL penicillin/streptomycin (Gibco, Life Technologies), 2 mM glutamine (Gibco, Life Technologies), ascorbic acid (50 µg/mL, Sigma-Aldrich-Meck) monothioglycerol (MTG, 15 mM, Sigma-Aldrich-Meck), BMP2 (5 ng/mL, Peprotech, NJ, USA) and VEGF (50 ng/mL, Miltenyi Biotec) and CHIR (930 ng/mL, Sigma-Aldrich-Meck) for the first 2 days. Then, until day 18 the medium was replenished and supplemented with a sequential cytokine cocktail, as shown in Table 4. Hematopoietic differentiation of iPSCs was then assessed at day 18 using flow

cytometry analyses for testing the differentiation at the megakaryocytic stage (by using CD41 and CD42).

	BMP4	CHIR	VEGF	bFGF	SCF	Flt3L	TPO	IL6
<i>Day 0</i>	5ng/mL	930ng/mL	50ng/mL					
<i>Day 1</i>	5ng/mL		50ng/mL	20ng/mL				
<i>Day 4</i>			15ng/mL	5ng/mL				
<i>Day 6</i>			50ng/mL	50ng/mL	50ng/mL	5ng/mL		
<i>Day 7</i>			50ng/mL	50ng/mL	50ng/mL	5ng/mL	50ng/mL	10ng/mL
<i>Day 8</i>			50ng/mL	50ng/mL	50ng/mL	5ng/mL	50ng/mL	10ng/mL
<i>Day 11</i>			50ng/mL	50ng/mL	50ng/mL	5ng/mL	50ng/mL	10ng/mL
<i>Day 13</i>			50ng/mL	50ng/mL	50ng/mL	5ng/mL	50ng/mL	10ng/mL
<i>Day 15</i>			50ng/mL	50ng/mL	50ng/mL	5ng/mL	50ng/mL	10ng/mL
<i>Day 18</i>			50ng/mL	50ng/mL	50ng/mL	5ng/mL	50ng/mL	10ng/mL

Table 4. iPSCs hematopoietic differentiation protocol.

High-throughput Screening (HTS) pipeline and cell treatment

For HTS, 480 pharmacologically active compounds of the LOPAC Library (Sigma-Aldrich-Meck) were screened in triplicate on AML-MSCs using a 10 μ M concentration. Cell seeding and drug treatment were performed through an Automated Pipetting Workstation (epMotion 5070, Eppendorf, Hamburg, Germany) to standardize the method. Briefly, AML-MSCs were seeded at 18,000 cells/cm² in StemMACSTM MSC Expansion Media (Miltenyi Biotec) and allowed to attach overnight in flat-bottom white-opaque 96-well plates (Corning®, Sigma-Aldrich-Meck). Then, compounds were added to medium at the final concentration of 10 μ M in a final volume of 100 μ L *per* well. Treatment with 0.5% DMSO (v/v) were considered the negative control. Cell viability were measured after 48 h of incubation (in a humidified incubator at 37°C) using CellTiter-Glo[®] reagent (Promega) according to the manufacturer's instructions. The luminescence from each well was captured using VICTOR3TM Multilabel plate reader (1420, Perkin Elmer) and normalized to negative control. The compounds were classified as active when cell viability resulted \leq 50% compared to negative control. The compounds resulted active were further screened on h-MSCs and then on AML cells lines, and those which decreased cell viability for less than 50% were considered specific and selective on AML-MSCs. Hit compounds, Lercanidipine-HCl and I-BET151 were sourced from Sigma-Aldrich-Meck, and Quizartinib from Selleckchem (Houston, TX, USA). For *in vivo* treatment, 5-Azacytidine and Thioridazine-HCl were sourced from Sigma-Aldrich-Merck. In

co-treatment experiments synergy scores were calculated as reported by Slinker ($CI = E_A + E_B / E_{AB}$, where E_{AB} represent the observed combination effect)¹⁹³.

Apoptosis analysis

Apoptosis was evaluated by double staining with Annexin-V/propidium iodide (Roche Biochemicals, Indianapolis, IN) and analyzed using Cytometer FC500 (Beckman Coulter). Increased apoptosis was calculated and expressed as the percentage of Annexin-V-positive and propidium iodide-positive cells compared to those exposed to DMSO.

Measurements of intracellular Ca^{2+}

The MSCs were plated on chamber slides and treated with 10 μ M of Lercanidipine-HCl for 48 hours. Then, intracellular Ca^{2+} levels were monitored by Fluo-4 AM (Thermo Fisher Scientific) fluorescence according to the manufacturer's instructions. Briefly, cells were washed in Hanks Balanced Salt Solutions, incubated with Fluo-4 AM 3 μ M diluted in the working buffer (0.02% w/v Pluronic and 0.2 mM sulfinpyrazone, both sourced from Sigma-Aldrich-Meck-Merck, in 10 mM HEPES-buffered Hanks) for 20' at RT. After incubation, cells were rinsed twice and incubated in working buffer for 30', to allow the de-esterification of Fluo-4 AM. Intracellular Ca^{2+} levels were then determined before and during the exogenous administration of Ca^{2+} ($CaCl_2$ solution 1 mM) by using a custom-built two-photon laser-scanning microscope (Thorlabs, Newton, NJ, USA) at an excitation wavelength of 488 nm and an emission wavelength of 525 nm. Data are presented as the relative change in fluorescence ($\Delta F/F$).

3D culture system set-up

Our 3D model consisted of a scaffold composed by 70% hydroxyapatite/30% collagen type I with 2% 1,4-butanediol diglycidyl ether (BDDGE), of 2 mm in height and diameter, which was produced by 'Istituto di Scienza e Tecnologia dei Materiali Ceramici' (ISTEC) of the 'Consiglio Nazionale delle Ricerche' (CNR) (Prof. A Tampieri, Faenza, Italy).

We used different 3D-culture conditions as following: i) with h-MSCs; ii) with AML-MSCs; iii) with AML-MSCs+OBs (osteoblasts differentiated from AML-MSCs for 7 days in ratio 2:1); iv) with AML-MSCs+HUVEC cells line (ratio 1:1). Briefly, scaffold were soaked in DMEM medium overnight prior to cell seeding. Then, medium was removed and 2×10^5 MSCs (or AML-MSCs+OBs or AML-MSCs+HUVEC for the condition iii and iv, respectively) resuspended in 10 μ L of StemMACS medium were slowly put on the upper surface of the scaffolds. Seeded scaffolds were

then incubated for 4 hours at 37°C, in order to facilitate cell penetration, prior to gently add 1 mL of StemMACS to each well. The scaffolds seeded with stromal cells were incubated for 7 days at 37°C. Then, the medium was removed and 4×10^5 AML primary cells in 10 μ L of proper medium (see “Cell lines and primary cells cultures”), were slowly pipetted on the upper surface of the MSCs coated-scaffold. Seeded scaffolds were then incubated for 15’ at 37°C, prior to gently add 1 mL of primary cells medium to each well. During the experiment, the medium was changed once a week up to 21 days. At the indicated time points, AML cells were extracted from the scaffold by pipetting and subjected to further indicated experiments.

3D cell viability assay

Cell viability were measured using CellTiter-Glo[®] 3D reagent (Promega) according to the manufacturer’s instructions. Briefly, scaffolds were individually transferred into wells of flat-bottom white-opaque 96-well plates (Corning®, Sigma-Aldrich-Meck) with 100 μ L of RPMI, then 100 μ L of CellTiter-Glo[®] 3D reagent were added into each well. Plates were shaken for 5’ to induce scaffold and cells lysis. Samples were then incubated for additional 20’ in the dark, at RT, to stabilize the bioluminescent signal, which was then recorded using VICTOR3[™] Multilabel plate reader (1420, Perkin Elmer). For the drug treatments in 3D, cell viability was compared to the control sample (scaffold treated with DMSO).

Colony-forming unit (CFU) assay

At the indicated time points, 2×10^3 primary AML cells harvested from 3D scaffolds were seeded into 500 μ L of MethoCult[™] (H4534, Stemcell Technologies, Meda MB, Italy), in 24-well plates and incubated at 37°C. After 4 weeks of culture, an adequate volume of a 1:6 solution of 3-[4,5-dimethylthiazol-2-yl]-2,5-diphenyltetrazolium bromide (MTT, Sigma-Aldrich-Meck) in Hanks’ was added to semisolid medium. Images were acquired by optical microscope with camera, and colonies were counted.

Immunohistochemistry

Harvested scaffolds were fixed overnight in Paraformaldehyde 4% in PBS1x. Fixed samples were then paraffin embedded and sectioned (6 μ m of thickness) for histological studies. Slides were incubated with human CD45 (Dako-Agilent Technologies) overnight, and then developed with the DAKO Envision Detection Kit (Dako-Agilent Technologies). Hematoxylin/eosin was performed to confirm the quality of the section.

Scanning Electron Microscope (SEM)

SEM was performed on the scaffold after 7 days of culture, at the ISTECCNR (Faenza, Italy). Briefly, the scaffolds were carefully washed with 0.1 M sodium cacodylate buffer pH 7.4, fixed in 2.5% glutaraldehyde (Sigma-Aldrich-Meck) in 0.1 M sodium cacodylate buffer pH 7.4 for 2 h at 4°C, washed in 0.1 M sodium cacodylate buffer pH 7.4 and dehydrated by freeze-drying. Dehydrated samples were sputter-coated with gold and observed using Stereoscan 360 SEM (Cambridge Instruments, UK).

Stable Isotope Labeling with Amino Acids in Cell Culture (SILAC)

MSCs were seeded in 3D model as previously described. After 7 days of culture, AML primary cells were added, in a RPMI cell culture media deficient in arginine and lysine (Gibco- Thermo Fisher Scientific) supplemented with dialyzed serum (Life Technologies-Thermo Fisher Scientific), 1,14 mM L-arginine-13C6 and 0,38 mM L-lysine-13C615N2 (Cambridge Isotope Laboratories Tewksbury, MA, USA) and appropriate cytokines as previously described (see 'Cell lines and primary cells cultures'). After 7 days of incubation, culture medium was carefully collected, floating cells and cellular debris were removed by centrifugation (4.500 rpm, 10 min) and medium subjected to Mass Spectrometry.

Mass Spectrometry: sample preparation

1.8 mL of 2% Trichloroacetic acid in isopropanol (W/V) was added to 0.18 mL of conditioned media to obtain proteins precipitation and the sample was incubated for 10 minute at room temperature before centrifugation (14.000 rpm, 5 min). Supernatant was removed and the protein pellet was then washed twice with 0.2 mL of MeOH and dried under vacuum. Before digestion, the pellet was resuspended in 50 mM of ammonium bicarbonate (pH~8) and protein amount was quantified by BCA assay. Sample was reduced by adding 100 mM dithiothreitol (DTT) at 60°C for 45', and alkylated by adding 100mM iodoacetamide (IAA) at RT for 30 min, in the dark. Overnight digestion was performed by adding MS sequencing grade trypsin in a 1:80 (trypsin:protein) ratio. The reaction was stopped by adding a 10% trifluoroacetic acid (TFA) solution. Digested proteins were finally dried under vacuum until analysis.

Mass Spectrometry: sample analysis

Digested samples have been resuspended in 40 µL of CH₃CN + 0.1% TFA before injection. An Ultimate 3000 HPLC system coupled to a Q Exactive (ThermoFisher) mass spectrometer was employed. The peptide mixtures were separated with a Biobasic C18 column, 5µm, using a 3-

45% linear gradient of CH₃CN + 0.1% TFA (mobile phase B) in H₂O + 0.1% TFA (mobile phase A) over at 110 min of analysis. Mass spec data have been acquired in data-dependent mode in the 300-1500 m/z mass range. Instrumental parameters were set as follow: source: ESI (+); precursor charge selection: from 2 to 5; precursor resolution: 10.000; fragments resolution: 60.000.

Mass Spectrometry: protein identification and quantization

LC-MS/MS data have been processed by Proteome Discoverer 2.2 (ThermoFisher) using the Sequest HT algorithm for proteins identification. Search parameters were set as follow: database, SwissProt; enzyme, Trypsin (max 2 missed cleavages); taxonomy, *homo sapiens*, *bos taururs* or *equus caballus*, when appropriate; precursor mass tolerance, 10 ppm, fragment mass tolerance, 0.02 Da. Fixed modifications: carbamidomethyl (C); label 13C6 (R), and label 13C615N2 (K). Dynamic modifications: oxidation (M, P); deamidation (N, Q), and phosphorylation (S, T, Y). An acceptable proteins false discovery rate (FDR) was set <0.01 and proteins were identified with 1 or 2 non-redundant peptides.

Luciferase transduction

For luciferase (LUC) transduction, the vial with the lentiviral particles (RediFect Red-FLuc-GFP, Perkin Elmer) was thawed and added to the SHI-1 cell line or primary AML cells previously seeded in a 24-well plate (multiplicity of infection, MOI= 30). The plate was incubated at 37°C for 24 hours and then cells were washed several times. After verification of GFP expression by flow cytometry (FC 500, Beckman Coulter), transduced cells were seeded on the MSCs-pre-seeded scaffolds, as previously reported (see '3D culture system set-up').

3D-AML *in vivo* model

All *in vivo* experimental procedures were performed in accordance with the Institutional Animal Care and Use Committee and with international laws (authorization n. 622/2017PR).

Primary AML samples were depleted of CD3⁺ T cells by immune-magnetic cell separation (Miltenyi Biotec) using CD3 MicroBead Kit (Miltenyi Biotec), to avoid the graft-versus host disease (GVHD). The scaffolds were seeded *in vitro* with 0,2x10⁶ AML-MSCs and after 24 hours with 1x10⁶ CD3-depleted primary AML cells. After 24 hours, 3D models (scaffold with AML-MSCs and primary AML cells) were implanted in a subcutaneous pocket in the back of mice (two 3D models *per* mouse). To monitor engraftment, peripheral blood samples were collected every two weeks to evaluate human CD45 expression by flow cytometry, otherwise, when using LUC-

transduced primary AML cells, *in vivo* luminescence activity of 3D implanted scaffold was measured after intra-peritoneal (i.p.) injection of XenoLight D-luciferin firefly (15mg/mL in PBS; Perkin Elmer, Waltham, MA) 10' before measurement by Xenogen IVIS Lumina II bioluminescence/optical imaging system (Xenogen Corporation, Alameda, CA). At the experimental end point, mice were sacrificed and scaffolds were explanted for histological and genetic analysis.

***In vivo* treatment of 3D-AML models**

For drug treatment, mice implanted with 3D scaffold containing AML-MSCs and LUC-transduced primary AML cells were randomized in 6 groups (n=3 *per* group) when LUC activity reached 10^5 total flux. Mice were treated daily with Venetoclax 100 mg/Kg (oral gavage, p.o.), AraC 50 mg/Kg (i.p.), 5-AZA 5 mg/Kg (i.p.), Thioridazine 8 mg/Kg (i.p.) I-BET151 30 mg/Kg (i.p.) or vehicle (ctrl, treated with DMSO) for 22 days, with washout during the weekend. Experimental end point was reached when total flux of ctrl group was 10^9 .

Data analysis

Statistical analysis was performed using Prism 6 (Graph Pad Software Inc., La Jolla, CA, USA) with details given in the respective figure legend. Experiments were performed in duplicate or triplicate, and results were presented as mean \pm standard error of the mean (s.e.m). Statistical significance of difference between two groups was evaluated by the unpaired Student's *t*-test, whereas one-way ANOVA was used for multiple comparisons. Differences were considered to be statistically significant at *p*-value of <0.05 (*), <0.01 (**), <0.001 (***), and <0.0001 (****).

Results

MSCs characterization AML-MSCs vs. h-MSCs

To investigate the characteristics of the leukemia BM microenvironment, we isolated MSCs from 62 BM sample derived from patients affected by *de novo* AML at diagnosis (AML-MSCs; see Table 1 in “Material and Methods” section for main biological and molecular features of the AML cases). We characterized these MSCs for morphology, immune-phenotype, cell proliferation, cell differentiation potential, anti-inflammatory/angiogenic ability, their role in co-cultures with healthy hematopoietic or leukemic cells to explore a potential transforming activity, as well as for gene expression profile (GEP). All these tests have been performed also in MSCs derived from BM of healthy donors (h-MSCs, n=9) in order to compare and study similarities and differences.

AML-MSCs display the same morphology and immunophenotype of h-MSCs

To characterize human MSCs specifically derived from AML, we first analyzed morphology and immuno-phenotype. Morphologically, AML-MSCs are polygonal or irregular shaped, as h-MSCs. These cells were cultured until the fifth passage, and characterized, according to the Internal Society for Cellular Therapy (ISTC), for their expression of typical mesenchymal stromal cell surface antigens, such as the CD73 and CD105, as well as for the absence of CD45 and CD11b, both typical hematopoietic cell markers. This flow-cytometry screening of AML-MSCs and h-MSCs revealed that CD73 and CD105 were expressed on both cell types at equal intensity. Neither CD45 nor CD11b was expressed on either AML-MSCs or h-MSCs (Figure 1A). Finally, AML-MSCs were confirmed to correctly differentiate into osteoblasts, adipocytes and chondrocytes *in vitro* at the same potential of the h-MSCs (Figure 1B).

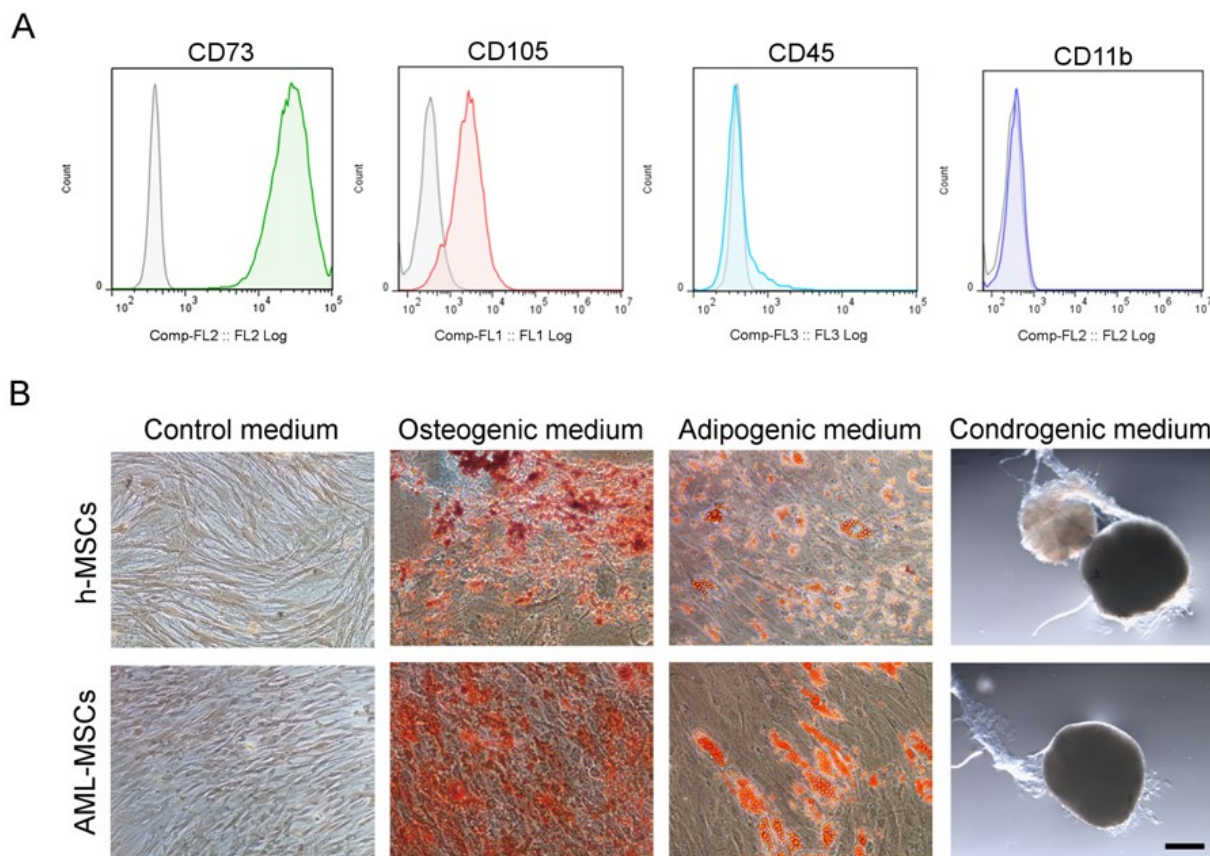


Figure 1. Phenotype and differentiation potential of AML-MSCs. (A) Representative histograms of CD73, CD105, CD45, and CD11b expression determined on AML-MSCs by flow cytometric analysis (grey line for the isotype control). (B) Three-lineage differentiation of h-MSCs and AML-MSCs at day 21 of culture. Control medium represents non-induced differentiated cells. Alizarin Red and Oil Red staining confirmed differentiation after 21 days of culture with a proper induction medium, while the formation and analysis of pellet confirmed chondrogenic differentiation of MSCs after 21 days. Representative micrographs of MSCs derived from healthy donors and AML patients at 10x magnification, scale bar = 200 μ m for control, osteogenic, and adipogenic medium; 5x magnification, scale bar = 100 μ m for chondrogenic medium.

AML-MSCs increase growth kinetics and osteogenic differentiation potential

To verify whether the MSCs culture from AML patients presented changes in their proliferative potential, we performed ATP proliferation assay every 24 hours until 96 hours of culture. Growth rate analysis of MSCs showed a statistically significant difference in cell growth between h-MSCs and AML-MSCs; particularly, AML-MSCs grew 1.5-fold more than h-MSCs at 72 and 96 h of culture (Figure 2), indicating that the increased proliferation kinetics of AML-MSCs could derive from the leukemia bone marrow niche microenvironment.

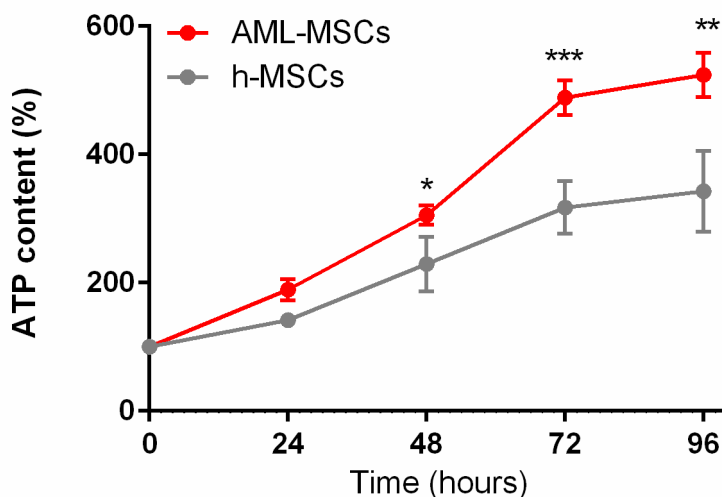


Figure 2. MSCs proliferation. Samples in triplicate have been used, error bars indicate s.e.m. Unpaired Student's *t*-test was used to detect statistically significant differences between h-MSCs (n=5) and AML-MSCs (n=11). *p*-values **p*<0.05, ***p*<0.01, ****p*<0.001.

In addition to alter proliferation, several works have reported that AML-MSCs had an increased¹⁸² or reduced⁷⁹ ability to differentiate into functional osteoblasts; this latter finding was reported in adult AML, but the role exerted by the AML blasts in mediating differentiation alteration potential of the MSCs is still unknown. We looked at the mRNA expression of some genes associated with osteogenic differentiation, including transcription factors *OPN* and the extracellular matrix-associated gene *TNAP*, confirming that these genes were up-regulated by 3.47- and 2.2-fold, respectively, in AML-MSCs with respect to h-MSCs (Figure 3A). Next, we extended our findings inducing osteogenic cell differentiation by culturing MSCs in an appropriate medium and revealed the osteogenic AML-MSCs and h-MSCs differentiation from day 7 to 21 of *in vitro* culture by Alizarin Red S staining. AML-MSCs on day 0 (before inducing osteogenic differentiation) were not positive for the staining, suggesting that these cells are osteo-progenitors not mature osteoblasts. Next, when exposed to osteogenic differentiation medium, we observed that AML-MSCs differentiated faster with respect to h-MSCs; particularly, AML-MSCs released calcium earlier than h-MSCs, between day 7 and 14 (Figure 3B), whereas for h-MSCs mineral calcium deposition were detectable only at the end point of differentiation process (day 21), as expected (Figure 3B). Trying to measure the Alizarin Red S staining by comparative quantification of absorbance (at 405 nm) we confirmed h-MSCs with a lower level of absorbance than of AML-MSCs at 21 days (*p*=ns, data not shown), sustaining that AML-MSCs are primed to differentiate into the osteogenic *lineage*.

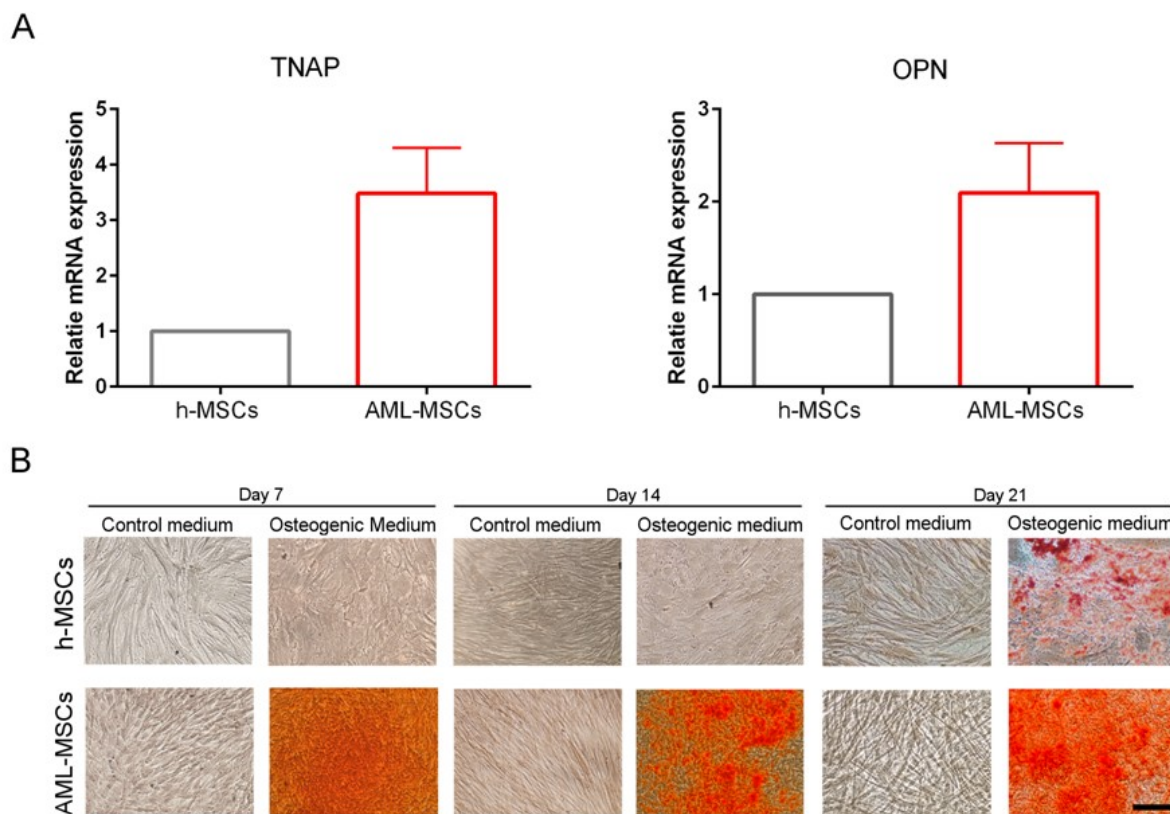


Figure 3. Osteogenic differentiation of AML-MSCs. (A) mRNA expression of osteoprogenitor-associated genes, *TNAP* and *OPN*, in h-MSCs (n=5, RQ=1 in the graph used as calibrator) and AML-MSCs (n=17) was measured by qRT-PCR. Histograms represent means + s.e.m. *GUS* served as equal loading control. (B) Representative Alizarin Red S staining in h-MSCs (n=3) and AML-MSCs (n=7) cultured without (Control medium) or with osteogenic differentiation medium for 21 days. At day 7, 14, and 21 cells were incubated with Alizarin Red S stain and images acquired (10x magnification, scale bar = 200 μ m).

AML-MSCs exert an aberrant anti-inflammatory potential

Concerning MSCs functions, it was reported that h-MSCs exerted immunomodulatory and anti-inflammatory properties on the microenvironment by the release of secreted proteins and factors to reduce angiogenesis, and maintain an anti-inflammatory niche to prevent tumor progression¹⁹⁴. On the other hand, several evidences demonstrated the involvement of the tumor niche in liquid tumors, such as AML, where an increased microvascular density and production of pro-angiogenic factors often was found to induce an inflammatory microenvironment^{195–197}. Furthermore, recent findings suggested a potential contribution of the non-hematopoietic niche cells, such as the MSCs, in the tumor angiogenesis¹⁹⁸. However, to date, the *in vitro* anti-inflammatory proprieties of MSCs from patients suffering from hematological malignancies remain unknown. Thus, we took advantage of an *in vitro* test that measure the ability of endothelial cells (HUVEC) to form three-dimensional

structures (tube formation) on collagen coated dish to measure a quick assessment of angiogenesis and explore if healthy and AML-MSCs exerted different anti-inflammatory properties. Briefly, MSCs were first expanded as an adherent monolayer until confluence, and were then stimulated for 24 h in the presence of IL 1 β , IL 6 and TNF- α to resemble the inflammatory milieu that MSCs find *in vivo*. MSCs supernatant was collected as conditional medium (CM) 18 h after cytokines withdrawal and used to culture HUVEC and study their proliferation. We confirmed that the soluble factors secreted by stimulating h-MSCs (namely st) strongly inhibited the ability of HUVEC cells to form tube networks; in contrast, un-stimulated h-MSCs (namely un) supernatant had no effects and tubes that were not affected (Figure 4, * p <0.05). These results confirmed that, in an inflammatory environment, h-MSCs opposed angiogenesis whereas the AML-MSCs no. It was interesting to note that, AML-MSCs did not alter HUVEC tube formation ability, in both conditions, also when cultured with inflammatory cytokines. Altogether, these findings indicate that AML-MSCs have peculiar properties that during an anti-inflammatory episode are not working to dampen the inflamed tumor microenvironment.

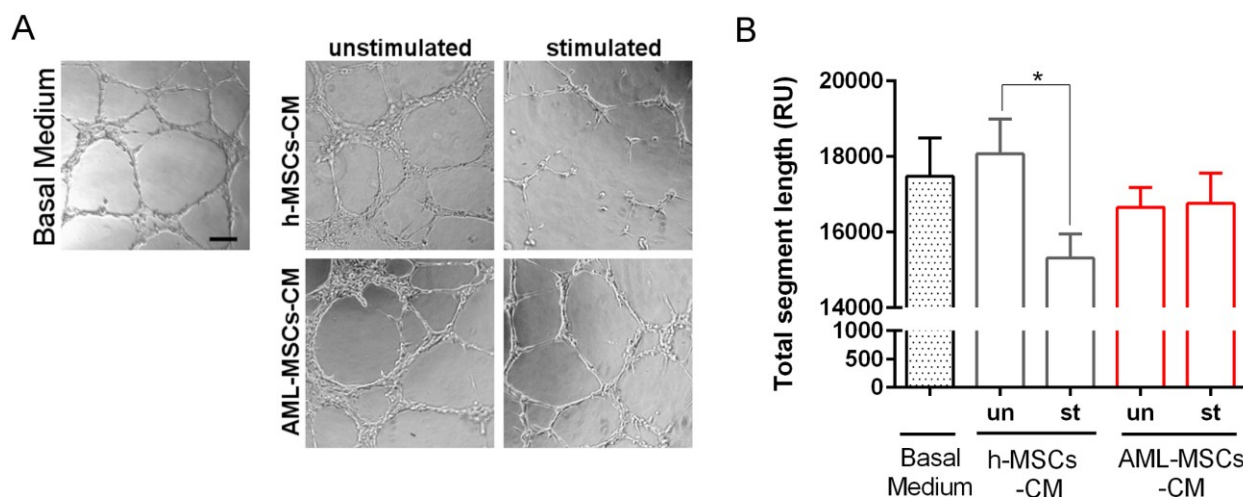


Figure 4. Effect of conditioned medium (CM) derived from human MSCs stimulated with pro-inflammatory cytokines on HUVEC tube formation ability. HUVEC cells were seeded on the top of a matrigel phase in the presence of conditional medium (CM) derived from un-stimulated (un) or stimulated (st) h-MSCs (n=7) or AML-MSCs (n=10) with pro-inflammatory cytokines. Basal medium represent the condition without conditional medium. (A) 4 h later, images were acquired with a phase contrast inverted microscope. (10x magnification, scale bar= 150 μ m). (B) Quantification of the tube segment length, express in Relative Units (RU, by ImageJ Angiogenesis Analyzer, * p <0.05).

AML-MSCs support hematopoietic stem cell proliferation

In light of these findings, AML-MSCs appeared to proliferate, differentiate and sustain an inflamed hematopoietic niche; hence we asked how hematopoietic cells react. First, we investigated healthy hematopoietic stem cells precursors (HSCPs) CD34⁺ purified from human umbilical cord blood

when co-cultured together with h-MSCs or AML-MSCs. CD34⁺ cells were cultured in cytokines-supplemented media (named stroma free condition, SF) as control in order to define the overall capacity of the different MSCs sources to support CD34⁺ cells survival. This experiment was conducted in 5 days period and revealed that CD34⁺ cells expanded as expected in SF condition, but significant differences were found in CD34⁺ cells when co-cultured with AML-MSCs or h-MSCs. In detail, CD34⁺ cells were found reducing their proliferation when co-cultured with AML-MSCs (Figure 5A), but maintained high CD34 expression when compared to the SF and h-MSCs conditions (Figure 5B). Furthermore, after 10 days of culture with AML-MSCs we measured a number of cells expressing CD34 being still significantly highly represented in the culture (43% respect to 29% in SF and 29% in h-MSCs conditions, Figure 5C). These results support that the leukemia BM microenvironment supports the stemness of healthy hematopoietic cells.

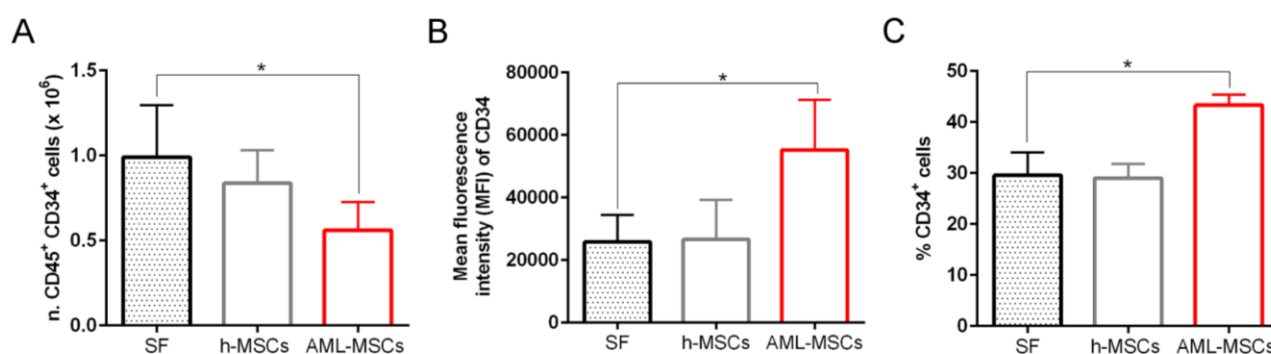


Figure 5. CD34⁺ cells characterization when co-cultured with h-MSCs or AML-MSCs. (A) *in vitro* expansion of normal CD34⁺ cells (1×10^5 CD34⁺ cells at day 0) when grown in stroma free (SF) condition or co-cultured with AML-MSCs and h-MSCs after 5 days (n=5 for each condition; * $p < 0.05$). (B) CD34 expression (flow cytometry, MFI) after 5 days of SF or co-cultured with MSCs (n=5 for each condition; * $p < 0.05$). (C) % of CD34⁺ after 10 days of co-cultures (n=3 for each condition; * $p < 0.05$).

Next, we used a model to test if there was a transforming potential intrinsic in the AML-MSCs by using a murine IL-3-dependent 32D cell line. 32D grows exclusively in the presence of interleukin-3 (IL 3) and in the IL 3 absence they undergo cell cycle arrest and apoptosis. This cell line is provided as cell model for studying the transformation abilities of various leukemia-associated oncogenes, such as *BCR/ABL* and *FLT3*, among others^{199,200}. For our approach, we considered to set up a two layer co-culturing system of 32D with h-MSCs or AML-MSCs without the IL 3, to evaluate how different sources of MSCs influenced 32D survival, ascribing an oncogenic potential to MSCs²⁰⁰. We observed that the co-culture of 32D with h-MSCs and without IL 3 did not permit proliferation and survival of 32D; extraordinary, we found that 32D cells co-cultured with AML-MSCs grew in the absence of IL 3 at similar rate of the IL 3 presence up to 72 hours (Figure 6).

Based on this finding, we speculate that the AML-MSCs have a supportive role to the 32D cells for survive in a cytokine-independent condition, supporting a role in mediating novel cellular activities towards putative transforming ability.

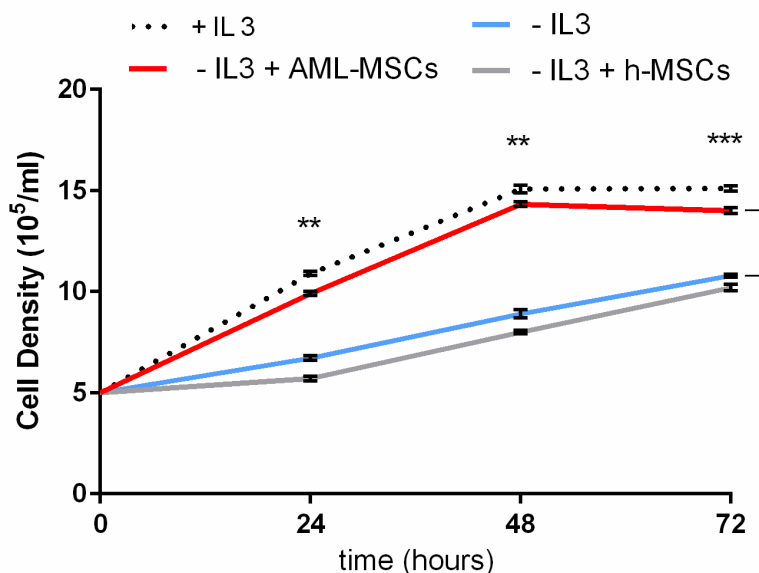


Figure 6. 32D cell line co-cultured with MSCs. Cell proliferative curves of IL 3-dependent 32D cell line cultured with IL 3 (black dotted line, n=6), or without IL 3 (blue line, n=8), compare to co-cultures with h-MSCs (grey line, n=6) or AML-MSCs (red line, n= 6). Cell density were determined in duplicate, at daily intervals, by trypan blue exclusion; ** $p < 0.01$, *** $p < 0.001$.

Collectively, these results highlighted that alteration of non-hematopoietic elements of the BM microenvironment, such as AML-MSCs, might induce hematopoietic dysfunction that can contribute to disease initiation or a pre-leukemic condition.

Hence, in order to address this hypothesis we set-up a model culturing AML-MSCs or h-MSCs with induced Pluripotent Stem Cells (iPSCs) derived from healthy CD34⁺ cells knocked-in with the AML pro-oncogenic *CBFA2T3-GLIS2* fusion gene^{188,201} and the iPSCs without the *CBFA2T3-GLIS2* translocation used as control (iPSCs CTRL). For this experiment we used AM-MSCs derived from an AML with the same *CBFA2T3-GLIS2* translocation found at diagnosis.

We performed a pilot experiment where we assessed the expression for megakaryocytic markers, such as CD41 and CD42, at the end point of the hematopoietic differentiation process as we expected a megakaryoblastic AML after the expression of the chimera *CBFA2T3-GLIS2* as previously demonstrated^{188,201}. Preliminary results demonstrated an accumulation of an abnormal population expressing low level of CD41 and CD42 in the culture condition with iPSCs *CBFA2T3-*

GLIS2 as expected to cells ascribed to megakaryoblasts. To note, the percentage of CD41^{low}CD42^{low} cells after 18 days of co-culture with AML-MSCs was triplicated with respect to the co-culture with h-MSCs (10.26% and 3.29% respectively) (Figure 7, lower panel). More interestingly, the aberrant population CD41^{low}CD42^{low} was present in lower percentage when AML-MSCs were co-cultured with iPSCs without *CBFA2T3-GLIS2* fusion (iPSCs CTRL) suggesting that the AML-MSCs, which derived from an AML harbouring the same *CBFA2T3-GLIS2* fusion gene, were probably modified by blasts to acquire the ability to induce a block of the differentiation in the iPSCs CTRL at the megakaryocyte stage. This abnormal population CD41^{low}CD42^{low} was never detected in the condition of h-MSCs (Figure 7, upper panel). To support this finding we confirmed that AML-MSCs did not carry the *CBFA2T3-GLIS2* fusion supporting that blasts acquired mutations and modify stromal cells characteristics. All together these preliminary data suggested that AML-MSCs acquired the capability to enhance the AML oncogenic activity sustaining and confirming their putative role in maintaining the AML progression. An intrinsic transforming ability towards the iPSCs CTRL could also be hypothesized, but further experiments are under investigation to finally dissect this point.

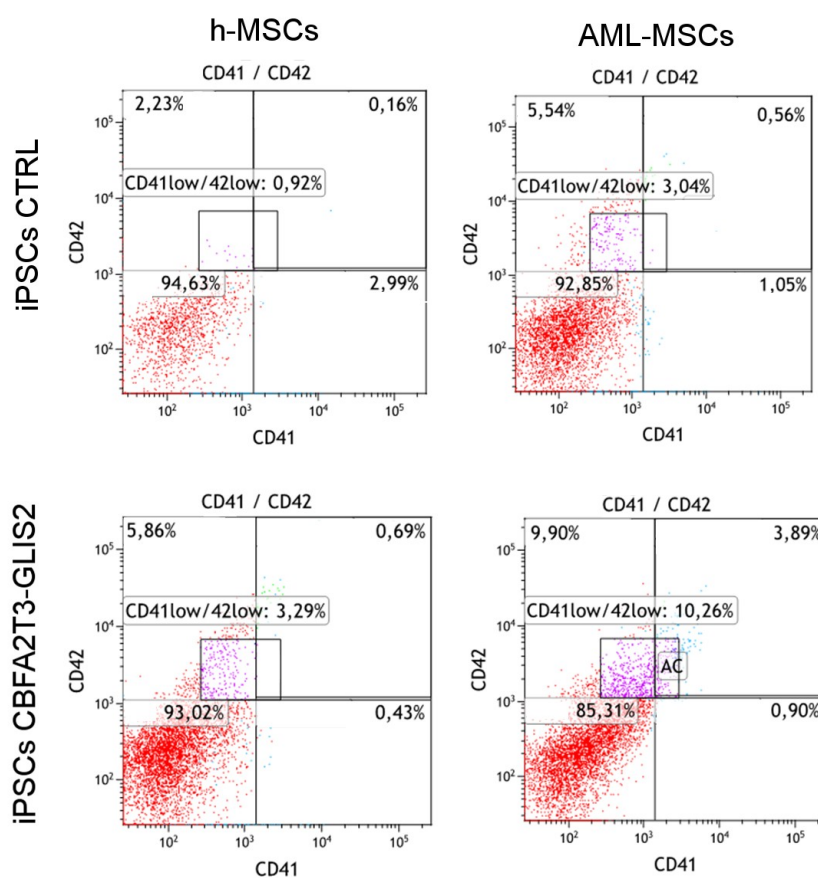


Figure 7. Flow cytometry analysis of megakaryocytic markers (CD41 and CD42) in iPSCs after cell differentiation induction. iPSCs CTRL (upper panel) and iPSCs *CBFA2T3-GLIS2* (lower panel) at day 18 of hematopoietic differentiation in co-cultures with h-MSCs (left) or AML-MSCs (right).

Specific gene expression profile of AML-MSCs

We next determined the global gene expression profile of h-MSCs and AML-MSCs. In order to depict AML-MSCs differences observed *in vitro*, we performed a comparative transcriptome analysis using AML-MSCs derived from 15 AML patients at diagnosis with different AML genetic subtypes¹⁷, and compared to 6 h-MSCs derived from healthy bone marrow donors. After the 3rd passage, total RNA was extracted and hybridized to GeneChipTM Human Genome U133 Plus 2.0 Arrays (Affymetrix, CA, USA) according to the manufacture's protocols. Results revealed 28 differentially expressed probes significantly de-regulated between AML-MSCs and h-MSCs (criterion: false discovery rate (FDR) <0.05; see Table 1). Especially, by Gene Ontology analysis these 28 probes were of genes of pathways regarding IL 17 signaling, response to hypoxia, cell differentiation, as well as for molecular functions associated with positive regulation of protein transport and positive regulation of cytokines production (Figure 8A). These latter pathways supported genes involved in MSCs functions as previously reported^{83,202,203}. The up-regulated genes in AML-MSCs, including *PTGS2*, *PEAR1*, *HES1*, *HK2*, *EGR1*, *CXCL2*, *ERG1*, *FOSB*, *ERRF1*, *AK4*, *GABPB1-AS1* and *NR4A2* respect to h-MSCs (Table 1), are in agreement with aberrancies and defects of the anti-inflammatory capability observed in AML-MSCs, supporting their role in sustaining an inflammatory environment. All these features being shared by the AML-MSC regardless of clinical and molecular AML features (Figure 8B).

Probe	Symbol	Description	Chr. position	AML-MSCs	h-MSCs
226612_at	UBE2QL1	ubiquitin conjugating enzyme E2 Q family like 1	5p15.31	5,04	6,88
203305_at	F13A1	coagulation factor XIII A chain	6p25.1	4,94	7,21
206373_at	ZIC1	Zic family member 1	3q24	5,17	7,25
205257_s_at	AMPH	amphiphysin	7p14.1	6,85	8,40
225016_at	APCDD1	APC down-regulated 1	18p11.22	6,65	8,56
209032_s_at	CADM1	cell adhesion molecule 1	11q23.3	7,21	9,22
213765_at	MFAP5	microfibrillar associated protein 5	12p13.31	6,88	9,42
243027_at	IGSF5	immunoglobulin superfamily member 5	21q22.2	4,11	5,65
209758_s_at	MFAP5	microfibrillar associated protein 5	12p13.31	8,51	10,95
213764_s_at	MFAP5	microfibrillar associated protein 5	12p13.31	6,81	9,34
209030_s_at	CADM1	cell adhesion molecule 1	11q23.3	8,49	10,25
204748_at	PTGS2	prostaglandin-endoperoxide synthase 2	1q31.1	6,24	3,96
228618_at	PEAR1	platelet endothelial aggregation receptor 1	1q23.1	7,86	5,69
203395_s_at	HES1	hes family bHLH transcription factor 1	3q29	7,61	5,79
203394_s_at	HES1	hes family bHLH transcription factor 1	3q29	9,65	7,62
202934_at	HK2	hexokinase 2	2p12	8,67	7,26
201693_s_at	EGR1	early growth response 1	5q31.2	10,01	8,53
1554997_a_at	PTGS2	prostaglandin-endoperoxide synthase 2	1q31.1	4,87	3,19
209774_x_at	CXCL2	C-X-C motif chemokine ligand 2	4q13.3	8,23	6,58
201694_s_at	EGR1	early growth response 1	5q31.2	11,60	10,49
202768_at	FOSB	FosB proto-oncogene, AP-1 transcription factor subunit	19q13.32	9,61	7,80
224657_at	ERRFI1	ERBB receptor feedback inhibitor 1	1p36.23	11,88	10,85
225342_at	AK4	adenylate kinase 4	1p31.3	7,19	5,53
235172_at	GABPB1-AS1	GABPB1 antisense RNA 1	15q21.2	5,43	4,21
202409_at				7,93	5,96
235274_at	GABPB1-AS1	GABPB1 antisense RNA 1	15q21.2	7,90	6,66
235419_at				8,54	7,30
216248_s_at	NR4A2	nuclear receptor subfamily 4 group A member 2	2q24.1	7,10	5,20

Table 1. Gene expression values (\log_2) of 28 differentially expressed probes between AML-MSCs and h-MSCs. Upper eleven probes indicate the over-expressed in h-MSCs, and *viceversa* for AML-MSCs.

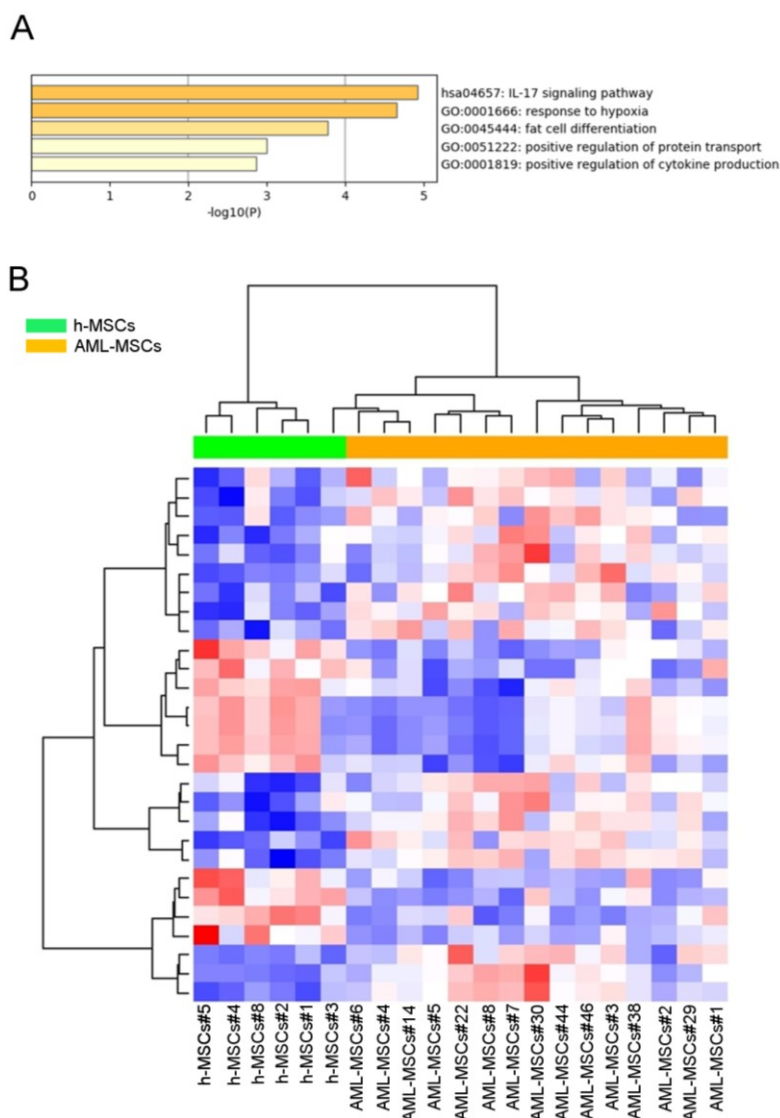


Figure 8. Gene Ontology and Heat map depicting clustering of genes differentially expressed between AML-MSCs and h-MSCs. (A) Gene Ontology, by Metascape analysis using a discrete color scale to represent statistical significance (p -value expressed in \log_{10}), indicates the most significant deregulated pathways in AML-MSCs with respect to h-MSCs. (B) Unsupervised hierarchical clustering of MSCs transcriptional profile of AML-MSCs at diagnosis (orange, $n=15$) and h-MSCs (green, $n=6$). Each column represents a sample and each row represent a gene. Red color indicates gene that are up-regulated and blue color indicates genes that are down-regulated. The analysis was performed using probes set with 90% of variants variability and clustering was performed using Euclidean distance and Wards method.

All together these data define another crucial biological characteristic of the AML-MSCs when compared to h-MSCs, and deal with a categorical question whether AML derives from primary defects of the hematopoietic stem cell or from the microenvironment-MSCs able to force their transformation. Although results from mouse models are consistent with both hypotheses^{47,69,91}, only few reports supported that niche cells are altered by the AML blasts⁷⁶. By the way, our iPSCs

model contrasts this latter hypothesis. Thus, to experimentally address this crucial point of AML *versus* MSCs driver role in initiate AML, we interrogated if AML-MSCs gene expression profile changed between diagnosis (n=15) and after treatment when the disease is in complete remission (R-MSCs, n=6; 4 cases were after chemotherapy alone and 2 cases after BM transplantation (HSCT), namely R-MSCs #4 and #66 showing no cluster differences). The heat-map of the differentially expressed genes showed a clear separation between the AML-MSCs and R-MSCs (Figure 9A). Using a ≥ 2.5 -fold change as a cut-off 1728 probes were found to be differentially expressed. Notably, we found 1186 probes up-regulated and 542 down-regulated in AML-MSCs with respect to R-MSCs. The top 50 down-expressed probes and over-expressed probes are listed in Table 2 and 3. By Principal Component Analysis (PCA) we confirmed the R-MSCs being far from the AML-MSCs (Figure 9B) supporting these cells being different when collected in the two different bone marrow conditions. To confirm these findings we analyzed three paired samples at diagnosis and remission (#1, #4, #44) finding same results (criterion: FDR <0.05; Figure 10). Gene Ontology analysis revealed that AML-MSCs differed from the R-MSCs for genes involved in regulation of cell adhesion, blood development, ossification, response to growth factors, as well as negative regulation of cell proliferation (Figure 11).

We finally attempted a comparative analysis of Gene Ontology among all the samples of R-MSCs, h-MSCs, and AML-MSCs analyzed by GEP in order to interpret if R-MSCs are similar to the h-MSCs or to the AML-MSCs. As shown in Figure 11, we appreciated more similarity (grey color) between R-MSCs and h-MSCs with respect to R-MSCs and AML-MSCs (enriched in orange color expressing dissimilarity). We looked at single probes finding that for 14 out of 21 probes (66%) their expression levels were similar in R-MSCs and h-MSCs with respect to the AML-MSCs (Figure 12), supporting that R-MSCs seemed to get back to h-MSCs gene expression profile when the complete remission was obtained, and that during the AML onset they acquired novel features. This latter observation supported that R-MSCs might exert same h-MSCs functions *in vitro*. So, we got back to the *in vitro* tests performed before and interrogated R-MSCs proliferation rate and transforming potential. As shown in Figure 13, R-MSCs exhibited a lower proliferation rate respect to AML-MSCs, as observed in the h-MSCs, and were not able to sustain 32D cell line proliferation in absence of IL 3 (Figure 13B). Taken together, these data clearly sustain a direct causal relationship between the presence of AML cells and the AML-MSCs properties, with peculiar stromal functions of h-MSCs recovered in the R-MSCs as soon as leukemia cells have been eradicated by therapy.

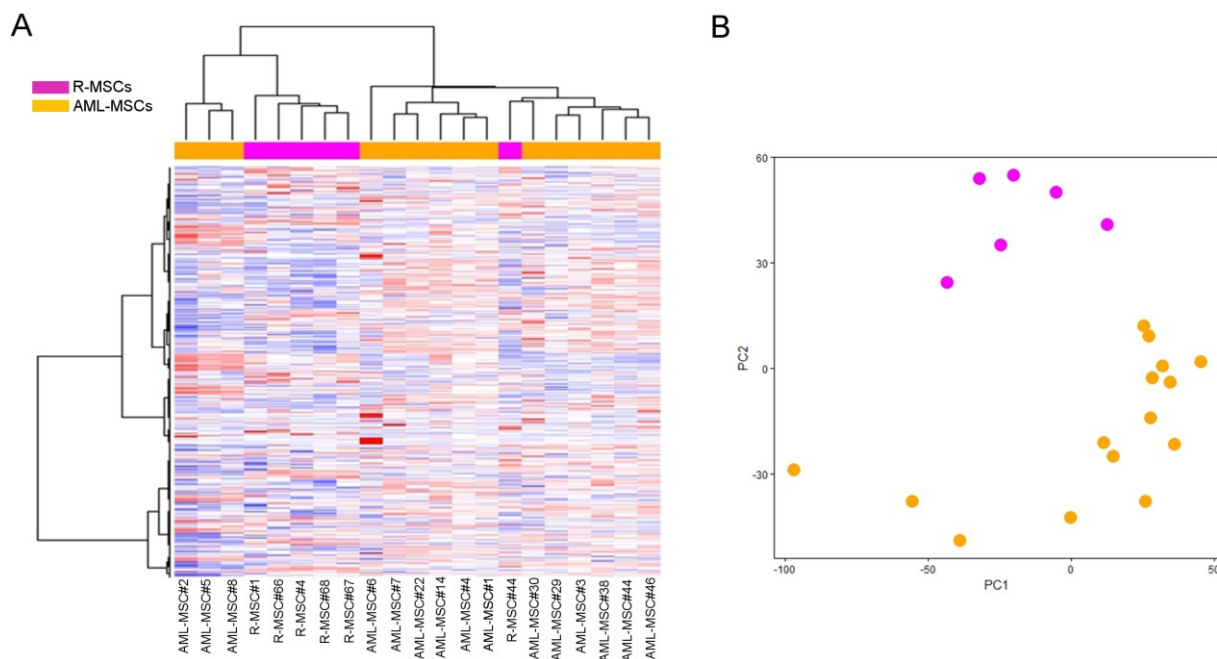


Figure 9. Unsupervised hierarchical clustering and principal component analysis (PCA). (A) Unsupervised hierarchical clustering of MSCs transcriptional profile of AML-MSCs (orange, n=15) and derived from R-MSCs (pink, n=6). Columns represent the sample. Colors represent relative levels of genes expression: bright red indicates the highest level of expression, and bright blue indicates the lowest level of expression. (B) Principle component analysis of the variance in mRNA expression of the sample depicted in the heat maps in AML-MSCs and in R-MSCs datasets. The x axis represents the first principal component, PC1, which accounts for the largest variance of mRNA expression and the y axis, PC2, explains the second largest variance.

Probe	Symbol	Description	Chr. Position	AML-MSCs	R-MSCs
205713_s_at	COMP	cartilage oligomeric matrix protein	19p13.11	7,38	11,32
213765_at	MFAP5	microfibrillar associated protein 5	12p13.31	6,88	10,22
213764_s_at	MFAP5	microfibrillar associated protein 5	12p13.31	6,81	10,07
220639_at	TM4SF20	transmembrane 4 L six family member 20	2q36.3	5,42	8,63
227006_at	PPP1R14A	protein phosphatase 1 regulatory inhibitor subunit 14A	19q13.2	4,35	7,56
208607_s_at				5,39	8,40
227550_at	GFRA1	GDNF family receptor alpha 1	10q25.3	6,87	9,83
209758_s_at	MFAP5	microfibrillar associated protein 5	12p13.31	8,51	11,42
205696_s_at	GFRA1	GDNF family receptor alpha 1	10q25.3	4,69	7,57
215704_at	FLG	filaggrin	1q21.3	5,59	8,42
202286_s_at	TACSTD2	tumor associated calcium signal transducer 2	1p32.1	8,91	11,70
229649_at	NRXN3	neurexin 3	14q24.3-q31.1	5,99	8,71
225895_at	SYNPO2	synaptopodin 2	4q26	5,44	8,14
202718_at	IGFBP2	insulin like growth factor binding protein 2	2q35	8,10	10,75
214456_x_at				6,80	9,40
204105_s_at	NRCAM	neuronal cell adhesion molecule	7q31.1	6,88	9,43
219529_at	CLIC3	chloride intracellular channel 3	9q34.3	6,38	8,88
212611_at	DTX4	deltex E3 ubiquitin ligase 4	11q12.1	5,66	8,15
215008_at	TLL2	tolloid like 2	10q24.1	3,45	5,88
206029_at	ANKRD1	ankyrin repeat domain 1	10q23.31	5,59	8,01
230163_at	GFRA1	GDNF family receptor alpha 1	10q25.3	5,70	8,09
214455_at				3,83	6,20
239218_at	PDE1C	phosphodiesterase 1C	7p14.3	5,05	7,41
201117_s_at	CPE	carboxypeptidase E	4q32.3	8,12	10,44
241749_at	CAVIN4	caveolae associated protein 4	9q31.1	4,69	6,99
1555471_a_at	FMN2	formin 2	1q43	4,38	6,67
203158_s_at	GLS	glutaminase	2q32.2	8,04	10,32
206825_at	OXTR	oxytocin receptor	3p25.3	6,28	8,55
201116_s_at	CPE	carboxypeptidase E	4q32.3	8,42	10,69
219054_at	NPR3	natriuretic peptide receptor 3	5p13.3	8,02	10,29
242002_at	NKAIN2	sodium/potassium transporting ATPase interacting 2	6q22.31	5,78	8,00
236193_at	HIST1H2BC	histone cluster 1 H2B family member c	6p22.2	4,62	6,80
208180_s_at	HIST1H4H	histone cluster 1 H4 family member h	6p22.2	4,86	7,04
236344_at	PDE1C	phosphodiesterase 1C	7p14.3	5,63	7,81
209343_at	EFHD1	EF-hand domain family member D1	2q37.1	6,12	8,28
1552378_s_at	RDH10	retinol dehydrogenase 10	8q21.11	6,71	8,86
210861_s_at	WISP3	WNT1 inducible signaling pathway protein 3	6q21	4,79	6,93
223618_at	FMN2	formin 2	1q43	5,00	7,14
225720_at	SYNPO2	synaptopodin 2	4q26	5,18	7,31
226961_at	PRR15	proline rich 15	7p14.3	4,75	6,87
242767_at	LMCD1	LIM and cysteine rich domains 1	3p25.3	6,79	8,91
204338_s_at	RGS4	regulator of G-protein signaling 4	1q23.3	4,58	6,69
205755_at	ITIH3	inter-alpha-trypsin inhibitor heavy chain 3	3p21.1	4,90	7,01
229566_at	WFDC21P	WAP four-disulfide core domain 21, pseudogene	17q23.1	7,12	9,23
227467_at	RDH10	retinol dehydrogenase 10	8q21.11	7,50	9,60
219789_at	NPR3	natriuretic peptide receptor 3	5p13.3	5,75	7,85
1555673_at				4,98	7,07
206439_at	EPYC	epiphycan	12q21.33	3,33	5,40
203157_s_at	GLS	glutaminase	2q32.2	8,64	10,72
1554195_a_at	C5orf46	chromosome 5 open reading frame 46	5q32	4,75	6,83

Table 2. Gene expression values (\log_2) of top 50 down-expressed probes in AML-MSCs with respect to R-MSCs.

Chromosome position and gene name are reported regarding the AML-MSCs with respect to R-MSCs. Empty rows are genes not clearly attributed to known genes or ncRNAs.

Probe	Symbol	Description	Chr. Position	AML-MSCs	R-MSCs
209687_at	CXCL12	C-X-C motif chemokine ligand 12	10q11.21	9,82	6,28
203666_at	CXCL12	C-X-C motif chemokine ligand 12	10q11.21	9,04	5,78
206932_at	CH25H	cholesterol 25-hydroxylase	10q23.31	9,01	5,96
208937_s_at	ID1	inhibitor of DNA binding 1, HLH protein	20q11.21	9,96	7,12
235743_at				7,92	5,14
205959_at	MMP13	matrix metalloproteinase 13	11q22.2	9,21	6,48
242918_at	NASP	nuclear autoantigenic sperm protein	1p34.1	6,70	4,07
208131_s_at	PTGIS	prostaglandin I2 synthase	20q13.13	7,62	5,01
203854_at	CFI	complement factor I	4q25	7,35	4,86
215506_s_at	DIRAS3	DIRAS family GTPase 3	1p31.3	8,57	6,12
232453_at				7,69	5,27
203423_at	RBP1	retinol binding protein 1	3q23	9,27	6,88
223044_at	SLC40A1	solute carrier family 40 member 1	2q32.2	7,13	4,75
209395_at	CHI3L1	chitinase 3 like 1	1q32.1	7,32	5,00
202202_s_at	LAMA4	laminin subunit alpha 4	6q21	8,03	5,73
228057_at	DDIT4L	DNA damage inducible transcript 4 like	4q24	8,08	5,79
221019_s_at	COLEC12	collectin subfamily member 12	18p11.32	10,54	8,27
216248_s_at	NR4A2	nuclear receptor subfamily 4 group A member 2	2q24.1	7,10	4,90
1564378_a_at				7,24	5,05
1555564_a_at	CFI	complement factor I	4q25	6,53	4,36
233090_at				8,22	6,07
210587_at	INHBE	inhibin beta E subunit	12q13.3	8,28	6,15
204622_x_at	NR4A2	nuclear receptor subfamily 4 group A member 2	2q24.1	7,43	5,37
209396_s_at	CHI3L1	chitinase 3 like 1	1q32.1	7,49	5,44
203395_s_at	HES1	hes family bHLH transcription factor 1	3q29	7,61	5,57
213125_at	OLFML2B	olfactomedin like 2B	1q23.3	10,06	8,02
204621_s_at	NR4A2	nuclear receptor subfamily 4 group A member 2	2q24.1	6,43	4,42
243993_at				7,98	5,98
231199_at				6,63	4,64
202350_s_at	MATN2	matrilin 2	8q22.1-q22.2	7,60	5,62
244341_at				7,56	5,59
241981_at	FAM20A	FAM20A, golgi associated secretory pathway pseudokinase	17q24.2	7,63	5,69
213506_at	F2RL1	F2R like trypsin receptor 1	5q13.3	8,55	6,63
221658_s_at	IL21R	interleukin 21 receptor	16p12.1	6,80	4,89
202768_at	FOSB	FosB proto-oncogene, AP-1 transcription factor subunit	19q13.32	9,61	7,74
238769_at				5,75	3,90
243296_at	NAMPT	nicotinamide phosphoribosyltransferase	7q22.3	6,98	5,13
209550_at	NDN	necdin, MAGE family member	15q11.2	9,85	8,00
204909_at	DDX6	DEAD-box helicase 6	11q23.3	6,93	5,09
1558732_at	MAP4K4	mitogen-activated protein kinase kinase kinase 4	2q11.2	7,25	5,42
200644_at	MARCKSL1	MARCKS like 1	1p35.1	9,93	8,10
203394_s_at	HES1	hes family bHLH transcription factor 1	3q29	9,65	7,82
241060_x_at				6,67	4,86
232541_at				7,01	5,22
236000_s_at				6,19	4,46
239571_at				6,75	5,03
1552736_a_at	NETO1	neuropilin and tolloid like 1	18q22.3	9,08	7,37
240262_at				5,26	3,56
208096_s_at	COL21A1	collagen type XXI alpha 1 chain	6p12.1	8,09	6,39
209687_at	CXCL12	C-X-C motif chemokine ligand 12	10q11.21	7,28	5,78

Table 3. Gene expression values (\log_2) of top 50 over-expressed probes in AML-MSCs with respect to R-MSCs. Chromosome position and gene name are reported regarding the AML-MSCs with respect to R-MSCs. Empty rows are genes not clearly attributed to known genes or ncRNAs.

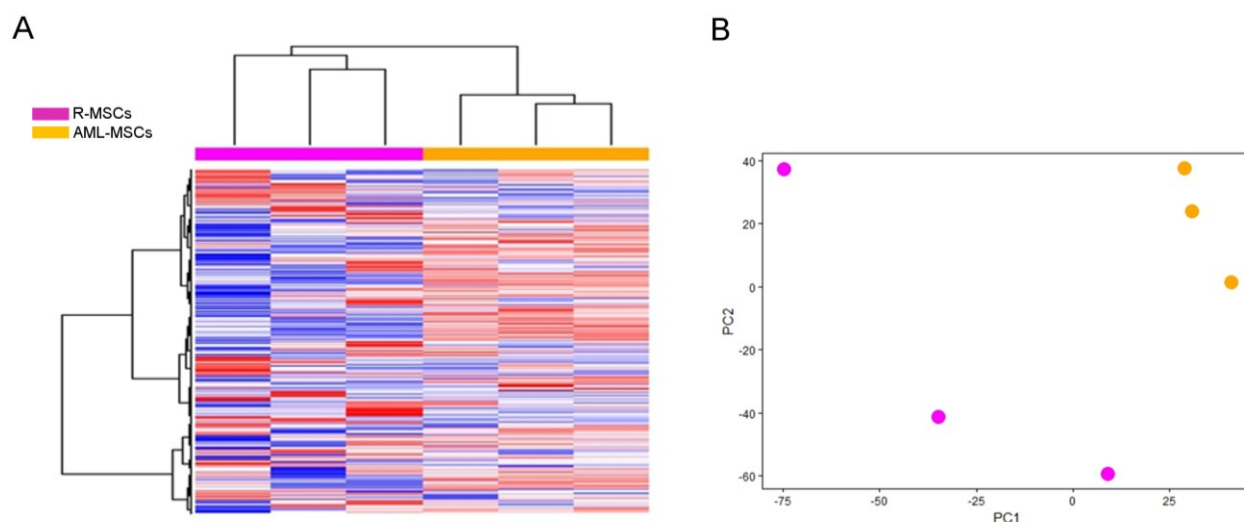


Figure 10. Unsupervised hierarchical clustering and principal component analysis (PCA) of three paired MSCs samples collected at diagnosis of AML and in remission. (A) Unsupervised hierarchical clustering of AML-MSCs transcriptional profile (orange, n=3) and R-MSCs (pink, n=3). Columns represent the sample. Each row represent the relative levels of expression of single gene, calculated as the number of standard deviation above (red) or below (blue) the mean expression level of that gene across the samples; FDR<0.05 (B) Principle component analysis of the variance in mRNA expression of the sample depicted in the heat maps in AML-MSCs (orange) and in R-MSCs (pink) datasets. The x axis represents the first principal component, PC1, which accounts for the largest variance of mRNA expression and the y axis, PC2, explains the second largest variance.

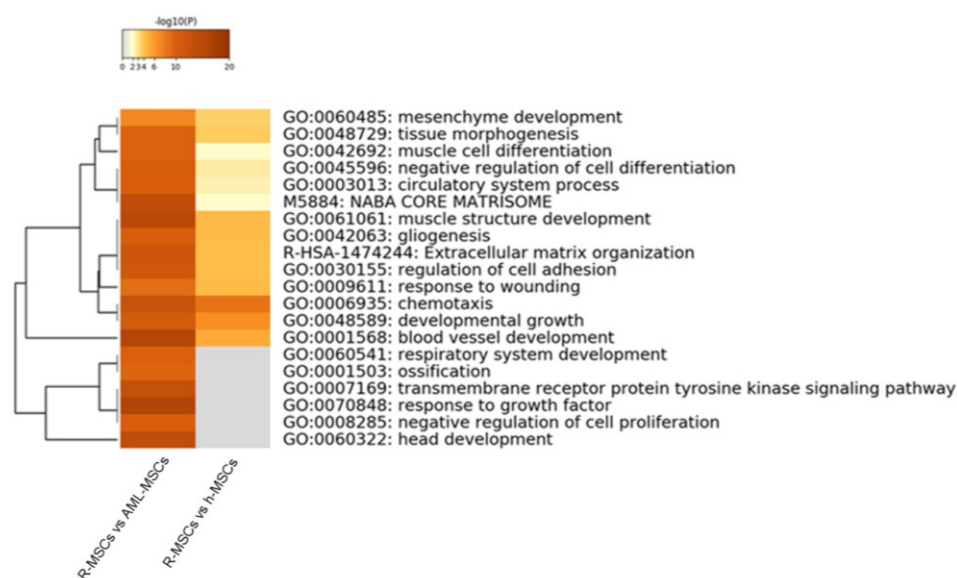


Figure 11. Gene Ontology comparative analysis. Gene Ontology annotation of biological processes enrichment performed on differentially expressed coding genes between the two analysis: AML-MSCs and R-MSCs (left) and R-MSCs and h-MSCs (right). Heat-map showing the top enrichment clusters, one row per cluster, using a discrete color scale to represent statistical significance, with dark orange indicating the lowest similarity, while the grey color indicates the highest similarity ($p=ns$).

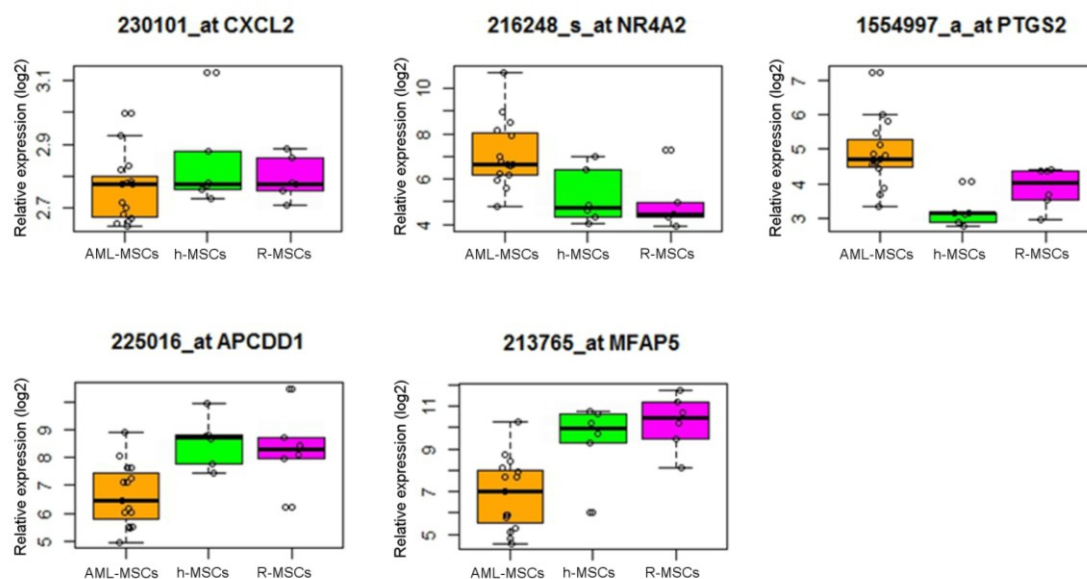


Figure 12. Expression levels of annotated genes in AML-MSCs versus h-MSCs and R-MSCs by GEP. Box plots show the expression of 5 representative genes in AML-MSCs (orange), h-MSCs (green) and R-MSCs (pink). Results represent mean values and are expressed as Log₂ values of the fold change.

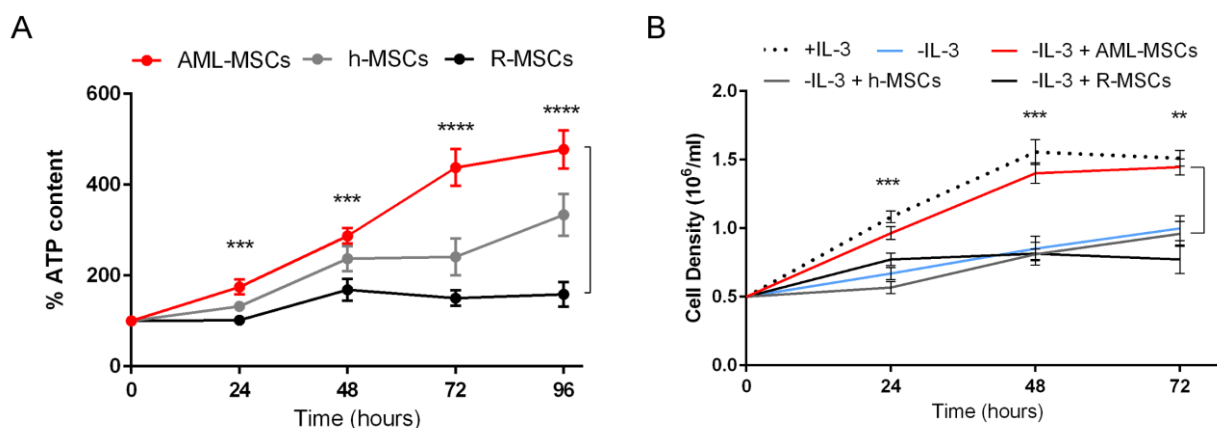


Figure 13. R-MSCs *in vitro* characterization. (A) R-MSCs, AML-MSCs, and h-MSCs proliferation rate over time. All points indicate mean of triplicate analysis and all error bars indicate s.e.m. Unpaired Student's *t*-test was used to detect statistically significant differences between R-MSCs (n=11), h-MSCs (n=6), and AML-MSCs (n=11) (**p < 0.01, ***p < 0.001, ****p < 0.0001). (B) Impact of R-MSCs on IL-3-independence growth of 32D cell line. Proliferative curves of murine IL-3-dependent 32D cell line cultured in suspension in presence of IL-3 (black dotted line) and in absence of IL-3 in suspension (blue line), in co-culture with R-MSCs (black line), or with h-MSCs (grey line) or with AML-MSCs (red line). Cell density was determined in duplicate, at daily intervals, by trypan blue exclusion (n=6, **p < 0.01, ***p < 0.001).

LOPAC^{®1280} high throughput drug screening on MSCs

Our AML-MSCs characterization revealed that AML-MSCs are playing a fundamental pro-tumoral function and prioritize them as novel potential target to treat AML. We performed a High-Throughput Screening (HTS) by using 480 compounds from a commercial Library of Pharmacologically Active Compounds (LOPAC^{®1280}), in order to discover drugs active with a novel indication for targeting the AML-MSCs. The HTS pipeline (Figure 14) established a treatment of 48 hours with drugs at 10 μ M on AML-MSCs, then on h-MSCs and finally on AML cell lines (e.g. SHI-1, ML-2, and HL-60) in order to select those active exclusively on AML-MSCs. The first step identified 47 compounds able to reduce at least 50% the AML-MSCs growth evaluated by ATP analysis. These 47 compounds were then used to treat h-MSCs in order to exclude toxicity on the h-MSCs: results revealed that 17 out of 47 compounds were active on these cells, and 30 were not. Finally, to refine drug selection we treated AML cell lines with the last 30 compounds and finally identified that 17 compounds out of 480 satisfying our criteria of selectively toward AML-MSCs (Figure 15). Interestingly, the 17 identified drugs belong to different classes of action (Table 4, Figure 16) by the way, two drugs, Lercanidipine-HCl and Nemadipine-A, have the same mechanism of action belonging to the class of dihydropyridines and block the inward movement of calcium by binding to the L-type calcium channels. Noteworthy, several data reported that the expression of the L-type calcium channels on MSCs has been linked to the proliferation and osteogenic differentiation ability of rat bone marrow-MSCs²⁰⁴, both pathways being found altered in our AML-MSCs characterization. However, data from mouse MSCs were inconsistent with these results, we decided to consider this discovery and choose Lercanidipine-HCl as the candidate compound to target AML-MSCs in the context of pediatric AML.

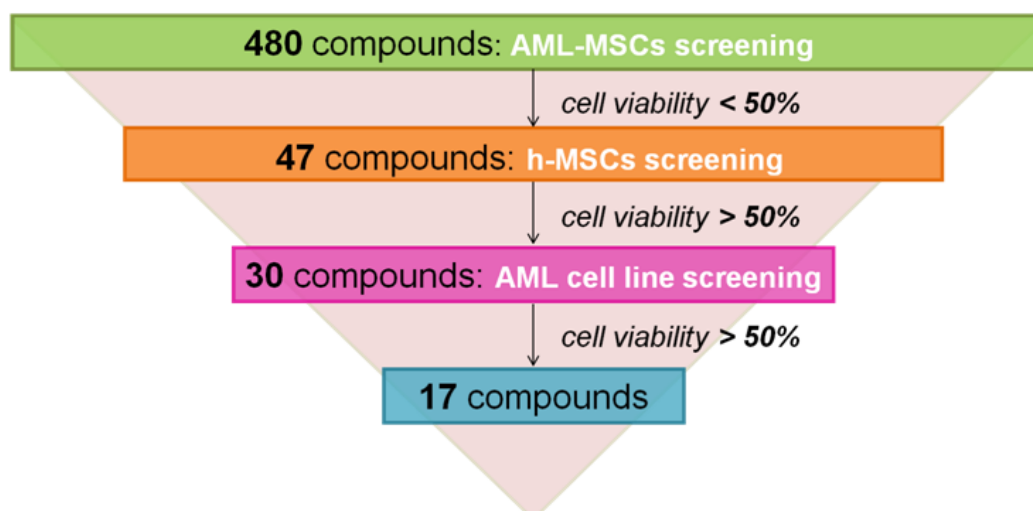


Figure 14. Pipeline of HTS to select among 480 compounds. Cell viability was considered the endpoint of this screening. Drugs able to reduce cell proliferation more than 50% AML-MSCs proliferation, but >50% in h-MSCs and AML cell lines were considered. A total of 17 out of 480 compounds satisfied these criteria.

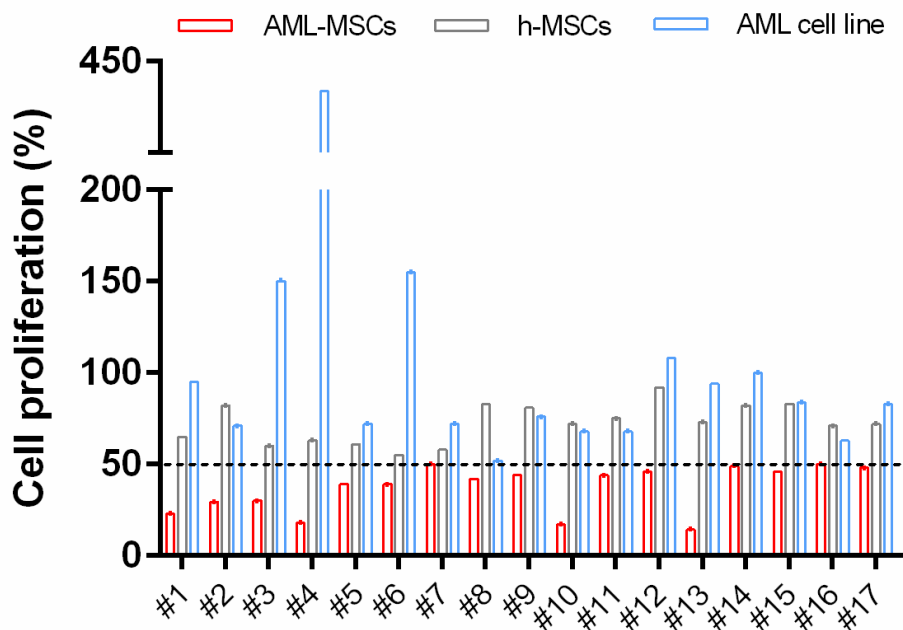


Figure 15. Drug screening on MSCs. Histogram represents ATP levels after drug screening of the 17 final active compounds on MSCs and AML cell lines. Drop line represents the IC₅₀ cut off below which these 17 effective drugs have been identified.

#	Compound	Activity
1	Lercanidipine-HCl	L-type Calcium channel inhibitor
2	Nemadipine-A	L-type Calcium channel inhibitor
3	O-(Carboxymethyl)hydroxylamine	Glucocorticoid receptor agonists
4	Paroxetine HCl hemihydrate	Serotonin reuptake inhibitors (SSRI)
5	Chlorpromazine hydrochloride	Dopamin antagonist
6	Caffeic acid phenethyl ester	Antimitogenic, anticarcinogenic, anti-inflammatory
7	Clomipramine hydrochloride	Inhibits the uptake of serotonin
8	UCL 2077	Potassium channel blocker
9	Tamoxifen	Estrogen receptor
10	GW2974	EGFR inhibitor
11	Fiduxosin hydrochloride	α 1-Adrenoceptor antagonist
12	Fluoxetine hydrochloride	Serotonin antagonist
13	JNJ-40418677	Gamma-secretase inhibitor
14	Methoctramine tetrahydrochloride	Muscarinic M2 receptor antagonist
15	AMN082	Glutamate receptor agonist
16	Nortriptyline hydrochloride	Dibenzocycloheptene-derivative tricyclic antidepressant
17	Ethopropazine hydrochloride	Antidyskinetic

Table 4. List of selected compounds. Seventeen compounds were prioritize from the HST for the ability to reduce AML-MSCs proliferation at least of 50%.

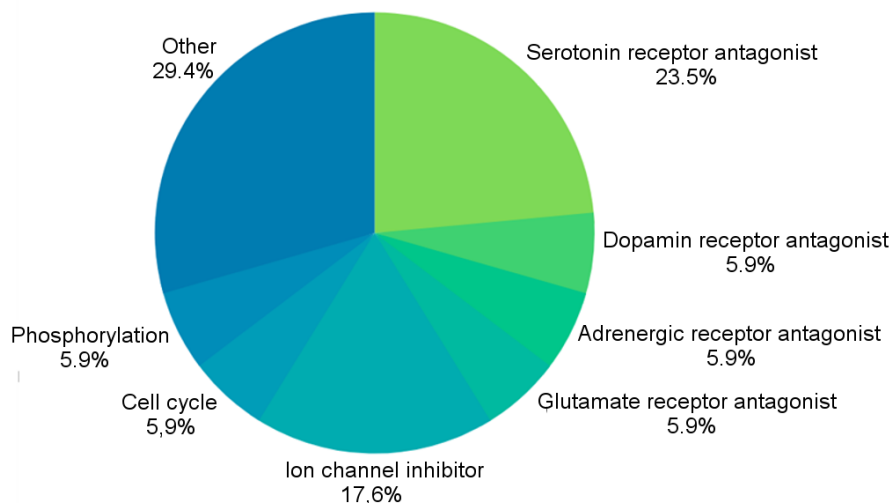


Figure 16. Selected compounds class of action. Representative diagram of the different class of action attributed to the 17 compounds resulted from the HST.

First of all we would support L-type channel antagonists effect on a large cohort of samples. We treated 6 AML-MSCs, 3 AML cell lines (SHI-1, ML-2, and HL-60), 6 different AML primary cells at diagnosis, and 2 healthy hematopoietic stem cells precursors CD34⁺ purified from human umbilical cord blood, confirming that this compound was inactive on AML and 34⁺ healthy cells, but was broadly active on all 6 samples of AML-MSCs, mediating a significant proliferation rate reduction measured by ATP assay (>50%) (Figure 17).

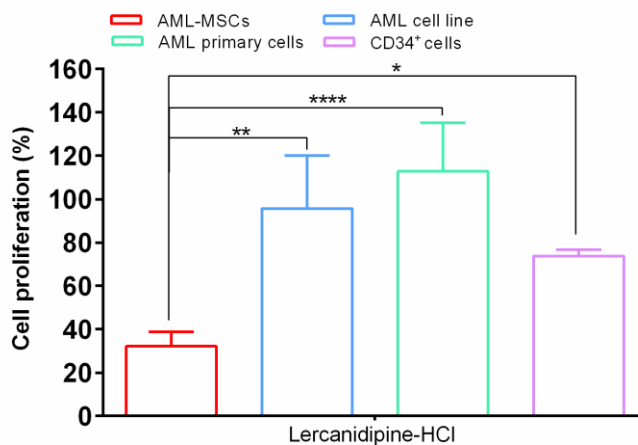


Figure 17. Lercanidipine-HCl treatment on different samples. Cell proliferation of AML-MSCs (n=6), AML cell lines (n=2), AML primary cells (n=6), and CD34⁺ cells (n=2) after 48 h of Lercanidipine-HCl treatment. Cell proliferation (%) was determined in triplicate, by ATP assay, normalizing the value with respect to the control group (DMSO=100%); * p <0.05, ** p <0.01, *** p <0.001.

Since we observed a reduction in ATP levels of the AML-MSCs, we asked if Lercanidipine-HCl exerted an influence on cell cycle inducing a proliferative block or by induction of death-apoptosis, both being important aspects to consider in the preservation of the pool of MSCs in the patient's BM niche. Hence, we measured the apoptosis induction concomitantly to the ATP levels in a long time Lercanidipine-HCl treatment of 9 days. Exposure to 10 μ M Lercanidipine-HCl for 24-72h did not result in general changes of cell viability (Annexin V and Propidium Iodide staining, average 82% at 72 h), but cell proliferation was reduced (by ATP, average 7 at 72 h, Figure 18, Table 5). Thereafter at 6 and 9 days of Lercanidipine-HCl treatment also cell viability was extremely impaired (AVPI at 9 days average at 11%) suggesting a late-effects of Lercanidipine-HCl on AML-MSCs survival. We attempted also a washout (w/o) of the drug after 24 h from the Lercanidipine-HCl administration. With this strategy, we demonstrated that after a first effect on cell proliferation observed in a window of 72 h, cells rescued proliferation in the long term, with a lowered rate of cell apoptosis, supporting the reversible effect of a daily treatment. These results open the discussion about a reliable use of Lercanidipine-HCl administration during chemotherapy preserving the MSCs pool after treatment (Figure 18).

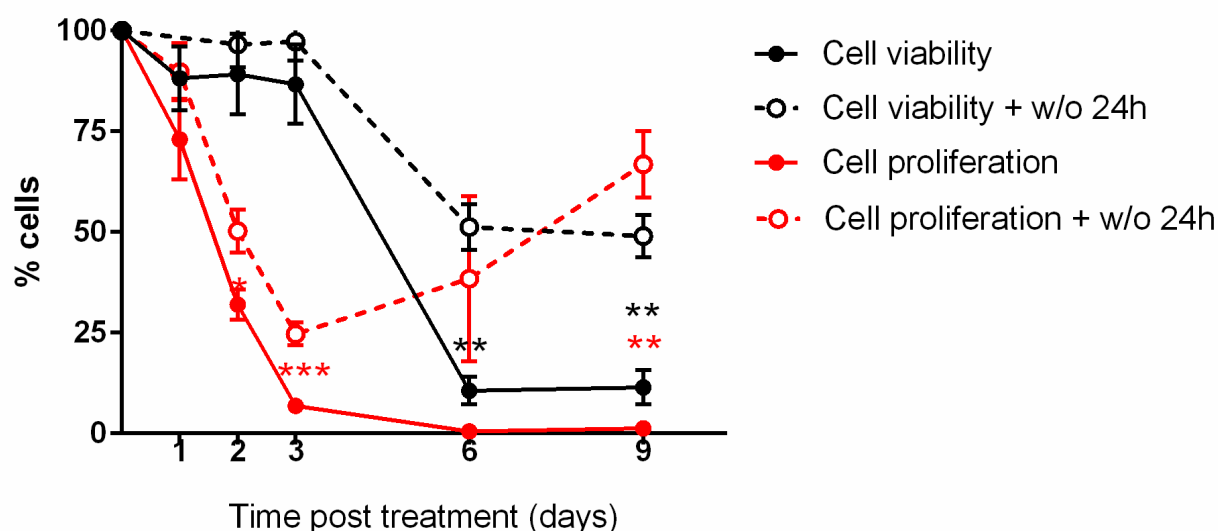
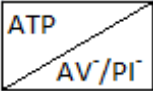


Figure 18. Annexin V/PI staining in AML-MSCs at up to 9 days of Lercanidipine-HCl treatment. Data represent the cell proliferation (red line) and cell viability (black line) of AML-MSCs after Lercanidipine-HCl treatment. Cells

were analyzed by ATP assay for cell proliferation and by Annexin V/PI staining for cell viability. Drop line represent the values of cell proliferation and cell viability after washout (w/o) drug experiment; n=5 ; ** $p < 0.01$, *** $p < 0.001$.

Time (days):	1	2	3	6	9
#1	63 80,2	38 76,1	5,3 92,3	1,07 16,6	- -
#2	83 96	19 78,5	4,5 84,7	0,34 -	- -
#3	- -	38 -	3,4 -	0,37 10	3,4 15
#4	- -	37 83	8,3 61	0,49 4,7	0,39 3
#5	- -	28 100	13 100	- -	0,18 16
Average	73 88	32 89	7 86	0,5 10	1,32 11,43



ATP
AV/PI

Table 5. Annexin V/PI and ATP comparison up to 9 days of Lercanidipine-HCl treatment. Data represent the values of cell proliferation (ATP) and cell viability expressed as viable cells being for the staining (AV/PI) in 5 different AML-MSCs samples.

These latter findings sustained Lercanidipine-HCl treatment for further clinical evaluation, thus we would identify its cellular target, the L-type calcium channel, named also CaV1.2. We used mRNA obtained from AML-MSCs and h-MSCs samples and found 3-fold lower expression levels of CaV1.2 in AML-MSC compared to h-MSCs (Figure 19A). Likewise, h-MSCs demonstrated also 3.5-fold higher Cav1.2 protein expression (expressed as MFI), by flow cytometry when compare to the AML-MSCs (Figure 19B and C). Finally, using the Calcium probe Fluo-4 AM, we monitored the entry of exogenous Ca^{2+} added after 48h of Lercanidipine-HCl treatment in h-MSCs and AML-MSC. Results showed that Ca^{2+} did not enter in AML-MSCs if Lercanidipine-HCl treated, whereas intra-cellular Ca^{2+} levels remained unaffected in h-MSCs treated and untreated (Figure 20). We revealed that Lercanidipine-HCl is extremely efficacious in AML-MSCs were the low expression of the CaV1.2 and the inhibitory effects of the drug completely abrogated Ca^{2+} flux disrupting its homeostasis and inducing AML-MSCs cell death.

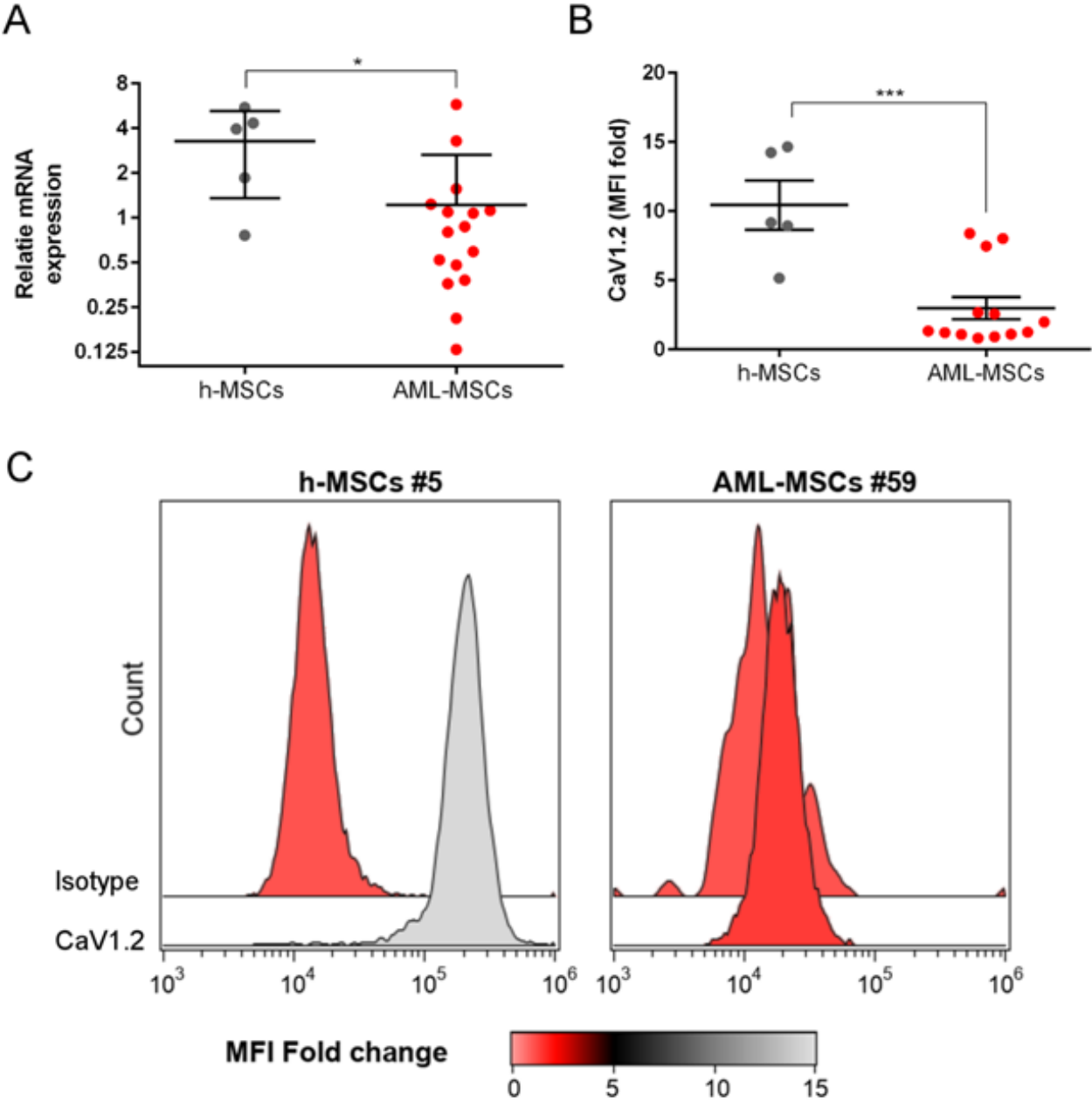


Figure 19. *CaV1.2* expression in AML-MSCs and h-MSCs. (A) relative mRNA expression of *CaV1.2*, in h-MSCs (n=5) and AML-MSCs (n=16) was measured by qRT-PCR. *GUS* served as an equal loading control; * $p < 0.05$. (B) Scatter plot of *CaV1.2* MFI fold change protein expression, by flow cytometry. Each dot represents the samples (h-MSCs, n=5; AML-MSCs, n= 13), presented as mean and error bars indicate s.e.m. *** $p < 0.001$. (C) Representative histograms of *CaV1.2* expression in h-MSCs (#5) and AML-MSCs (#59), by flow cytometry. Color scale represents fold change values respect to the relative isotypic control.

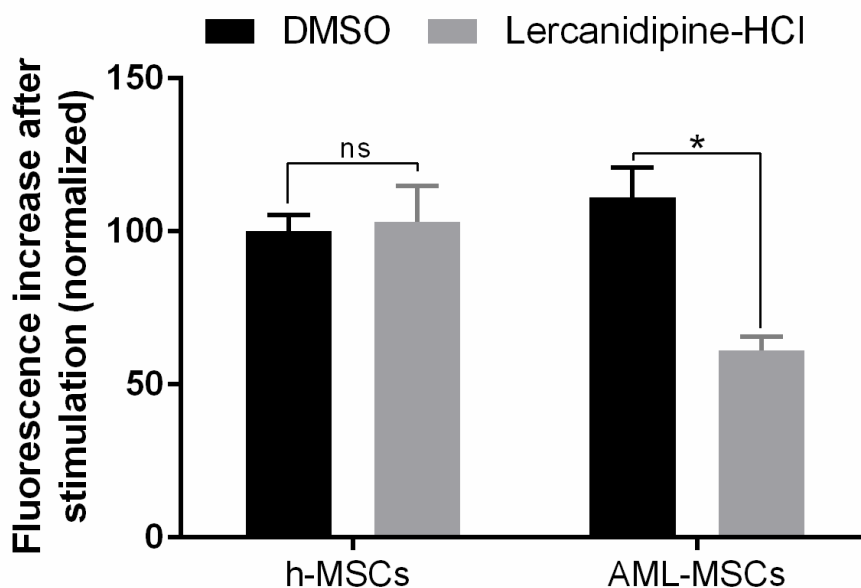


Figure 20. MSCs Ca^{2+} uptake under Lercanidipine-HCl treatment. MSCs were loaded with calcium indicator Fluo-4 AM probe after 48 h of Lercanidipine-HCl treatment. Histograms indicates the increase fluorescence levels during CaCl_2 (1mM) addition to culture medium on h-MSCs or AML-MSCs under Lercanidipine-HCl or vehicle (DMSO) treatment (n=3). Data represent the mean + standard deviation (SD); * p <0.05.

In addition, in order to confirm the selectivity of Lercanidipine-HCl towards L-type channel $\text{CaV}1.2$, we perform a Lercanidipine-HCl treatment in combination with Calcium $\text{CaV}1.2$ agonists, as BAY-K8644 and FPL 64176, demonstrating a partial rescue (+ 20%) of the AML-MSCs proliferation rate, indicating that $\text{CaV}1.2$ is the target (Figure 21A). Next, we decided to test two different Ca^{2+} channel blockers, such as Verapamil and Diltiazem that referred to other classes of action (Phenylalkylamine and Benzothiazepine, respectively) with respect to Lercanidipine-HCl and Nemedipine-A. As shown in Figure 21B, when we tested the effects of these Ca^{2+} channel blockers compared with Lercanidipine-HCl and Nemedipine-A effects on AML-MSCs, we confirmed they activity with respect to DMSO (100% in the figure), but observed a significant reduced activity of both compounds in AML-MSCs proliferation, supporting the specificity and selectivity of our candidate compound.

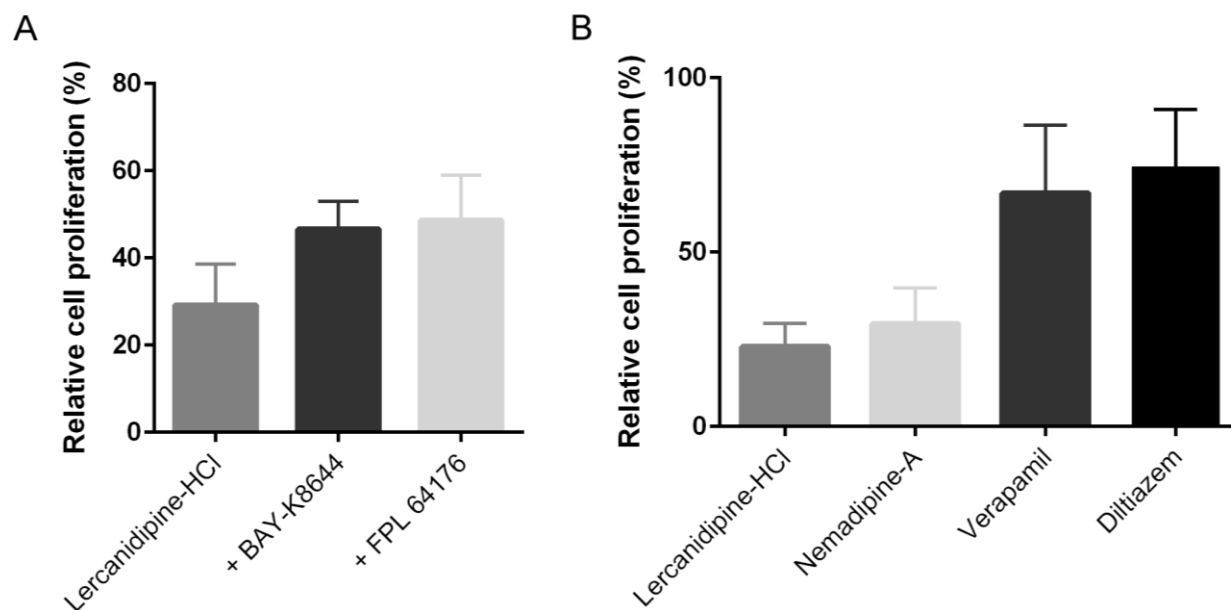


Figure 21. Lercanidipine-HCl specifically targets CaV1.2 channels. (A) AML-MSCs proliferation after 48 h of combination treatment with Lercanidipine-HCl and CaV1.2 agonists, BAY-K8644 and FPL 64176 (10 μ M, n=3). (B) Cell proliferation of AML-MSCs after 48 h of treatment with CaV1.2 antagonists, Verapamil and Diltiazem (10 μ M, n=3). Cell proliferation (%) was determined in triplicate, by ATP assay, normalizing the value with respect to the control group (DMSO=100%).

3D-AML long term cultures set up

In the last years, many efforts have been spent in studying leukemia pathogenesis and the three-dimensional (3D) AML cultures, to simultaneously investigate the stromal cells role in leukemia progression, have been proposed as the eligible model to study new therapeutic approaches^{123,152,205}. The 3D hematopoietic culture models were designed to mimic the structure and the composition of the bone marrow niche, thus resembling the leukemic microenvironment. Hence, these 3D co-culture models were set up to contain AML primary leukemia cells and stroma bone marrow components, such as mesenchymal, endothelial and osteoblastic cells, on different scaffolds types^{132,142,206}. Here, we aimed to create a 3D model for pediatric AML studies and used an hydroxyapatite–Collagen type I scaffold, considering that hydroxyapatite is a close analogue of bone apatite, which is the foundation of the hard tissue in all vertebrates and is produced by bio-mineralization in the body, and of Collagen type I being is essential non-cell-component of the bone marrow niche.

3D-AML scaffold mimics the leukemia bone marrow niche *in vitro*

We selected a cohort of 22 AML bone marrow samples from patients at diagnosis of AML *de novo* (Table 1 “Material and Methods” section). Three different cell-stroma media conditions were used to test if the different components supported different AML primary cells proliferation and maintained the AML original characteristics detected at diagnosis. In detail, we used i) AML-MSCs; ii) a mixture of AML-MSCs and osteoblasts (OBs) cells (differentiated from AML-MSCs); iii) a mixture of AML-MSCs and HUVEC endothelial cells (Figure 22). The two last conditions have been evaluated since it’s well known that OBs and endothelial cells, such as mesenchymal stromal cells, are crucial components of the BM niche²⁰⁷. After seeding MSCs in the scaffold for 7 days, the cells grew along the inner surfaces of bone trabecular pores and formed a stable fibrous 3D structure. On scanning electron and inverted microscopy, the cells resulted tightly attached to the surface of bone trabecular. We observed the assessment of AML cells adherent to the scaffolds and to stroma surface. The Scanning Electron Microscopy (SEM) analysis showed the surface of the scaffold covered by MSCs, which exhibit cytoplasmic extensions. This finding guarantees the connection between cells and the anchor to the material and suggests a good cyto-compatibility and a high level of interaction with the biomaterial surface (Figure 23A-a,b,c). After confirming that the scaffold was well populated by stromal cells, thus resembling the BM niche, we seeded the AML primary cells. AML primary cells were cultured for 7, 14, and 21 days on these 3D structures and analyzed by SEM too (Figure 23A-d, white arrows). Additionally, to determine the robustness of the niche, the presence of cell-cell interaction and the distribution of feeder cells were also

visualized after 7, 14, and 21 days of cultures by immune-staining. In detail, immuno-fluorescence for phalloidin staining (Figure 23B) and immuno-histochemistry staining for CD45 were performed on scaffolds slides (Figure 23C). As illustrated in Figure 23, the scaffolds were populated after 21 days of cultures.

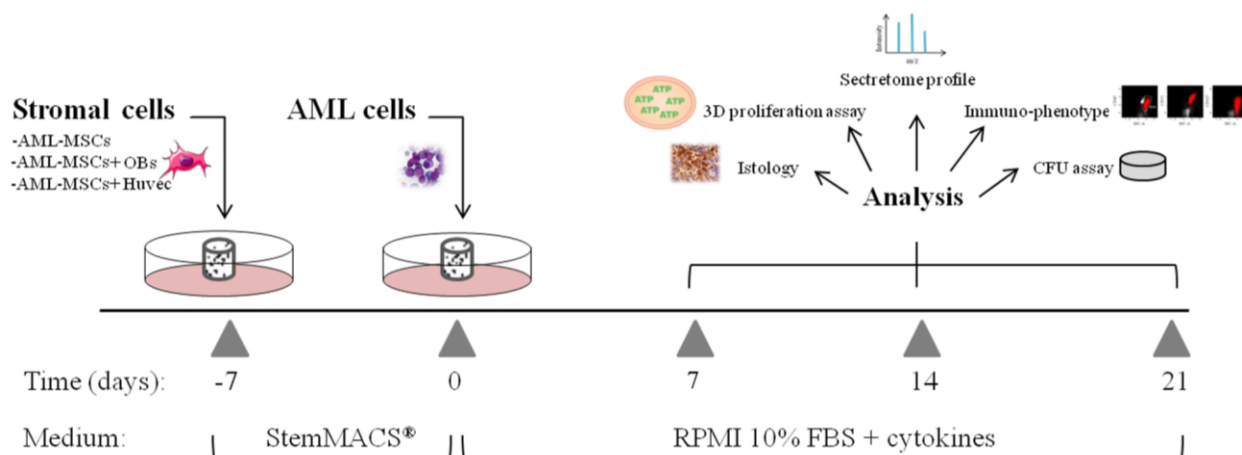


Figure 22. Scheme of the *in vitro* 3D culture set up procedure. Scaffolds were seeded with different human stromal cells, alone or with other components, and cultured in StemMACS® media for 1 week. AML primary cells were then added and cultured for 3 weeks in cytokines-supplemented media. Medium change was performed once per week, and differential analysis were also conducted at day 7,14, and 21. The 3D-leukemic cultures were maintained for 3 weeks in static environment.

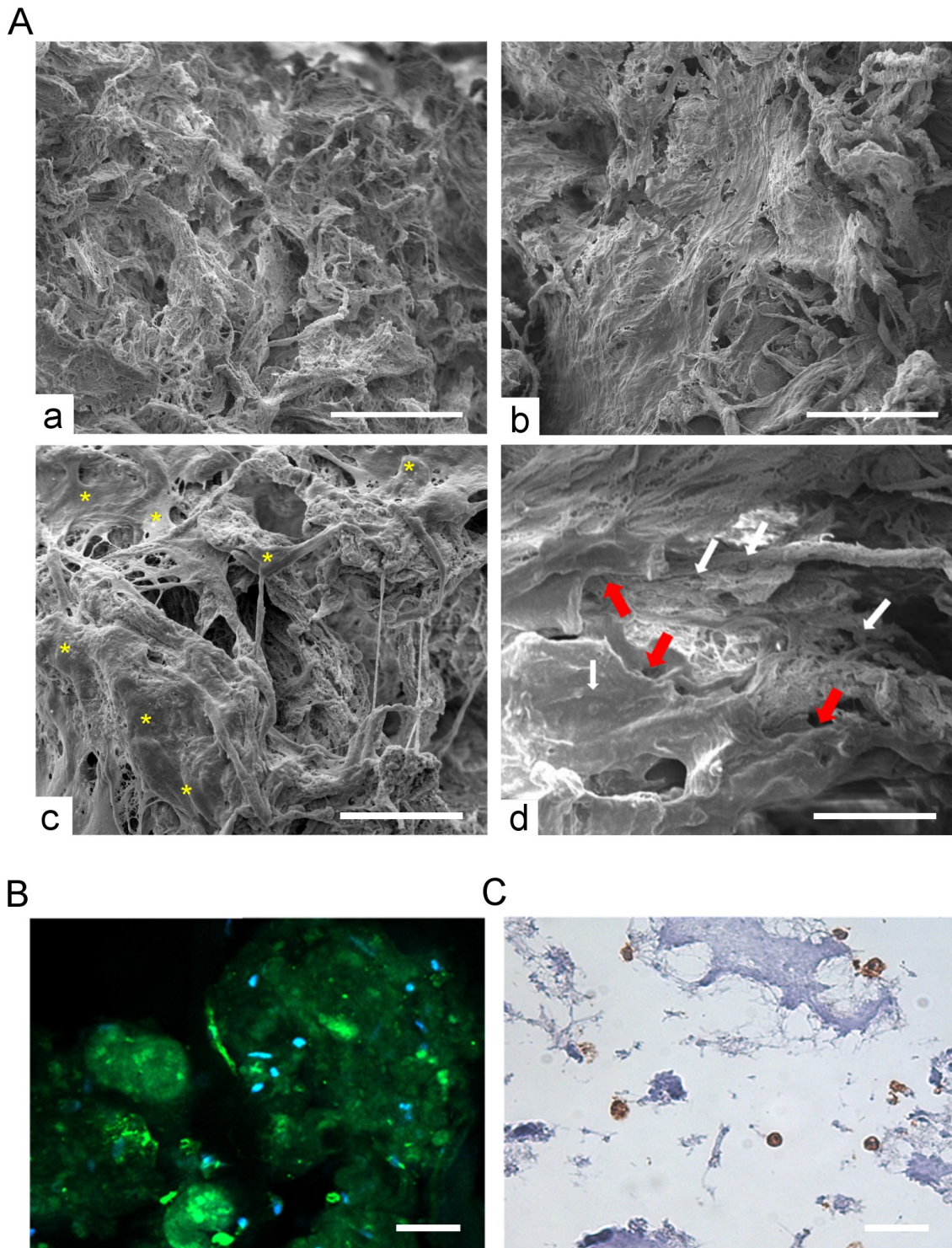


Figure 23. Scaffolds and 3D-AML cultures *in vitro* characterization. (A) SEM of upper surface of the freeze-dried hybrid scaffold MgHA/Coll (a). MSCs layer grown on the scaffold (b). MSCs (yellow asterisks) interacting with the scaffold surface (c). MSCs (red arrow) and AML primary cells (white arrow) after 7 days of co-culture (d). Scale bars= (a, b) 300 μ m; (c) 50 μ m; (d) 20 μ m. (B) immuno-fluorescence staining for phalloidin with 4',6-diamidino-2-phenylindole dihydrochloride (DAPI) nuclear counterstain (40x magnification, scale bar= 50 μ m). (C) DAB peroxidase stain of AML cells (CD45-positive cells) on 3D scaffold through inverted microscope after 21 days of 3D culture (40x magnification, scale bar= 50 μ m).

In order to determine whether the mesenchymal, endothelial, or osteoblastic cells in the 3D system were able to supply AML long-term cultures *in vitro*, the frequency of metabolically active proliferating cells, on 3D scaffold after 7, 14, and 21 days was investigated by ATP-3D assay. We found that AML primary cells proliferated in both AML-MSCs and AML-MSCs+OBs co-culture systems (Figure 24A). We appreciated that AML cells growth at maximum from day 7 and 14, and lowered but still proliferating until day 21. On the contrary, we noted that AML-MSCs with HUVEC reduced AML cells proliferation probably engulfing the 3D scaffold. This latter system was excluded from the rest of the experiments.

Then, we explored the 3D model for its ability to preserve the characteristic of the original patient' tumor in terms of clonogenic potential and the immuno-phenotype. We extracted cells from the 3D and seeded them in methylcellulose to determine whether the different artificial microenvironment affected AML precursors. We observed that colonies were formed from cells after 7 days in 3D, nevertheless, cells from the 3D culture containing AML-MSCs+OBs had a significant reduction of clonogenic potential at 14 and 21 days of culture with respect to the 3D culture containing AML-MSCs (Figure 24B). To study if the 3D long-term cultures maintained AML cell immune-phenotype as the original AML we analyzed several marker expressed and compared to diagnosis. AML cells after 7, 14, and 21 days in 3D cultures were found to maintain same immune-phenotype of day 0 (Figure 25).

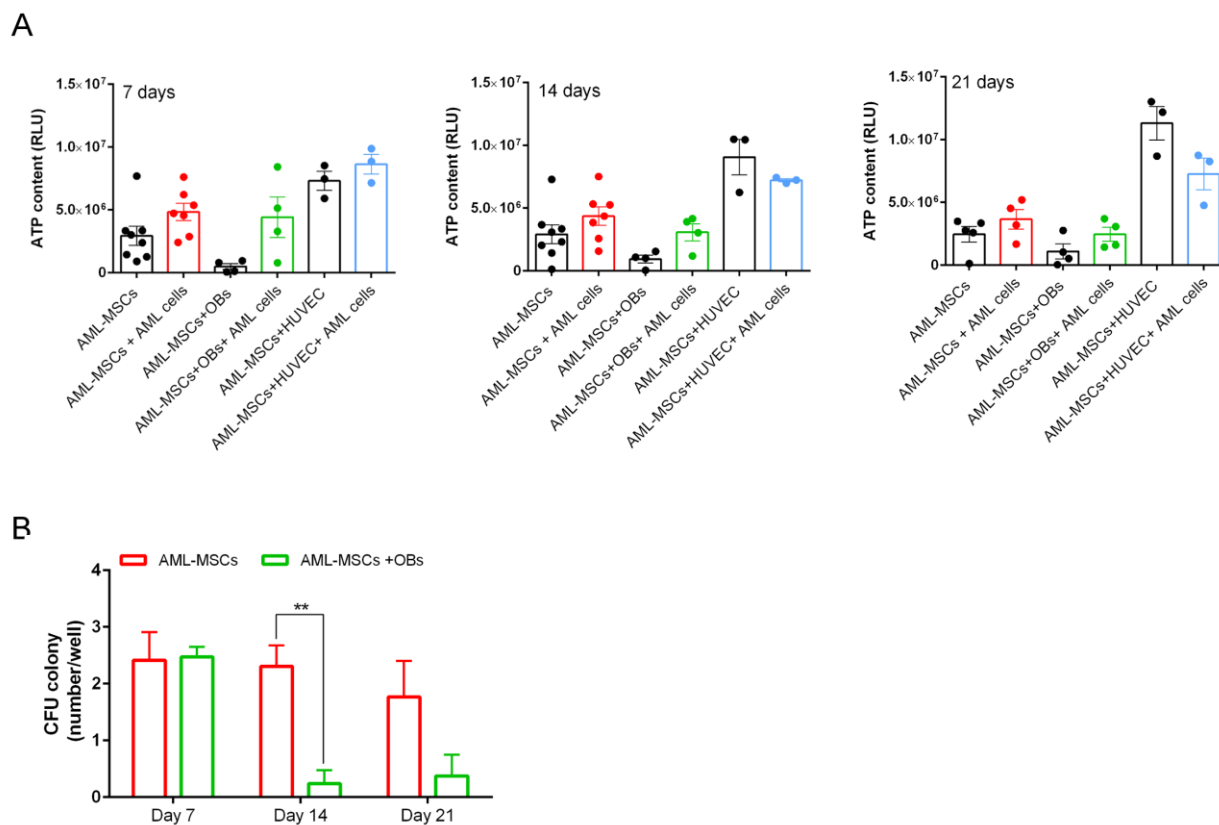


Figure 24. AML blasts proliferation in 3D. (A) Cell proliferation rate in the different 3D culture systems: AML blasts +AML-MSCs (red, n=7), AML-MSC+ OBs (green, n=4), and AML-MSCs+HUVEC (blue, n=3) at day 7, 14, and 21. Black column represent the ATP level of 3D culture system without AML cells. Data represent the average of 3D-ATP levels, expressed in relative luminescent unit (RLU), and error bars correspondent to s.e.m; three independent scaffolds for each experiment and for each time point were analyzed. (B) Average number of colonies grown from AML cells harvested from two different 3D culture systems (AML +AML-MSCs and AML + AML-MSCs +OBs) at different time points (** $p < 0.01$).

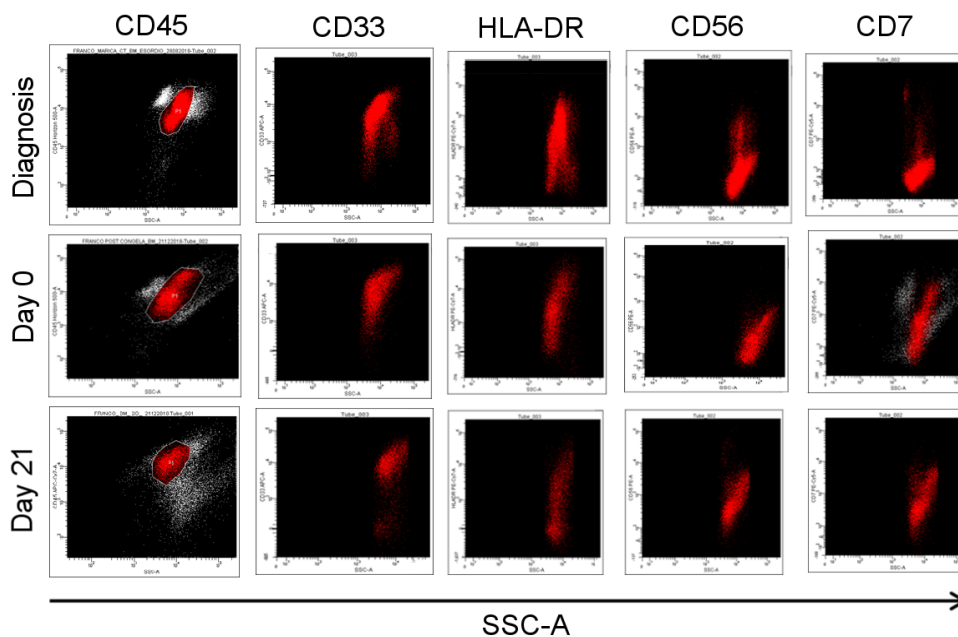


Figure 25. AML immune-phenotype in 3D cultures. Flow-citometry analysis comparative analysis of immunophenotype, of AML cells derived from AML patients at diagnosis, after thawing (day 0), and 21 days of 3D culture with AML-MSCs (n=3).

We concluded this *in vitro* analysis by determining the creation of a new 3D model for culturing AML in a niche together with AML-MSCs. This system allows leukemia proliferation with the maintenance of the original characteristics for long term.

3D-AML cultures secretome

It is still debated whether AML cells alter bone marrow niche microenvironment, but it was previously shown that the cytokine-mediated crosstalk between AML cells and MSCs can support leukemia²⁰⁸ and mediate resistance against chemotherapy²⁰⁹. In order to investigate if AML-MSCs contribute to AML support and proliferation with specific factors secretion, we studied the microenvironment created in our 3D-AML model by co-culturing AML-MSCs or h-MSCs with AML blasts. To reach this goal, we took advantage of SILAC labeling technique that is capable to detect any new expressed proteins in the medium if combined with Liquid chromatography-Mass Spectrometry (LC-MS/MS). MSCs and AML primary cells were co-cultured for 7, 14, and 21 days in appropriate medium (see Material and Method at SILAC section) and the production of new soluble factors in the 3D system was detected and measured by LC-MS/MS (Figure 26). LC-MS/MS results revealed a different secretome of our cultures. In detail, 22 different label-proteins secreted by AML-MSCs when compared to h-MSCs (criterion: FDR <0.01) were identified. 15 proteins showed at least two heavy-labeled peptides *per* protein and highly predicted to be newly synthesized and secreted in the 3D culture. On the contrary, there were 7 proteins that showed only

one labeled peptide *per* protein, including HSD3B2, MMP16, A2M, LUZP2, COL2A1, COL6A2, and ITIH6 with low confidential strength. Among the 22 proteins we found known factors in cancer such as CHI3L1²¹⁰, SERPINE1²¹¹, SPARC²¹², and BGN²¹³ (Table 6). Furthermore, we noticed that protein levels were stable over the 3 weeks experiment course, indicating a robustness for the 3D-AML environment (Table 6). In a comparative analysis of the secreted heavy-labeled proteins (with at least 2 peptides labelled) between h-MSCs and AML-MSCs we highlighted that CHI3L1 and SERPINE1 proteins were secreted was 16 and 10 time higher in AML-MSCs than those in h-MSCs (Figure 27 and 28). In addition, a new extrinsic oncosuppressor, PTX3²¹⁴, was completely absent at 7 days of AML-MSCs culture, and still 13 and 9 times lower than the level produced by h-MSCs at day 14 and 21, supporting that also by secretome AML-MSCs are supporting AML growth (Figure 28).

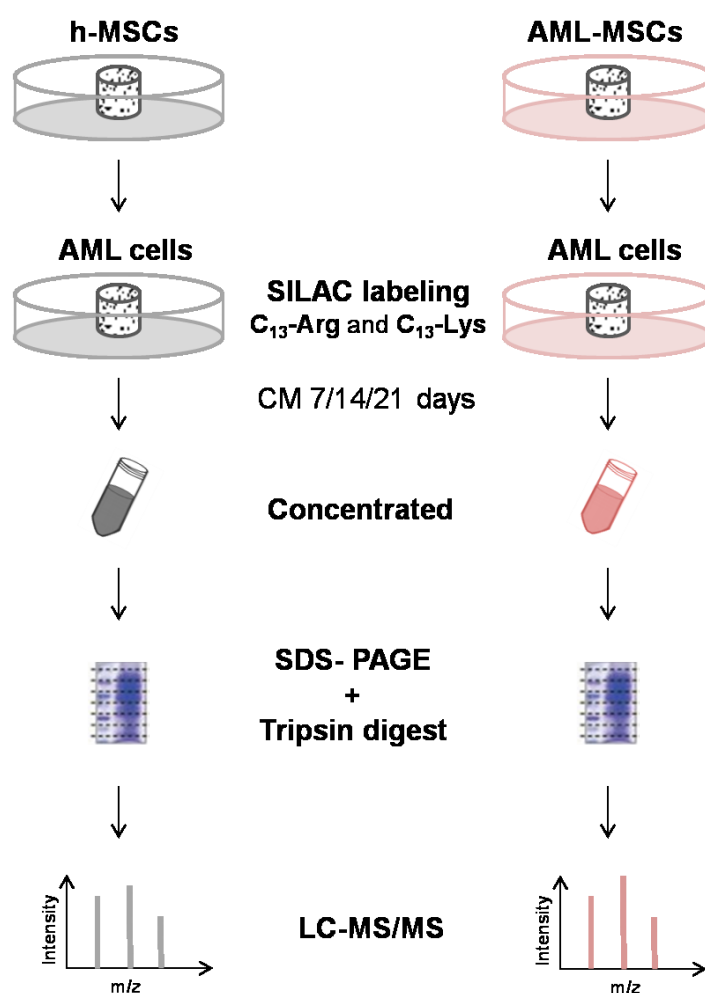


Figure 26. Secretome analysis pipeline. Schematic overview of the quantitative 3D secretome analysis performed after 7, 14, and 21 days of AML cells co-culture with AML or h-MSCs (n=3).

Protein ID	Protein name	Gene symbol	Ratio h-/AML-MSCs		Angiogenesis	inflammation	tumorigenesis
			7 days	21 days			
≥ 2 peptides label							
P36222	Chitinase-3-like protein1	CHI3L1	0,064	0,143		x	
P05121	Plasminogen activator inhibitor 1	SERPINE1	0,066	0,457			
P09486	Sparc	SPARC	0,405	0,364			x
P07858	Cathepsin B	CTSB	0,581	0,934			x
P12109	Collagen alpha-1(VI) chain	COL6A1	0,763	1,077			
P07585	Decorin	DCN	0,765	0,512	x		x
P01033	Metalloproteinase inhibitor 1	TIMP1	0,903	0,779			
P02452	Collagen alpha-1(I) chain	COL1A1	0,948	1,061			
P21810	Biglycan	BGN	0,997	0,871			
Q15063-3	Isoform 3 of Periostin	POSTN	1,182	0,705			x
P02751	Fibronectin	FN1	1,869	0,899			
P08123	Collagen alpha-2(I) chain	COL1A2	2,431	0,891			
P08253	72kDa type IV collagenase	MMP2	2,957	1,028	x		x
P07996	Thrombospondin-1	THBS1	5,899	0,737	x		x
P26022	Pentraxin-related protein PTX3	PTX3	n.d	9,994	x	x	x

Table 6. Secretome mass spectrometry analysis results. List of the 15 identified and quantified labeled peptides (two *per* protein) in 3D-AML culture. Ratio values represent the difference in the average of intensity for the heavy- peptides matches per protein between h-MSCs and AML-MSCs secretome. PTX3 at day 7 was not detected in the AML-MSCs condition.

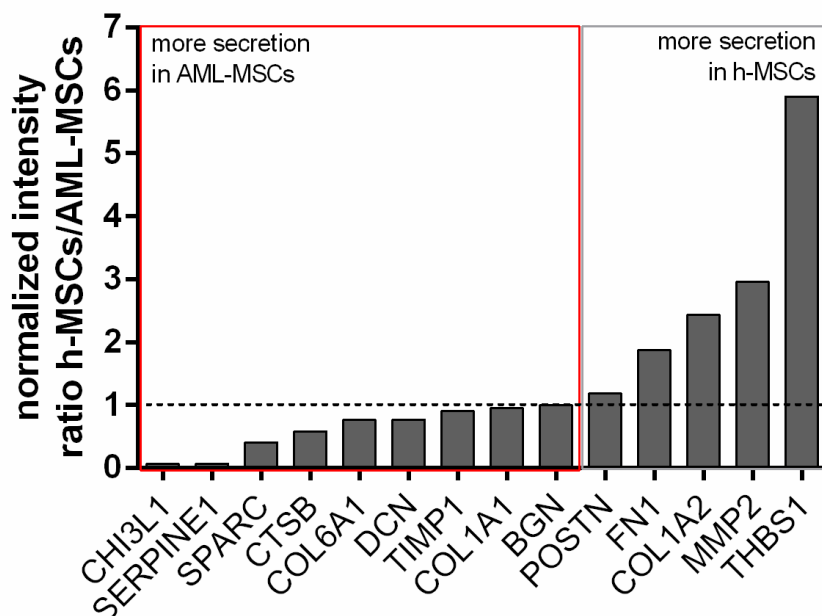


Figure 27. Histogram of proteins differentially secreted in AML-MSCs and h-MSCs 3D-AML culture at day 7. Drop line indicates the normalized intensity ratio h-MSCs/AML-MSCs: <1 define proteins more secreted in AML-MSCs cultures; >1 defines proteins more secreted in h-MSCs cultures.

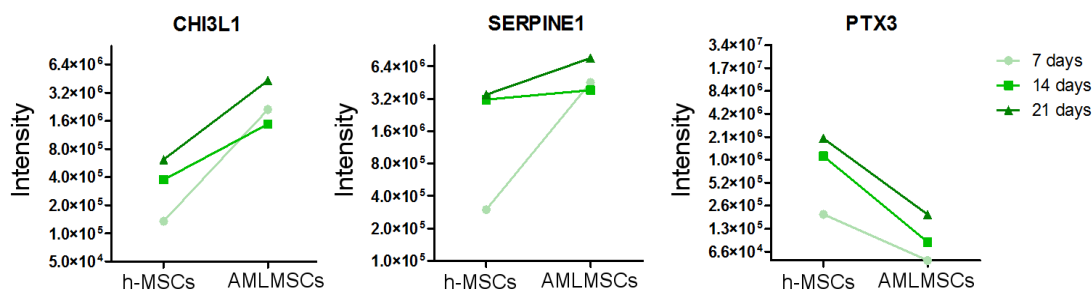


Figure 28. Representative protein expression in 3D-AML cultures secretome. Three representative proteins differentially expressed between AML-MSCs and h-MSCs in 3D-AML culture with similar trend at 7,14, and 21 days. Data indicate the average intensity for the heavy- peptides matches per protein.

Finally, to assess the relationship among the 22 heavy-labeled proteins identified by the LC-MS/MS, we tried an association network analysis by using STRING 11.0. We found all proteins interconnected through one association, with the exception of ITIH6, LUZP2 and HSD3B2. This finding suggests that AML-MSCs are distinctly expressing various proteins all linked together (Figure 29).

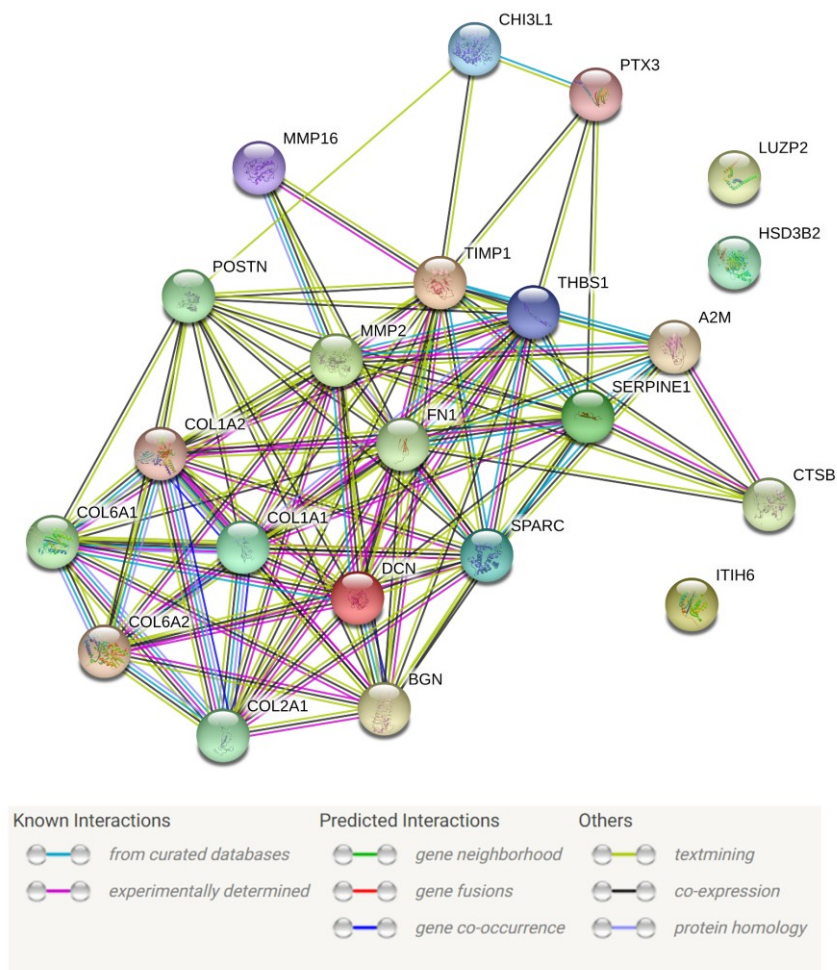


Figure 29. String analysis for the protein being differentially secreted in 3D-AML cultures. Meaning of network edges: evidence: line color indicates the type of interaction. Edge thickness indicated confidence of 0,9.

Gene Ontology revealed that proteins were mainly related to extracellular matrix, response to cytokines, response to oxygen-containing compound, and ossification pathways (Table 7); additionally, we recognized that the secretome of AML-MSCs contains a broad spectrum of over-produced factors implicated in angiogenesis, inflammation and cancerogenesis, as CHI3L1^{210,215} and SERPINE1^{211,216}. The above findings led us to consider a potential contribution of AML-MSCs to the state of inflammation present in the bone marrow niche during leukemia progression, as previously suggested^{195–197}, and support AML-MSCs to be targeted in patients with AML.

#pathway ID	pathway description	observed gene count	false discovery rate	matching proteins in your network (labels)
GO:0030198	extracellular matrix organization	15	3.95E-20	A2M,BGN,COL1A1,COL1A2,COL2A1,COL6A1,COL6A2,DCN, FN1,MMP16, MMP2,SERPINE1,SPARC,THBS1,TIMP1
GO:0002576	platelet degranulation	6	1.07E-06	A2M, FN1,SERPINE1,SPARC,THBS1,TIMP1
GO:0010033	response to organic substance	15	1.07E-06	BGN,CHI3L1,COL1A1,COL1A2,COL2A1,COL6A1,COL6A2,CTSB,DCN, FN1, MMP2,SERPINE1,SPARC,THBS1,TIMP1
GO:0070208	protein heterotrimerization	4	1.07E-06	COL1A1,COL1A2,COL6A1,COL6A2
GO:0071310	cellular response to organic substance	14	1.07E-06	BGN,CHI3L1,COL1A1,COL1A2,COL2A1,COL6A1,CTSB,DCN, FN1, MMP2,S ERPINE1,SPARC,THBS1,TIMP1
GO:0001501	skeletal system development	8	2.28E-06	CHI3L1,COL1A1,COL1A2,COL2A1,MMP16,MMP2,SPARC,TIMP1
GO:0045055	regulated exocytosis	9	2.44E-06	A2M,CHI3L1,CTSB, FN1,PTX3,SERPINE1,SPARC,THBS1,TIMP1
GO:0034097	response to cytokine	10	4.35E-06	BGN,CHI3L1,COL1A1,COL1A2,DCN, FN1,MMP2,SPARC,THBS1,TIMP1
GO:0071345	cellular response to cytokine stimulus	9	2.49E-05	BGN,CHI3L1,COL1A1,COL1A2,DCN, FN1,MMP2,THBS1,TIMP1
GO:0042060	wound healing	7	2.86E-05	A2M,COL1A1,COL1A2,DCN, FN1,SPARC,TIMP1
GO:0032963	collagen metabolic process	4	2.87E-05	COL1A1,CTSB,MMP16,MMP2
GO:0022617	extracellular matrix disassembly	4	3.33E-05	A2M,MMP16,MMP2,TIMP1
GO:0018149	peptide cross-linking	4	3.35E-05	BGN,DCN, FN1,THBS1
GO:0050790	regulation of catalytic activity	12	3.35E-05	A2M,BGN,CHI3L1,CTSB,DCN, FN1,ITIH6,MMP16,PTX3,SERPINE1,THBS1, TIMP1
GO:0071230	cellular response to amino acid stimulus	4	3.35E-05	COL1A1,COL1A2,COL6A1,MMP2
GO:1901700	response to oxygen-containing compound	10	3.75E-05	COL1A1,COL1A2,COL6A1,COL6A2,DCN,MMP2,SERPINE1,SPARC,THBS1, TIMP1
GO:0043086	negative regulation of catalytic activity	8	5.12E-05	A2M,BGN,DCN,ITIH6,PTX3,SERPINE1,THBS1,TIMP1
GO:0072359	circulatory system development	8	5.12E-05	COL1A1,COL1A2,COL2A1, FN1,MMP2,SERPINE1,SPARC,THBS1
GO:0001503	ossification	5	0.00012	COL1A1,COL2A1,MMP16,MMP2,SPARC
GO:0001958	endochondral ossification	3	0.00015	COL1A1,COL2A1,MMP16
GO:0016525	negative regulation of angiogenesis	4	0.00015	DCN,SERPINE1,SPARC,THBS1
GO:0052547	regulation of peptidase activity	6	0.00015	A2M, FN1,ITIH6,SERPINE1,THBS1,TIMP1

Table 7. Gene Ontology analysis of 3D-AML cultures. Distribution into biological processes of the 22 proteins differentially secreted in AML-MSCs and h-MSCs 3D culture.

Drug screening in 3D-AML cultures

Treatment of patients with leukemia means treating leukemia cells within their niche, including non-hematopoietic stromal cells. Our 3D model provides an opportunity to study drug response in a physiological three-dimensional context. Thus, we moved toward assessing an innovative 3D-AML model to test drug's efficacy since the 3D model might recapitulate the leukemia niche. Furthermore, this 3D model permitted to 1) combine treatments to attest new synergistic therapeutic effects, 2) to reduce the doses of chemotherapies (thus toxicity), and 3) to minimize or delay the induction of drug resistance, with the final aim that new treatment combinations would give great benefits to children. For these reasons, we decided to combine the targeting of AML-MSCs by applying less intensive treatment towards AML. We used targeted AML drugs, such as the Quizartinib and I-BET151, a *FLT3* inhibitor and a Bromodomain and Extra-Terminal motif (BET) inhibitor, respectively to treat primary cultures harboring *FLT3ITD* mutation²¹⁷ and *MLL*-rearrangements²¹⁸ by following the treatment pipeline described in Figure 30. In this pilot 3D treatment we pursued the idea that AML-drugs would be effective exclusively on blast without effects over AML-MSCs, as we performed for the AML-MSCs selecting a drug that did not destroy

AML cells (see Figure 17). Thus, Quizartinib and I-BET151 doses were tested on AML-MSCs to support their use: we appreciated that after 72 h of Quizartinib and I-BET151 treatment there was a significant decrease in the proliferative response of AML cells in 2D conditions with increased doses, with an IC_{50} at 0.2 and 0.5 μ M, respectively (Figure 31A and B), with no effects exerted on AML-MSCs. To note, we cannot have a 3D- IC_{50} for AML drugs because blasts cannot grow alone in 3D, but need the MSCs. Subsequently, we defined the IC_{50} of Lercanidipine-HCl on AML-MSCs in 2D and in 3D systems. After 72 h of Lercanidipine-HCl treatment, there was a significant decrease in the proliferative response of AML-MSCs in 2D condition with increased doses, with an IC_{50} of 4.5 μ M (Figure 31C), this latter increasing when in 3D being found of 35 μ M (Figure 31D). This comparison of IC_{50} in 2D and 3D systems indicated that 3D co-culture conditions increased the efficacious dose when compared to 2D condition, confirming the greater relevance of 3D model and the limit of a treatment over-estimation effects in 2D cultures. The same experiment was performed using the 3D model with h-MSCs, as negative control, and after 72 hours from the treatment we could appreciate significant differences in treatment to obtained the AML-MSCs decreased proliferation <50%, and the h-MSCs being still more proliferative at these higher doses (Figure 31D, previously we used Lercanidipine-HCl in 2D at 10 μ M).

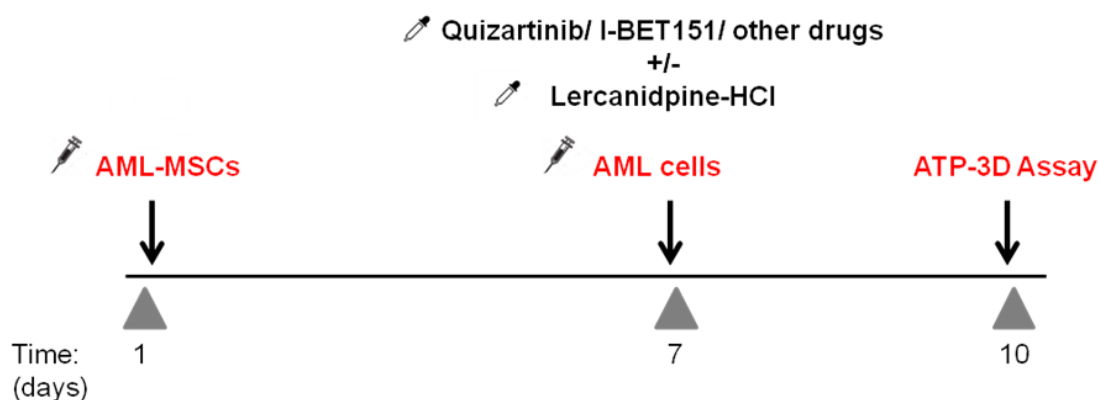


Figure 30. Scheme of drug combination treatment on 3D-AML cultures *in vitro*. AML-MSCs were seeded in the scaffold and cultured in StemMACS[®] media for MSCs expansion for 1 week. Then, AML primary cells were added into the scaffold and exposed to drugs (Quizartinib or I-BET151) alone, or in combination with Lercanidipine-HCl in cytokines-supplemented media for AML expansion. Proliferation of the whole system was performed after 3 days of treatment by 3D ATP assay.

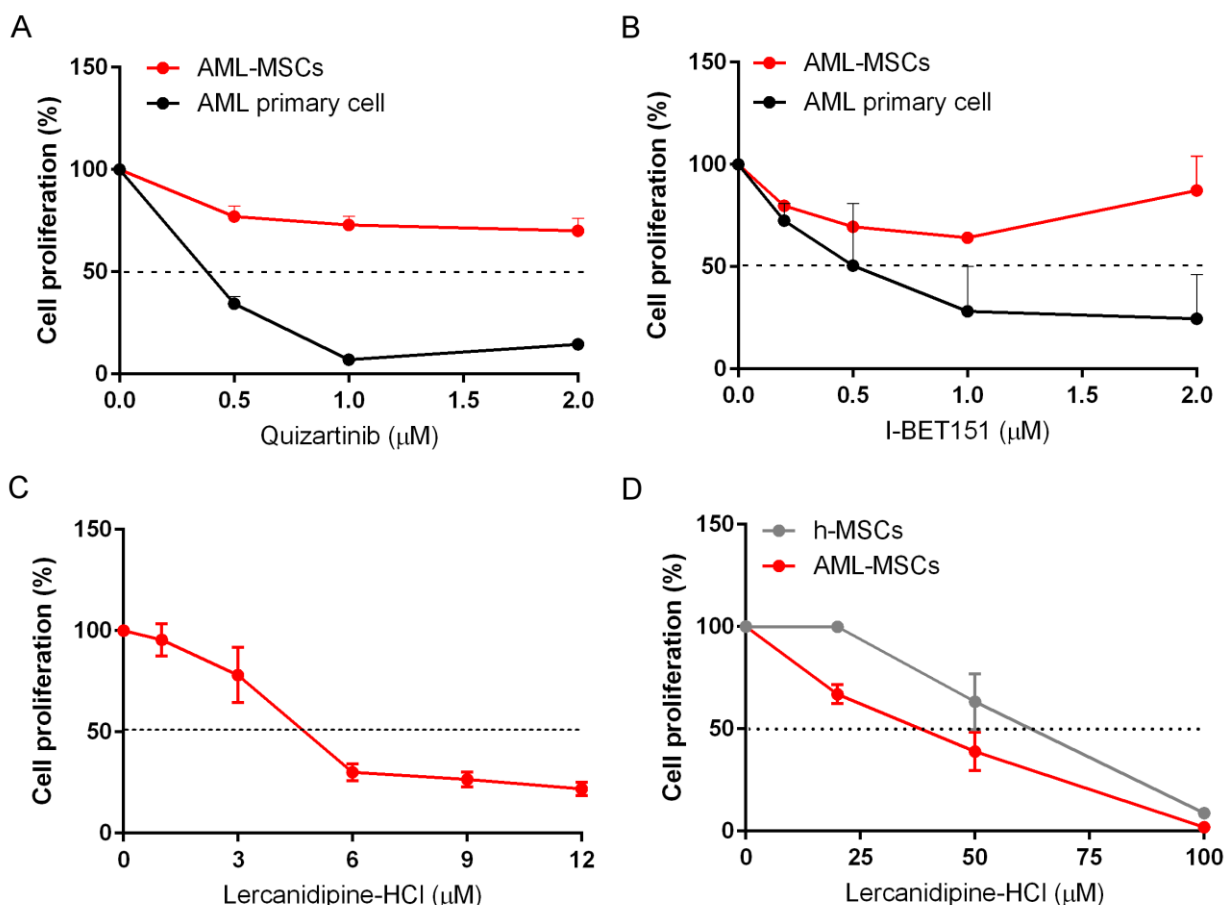


Figure 31. (A) Quizartinib and (B) I-BET151 dose-dependent proliferation reduction of AML primary cells and AML-MSCs after 72 hours of treatment in 2D (n=3). (C) Lercanidipine-HCl dose-dependent proliferation reduction of AML-MSCs in 2D after 72 hours of treatment (n=3). (D) Lercanidipine-HCl dose-dependent proliferation in 3D culture after 72 h of treatment of AML-MSCs (red line) and h-MSCs (grey line); two independent scaffolds for each experiment and for time points were analyzed (n=3). Drop line show the IC₅₀ cut off.

Hence we performed a 3D drug testing with primary AML and AML-MSCs at the indicated concentration of drugs (Quizartinib 0.2 μM or I-BET151 0.5 μM) except for the dose of Lercanidipine-HCl in which we used the dose corresponding to IC₂₅ in order to appreciate the synergistic effect. To note, in our 3D co-culture system, AML and AML-MSCs grew together and we evaluated the proliferative response/cytotoxicity to chemotherapy in 3D cell culture system by the 3D-ATP assay after 72 h of treatment. As shown in Figure 32, there was no significant cytotoxicity in 3D at 0.2 and 0.5 μM concentration of Quizartinib and I-BET151 that correspond to IC₅₀ in 2D, and a lower effect of Lercanidipine-HCl in the 3D when used alone (IC₂₅). Finally, we determined the cytotoxic potency of this assay showing the combined treatment significantly synergistic (Figure 32A and B, combination index (CI)= 0.5). Finally, we expanded the study including another targeted drug for *c-KIT* mutated AML, the Dasatinib. Similarly, to the previous experiments this combined treatment with Lercanidipine-HCl showed a reduction of cell proliferation with an additive effect (CI=1) respect to the single treatment (Figure 32C).

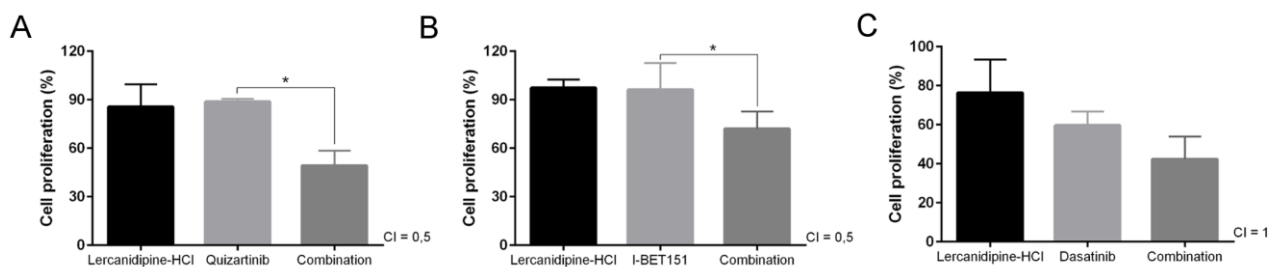


Figure 32. Combined drug treatment in 3D-AML cultures. Cell proliferation of AML-MSCs and AML harboring *FLT3* mutations (A), *MLL*-rearrangement (B) and *c-KIT* mutation (C) were analyzed after 72 h of single treatment, Quizartinib (A) I-BET151 (B), Dasatinib (C) or in combined therapy with Lercanidipine-HCl. Graphs represent cell viability of single and combined therapies normalized to the respective controls (DMSO), whose value is set to 100%. Data are the average of 3D-ATP levels measurements and error bars correspondent to s.e.m. (n=3 (A and B), n=1 (C), two independent scaffolds for each experiments were analyzed, * $p < 0.05$); combination index (CI) was calculated using the method of constant ratio drug combination proposed by Slinker¹⁹³.

Use of the humanized 3D-AML niche to improve AML dissemination and engraftment *in vivo*

To date, *in vivo* experimentation represents the pre-clinical model for a drug testing. However, AML cells engraftment in mice showed low success rate mostly because the engraftment capability varies considerably depending on AML risk group, the quality of the sample and many other variables still obscure²¹⁹. In recent years the use of humanized bone marrow organoids or ossicles *in vivo* has been evaluated as a strategy to improve the engraftment of leukemia, mostly in adults AML context^{133,181,185}. To date, for pediatric AML no available results have been reported. At this purpose we studied several strategies, and first of all we tried to translate our 3D *in vitro* model in *in vivo* in order to determine whether AML-MSCs and AML cells seeded on hydroxyapatite scaffolds could establish an ectopic human bone marrow environment able to sustain AML proliferation and dissemination in the mice bone marrow. We used two different immunodeficient mice strains: common NSG (NOD.Cg-Prkdcscid Il2rgtm1Wjl/SzJ) and transgenic humanized mice expressing human IL 3 and human GM-CSF (NOD.Cg-Prkdcscid Il2rgtm1Sug Tg(SV40/HTLV-IL3,CSF2)10-7Jic/JicTac). In addition, young mice of 4-6 weeks old were used, and AML samples were depleted of the T cells (CD3⁺) in order to avoid graft-versus host disease risk.

3D-humanized AML niche implantation in NSG mice

A cohort of 15 patients affected by AML *de novo* (Table 8) was selected for establishing the 3D-AML cultures to be then implanted in mice (a number of 3 to 5 implanted mice *per* AML sample).

Patient ID	Molecular	Risk	Age	Gender
AML#1	negative	IR	17	M
AML#2	NUP98-NSD1, FLT3-ITD	HR	4	M
AML#3	negative	IR	10	M
AML#4	MLL-AF6	HR	16	M
AML#5	NUP98-NSD1, FLT3-ITD	HR	17	M
AML#6	MLL-AF6	HR	12	M
AML#7	NPM1 ^{MUT} , FLT3-ITD	HR	5	F
AML#8	MLL-AF10	HR	7	M
AML#9	FLT3-ITD	HR	18	M
AML#10	negative	IR	15	F
AML#11	negative	IR	2	M
AML#12	MLL-MLL (PTD), FLT3-ITD	HR	13	F
AML#13	NPM1 ^{MUT}	SR	9	F
AML#14	NUP98-NSD1, FLT3-ITD	HR	6	M
AML#15	NPM1 ^{MUT} -MLF1, FLT3-ITD	HR	7	M

Table 8. Biological and clinical characteristics of the AML patients' samples enrolled in *in vivo* experiments. Risk classes according to LAM2013-AIEOP trial^{4,189}. SR, standard risk; IR, intermediate risk; HR, high risk; negative, no mutations found by the current genetic screening; Age in years; M, male; F, female.

Briefly, in this model, leukemia cells were injected in the scaffolds before coated for 24 h with AML-MSCs *in vitro*; then the AML cells were seeded in AML-MSCs-scaffolds, and were implanted subcutaneously in the back of NSG mice (Figure 33A). Animals were sacrificed in a time ranging from 3 weeks to 12 months after scaffolds implantation without any sign of disseminated leukemia (humanCD45 cells monitored in the peripheral blood every 15 days). Thus, we studied leukemia niche *in vivo* by harvesting the scaffolds at various time points (at 1, 3, and 6 months) and with different immuno-histochemical stainings. As shown in Figure 33B, human CD45-positive cells were found still in the scaffolds. Analysis of the scaffolds at 3 weeks were performed to test the *bona fide* of this niche and revealed mouse vascularization pervading the exogenous structure, the presence of osteoblasts derived from human MSCs, both analyses suggesting that human MSCs survived in 3D and differentiated creating an ectopic human bone marrow microenvironment (Figure 33B). Next AML cells were also investigated and found in the scaffold by luciferase intensity after 3 months from the transplantation (Figure 33C), and longer, up to 12 months.

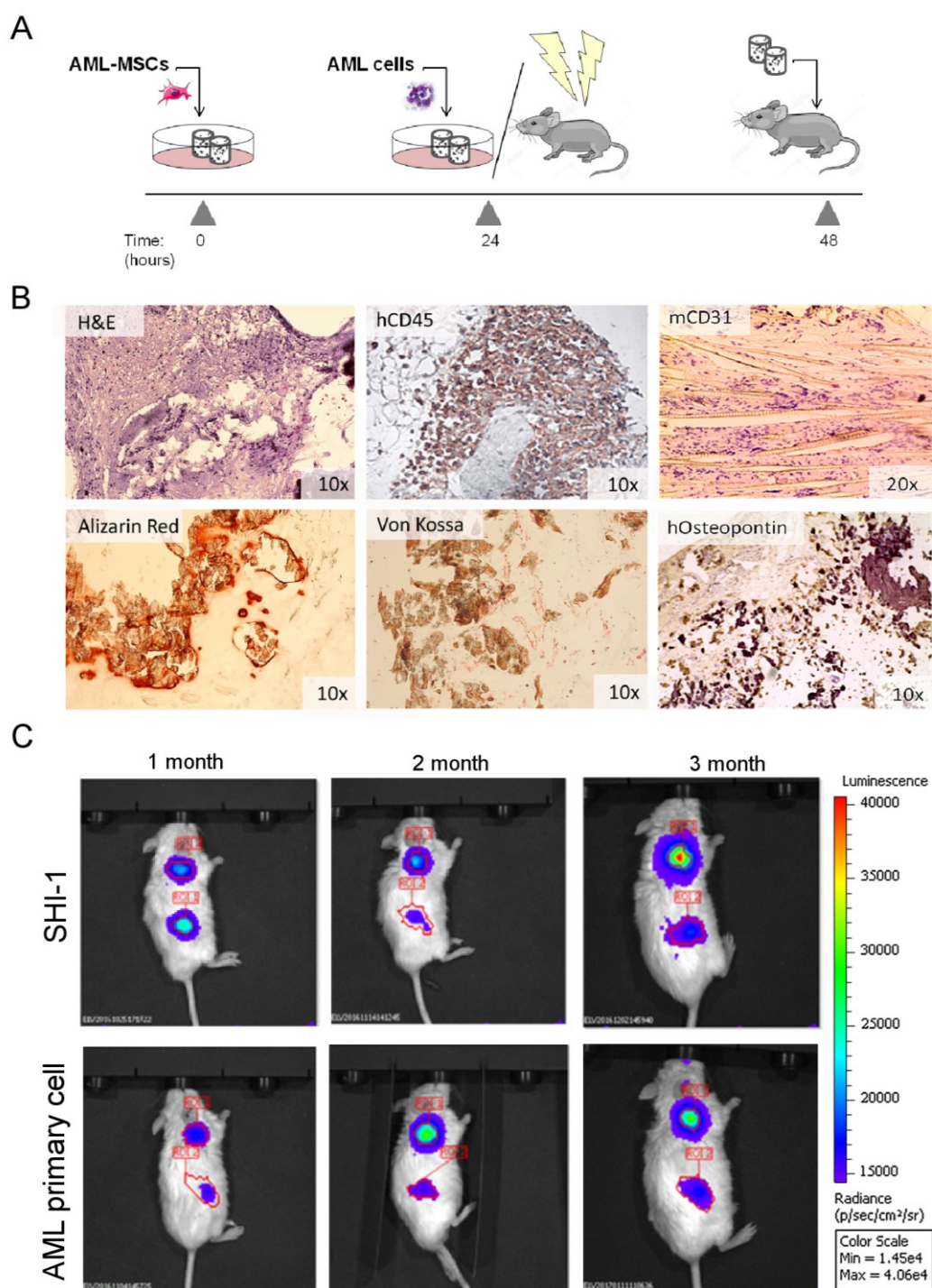


Figure 33. Evaluation of humanized 3D-AML niche *in vivo*. (A) Pipeline of 3D-AML culture preparation for *in vivo* implant by the pre-seeding of AML cells 24h before *in vitro*. (B) Histochemical stainings on 3D scaffolds after 3 weeks post-implantation: representative image of H&E stain, DAB peroxidase stain for human CD45 (brown) and for murine CD31, Alizarin Red stain, Von Kossa stain and DAB peroxidase stain for human Osteopontin (brown). (C) AML cells (after being transduced with luciferase gene) proliferation in 3D *in vivo*. Time lapse of bioluminescence of AML cells line (SHI-1) and AML primary cells were confirmed up to 3 months post-implantation. Radiance intensity is shown as colors scale.

Next, we asked if AML grew in the ectopic niche preserving its features of diagnosis. We investigated the molecular marker found at diagnosis, when present, by Trizol reagent for RNA extraction and the dissociation of the 3D scaffolds. Results by PCR confirmed that 4 out of 5 samples, collected in a ranging time of 4 to 12 months from implantation, still harbored the genetic rearrangements of the leukemia of the patient at diagnosis.

Finally we concluded that MSCs-3D-AML niche resulted in a functional human hematopoietic microenvironment integrated in the bone marrow of the murine host where AML cells survived and proliferated in the humanized niche. The scaffolds were well tolerated in the NSG hosts, without infection nor ulceration. To note, after 7 months from the implantation only one mouse model (AML#8) out of the 15 AML cases (38 injected mice) gave rise to an AML in mice. However, to date, 12 months later AML cells were present in the 3D, suggesting their preferentially reside into the human microenvironment recreated. Furthermore, the implementation with pharmacological mobilization strategy, by AMD3100 administration²²⁰, did not give any sign of AML dissemination out of the 3D.

Humanized 3D-AML model for a local drug testing *in vivo*

Considering that numerous findings about the interaction between AML cells and leukemia bone marrow niche had revealed a key role of MSCs in chemo-protective role³⁶, we therefore asked whether the humanized bone marrow niche in mice could be used as a platform for drug testing, mimicking the patient' response to treatment and focusing on new drugs that are moving to clinic now or that target BM stromal components. Our data demonstrated that the 3D structure maintained AML cells viable *in vivo*, opening for the possibility to perform preliminary 3D drug screening *in loco* by transducing AML cells with luciferase before transplantation and measuring luciferase reduction as the read-out of drug efficacy.

Up to now, we performed a pilot test with AML cell line (SHI-1, luciferase positive cells) being injected in scaffolds and implanted in NSG mice as described in figure 34A. All mice had AML in the 3D scaffolds after 10 days from the implantation, thus mice were divided into six treatment groups: one received DMSO as vehicle, one received Venetoclax (100 mg/Kg) by oral administration for 22 days, and the other four groups received by intraperitoneal injection for 22 days of AraC (50mg/Kg), Thioridazine (8 mg/Kg), I-BET151 (30 mg/Kg), and 5-Azacitidine (5 mg/Kg). The long-term follow-up of these animals showed great results in terms of drug efficacy. Briefly, all treated mice reduced luciferase intensity of the AML with respect to DMSO-treated

mice in the 3D (Figure 34). In particular a significant reduction of AML proliferation after I-BET151, Thioridazine, and 5-Azacytidine was observed. However, such as for the above experiments, AML did not show any systemic invasiveness or tissue destruction in all these animals. The first pilot study with an AML-luciferase primary culture with AML-MSCs in 3D scaffolds is under evaluation with the combined treatment AraC+ Lercanidipine-HCl.

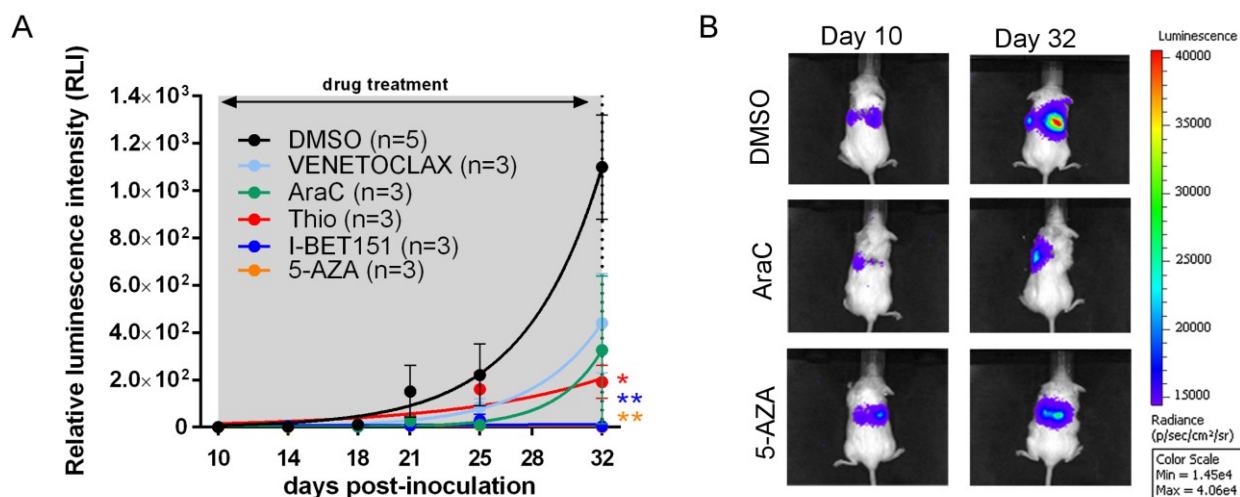


Figure 34. *In vivo in loco* 3D-AML drug screening. (A) Luminescence detection of luciferase-transduced SHI-1 cells at the indicated time points, representing the AML proliferation rate in the 3D niche. All values normalized to the initial intensity before starting treatment. Mice were treated daily from day 10 at following doses: Venetoclax 100mg/Kg (p.o.), AraC 50mg/Kg (i.p.), Thioridazine 8mg/Kg (i.p.), I-BET151 30mg/Kg (i.p.), 5-Azacytidine 5mg/Kg (i.p.); * $p < 0.05$, ** $p < 0.01$ (B) Representative time lapse of luciferase-AML cell line SHI-1 in mice *in loco*, in the 3D scaffolds, at day 10 (the start of treatment) and at day 32 (the end of treatment).

Discussion and Conclusion

The BM microenvironment have been shown to play a role in the pathogenesis of a variety of hematological malignances, including AML, MM, lymphomas, and MDS^{91,221}, with MSCs as key components of the BM milieu^{52,166}. MSCs regulate normal hematopoiesis through cell-cell interaction with HSCs or via the release of paracrine factors within functional BM niche; on the other hand, MSCs contribute to the maintenance of hematopoiesis by regulating self-renewal, differentiation, survival and apoptosis. In hematopoietic malignancies, BM stroma is likely to be considered accessory to tumor development, promoting the microenvironment to support tumor proliferation, clonal evolution, cell migration and chemoresistance, thus permitting tumor progression and immune escape¹⁰³. Furthermore, studies using animal models reported peculiar changes in the BM niche cells after leukemia engraftment thus sustaining its modification during tumor initiation^{70,71,73}. Regardless, a deeper understanding of the MSCs role in pediatric AML may lead to novelty in treatment opportunities and leukemogenesis.

Here, we report a detailed functional *in vitro* characterization of MSCs derived from a large cohort of pediatric AML bone marrow samples in comparison with those derived from healthy donors. This first part of the study showed a higher proliferation rate of the AML-MSCs with respect to h-MSCs. In support with this finding, other studies documented an altered AML-MSCs growth with changes in cell number in leukemia patients^{72,82,182}, suggesting MSCs plasticity and their role in remodeling the niche cellular composition during leukemia progression. Moreover, osteogenic differentiation capability of the MSCs were also described in adult AML patients¹⁸². Our analysis confirmed an higher osteogenic differentiation potential of the AML-MSCs when compared to h-MSCs; in particular, AML-MSCs produced mineral calcium deposition at the very beginning of the induced differentiation process with respect to the h-MSCs that completed their differentiation later. This latter finding was supported by an higher expression levels of some osteo-progenitor-associated genes, including *TNAP* and *OPN* associated to AML-MSCs. Taken together, these data sustain that AML may induce a primed osteoblasts/osteo-progenitors populated niche to enhance AML cells expansion, thus conferring to MSCs a role in promoting disease progression.

MSCs are known for their immunomodulatory and anti-inflammatory properties by the release of secreted cytokines and proteins, reducing the *in vitro* and *in vivo* angiogenesis, as well as preventing tumor progression¹⁹⁴. In solid tumors a concrete evidence of an immune suppression mediated by

altered stromal environment enabling cancer cell growth was previously demonstrated²²². However, similar role for MSCs in AML has never been depicted. This is partially due to the fact that there is a lack of studies addressing the anti-inflammatory nature of MSCs derived from AML patients. Nevertheless, an high microvascular density is known to occur in the BM of patients with hematological malignancies, correlating with therapy resistance, support angiogenetic process also within the leukemic niche¹⁹⁵⁻¹⁹⁷. We tried to explore this phenomenon *in vitro*, and observed a different HUVEC capability to form capillary-like tubes when co-cultured with AML-MSCs or h-MSCs. In particular, AML-MSCs did not exert an anti-angiogenic ability dampening or maintaining the inflamed tumor microenvironment, whereas the h-MSCs abolished this angiogenic-like HUVEC capability thanks to their physiological activity being exerted.

In the light of all these results we supposed a pivotal role of MSCs in regulating hematopoietic niche and inferred whether also hematopoiesis could be affected. We explored this theory by culturing healthy CD34⁺ hematopoietic progenitor derived from cord blood cells together with AML-MSCs or h-MSCs. In this experimental model we observed a lower overall expansion and differentiation potential of healthy CD34⁺ hematopoietic progenitors when co-cultured with AML-MSCs. This observation suggests that h-MSCs support the normal hematopoietic differentiation process, whereas AML-MSCs maintain the undifferentiated CD34⁺ cells for longer time during which, potentially, the transformation process could initiate. It is unclear whether hematopoietic differentiation is delayed or blocked by AML-MSCs; however, further time-course analyses would elucidate this aspect. It has been reported that several factors and proteins, such as Osteopontin (OPN), are able to modulate the HSCs proliferative capacity within the BM microenvironment²²³. Corroborating this notion, we demonstrated that the *OPN* mRNA expression in AML-MSCs was increased with respect to the h-MSCs. Based on these observation, we hypothesized that AML-MSCs might be reprogrammed to control the proliferation of HSCs, thereby limiting their contribution to hematopoiesis in the BM and promoting leukemia progression through unbalanced competition. Hence, the AML-MSCs remodeling of the niche, resulting in an aberrant microenvironment, may be a pathogenic mechanism of the leukemia itself. Afterwards, we developed a cell co-culture model to test if a transformation potential was intrinsic of the MSCs when derived from the AML by using murine IL 3-dependent 32D cell line^{199,200}. We evaluated that the presence of AML-MSCs allowed 32D cells growth independently of IL 3, ascribing a potential oncogenic role to these cells which permitted to the 32D cells to survive in a cytokine-independent conditions.

In view of these biological and functional properties being peculiar of the AML-MSCs, we hypothesized that the gene expression pattern of these cells could be different from those of the h-MSCs. Accordingly, we performed GEP analysis and found a peculiar gene expression signature in AML-MSCs with networks involved in IL 17, response to hypoxia, cell differentiation, as well as regulation of protein transport and cytokines production. Interestingly, IL 17 plays a crucial role in both acute and chronic inflammatory response, supporting our *in vitro* results about the reduced anti-inflammatory capability observed for the AML-MSCs, and supporting the concept that leukemia niche is an inflammatory microenvironment²⁰². Furthermore, many genes de-regulated in AML-MSCs were highly enriched among GO categories related to “cytokines production” implicating an involvement of excessive cytokine activity in the leukemia context. In line with these results, recent animal studies demonstrated that an excessive cytokine secretion could drive niche alteration^{79,194,222}; however, a study of the cytokines and factors produced by AML-MSCs is necessary in order to appoint a role to MSCs in the pathogenesis of leukemia.

All together these data open for a categorical question: whether acute myeloid leukemia derived from primary defects of HSCs or microenvironment modifications are leading to hematopoietic cell transformation. In other words, we wonder if stromal cells acquire mutations as primary events and then induce the hematopoietic cell transformation and disease onset, or if the AML-MSCs represent an adaptations of the h-MSCs to leukemia cells occupying the niche. Previous results from mouse models were produced to support both hypotheses^{47,69,91}, but more recently published reports supported leukemia onset able to alter microenvironment in AML patients^{65,70,76}. Accordingly, we attempted to use GEP to clarify this point. GEP of the AML-MSCs and the MSCs collected after treatment and in disease remission (R-MSCs) was compared. Interestingly, we found a distinct clustering of the transcriptome profiling of the AML-MSCs and R-MSCs, with gene ontology analysis showing a strong enrichment for biological processes involved in the regulation of cell adhesion, blood development, ossification, response to growth factors, as well as negative regulation of cell proliferation. To note, these results reflected the *in vitro* documented AML-MSCs features that were not maintained in the R-MSCs by GEP. We finally explored a gene ontology comparative analysis considering the three different conditions used to derive MSCs, the healthy, AML and disease remission, evidencing that R-MSCs mirrored the h-MSCs transcriptome profile. In addition, we performed *in vitro* studies of R-MSCs proliferation and transforming abilities confirming their similarity to h-MSCs. These latter findings suggest a direct causal relationship between AML cells and the AML-MSCs, with peculiar stromal functions of h-MSCs restored in R-MSCs as soon as leukemic cells have been eradicated by therapy. These findings confirm that

leukemic cells alter MSCs transcriptome profile to confer aberrant proliferation, differentiation, and main physiologic functions towards transforming abilities.

In line with these findings, we produced preliminary data on an experimental model of iPSCs with inducible expression of the *CBFA2T3-GLIS2* translocation known to originate a megakaryoblastic AML^{188,201}. Our results suggested that AML-MSCs when cultured together with *CBFA2T3-GLIS2*-translocated blasts were able to trigger (as driving force) or/and enhance (or anticipate) the hematopoietic differentiation block concurring to produce the megakaryoblasts expansion *in vitro*. Same abilities were observed in the iPSCs without the chimera expression when put in contact with the AML-MSCs alone, thus supporting their modification being previously induced by the blasts expressing the chimera within the BM of the patients (AML-MSCs were derived from a BM of AML with t(16,16) *CBFA2T3-GLIS2*). These findings will be further dissected to better clarify the role of AML-MSCs in the leukemogenesis, but strengthen our GEP and *in vitro* results confirming and supporting that AML blasts modify the microenvironment to fulfil their oncogenic functions.

Overall, AML-MSCs exhibit functional and transcriptome abnormalities, as well as a pro-leukemia potential, suggesting that their targeting in patients with AML. Here, we proposed the targeting of AML-MSCs as a new strategy to block leukemia growth and help to reach the complete remission with non-toxic doses of chemotherapy. In fact, we performed an HST of 480 and discovered new potential drugs active on reducing AML-MSCs proliferation. We considered the HTS, by using a LOPAC[®] Library, an interesting method to discover effective drugs that can be quickly repositioned²²⁴ in a low cost and time-consuming process for new indications. This screening uncovered 17 compounds active in reducing AML-MSCs viability, with no effects on h-MSCs or AML cells. This concept is fundamental in the targeted-therapy with new treatments reducing side-effects on healthy cells, and preserving the pool of healthy stromal and stem cells in the BM. Interestingly, 2 out of 17 identified compounds, Lercanidipine-HCl and Nemadipine-A, are known to block the L-type calcium channels and Lercanidipine-HCl is currently used in adult hypertension treatment²²⁵. Previously, several data reported the expression of the L-type calcium channel in MSCs (namely CaV1.2) with a role in their proliferation and osteogenic differentiation²⁰⁴. Here, we found both pathways being altered in the AML-MSCs, and produced new data on CaV1.2 RNA and protein expression and function in the context of AML. We uncovered that AML-MSCs had a different sensitivity to Lercanidipine-HCl due to CaV1.2 lower expression with respect to h-MSCs, as reported in the majority of cancer types, including brain, lymphoma, ovarian, bladder, prostate, renal, salivary gland, cervix and colorectal cancers, compared with normal tissue^{226,227}. Furthermore, the treatment in combination with CaV1.2 agonists showed to directly restore the

proliferation of AML-MSCs, indicating that CaV1.2 is the main target of Lercanidipine-HCl. In addition, long-term treatment with Lercanidipine-HCl revealed that the effect on AML-MSCs viability was reversible after drug washout. This crucial observation revealed this drug able to block the cross-talk between the AML-MSCs and AML, with potentiality in enhancing chemotherapy efficacy over cancer cell and, more importantly, permitting to restore h-MSCs during BM niche recovery. By the way, the involvement and the remodeling of calcium channels in leukemia development and progression remains still largely obscure; however, published reports suggested that alterations in CaV1.2 expression may have an adverse effect on tissue homeostasis, which may result in pro-leukemia potential or tumorigenesis²²⁷, this latter supporting our targeting for further experimentation *in vivo*.

Taken together these findings suggest that leukemia-induced remodeling of the niche, resulting in a deteriorated microenvironment, is another pathogenic mechanism of cancer. Nevertheless, the lack of suitable *in vitro* and *in vivo* models for underpinning the BM microenvironment limited knowledge in this field. Despite many attempts, the culturing method of leukemic primary cells *in vitro* is still extremely challenging²²⁸, and no appropriate culture models have been developed so far. Traditionally, AML culture has relied on the 2D growth configuration provided by flask or well-plates, which did not recapitulate the BM niche inductive microenvironment required for leukemia support. Recently, more and more studies have indicated that BM niche is crucial to determine leukemia fate, with the stromal cells in the niche providing a sanctuary in which leukemic cells acquire a drug-resistance phenotype and evade chemotherapy-induced death²²⁹. To note, the BM niche is a three-dimensional (3D) tissue and the close reconstruction of it in *in vitro* and *in vivo* systems is considered an amazing opportunity to develop new culture strategies to specifically investigate the balance of leukemia onset or progression.

The hematopoietic niche in BM, together with MSCs, also endothelial cells and osteoblast cells have long been revealed to be part and support the maintenance, proliferation and differentiation of hematopoietic cells²²⁹. Therefore, in this study we selected MSCs, HUVECs and osteoblasts derived from MSCs as the candidates feeder cells to create a culture system *in vitro* that could mimic the leukemia niche. To better reproduce the physical conditions of BM niche, we adopted a 3D scaffold made of hydroxyapatite and Collagen I as substrate for culturing stromal cells. The MSCs after seeding were observed to grow in the porous network of the bone trabecular and form a meshwork-like structure, while leukemia cells embedded and grew in the intercellular space similar to the *in vivo* marrow-microenvironment²³⁰. An ideal leukemia culture system should possess the ability both to continuously promote leukemia cells pool proliferation and to maintain their self-renewal

potential in long-term. We thus assessed the supportive effects of our set up 3D culture system on AML cells proliferation, with the exception of the system containing HUVEC in which the proliferation was found impaired, suggesting that HUVEC saturated the system potentially arresting AML cell cycle. We also interrogated this 3D system for its ability to maintain the stem-clonogenic potential and demonstrated that only the 3D culture method containing AML-MSCs gave rise to constant number of colonies up to 21 days, preserving AML cells self-renewal and reducing their differentiation. Finally, we confirmed that AML cells, after 21 days of 3D culture, maintained the immunophenotypic profile detected in the AML sample at diagnosis. This latter finding, confirmed the preservation of the original patient' tumor AML characteristics, which is a fundamental and necessary condition for *in vitro* models that would serve to pharmacological screenings. To note, even if it is not known how AML cells can alter the biological functions of MSCs, it has been previously demonstrated the role of cytokine-mediated crosstalk between AML cells and stromal cells supporting both leukemia growth²⁰⁸ and resistance against the anti-leukemic chemotherapy²⁰⁹. In line with this issue, we studied the factors secreted by AML-MSCs in our humanized 3D model, by comparison with those secreted from h-MSCs when cultured together with AML cells. This study represents the first secretome investigation in a 3D long term AML cultures. The major observation of this experiment was the discovery that AML-MSCs produced 22 different heavy-labeled proteins with respect to h-MSCs, with a broad spectrum of them found implicated in angiogenesis, inflammation and cancerogenesis. Consistently, several of these proteins have been previously mentioned in the context of AML pathogenesis, including CHI3L1^{231,232}, SERPINE1²³³, and PTX3^{234,235}. More interestingly, we observed a reduction in the secretion of PTX3 from AML-MSCs compared with h-MSCs in 3D culture. It has been reported that PTX3, secreted by MSCs, is an essential component of the humoral arm of innate immunity, acting as an extrinsic oncosuppressor gene by regulating complement-dependent and tumor-promoting inflammation. In accordance with our results, PTX3 expression previously was found repressed in some human tumors¹⁹⁵⁻¹⁹⁷, suggesting inflammation as one of the main feature of the bone marrow niche and its putative role also in the pathogenesis of AML. As a matter of fact, these findings stressed the crucial role of the leukemia niche and its targeting for counteract disease progression, and raise our innovative 3D-AML model useful for testing novel combined therapeutic strategies.

Ultimately, the goal of this research was the use of our 3D system *in vitro* and *in vivo* to study and reliably predict drug response, since treating AML patients means that a drug fluctuate in a 3D context within several diverse compartments and cells. Our model provides an opportunity to study this collective response in 3D and we decided to test classic chemotherapies or new drugs currently in clinical trials, such as Quizartinib²¹⁷, I-BET151²¹⁸, and Dasatinib²³⁶, for targeting genetic

mutations recurrently found in high risk AML subtypes. This method would be helpful to determine effective drug doses, since the 3D model might recapitulate a more physiological condition²³⁷, and would strengthen the potential use of this 3D system in a pre-clinical testing of large numbers of compounds. Furthermore, we improved this task, by considering to target the niche and explore how the block of the crosstalk between AML and AML-MSCs by Lercanidipine-HCl could improve disease clearance. The results described in this thesis showed that treatments in 3D-AML model resulted in a synergistic effect on the reduction of AML proliferation *in vitro*. To notice, this current thesis is the first study that evaluates the repositioning of known drugs commonly used for adult hypertension for sensitizing leukemia microenvironment. The impact of L-type calcium channel blockers on the survival of patients with AML is largely unknown; nevertheless, it has been shown that patients with breast cancer²³⁸ and melanoma²³⁹, who received calcium channel inhibitors, have extended survival. In support of the use of anti-hypertensives in targeting leukemia niche, there are certain evidence suggesting that commonly prescribed anti-hypertensives can exert biological effect also in AML²⁴⁰. Interestingly, it was reported that components of the renin angiotensin system, targetable from Lercanidipine-HCl, are expressed in the BM microenvironment of AML cells and are postulated to exert a regulatory function by participating in autocrine and paracrine loops²⁴¹. In addition, it was reported that Lercanidipine-HCl demonstrated anti-inflammatory and antioxidant properties²²⁵. These findings further support our proposal to use Lercanidipine-HCl in combination with chemotherapy in our AML patients; inasmuch our data reported that the leukemic niche have altered inflammation- and angiogenesis-related pathways. Taken together, we strongly support our *in vitro* 3D model a new tool to selectively and efficiently test new treatment strategies with more information regarding drug sensitivity and effective doses.

Finally, considering the huge difficulty to obtain AML mouse models and given the promising results achieved *in vitro* in mimicking the leukemic niche, we investigated if the presence of the humanized 3D niche in mice would increase the *in vivo* engraftment rate of pediatric AML. To date, the engraftment capability of AML still considerably varies from high to no engraftment at all, mostly depending on AML risk group, with the high risk being the most represented²¹⁹. Several attempts to improve engraftment, such as the use of transgenic mice expressing human cytokines or the implantation of ossicles or organoids to mimic a human BM niche have already been conducted, without success for pediatric AML^{120,175}. Here, we implanted our optimized *in vitro* 3D-AML model, containing both AML-MSCs and AML cells. The scaffold was shown supporting blood vessels formation, mimicking human BM stromal network that enabled growth and maintenance of AML cells, including their genetic and immune-phenotype. Furthermore, the contact of the MSCs with the scaffold *in vivo* appeared to induce their differentiation along the osteogenic *lineage*.

The injected leukemia cells were evaluated for survival and proliferation, showing that leukemia progressed in the scaffold for more than 12 months. Nevertheless, AML did not disseminate in the murine peripheral blood, BM, liver nor spleen after 1 year from implantation, suggesting the preference of the human AML to grow in the humanized microenvironment. We tried to overcome this issue and try the cell mobilization by treatment with CXCR4 antagonist, such as AMD3100²²⁰, which disrupts the chemokines/chemoreceptor signaling axis of SDF-1 and CXCR4. Regrettably, we did not observe any sign of AML outside of the scaffolds. Up to now, 12 months later from the implantation of scaffolds, our experiments did not give positive engraftments, except in 1 case out of 15, which engrafted after 7 months from the implantation. This failure is in line with the results observed in another study on acute myeloid leukemia¹⁶⁶. Nevertheless, we demonstrated that our 3D structure maintained AML cells viable *in vivo*, opening for the possibility to perform preliminary 3D drug screening *in vivo in loco*, by transducing AML cells with luciferase before transplantation, and using luciferase-positive cells reduction as main read-out of new treatments' efficacy. Furthermore, our innovative system will lay the groundwork for biologically relevant pre-clinical models able to investigate the dynamic interactions between leukemia cells and the BM microenvironment, since the scaffold can be easily manipulated and removed for histological and molecular analyses without disrupting the niche interactions. This latter option of an *in vivo in loco* monitoring, by the pre-seeding of the AML cells before scaffold implantation in mice, circumvents the limitations of standard intravenous cells injections, including poor delivery and poor retention of cells at the intended site, and can be considered a feasible and interesting tool for new *in vivo* approaches for combined drug screening towards AML and MSCs.

In conclusion this project rises with important results for future investigations on the pathogenesis of AML, AML microenvironment and new treatment approaches. We improve knowledge on leukemia MSCs with an aberrant selective activity within the niche strongly supporting and maintaining AML proliferation, with further investigations to unveil the role of microenvironment in tumor onset being currently still under evaluation. Furthermore, the new synergistic strategy which combines the targeting of stromal microenvironment with the current front-line chemotherapy, in order to face the residual disease and relapse occurrence in AML is of crucial importance in the pediatric field, where front-line therapy improvements are completely absent²⁴². This novel system represents a new platform for rapid drug testing, and can be used for determining the best combination approaches efficacy, as well as the definition of individualized treatment modalities for AML patients. This original and novel 3D-modeling for long-term cultures with primary AML cells represents an incredible tool for understanding the role of leukemia niche in the

progression of disease, and in phenomena related to therapy resistance, both arguments being under investigation.

This thesis poses the basis for further discoveries in the pediatric AML field, both mechanistic and clinical, with great chances to reach the goals of improving children survival, reduce relapse incidence and the late effects related to cytotoxicity that are severely influencing the future of our children with cancer.

References

1. Zhou, H. S., Carter, B. Z. & Andreeff, M. Bone marrow niche-mediated survival of leukemia stem cells in acute myeloid leukemia: Yin and Yang. *Cancer Biology and Medicine* **13**, 248–259 (2016).
2. Hoggatt, J., Kfoury, Y. & Scadden, D. T. Hematopoietic Stem Cell Niche in Health and Disease. *Annu. Rev. Pathol. Mech. Dis.* (2016). doi:10.1146/annurev-pathol-012615-044414
3. Kumar, C. C. Genetic abnormalities and challenges in the treatment of acute myeloid Leukemia. *Genes and Cancer* (2011). doi:10.1177/1947601911408076
4. Pession, A. *et al.* Results of the AIEOP AML 2002/01 multicenter prospective trial for the treatment of children with acute myeloid leukemia. *Blood* **122**, 170–8 (2013).
5. de Rooij, J. D. E., Zwaan, C. M. & van den Heuvel-Eibrink, M. Pediatric AML: From Biology to Clinical Management. *J. Clin. Med.* **4**, 127–49 (2015).
6. Jan, M. *et al.* Clonal evolution of preleukemic hematopoietic stem cells precedes human acute myeloid leukemia. *Sci. Transl. Med.* **4**, 149ra118 (2012).
7. Corces-Zimmerman, M. R. & Majeti, R. Pre-leukemic evolution of hematopoietic stem cells: the importance of early mutations in leukemogenesis. *Leukemia* **28**, 2276–82 (2014).
8. Ding, L. *et al.* Clonal evolution in relapsed acute myeloid leukaemia revealed by whole-genome sequencing. *Nature* **481**, 506–10 (2012).
9. Klco, J. M. *et al.* Functional heterogeneity of genetically defined subclones in acute myeloid leukemia. *Cancer Cell* **25**, 379–92 (2014).
10. Masetti, R. *et al.* Genomic complexity and dynamics of clonal evolution in childhood acute myeloid leukemia studied with whole-exome sequencing. *Oncotarget* (2016). doi:10.18632/oncotarget.10778
11. Conway O'Brien, E., Prideaux, S. & Chevassut, T. The Epigenetic Landscape of Acute Myeloid Leukemia. *Adv. Hematol.* (2014). doi:10.1155/2014/103175
12. Ley, T. J. *et al.* DNA sequencing of a cytogenetically normal acute myeloid leukaemia genome. *Nature* (2008). doi:10.1038/nature07485
13. Ley, T. J. *et al.* DNMT3A Mutations in Acute Myeloid Leukemia Supplementary. *N. Engl. J. Med.* (2010). doi:10.1056/NEJMoa1005143
14. Pui, C. H., Carroll, W. L., Meshinchi, S. & Arceci, R. J. Biology, risk stratification, and therapy of pediatric acute leukemias: An update. *Journal of Clinical Oncology* (2011). doi:10.1200/JCO.2010.30.7405
15. Creutzig, U. *et al.* Diagnosis and management of acute myeloid leukemia in children and adolescents: recommendations from an international expert panel, on behalf of the AML Committee of the International BFM Study Group. *Blood* (2012). doi:10.1182/blood-2012-

03-362608

16. Masetti, R. *et al.* Acute Myeloid Leukemia in Infants: Biology and Treatment. *Front. Pediatr.* (2015). doi:10.3389/fped.2015.00037
17. Bennett, J. M. *et al.* Proposals for the Classification of the Acute Leukaemias French- American- British (FAB) Co- operative Group. *Br. J. Haematol.* (1976). doi:10.1111/j.1365-2141.1976.tb03563.x
18. Vardiman, J. W. *et al.* The 2008 revision of the World Health Organization (WHO) classification of myeloid neoplasms and acute leukemia: Rationale and important changes. *Blood* (2009). doi:10.1182/blood-2009-03-209262
19. Duque-Afonso, J. & Cleary, M. L. The AML salad bowl. *Cancer Cell* **25**, 265–7 (2014).
20. Arber, D. A. *et al.* The 2016 revision to the World Health Organization classification of myeloid neoplasms and acute leukemia. *Blood* (2016). doi:10.1182/blood-2016-03-643544
21. Leung, W. *et al.* High success rate of hematopoietic cell transplantation regardless of donor source in children with very high-risk leukemia. *Blood* **118**, 223–30 (2011).
22. Suh, J. K. *et al.* Hematopoietic stem cell transplantation in pediatric patients with acute myeloid leukemia without favorable cytogenetics. *Pediatr. Transplant.* **21**, (2017).
23. Locatelli, F. *et al.* Outcome of children with acute leukemia given HLA-haploidentical HSCT after $\alpha\beta$ T-cell and B-cell depletion. *Blood* **130**, 677–685 (2017).
24. Horan, J. T. *et al.* Impact of disease risk on efficacy of matched related bone marrow transplantation for pediatric acute myeloid leukemia: The Children’s Oncology Group. *J. Clin. Oncol.* (2008). doi:10.1200/JCO.2007.13.5244
25. Pession, A. *et al.* Treatment and long-term results in children with acute myeloid leukaemia treated according to the AIEOP AML protocols. *Leukemia* **19**, 2043–2053 (2005).
26. Riley, L. C., Hann, I. M., Wheatley, K. & Stevens, R. F. Treatment-related deaths during induction and first remission of acute myeloid leukaemia in children treated on the Tenth Medical Research council Acute Myeloid Leukaemia Trial (MRC AML10). *Br. J. Haematol.* **106**, 436–444 (1999).
27. Creutzig, U. *et al.* Early deaths and treatment-related mortality in children undergoing therapy for acute myeloid leukemia: Analysis of the multicenter clinical trials AML-BFM 93 and AML-BFM 98. *J. Clin. Oncol.* **22**, 4384–4393 (2004).
28. Rubnitz, J. E. *et al.* Death during induction therapy and first remission of acute leukemia in childhood: The St. Jude experience. *Cancer* **101**, 1677–1684 (2004).
29. Slats, A. M. *et al.* Causes of death - Other than progressive leukemia - In childhood acute lymphoblastic (ALL) and myeloid leukemia (AML): The Dutch Childhood Oncology Group experience. *Leukemia* **19**, 537–544 (2005).
30. Mulrooney, D. A. *et al.* Cardiac outcomes in a cohort of adult survivors of childhood and adolescent cancer: Retrospective analysis of the childhood cancer survivor study cohort. *BMJ* (2009). doi:10.1136/bmj.b4606
31. Grosso, D. A., Hess, R. C. & Weiss, M. A. Immunotherapy in acute myeloid leukemia.

- Cancer* **121**, 2689–2704 (2015).
32. Itzykson, R. & Fenaux, P. Epigenetics of myelodysplastic syndromes. *Leukemia* **28**, 497–506 (2014).
 33. Quintás-Cardama, A. *et al.* Epigenetic therapy is associated with similar survival compared with intensive chemotherapy in older patients with newly diagnosed acute myeloid leukemia. *Blood* **120**, 4840–4845 (2012).
 34. Abedin, S. M., Boddy, C. S. & Munshi, H. G. BET inhibitors in the treatment of hematologic malignancies: Current insights and future prospects. *OncoTargets and Therapy* (2016). doi:10.2147/OTT.S100515
 35. Chen, Y. *et al.* Tyrosine kinase inhibitors targeting FLT3 in the treatment of acute myeloid leukemia. *Stem cell Investig.* **4**, 48 (2017).
 36. Meads, M. B., Hazlehurst, L. A. & Dalton, W. S. The bone marrow microenvironment as a tumor sanctuary and contributor to drug resistance. *Clin. Cancer Res.* **14**, 2519–2526 (2008).
 37. Rashidi, A. & DiPersio, J. F. Targeting the leukemia-stroma interaction in acute myeloid leukemia: rationale and latest evidence. *Ther. Adv. Hematol.* **7**, 40–51 (2016).
 38. Ferraro, F., Lo Celso, C. & Scadden, D. Adult stem cells and their niches. *Advances in Experimental Medicine and Biology* (2010). doi:10.1007/978-1-4419-7037-4_11
 39. Schofield, R. The relationship between the spleen colony-forming cell and the haemopoietic stem cell. *Blood Cells* (1978).
 40. Kunisaki, Y. *et al.* Arteriolar niches maintain haematopoietic stem cell quiescence. *Nature* (2013). doi:10.1038/nature12612
 41. Acar, M. *et al.* Deep imaging of bone marrow shows non-dividing stem cells are mainly perisinusoidal. *Nature* **526**, 126–30 (2015).
 42. Asada, N., Takeishi, S. & Frenette, P. S. Complexity of bone marrow hematopoietic stem cell niche. *International Journal of Hematology* (2017). doi:10.1007/s12185-017-2262-9
 43. Calvi, L. M. *et al.* Osteoblastic cells regulate the haematopoietic stem cell niche. *Nature* (2003). doi:10.1038/nature02040
 44. Mendez-Ferrer, S., Enikolopov, G. N., Lira, S. & Frenette, P. S. Mesenchymal Stem Cells, Regulated by the Sympathetic Nervous System, Form the Hematopoietic Stem Cell Niche. *Blood* **112**, (2008).
 45. Yamazaki, S. *et al.* Nonmyelinating Schwann cells maintain hematopoietic stem cell hibernation in the bone marrow niche. *Cell* **147**, 1146–58 (2011).
 46. Naveiras, O. *et al.* Bone-marrow adipocytes as negative regulators of the haematopoietic microenvironment. *Nature* **460**, 259–63 (2009).
 47. Kode, A. *et al.* Leukaemogenesis induced by an activating β -catenin mutation in osteoblasts. *Nature* **506**, 240–4 (2014).
 48. Fujisaki, J. *et al.* In vivo imaging of Treg cells providing immune privilege to the haematopoietic stem-cell niche. *Nature* **474**, 216–9 (2011).

49. Guezguez, B. *et al.* Regional localization within the bone marrow influences the functional capacity of human HSCs. *Cell Stem Cell* (2013). doi:10.1016/j.stem.2013.06.015
50. Yin, T. & Li, L. The stem cell niches in bone. *Journal of Clinical Investigation* (2006). doi:10.1172/JCI28568
51. Kopp, H.-G., Avecilla, S. T., Hooper, A. T. & Rafii, S. The bone marrow vascular niche: home of HSC differentiation and mobilization. *Physiology (Bethesda)*. **20**, 349–56 (2005).
52. Calvi, L. M. & Link, D. C. Cellular complexity of the bone marrow hematopoietic stem cell niche. *Calcif. Tissue Int.* **94**, 112–24 (2014).
53. Morrison, S. J. & Scadden, D. T. The bone marrow niche for haematopoietic stem cells. *Nature* **505**, 327–34 (2014).
54. Deguchi, K. *et al.* Excessive extramedullary hematopoiesis in Cbfa1-deficient mice with a congenital lack of bone marrow. *Biochem. Biophys. Res. Commun.* **255**, 352–359 (1999).
55. Shiozawa, Y., Havens, A. M., Pienta, K. J. & Taichman, R. S. The bone marrow niche: habitat to hematopoietic and mesenchymal stem cells, and unwitting host to molecular parasites. *Leukemia* **22**, 941–50 (2008).
56. Méndez-Ferrer, S. *et al.* Mesenchymal and haematopoietic stem cells form a unique bone marrow niche. *Nature* (2010). doi:10.1038/nature09262
57. Friedenstein, A. J., Petrakova, K. V, Kurolesova, A. I. & Frolova, G. P. Heterotopic of bone marrow. Analysis of precursor cells for osteogenic and hematopoietic tissues. *Transplantation* (1968).
58. Gao, F. *et al.* Mesenchymal stem cells and immunomodulation: current status and future prospects. *Cell death & disease* (2016). doi:10.1038/cddis.2015.327
59. Crane, G. M., Jeffery, E. & Morrison, S. J. Adult haematopoietic stem cell niches. *Nat. Rev. Immunol.* **17**, 573–590 (2017).
60. Le Blanc, K., Tammik, L., Sundberg, B., Haynesworth, S. E. & Ringdén, O. Mesenchymal stem cells inhibit and stimulate mixed lymphocyte cultures and mitogenic responses independently of the major histocompatibility complex. *Scand. J. Immunol.* (2003).
61. Sotiropoulou, P. A., Perez, S. A., Gritzapis, A. D., Baxevanis, C. N. & Papamichail, M. Interactions between human mesenchymal stem cells and natural killer cells. *Stem Cells* **24**, 74–85 (2006).
62. Corcione, A. *et al.* Human mesenchymal stem cells modulate B-cell functions. *Blood* (2006). doi:10.1182/blood-2005-07-2657
63. Frenette, P. S., Pinho, S., Lucas, D. & Scheiermann, C. Mesenchymal stem cell: keystone of the hematopoietic stem cell niche and a stepping-stone for regenerative medicine. *Annu. Rev. Immunol.* **31**, 285–316 (2013).
64. Boulais, P. E. & Frenette, P. S. Making sense of hematopoietic stem cell niches. *Blood* **125**, 2621–9 (2015).
65. Schepers, K., Campbell, T. B. & Passegué, E. Normal and leukemic stem cell niches: insights and therapeutic opportunities. *Cell Stem Cell* **16**, 254–67 (2015).

66. Sugiyama, T., Kohara, H., Noda, M. & Nagasawa, T. Maintenance of the hematopoietic stem cell pool by CXCL12-CXCR4 chemokine signaling in bone marrow stromal cell niches. *Immunity* **25**, 977–88 (2006).
67. Dominici, M. *et al.* Minimal criteria for defining multipotent mesenchymal stromal cells. The International Society for Cellular Therapy position statement. *Cytotherapy* (2006). doi:10.1080/14653240600855905
68. Konopleva, M. *et al.* Stromal cells prevent apoptosis of AML cells by up-regulation of anti-apoptotic proteins. *Leukemia* **16**, 1713–24 (2002).
69. Frisch, B. J. *et al.* Functional inhibition of osteoblastic cells in an in vivo mouse model of myeloid leukemia. *Blood* (2012). doi:10.1182/blood-2011-04-348151
70. Zhang, B. *et al.* Altered microenvironmental regulation of leukemic and normal stem cells in chronic myelogenous leukemia. *Cancer Cell* **21**, 577–92 (2012).
71. Schepers, K. *et al.* Myeloproliferative neoplasia remodels the endosteal bone marrow niche into a self-reinforcing leukemic niche. *Cell Stem Cell* (2013). doi:10.1016/j.stem.2013.06.009
72. Arranz, L. *et al.* Neuropathy of haematopoietic stem cell niche is essential for myeloproliferative neoplasms. *Nature* **512**, 78–81 (2014).
73. Hanoun, M. *et al.* Acute myelogenous leukemia-induced sympathetic neuropathy promotes malignancy in an altered hematopoietic stem cell niche. *Cell Stem Cell* **15**, 365–375 (2014).
74. Blau, O. *et al.* Chromosomal aberrations in bone marrow mesenchymal stroma cells from patients with myelodysplastic syndrome and acute myeloblastic leukemia. *Exp. Hematol.* **35**, 221–9 (2007).
75. Blau, O. *et al.* Mesenchymal stromal cells of myelodysplastic syndrome and acute myeloid leukemia patients have distinct genetic abnormalities compared with leukemic blasts. *Blood* (2011). doi:10.1182/blood-2011-03-343467
76. Kim, J.-A. *et al.* Microenvironmental remodeling as a parameter and prognostic factor of heterogeneous leukemogenesis in acute myelogenous leukemia. *Cancer Res.* **75**, 2222–31 (2015).
77. Geyh, S. *et al.* Insufficient stromal support in MDS results from molecular and functional deficits of mesenchymal stromal cells. *Leukemia* **27**, 1841–51 (2013).
78. Chandran, P. *et al.* Mesenchymal stromal cells from patients with acute myeloid leukemia have altered capacity to expand differentiated hematopoietic progenitors. *Leuk. Res.* **39**, 486–93 (2015).
79. Geyh, S. *et al.* Functional inhibition of mesenchymal stromal cells in acute myeloid leukemia. *Leukemia* **30**, 683–91 (2016).
80. Diaz de la Guardia, R. *et al.* Detailed Characterization of Mesenchymal Stem/Stromal Cells from a Large Cohort of AML Patients Demonstrates a Definitive Link to Treatment Outcomes. *Stem cell reports* **8**, 1573–1586 (2017).
81. Kornblau, S. M. *et al.* Distinct protein signatures of acute myeloid leukemia bone marrow-derived stromal cells are prognostic for patient survival. *Haematologica* **103**, 810–821

- (2018).
82. Corradi, G. *et al.* Mesenchymal stromal cells from myelodysplastic and acute myeloid leukemia patients display in vitro reduced proliferative potential and similar capacity to support leukemia cell survival. *Stem Cell Res. Ther.* **9**, (2018).
 83. Schroeder, T., Geyh, S., Germing, U. & Haas, R. Mesenchymal stromal cells in myeloid malignancies. *Blood Research* (2016). doi:10.5045/br.2016.51.4.225
 84. Vader, P., Breakefield, X. O. & Wood, M. J. A. Extracellular vesicles: Emerging targets for cancer therapy. *Trends in Molecular Medicine* **20**, 385–393 (2014).
 85. Camacho, V., McClearn, V., Patel, S. & Welner, R. S. Regulation of normal and leukemic stem cells through cytokine signaling and the microenvironment. *International Journal of Hematology* **105**, 566–577 (2017).
 86. Zhang, S., Yang, X., Wang, L. & Zhang, C. Interplay between inflammatory tumor microenvironment and cancer stem cells (Review). *Oncology Letters* **16**, 679–686 (2018).
 87. Rupec, R. A. *et al.* Stroma-mediated dysregulation of myelopoiesis in mice lacking I kappa B alpha. *Immunity* **22**, 479–91 (2005).
 88. Walkley, C. R. *et al.* A microenvironment-induced myeloproliferative syndrome caused by retinoic acid receptor gamma deficiency. *Cell* **129**, 1097–110 (2007).
 89. Walkley, C. R., Shea, J. M., Sims, N. A., Purton, L. E. & Orkin, S. H. Rb regulates interactions between hematopoietic stem cells and their bone marrow microenvironment. *Cell* **129**, 1081–95 (2007).
 90. Kim, Y.-W. *et al.* Defective Notch activation in microenvironment leads to myeloproliferative disease. *Blood* **112**, 4628–38 (2008).
 91. Raaijmakers, M. H. G. P. *et al.* Bone progenitor dysfunction induces myelodysplasia and secondary leukaemia. *Nature* **464**, 852–7 (2010).
 92. Zambetti, N. A. *et al.* Mesenchymal Inflammation Drives Genotoxic Stress in Hematopoietic Stem Cells and Predicts Disease Evolution in Human Pre-leukemia. *Cell Stem Cell* (2016). doi:10.1016/j.stem.2016.08.021
 93. Wiseman, D. H. Donor cell leukemia: a review. *Biol. Blood Marrow Transplant.* **17**, 771–89 (2011).
 94. Greenberger, J. S. *et al.* Role of bone marrow stromal cells in irradiation leukemogenesis. *Acta Haematol.* **96**, 1–15 (1996).
 95. Barcellos-Hoff, M. H., Park, C. & Wright, E. G. Radiation and the microenvironment - tumorigenesis and therapy. *Nat. Rev. Cancer* **5**, 867–75 (2005).
 96. Damiano, J. S., Cress, A. E., Hazlehurst, L. A., Shtil, A. A. & Dalton, W. S. *Cell Adhesion Mediated Drug Resistance (CAM-DR): Role of Integrins and Resistance to Apoptosis in Human Myeloma Cell Lines.*
 97. Frassanito, M. A., Cusmai, A., Iodice, G. & Dammacco, F. Autocrine interleukin-6 production and highly malignant multiple myeloma: Relation with resistance to drug-induced apoptosis. *Blood* (2001). doi:10.1182/blood.V97.2.483

98. Zeng, Z. *et al.* Inhibition of CXCR4 with the novel RCP168 peptide overcomes stroma-mediated chemoresistance in chronic and acute leukemias. *Mol. Cancer Ther.* (2006). doi:10.1158/1535-7163.mct-06-0228
99. Dias, S. *et al.* Bcl-2 expression and apoptosis inhibition VEGF 165 promotes survival of leukemic cells by Hsp90-mediated induction of Bcl-2 expression and apoptosis inhibition. (2014). doi:10.1182/blood.V99.7.2532
100. Kremer, K. N. *et al.* Osteoblasts protect AML cells from SDF-1-induced apoptosis. *J. Cell. Biochem.* **115**, 1128–37 (2014).
101. Tabe, Y. & Konopleva, M. Advances in understanding the leukaemia microenvironment. *Br. J. Haematol.* **164**, 767–78 (2014).
102. Rogers, R. S. & Bhattacharya, J. When cells become organelle donors. *Physiology* **28**, 414–422 (2013).
103. Moschoi, R. *et al.* Protective mitochondrial transfer from bone marrow stromal cells to acute myeloid leukemic cells during chemotherapy. *Blood* **128**, 253–64 (2016).
104. Marlein, C. *et al.* Bone Marrow Mesenchymal Stromal Cells Transfer Their Mitochondria to Acute Myeloid Leukaemia Blasts to Support Their Proliferation and Survival. *Blood* **128**, (2016).
105. Nervi, B. *et al.* Chemosensitization of acute myeloid leukemia (AML) following mobilization by the CXCR4 antagonist AMD3100. *Blood* **113**, 6206–14 (2009).
106. Zeng, Z. *et al.* Targeting the leukemia microenvironment by CXCR4 inhibition overcomes resistance to kinase inhibitors and chemotherapy in AML. *Blood* (2009). doi:10.1182/blood-2008-05-158311
107. Matsunaga, T. *et al.* Interaction between leukemic-cell VLA-4 and stromal fibronectin is a decisive factor for minimal residual disease of acute myelogenous leukemia. *Nat. Med.* **9**, 1158–65 (2003).
108. Winkler, I. G. *et al.* Vascular niche E-selectin regulates hematopoietic stem cell dormancy, self renewal and chemoresistance. *Nat. Med.* **18**, 1651–7 (2012).
109. Jin, L., Hope, K. J., Zhai, Q., Smadja-Joffe, F. & Dick, J. E. Targeting of CD44 eradicates human acute myeloid leukemic stem cells. *Nat. Med.* (2006). doi:10.1038/nm1483
110. Krause, D. S., Lazarides, K., von Andrian, U. H. & Van Etten, R. A. Requirement for CD44 in homing and engraftment of BCR-ABL-expressing leukemic stem cells. *Nat. Med.* **12**, 1175–80 (2006).
111. Burger, M. *et al.* Small peptide inhibitors of the CXCR4 chemokine receptor (CD184) antagonize the activation, migration, and antiapoptotic responses of CXCL12 in chronic lymphocytic leukemia B cells. *Blood* **106**, 1824–30 (2005).
112. Juarez, J., Bradstock, K. F., Gottlieb, D. J. & Bendall, L. J. Effects of inhibitors of the chemokine receptor CXCR4 on acute lymphoblastic leukemia cells in vitro. *Leukemia* **17**, 1294–300 (2003).
113. Uy, G. L. *et al.* A phase 1/2 study of chemosensitization with the CXCR4 antagonist plerixafor in relapsed or refractory acute myeloid leukemia. *Blood* **119**, 3917–24 (2012).

114. Hsieh, Y. Te *et al.* Integrin alpha4 blockade sensitizes drug resistant pre-B acute lymphoblastic leukemia to chemotherapy. *Blood* (2013). doi:10.1182/blood-2012-01-406272
115. Layani-Bazar, A. *et al.* Redox modulation of adjacent thiols in VLA-4 by AS101 converts myeloid leukemia cells from a drug-resistant to drug-sensitive state. *Cancer Res.* **74**, 3092–103 (2014).
116. Karp, J. E. *et al.* Targeting vascular endothelial growth factor for relapsed and refractory adult acute myelogenous leukemias: Therapy with sequential 1- β -D-arabinofuranosylcytosine, mitoxantrone, and bevacizumab. *Clin. Cancer Res.* (2004). doi:10.1158/1078-0432.CCR-03-0627
117. Coltella, N., Valsecchi, R., Ponente, M., Ponzoni, M. & Bernardi, R. Synergistic Leukemia Eradication by Combined Treatment with Retinoic Acid and HIF Inhibition by EZN-2208 (PEG-SN38) in Preclinical Models of PML-RAR α and PLZF-RAR α -Driven Leukemia. *Clin. Cancer Res.* **21**, 3685–94 (2015).
118. Smith, C. C. *et al.* Validation of ITD mutations in FLT3 as a therapeutic target in human AML. *Nature* **485**, 260–263 (2012).
119. Sanchez, P. V. *et al.* A robust xenotransplantation model for acute myeloid leukemia. *Leukemia* **23**, 2109–2117 (2009).
120. Wunderlich, M. *et al.* AML xenograft efficiency is significantly improved in NOD/SCID-IL2RG mice constitutively expressing human SCF, GM-CSF and IL-3. *Leukemia* **24**, 1785–8 (2010).
121. Horvath, P. *et al.* Screening out irrelevant cell-based models of disease. *Nature Reviews Drug Discovery* (2016). doi:10.1038/nrd.2016.175
122. Aljitiawi, O. S. *et al.* A novel three-dimensional stromal-based model for in vitro chemotherapy sensitivity testing of leukemia cells. *Leuk. Lymphoma* (2014). doi:10.3109/10428194.2013.793323
123. Houshmand, M. *et al.* Mimicking the Acute Myeloid Leukemia Niche for Molecular Study and Drug Screening. *Tissue Eng. Part C. Methods* **23**, 72–85 (2017).
124. Bray, L. J. *et al.* A three-dimensional ex vivo tri-culture model mimics cell-cell interactions between acute myeloid leukemia and the vascular niche. *Haematologica* **102**, 1215–1226 (2017).
125. Dexter, T. M., Wright, E. G., Krizsa, F. & Lajtha, L. G. Regulation of haemopoietic stem cell proliferation in long term bone marrow cultures. *Biomedicine* (1977).
126. Griessinger, E. *et al.* A Niche-Like Culture System Allowing the Maintenance of Primary Human Acute Myeloid Leukemia-Initiating Cells: A New Tool to Decipher Their Chemoresistance and Self-Renewal Mechanisms. *Stem Cells Transl. Med.* (2014). doi:10.5966/sctm.2013-0166
127. Hartwell, K. A. *et al.* Niche-based screening identifies small-molecule inhibitors of leukemia stem cells. *Nat. Chem. Biol.* **9**, 840–848 (2013).
128. van Gosliga, D. *et al.* Establishing long-term cultures with self-renewing acute myeloid leukemia stem/progenitor cells. *Exp. Hematol.* **35**, 1538–1549 (2007).

129. Ito, S. *et al.* Long term maintenance of myeloid leukemic stem cells cultured with unrelated human mesenchymal stromal cells. *Stem Cell Res.* **14**, 95–104 (2015).
130. Panoskaltsis, N., Mantalaris, A. & Wu, J. H. D. Engineering a mimicry of bone marrow tissue ex vivo. *J. Biosci. Bioeng.* **100**, 28–35 (2005).
131. Owen, S. C. & Shoichet, M. S. Design of three-dimensional biomimetic scaffolds. *Journal of Biomedical Materials Research - Part A* **94**, 1321–1331 (2010).
132. Di Maggio, N. *et al.* Toward modeling the bone marrow niche using scaffold-based 3D culture systems. *Biomaterials* **32**, 321–329 (2011).
133. Reinisch, A. *et al.* A humanized bone marrow ossicle xenotransplantation model enables improved engraftment of healthy and leukemic human hematopoietic cells. *Nat. Med.* **22**, 812–21 (2016).
134. Sharma, M. B., Limaye, L. S. & Kale, V. P. Mimicking the functional hematopoietic stem cell niche in vitro: Recapitulation of marrow physiology by hydrogel-based three-dimensional cultures of mesenchymal stromal cells. *Haematologica* **97**, 651–660 (2012).
135. Leisten, I. *et al.* 3D co-culture of hematopoietic stem and progenitor cells and mesenchymal stem cells in collagen scaffolds as a model of the hematopoietic niche. *Biomaterials* (2012). doi:10.1016/j.biomaterials.2011.11.034
136. Torisawa, Y. S. *et al.* Bone marrow-on-a-chip replicates hematopoietic niche physiology in vitro. *Nat. Methods* (2014). doi:10.1038/nmeth.2938
137. Wang, T. Y., Brennan, J. K. & Wu, J. H. Multilineal hematopoiesis in a three-dimensional murine long-term bone marrow culture. *Exp. Hematol.* **23**, 26–32 (1995).
138. Kotha, S. S. *et al.* Engineering a multicellular vascular niche to model hematopoietic cell trafficking. *Stem Cell Res. Ther.* (2018). doi:10.1186/s13287-018-0808-2
139. Bray, L. J. *et al.* A three-dimensional tri-culture model for the ex vivo study of acute myeloid leukemia. (2017). doi:10.3324/haematol.2016.157883
140. Tan, J. *et al.* Maintenance and expansion of hematopoietic stem/progenitor cells in biomimetic osteoblast niche. *Cytotechnology* **62**, 439–48 (2010).
141. Karimpoor, M. *et al.* Alginate foam-based three-dimensional culture to investigate drug sensitivity in primary leukaemia cells. *J. R. Soc. Interface* **15**, (2018).
142. Fujita, A. *et al.* Hematopoiesis in regenerated bone marrow within hydroxyapatite scaffold. *Pediatr. Res.* (2010). doi:10.1203/PDR.0b013e3181e1cfce
143. Beniash, E., Hartgerink, J. D., Storrer, H., Stendahl, J. C. & Stupp, S. I. Self-assembling peptide amphiphile nanofiber matrices for cell entrapment. *Acta Biomater.* **1**, 387–97 (2005).
144. Tortelli, F., Tasso, R., Loiacono, F. & Cancedda, R. The development of tissue-engineered bone of different origin through endochondral and intramembranous ossification following the implantation of mesenchymal stem cells and osteoblasts in a murine model. *Biomaterials* **31**, 242–249 (2010).
145. Villa-Bellosta, R., Millan, A. & Sorribas, V. Role of calcium-phosphate deposition in vascular smooth muscle cell calcification. *Am. J. Physiol. Cell Physiol.* **300**, C210-20 (2011).

146. Severn, C. E. *et al.* Polyurethane scaffolds seeded with CD34 + cells maintain early stem cells whilst also facilitating prolonged egress of haematopoietic progenitors. *Sci. Rep.* **6**, (2016).
147. Bray, L. J., Binner, M., Freudenberg, U. & Werner, C. Hydrogel-based in vitro models of tumor angiogenesis. in *Methods in Molecular Biology* **1612**, 39–63 (Humana Press Inc., 2017).
148. Fischbach, C. *et al.* Engineering tumors with 3D scaffolds. *Nat. Methods* **4**, 855–860 (2007).
149. Mousavi, S. H., Abroun, S., Soleimani, M. & Mowla, S. J. 3-Dimensional nano-fibre scaffold for ex vivo expansion of cord blood haematopoietic stem cells. *Artif. cells, nanomedicine, Biotechnol.* **46**, 740–748 (2018).
150. Papadimitropoulos, A. *et al.* Expansion of human mesenchymal stromal cells from fresh bone marrow in a 3D scaffold-based system under direct perfusion. *PLoS One* (2014). doi:10.1371/journal.pone.0102359
151. Sadat Hashemi, Z., Forouzandeh Moghadam, M. & Soleimani, M. Comparison of the Ex Vivo Expansion of UCB-Derived CD34+ in 3D DBM/MBA Scaffolds with USSC as a Feeder Layer. *Iran. J. Basic Med. Sci.* **16**, 1075–87 (2013).
152. Li, G., Liu, X., Du, Q., Gao, M. & An, J. Three dimensional de novo micro bone marrow and its versatile application in drug screening and regenerative medicine. *Exp. Biol. Med.* **240**, 1029–1038 (2015).
153. Choi, J. S., Mahadik, B. P. & Harley, B. A. C. Engineering the hematopoietic stem cell niche: Frontiers in biomaterial science. *Biotechnology Journal* **10**, 1529–1545 (2015).
154. Nichols, J. E. *et al.* In vitro analog of human bone marrow from 3D scaffolds with biomimetic inverted colloidal crystal geometry. *Biomaterials* **30**, 1071–9 (2009).
155. Cukierman, E., Pankov, R., Stevens, D. R. & Yamada, K. M. Taking cell-matrix adhesions to the third dimension. *Science (80-.)*. **294**, 1708–1712 (2001).
156. Beningo, K. A., Dembo, M. & Wang, Y. Responses of fibroblasts to anchorage of dorsal extracellular matrix receptors. *Proc. Natl. Acad. Sci. U. S. A.* **101**, 18024–9 (2004).
157. Ferrarini, M. *et al.* Ex-vivo dynamic 3-D culture of human tissues in the RCCS™ bioreactor allows the study of Multiple Myeloma biology and response to therapy. *PLoS One* **8**, e71613 (2013).
158. Hidalgo, M. *et al.* Patient-Derived Xenograft Models: An Emerging Platform for Translational Cancer Research. *Cancer Discov.* (2014). doi:10.1158/2159-8290.cd-14-0001
159. Kohnken, R., Porcu, P. & Mishra, A. Overview of the Use of Murine Models in Leukemia and Lymphoma Research. *Front. Oncol.* (2017). doi:10.3389/fonc.2017.00022
160. Zuber, J. *et al.* Mouse models of human AML accurately predict chemotherapy response. *Genes Dev.* **23**, 877–889 (2009).
161. Walrath, J. C., Hawes, J. J., Van Dyke, T. & Reilly, K. M. Genetically engineered mouse models in cancer research. *Adv. Cancer Res.* **106**, 113–64 (2010).
162. Thanopoulou, E. *et al.* Engraftment of NOD/SCID-beta2 microglobulin null mice with

- multilineage neoplastic cells from patients with myelodysplastic syndrome. *Blood* **103**, 4285–93 (2004).
163. Pearce, D. J. *et al.* AML engraftment in the NOD/SCID assay reflects the outcome of AML: implications for our understanding of the heterogeneity of AML. *Blood* **107**, 1166–73 (2006).
164. Milan, T. *et al.* Pediatric leukemia: Moving toward more accurate models. *Experimental Hematology* **74**, 1–12 (2019).
165. Theocharides, A. P. A., Rongvaux, A., Fritsch, K., Flavell, R. A. & Manz, M. G. Humanized hemato-lymphoid system mice. *Haematologica* **101**, 5–19 (2016).
166. Grey, W. *et al.* Modeling the human bone marrow niche in mice: From host bone marrow engraftment to bioengineering approaches. *J. Exp. Med.* (2018). doi:10.1084/jem.20172139
167. Dao, M. A., Pepper, K. A. & Nolta, J. A. Long-term cytokine production from engineered primary human stromal cells influences human hematopoiesis in an in vivo xenograft model. *Stem Cells* (1997). doi:10.1002/stem.150443
168. Nicolini, F. E., Cashman, J. D., Hogge, D. E., Humphries, R. K. & Eaves, C. J. NOD/SCID mice engineered to express human IL-3, GM-CSF and Steel factor constitutively mobilize engrafted human progenitors and compromise human stem cell regeneration. *Leukemia* **18**, 341–7 (2004).
169. Yoshimi, A. *et al.* Robust patient-derived xenografts of MDS/MPN overlap syndromes capture the unique characteristics of CMML and JMML. *Blood* **130**, 397–407 (2017).
170. Rongvaux, A. *et al.* Development and function of human innate immune cells in a humanized mouse model. *Nat. Biotechnol.* **32**, 364–72 (2014).
171. Saito, Y. *et al.* Peripheral blood CD34+ cells efficiently engraft human cytokine knock-in mice. *Blood* **128**, 1829–1833 (2016).
172. Ellegast, J. M. *et al.* inv(16) and NPM1mut AMLs engraft human cytokine knock-in mice. *Blood* (2016). doi:10.1182/blood-2015-12-689356
173. Medyouf, H. *et al.* Myelodysplastic cells in patients reprogram mesenchymal stromal cells to establish a transplantable stem cell niche disease unit. *Cell Stem Cell* **14**, 824–37 (2014).
174. Cosgun, K. N. *et al.* Kit regulates HSC engraftment across the human-mouse species barrier. *Cell Stem Cell* (2014). doi:10.1016/j.stem.2014.06.001
175. Carretta, M. *et al.* Genetically engineered mesenchymal stromal cells produce IL-3 and TPO to further improve human scaffold-based xenograft models. *Exp. Hematol.* (2017). doi:10.1016/j.exphem.2017.04.008
176. Ho, M. S. H., Medcalf, R. L., Livesey, S. A. & Traianedes, K. The dynamics of adult haematopoiesis in the bone and bone marrow environment. *British Journal of Haematology* (2015). doi:10.1111/bjh.13445
177. Holzapfel, B. M. *et al.* Tissue engineered humanized bone supports human hematopoiesis in vivo. *Biomaterials* **61**, 103–14 (2015).
178. Flores-Figueroa, E. & Gratzinger, D. Beyond the niche: Myelodysplastic syndrome topobiology in the laboratory and in the clinic. *International Journal of Molecular Sciences*

- (2016). doi:10.3390/ijms17040553
179. Nelson, M. R. & Roy, K. studying hematopoietic stem and progenitor. *J. Mater. Chem. B* (2016). doi:10.1039/C5TB02644J
180. Vaiselbuh, S. R., Edelman, M., Lipton, J. M. & Liu, J. M. Ectopic human mesenchymal stem cell-coated scaffolds in NOD/SCID mice: an in vivo model of the leukemia niche. *Tissue Eng. Part C. Methods* **16**, 1523–31 (2010).
181. Antonelli, A. *et al.* Establishing human leukemia xenograft mouse models by implanting human bone marrow-like scaffold-based niches. *Blood* (2016). doi:10.1182/blood-2016-05-719021
182. Battula, V. L. *et al.* AML-induced osteogenic differentiation in mesenchymal stromal cells supports leukemia growth. *JCI insight* **2**, (2017).
183. Martine, L. C. *et al.* Engineering a humanized bone organ model in mice to study bone metastases. *Nat. Protoc.* **12**, 639–663 (2017).
184. Passaro, D., Abarategi, A., Foster, K., Ariza-McNaughton, L. & Bonnet, D. Bioengineering of Humanized Bone Marrow Microenvironments in Mouse and Their Visualization by Live Imaging. *J. Vis. Exp.* (2017). doi:10.3791/55914
185. Gribben, J. *et al.* Versatile humanized niche model enables study of normal and malignant human hematopoiesis. *J. Clin. Invest.* (2017). doi:10.1172/jci89364
186. Chen, Y. *et al.* Human extramedullary bone marrow in mice: A novel in vivo model of genetically controlled hematopoietic microenvironment. *Blood* (2012). doi:10.1182/blood-2011-11-389957
187. Reinisch, A., Hernandez, D. C., Schallmoser, K. & Majeti, R. Generation and use of a humanized bone-marrow-ossicle niche for hematopoietic xenotransplantation into mice. *Nat. Protoc.* (2017). doi:10.1038/nprot.2017.088
188. Masetti, R. *et al.* CBFA2T3-GLIS2 fusion transcript is a novel common feature in pediatric, cytogenetically normal AML, not restricted to FAB M7 subtype. *Blood* **121**, 3469–3472 (2013).
189. Bisio, V. *et al.* NUP98-fusion transcripts characterize different biological entities within acute myeloid leukemia: A report from the AIEOP-AML group. *Leukemia* **31**, 974–977 (2017).
190. Manara, E. *et al.* MLL-AF6 fusion oncogene sequesters AF6 into the nucleus to trigger RAS activation in myeloid leukemia. *Blood* **124**, 263–272 (2014).
191. Gregory, C. A., Gunn, W. G., Peister, A. & Prockop, D. J. An Alizarin red-based assay of mineralization by adherent cells in culture: comparison with cetylpyridinium chloride extraction. *Anal. Biochem.* **329**, 77–84 (2004).
192. Chou, B.-K. *et al.* A facile method to establish human induced pluripotent stem cells from adult blood cells under feeder-free and xeno-free culture conditions: a clinically compliant approach. *Stem Cells Transl. Med.* **4**, 320–32 (2015).
193. Slinker, B. K. The statistics of synergism. *Journal of Molecular and Cellular Cardiology* **30**, 723–731 (1998).

194. Bassi, Ê. J., de Almeida, D. C., Moraes-Vieira, P. M. M. & Câmara, N. O. S. Exploring the role of soluble factors associated with immune regulatory properties of mesenchymal stem cells. *Stem Cell Rev.* **8**, 329–42 (2012).
195. Mead, A. J. *et al.* Niche-mediated depletion of the normal hematopoietic stem cell reservoir by Flt3-ITD-induced myeloproliferation. *J. Exp. Med.* **214**, 2005–2021 (2017).
196. Passaro, D. *et al.* Increased Vascular Permeability in the Bone Marrow Microenvironment Contributes to Disease Progression and Drug Response in Acute Myeloid Leukemia. *Cancer Cell* (2017). doi:10.1016/j.ccell.2017.08.001
197. Duarte, D. *et al.* Inhibition of Endosteal Vascular Niche Remodeling Rescues Hematopoietic Stem Cell Loss in AML. *Cell Stem Cell* **22**, 64–77.e6 (2018).
198. Roorda, B. D., ter Elst, A., Kamps, W. A. & de Bont, E. S. J. M. Bone marrow-derived cells and tumor growth: contribution of bone marrow-derived cells to tumor micro-environments with special focus on mesenchymal stem cells. *Crit. Rev. Oncol. Hematol.* **69**, 187–98 (2009).
199. Laneuville, P., Heisterkamp, N. & Groffen, J. Expression of the chronic myelogenous leukemia-associated p210bcr/abl oncoprotein in a murine IL-3 dependent myeloid cell line. *Oncogene* **6**, 275–82 (1991).
200. Yamamoto, Y. *et al.* Activating mutation of D835 within the activation loop of FLT3 in human hematologic malignancies. *Blood* **97**, 2434–2439 (2001).
201. Gruber, T. A. *et al.* An Inv(16)(p13.3q24.3)-Encoded CBFA2T3-GLIS2 Fusion Protein Defines an Aggressive Subtype of Pediatric Acute Megakaryoblastic Leukemia. *Cancer Cell* **22**, 683–697 (2012).
202. Han, X. *et al.* Interleukin-17 enhances immunosuppression by mesenchymal stem cells. *Cell Death Differ.* **21**, 1758–1768 (2014).
203. Abdul-Aziz, A. M. *et al.* Hypoxia Drives AML Proliferation in the Bone Marrow Microenvironment Via Macrophage Inhibitory Factor. *Blood* **128**, (2016).
204. Wen, L. *et al.* L-type calcium channels play a crucial role in the proliferation and osteogenic differentiation of bone marrow mesenchymal stem cells. *Biochem. Biophys. Res. Commun.* **424**, 439–45 (2012).
205. Aljritawi, O. S. *et al.* A novel three-dimensional stromal-based model for in vitro chemotherapy sensitivity testing of leukemia cells. *Leuk. Lymphoma* **55**, 378–91 (2014).
206. Leisten, I. *et al.* 3D co-culture of hematopoietic stem and progenitor cells and mesenchymal stem cells in collagen scaffolds as a model of the hematopoietic niche. *Biomaterials* **33**, 1736–47 (2012).
207. Guerrouahen, B. S., Al-Hijji, I. & Tabrizi, A. R. Osteoblastic and vascular endothelial niches, their control on normal hematopoietic stem cells, and their consequences on the development of leukemia. *Stem Cells International* (2011). doi:10.4061/2011/375857
208. Reikvam, H. *et al.* The cytokine-mediated crosstalk between primary human acute myeloid cells and mesenchymal stem cells alters the local cytokine network and the global gene expression profile of the mesenchymal cells. *Stem Cell Res.* (2015). doi:10.1016/j.scr.2015.09.008

209. Kojima, K. *et al.* p53 activation of mesenchymal stromal cells partially abrogates microenvironment-mediated resistance to FLT3 inhibition in AML through HIF-1 α -mediated down-regulation of CXCL12. *Blood* **118**, 4431–9 (2011).
210. Libreros, S., Garcia-Areas, R. & Iragavarapu-Charyulu, V. CHI3L1 plays a role in cancer through enhanced production of pro-inflammatory/pro-tumorigenic and angiogenic factors. *Immunol. Res.* **57**, 99–105 (2013).
211. Li, S. *et al.* Plasminogen activator inhibitor-1 in cancer research. *Biomedicine and Pharmacotherapy* **105**, 83–94 (2018).
212. Tai, I. T. & Tang, M. J. SPARC in cancer biology: Its role in cancer progression and potential for therapy. *Drug Resist. Updat.* **11**, 231–246 (2008).
213. Zhu, Y.-H. *et al.* High expression of biglycan is associated with poor prognosis in patients with esophageal squamous cell carcinoma. *Int. J. Clin. Exp. Pathol.* **6**, 2497 (2013).
214. Bonavita, E. *et al.* PTX3 is an extrinsic oncosuppressor regulating complement-dependent inflammation in cancer. *Cell* **160**, 700–714 (2015).
215. Qiu, Q. C. *et al.* CHI3L1 promotes tumor progression by activating TGF- β signaling pathway in hepatocellular carcinoma. *Sci. Rep.* **8**, (2018).
216. Wu, J. *et al.* Plasminogen activator inhibitor-1 inhibits angiogenic signaling by uncoupling vascular endothelial growth factor receptor-2- α V β 3 integrin cross talk. *Arterioscler. Thromb. Vasc. Biol.* **35**, 111–20 (2015).
217. Sexauer, A. N. & Tasian, S. K. Targeting FLT3 signaling in childhood acute myeloid leukemia. *Frontiers in Pediatrics* **5**, (2017).
218. Dawson, M. A. *et al.* Inhibition of BET recruitment to chromatin as an effective treatment for MLL-fusion leukaemia. *Nature* **478**, 529–533 (2011).
219. Griessinger, E. *et al.* Acute myeloid leukemia xenograft success prediction: Saving time. *Exp. Hematol.* **59**, 66–71.e4 (2018).
220. Welschinger, R. *et al.* Plerixafor (AMD3100) induces prolonged mobilization of acute lymphoblastic leukemia cells and increases the proportion of cycling cells in the blood in mice. *Exp. Hematol.* **41**, (2013).
221. Walkley, C. R. *et al.* A microenvironment-induced myeloproliferative syndrome caused by retinoic acid receptor gamma deficiency. *Cell* **129**, 1097–110 (2007).
222. Quail, D. F. & Joyce, J. A. Microenvironmental regulation of tumor progression and metastasis. *Nature Medicine* **19**, 1423–1437 (2013).
223. Nilsson, S. K. *et al.* Osteopontin, a key component of the hematopoietic stem cell niche and regulator of primitive hematopoietic progenitor cells. *Blood* **106**, 1232–1239 (2005).
224. Andresen, V. & Gjertsen, B. T. Drug repurposing for the treatment of acute myeloid leukemia. *Frontiers in Medicine* **4**, (2017).
225. Grassi, G., Robles, N. R., Seravalle, G. & Fici, F. Lercanidipine in the management of hypertension: An update. *Journal of Pharmacology and Pharmacotherapeutics* **8**, 155–165 (2017).

226. Buchanan, P. J. & McCloskey, K. D. CaV channels and cancer: canonical functions indicate benefits of repurposed drugs as cancer therapeutics. *European Biophysics Journal* **45**, 621–633 (2016).
227. Phan, N. N. *et al.* Voltage-gated calcium channels: Novel targets for cancer therapy. *Oncol. Lett.* **14**, 2059–2074 (2017).
228. Walasek, M. A., van Os, R. & de Haan, G. Hematopoietic stem cell expansion: challenges and opportunities. *Ann. N. Y. Acad. Sci.* **1266**, 138–50 (2012).
229. Behrmann, L., Wellbrock, J. & Fiedler, W. Acute myeloid leukemia and the bone marrow niche - Take a closer look. *Frontiers in Oncology* **8**, (2018).
230. Takaku, T. *et al.* Hematopoiesis in 3 dimensions: Human and murine bone marrow architecture visualized by confocal microscopy. *Blood* (2010). doi:10.1182/blood-2010-02-268466
231. Hurmale, A. K. *et al.* Overexpression of chitinase like protein YKL-40 in leukemia patients. *J. BioSci. Biotech* **2013**, 215–220
232. Bergmann, O. J. *et al.* High serum concentration of YKL-40 is associated with short survival in patients with acute myeloid leukemia. *Clin. Cancer Res.* **11**, 8644–52 (2005).
233. French, D. *et al.* A PAI-1 (SERPINE1) polymorphism predicts osteonecrosis in children with acute lymphoblastic leukemia: A report from the children's oncology group. *Blood* **111**, 4496–4499 (2008).
234. Biagi, E. *et al.* PTX3 as a potential novel tool for the diagnosis and monitoring of pulmonary fungal infections in immuno-compromised pediatric patients. *J. Pediatr. Hematol. Oncol.* **30**, 881–5 (2008).
235. Greco, R. *et al.* Pentraxin 3 As a Novel Diagnostic and Prognostic Biomarker for Acute GvHD and Fungal Infections in Adult Allogeneic HSCT Recipients. *Blood* **128**, (2016).
236. Paschka, P. *et al.* Adding dasatinib to intensive treatment in core-binding factor acute myeloid leukemia-results of the AMLSG 11-08 trial. *Leukemia* **32**, 1621–1630 (2018).
237. Langhans, S. A. Three-dimensional in vitro cell culture models in drug discovery and drug repositioning. *Frontiers in Pharmacology* **9**, (2018).
238. Barron, T. I., Connolly, R. M., Sharp, L., Bennett, K. & Visvanathan, K. Beta blockers and breast cancer mortality: A population-based study. *J. Clin. Oncol.* **29**, 2635–2644 (2011).
239. Lemeshow, S. *et al.* β -blockers and survival among danish patients with malignant melanoma: A population-based cohort study. *Cancer Epidemiol. Biomarkers Prev.* **20**, 2273–2279 (2011).
240. Chae, Y. K., Dimou, A., Pierce, S., Kantarjian, H. & Andreeff, M. The effect of calcium channel blockers on the outcome of acute myeloid leukemia. *Leuk. Lymphoma* **55**, 2822–2829 (2014).
241. Aksu, S. *et al.* Over-expression of angiotensin-converting enzyme (CD 143) on leukemic blasts as a clue for the activated local bone marrow RAS in AML. *Leuk. Lymphoma* **47**, 891–896 (2006).

242. Zwaan, C. M. *et al.* Collaborative efforts driving progress in pediatric acute myeloid leukemia. *Journal of Clinical Oncology* (2015). doi:10.1200/JCO.2015.62.8289

Secondary projects

1. Epigenetic heterogeneity affects the risk of relapse in children with t(8;21)RUNX1-RUNX1T1-rearranged AML. *Leukemia*. 2018 May; (32):1124-1134.

2. The long noncoding RNA *BALR2* controls new transcriptional circuits conferring chemotherapy resistance in acute leukemia. *Blood*
Under revision

1. Epigenetic heterogeneity affects the risk of relapse in children with t(8;21)*RUNX1-RUNX1T1*-rearranged AML

Matteo Zampini^{1*}, Claudia Tregnago^{2*}, Valeria Bisio², Luca Simula³, **Giulia Borella**², Elena Manara¹, Carlo Zanon¹, Francesca Zonta², Valentina Serafin², Benedetta Accordi², Silvia Campello⁴, Barbara Buldini², Andrea Pession⁵, Franco Locatelli⁶, Giuseppe Basso², Martina Pigazzi²

* These authors contributed equally to this work

Affiliations:

1) Istituto di Ricerca Pediatrica (IRP) – Fondazione Città della Speranza, Haematology-Oncology Lab, Padova, Italy. 2) University of Padova, Women and Child Health Department, Haematology-Oncology Clinic and Lab, Padova, Italy. 3) Department of Biology, University of Rome Tor Vergata, Italy; Department of Pediatric Haematology and Oncology, IRCCS Bambino Gesù Children's Hospital, Rome, Italy. 4) Department of Biology, University of Rome Tor Vergata, Italy; IRCCS, Fondazione Santa Lucia, Rome, Italy. 5) Department of Pediatrics, Sant'Orsola Hospital, University of Bologna, Italy. 6) Department of Pediatric Onco-Haematology, IRCCS Bambino Gesù Children's Hospital, Rome, University of Pavia, Italy.

Leukemia. 2018 May; (32):1124-1134.

Manuscript is available online

doi: 10.1038/s41375-017-0003-y.

Abstract

The somatic translocation t(8;21)(q22;q22)/RUNX1-RUNX1T1 is one of the most frequent rearrangements found in children with standard-risk acute myeloid leukemia (AML). Despite the favorable prognostic role of this aberration, we recently observed a higher than expected frequency of relapse. Here, we employed an integrated high throughput approach aimed at identifying new biological features predicting relapse among 34 t(8;21)-rearranged patients. We found that the DNA methylation status of patients who suffered from relapse was peculiarly different from that of children maintaining complete remission. The epigenetic signature, made up of 337 differentially methylated regions, was then integrated with gene and protein expression profiles, leading to a network, where cell-to-cell adhesion and cell-motility pathways were found to be aberrantly activated in relapsed patients. We identified most of these factors as RUNX1-RUNX1T1 targets, with Ras Homolog Family Member (RHOB) overexpression being the core of this network. We documented how RHOB re-organized the actin cytoskeleton through its downstream ROCK-LIMK-COFILIN axis: this increases blast adhesion by stress fiber formation, and reduces mitochondrial apoptotic cell death after chemotherapy treatment. Altogether, our data show an epigenetic heterogeneity within t(8;21)-rearranged AML patients at diagnosis able to influence the program of the chimeric transcript, promoting blast re-emergence and progression to relapse.

2. The long noncoding RNA *BALR2* controls new transcriptional circuits conferring chemotherapy resistance in acute leukemia

Valeria Bisio^{1†}, Maddalena Benetton^{1†}, Elena Porcù^{1†}, Matteo Bordi², Carlo Zanon³, **Giulia Borella**¹, Ambra Da Ros¹, Giuseppe Germano³, Sabrina Manni⁴, Claudia Tregnago¹, Silvia Campello², Dinesh S. Rao⁵, Franco Locatelli⁶, Martina Pigazzi^{1,3*}

† Authors contributed equally to the manuscript

Affiliations:

1) Women and Child Health Department, Hematology-Oncology Clinic and Lab, University of Padova, Padova, Italy. 2) Department of Biology, University of Rome Tor Vergata, Rome, Italy. 3) Istituto di Ricerca Pediatrica - Città della Speranza, Padova, Italy. 4) Department of Medicine, Hematology and Clinical Immunology Branch, University of Padova, Padova, and Veneto Institute of Molecular Medicine (VIMM), Padova, Italy. 5) Department of Pathology and Laboratory Medicine, UCLA, Los Angeles, USA. 6) Department of Pediatric Hematology and Oncology, Bambino Gesù Children's Hospital, Sapienza University of Rome, Roma, Italy.

Key points:

1. *BALR2* expression identifies pediatric AML patients with higher incidence of therapy resistance
2. *BALR2* levels influence AML cells mitochondrial mass, thus mitochondrial targeting may represent a strategy to enhance chemo-sensitivity

Abstract

In AML, the assessment of post-induction minimal residual disease (MRD) is largely utilized for choosing post-remission therapies aimed at maintaining complete remission and preventing relapse. This latter is still the major cause of treatment failure in pediatric AML, and even if several efforts have been spent to validate MRD as a prognostic marker, numerous studies demonstrated that MRD negativity cannot be considered a completely reliable surrogate biomarker predicting outcome, since it does not exclude a relapse. We, thus, hypothesized that other markers need to be explored to re-interpret leukemia progression. We found an overall hyper-expression of the lncRNA *BALR2* in 132 *de novo* AML, and produced important advances by gene expression profile in identifying *BALR2* as a robust novel molecular marker of a new subgroup of AML characterized by a high rate of resistance to induction therapy. We demonstrated *in vitro* that *BALR2* controlled bi-directionally its neighbor gene, *CDK6*, to exert a genomic pressure creating novel transcriptional circuits able to impair *RUNX1*-driven hematopoietic differentiation process and mitochondrial biogenesis and mass in both AML and healthy CD34+ human stem cell precursors. Consistently, a mitochondria inhibitor, when used alone or coupled with *BALR2* silencing, was shown to induce AML blasts differentiation and cell death, both events increasing leukemia sensitivity to chemotherapy. Our findings attribute a distinct role to *BALR2* in the block of myeloid stem cell differentiation occurring during leukemogenesis, and sustained that novel personalized mitochondria-oriented therapeutic approaches in defined AML subgroups, could be pursued to optimize the outcome of childhood AML.

Introduction

In acute myeloid leukemia (AML), assessment of post-induction minimal residual disease (MRD) is largely utilized for choosing post-remission therapies aimed at maintaining complete remission and preventing relapse, which still represents the major cause of treatment failure¹. In the last decade, pediatric trials incorporated flow-cytometry monitoring of MRD for stratification of patients in groups at different risk of leukemia recurrence²⁻⁴. Although MRD negativity assessed by evaluation of leukemia-associated immunophenotypic patterns, quantitative polymerase chain reaction (PCR), next generation sequencing and digital PCR^{5,6} has a remarkable prognostic value, it does not completely exclude the occurrence of relapse and, thus, cannot be considered a completely reliable biomarker predicting outcome^{2,7-9}. Molecular techniques for MRD detection depend mainly on monitoring chimeric or oncogenic protein-coding genes and do not consider that chemotherapy resistance may arise from other genetic alterations, or from still unknown phenomena related to leukemia stem cell properties, cancer microenvironment factors, DNA methylation, and non-coding RNA (ncRNA) pressure¹⁰⁻¹². We and others previously showed the ability of a subset of ncRNAs and microRNAs of controlling AML oncogene expression, their functional role independently predicting a higher risk of relapse^{13,14}. Until recently, relatively fewer efforts have been spent to understand the role played by a large class of ncRNAs, the long non-coding RNAs (lncRNAs), with recent findings demonstrating their aberrant hyperactivation leading to resistance mechanisms in different neoplasia, including acute leukemia^{15,16}. LncRNAs are transcripts of more than 200 nucleotides, which can be localized into the nucleus or cytoplasm, playing diverse roles, including that of intergenic transcripts, enhancers, sense/antisense transcripts, regulation of nuclear domains¹⁷⁻²³ and transcriptional regulators both *in cis* or *trans*²⁴. Although the delineation of non-coding gene expression profiles is certainly recognized to be a useful tool to define pathways and genetic subgroups in cancer, there is a lack of functional validation and characterization of prioritized candidates.

In this study, we focused on a lncRNA, known as *BALR2* (LOC101927497). *BALR2* was prioritized from differentially expressed lncRNAs and mRNAs in cancer cells and it was shown to correlate with poor overall survival and diminished response to prednisone treatment in acute lymphoblastic leukemia¹¹, as well as to play a role in human gastric epithelial tumorigenesis²⁵.

We demonstrate the ability of *BALR2* to contribute to its own transcriptional activation and to that of its neighbor gene *CDK6*, influencing transcriptionally novel networks creating circuits able to impair RUNX1-driven hematopoietic differentiation process and to enhance mitochondrial biogenesis, both these phenomena resulting into lower chemo-sensitivity of AML blasts.

Methods

Patients' samples. Patients with *de novo* AML (n=132) other than acute promyelocytic leukemia, aged 0–18 years, diagnosed between 2002 and 2014 in one of the centers affiliated to AIEOP (Associazione Italiana Ematologia Oncologia Pediatrica) were included in these study. (see Supplementary Methods).

Gene expression analysis (GEP). RNA from BM cells collected at diagnosis from all patients for RQ-PCR analysis, and 58 for GeneChip® Human Transcriptome Array 2.0 as previously reported GSE75461 (HTA, Affymetrix, Santa Clara, CA, USA). In order to investigate the *BALR2* interaction network from gene expression data, we ranked the genes according to their absolute Spearman's rank correlation coefficient across all the selected samples with the expression profile of the probe detecting the first exon of both *CDK6* and *BALR2*, using the 'cor' function within the 'stats' package of the R software. The top 1% correlated values associated to 251 probes, and mapping to 337 RefSeq transcripts, used to perform an unsupervised clustering (see Supplemental Methods).

Cell culture. The SHI-1 leukemia cell line (DSMZ, Germany) was cultured in DMEM (Invitrogen, Carlsbad, CA) with 10% FBS, as previously described ²⁶. Human Cord Blood (CB) was collected after obtaining a written informed consent for research use from the delivering women. Mononuclear cells were isolated from CB to isolate CD34+ and CD34- cells by anti-human CD34 microbeads (Miltenyi Biotec, Bergisch-Gladbach, DE). Cell treatment with Tigecycline and AraC were used to test colony formation in semisolid medium, phagocytosis capability, mitochondria membrane potential and cell cycle as described in supplemental methods.

Immunoblotting and Immunofluorescence were performed as previously described ^{27,28}.

In situ proximity ligation assay. PLA experiments were performed by using DuoLink II (Sigma-Aldrich S.r.l., Milan, IT) as described in supplemental methods.

Cell transfection and lentiviral transduction. Three specific p2CZL short hairpin RNAs (shRNAs1, 2 and 3), kindly provided by Dr. Rao et al. ¹¹, were mixed to transiently transfect AML cell lines to silence *BALR2*. Third-generation lentiviral vectors were produced to generate *BALR2* stable knockdown (KD) constructs, as previously described ¹¹ (see supplemental methods). We referred to shRNA 1 colony 2 (namely as shBALR2-1col2 in main figures) for the high downregulation of both *BALR2* and *CDK6*, but other independent clones are presented in supplemental figures.

Plasmids construction and promoter activity assay. We generated reporter vectors to verify *CDK6-BALR2* bidirectional promoter activity. By *in silico* prediction, we selected a 1.17 kb

genomic fragment and cloned it into the pGL4.28[*luc2CP*/minP/Hygro] luciferase vector (Promega), obtaining pGL4-BALR2/CDK6-LUC plasmid. We subsequently constructed a double *luc2CP* vector by cloning the *luc2CP* gene also in 3'-5' direction upstream the promoter region, obtaining pGL4-LUC-BALR2/CDK6-LUC plasmid. Then, we knocked-out LUC from pGL4-BALR2/CDK6-LUC plasmid, by mutagenesis of the ATG start codon (Q5® site-directed mutagenesis Kit, New England BioLab), producing the pGL4-BALR2/CDK6-ΔLUC control plasmid. Luciferase activity was measured after transfection of 1 µg of each vector in SHI-1 shNEG and shBALR2-1 col 2 stable cell lines with 0.1 µg of Renilla by electroporation (Amaxa Nucleofector, Lonza) following manufacturer's instructions (Dual-Luciferase Reporter Assay, Promega).

Data evaluation and statistical analyses. p-value<0.05, *p-value<0.01, ***p-value<0.001, ****p-value<0.0001 were considered to be statistically significant, see also supplemental methods.

Results

***BALR2* expression distinguishes AML subgroups with different transcriptional profile**

We retrospectively analyzed the expression of *BALR2* in leukemia blasts of 132 patients with *de novo* AML enrolled in the AIEOP AML 2002/01 protocol ² harboring different genetic abnormalities: *CBF* rearrangement such as t(8;21)*RUNX1-RUNX1T1* and inv(16)*CBFB-MYH11* (n=20), *MLL*-translocations (n=37), *NUP98*-translocations (n=15), *FLT3-ITD* (n=15), rare translocations (n=9), and 36 patients without any recurrent molecular lesion. Overall expression of *BALR2* was significantly higher (p<0.05) in all AML samples when compared with healthy BM samples (HBM, RQ=1, Figure 1A). Furthermore, selecting a subgroup of patients harboring known fusion genes and molecularly monitored for MRD during follow-up, we noticed that, under treatment, *BALR2* expression levels reduced similarly to the known molecular marker (Supplemental Figure 1A), supporting the hypothesis that *BALR2* could serve as a new biomarker for evaluating AML response to therapy. The level of *BALR2*, in fact, decreased, at the different time points evaluated, in patients responding to treatment, while it increased again when leukemia relapse occurred (Patient C, Supplemental Figure 1A). We subdivided patients according to *BALR2* quartile expression (Figure 1B) finding heterogeneous and increasing levels of expression from quartile 1 to 4. This different *BALR2* expression distribution was maintained also subdividing patients according to genetic abnormalities identified at diagnosis (p<0.05, Supplemental Figure 1B). To interrogate a biological role for *BALR2*, we examined the gene expression profiles of 58 out of the 132 AML patients, of whom 18 cases had the highest Q4 *BALR2* (Q4-AML) expression,

and 40 were included in Q1, Q2, Q3 (Q123-AML) quartiles (GSE75461, Figure 1C). Of note, the unsupervised analysis showed a statistical significant clustering of Q4-AML from the remaining cases independently of their genetic lesions for 57 coding and 12 ncRNAs (with a Fold Change ≥ 2 , p -value <0.01 , Figure 1C; or 247 coding genes and 83 ncRNAs with a Fold Change ≥ 1.5 , p -value <0.01 , Supplemental Figure 2AB and Supplemental Table 1AB). Among the most differentially expressed genes in Q4-AML, we identified, together with *BALR2*, its adjacent gene *CDK6*, located at 7q21.2 (Supplemental Figure 2C and Supplemental Table 1B). Given that lncRNAs are known to transcriptionally regulate protein or RNA genes *in cis*, we interrogated *CDK6* and *SAMD9*, the other neighbor gene localized at 7q21.2. An overall significant positive correlation between *BALR2* and *CDK6* expression was confirmed (Figure 1D, Pearson correlation $r=0.7$, p -value <0.001), but not between *BALR2* and *SAMD9* (data not shown, Pearson correlation $r=0.11$, p -value $=0.4$). In particular, a strong correlation was observed for the majority of the groups of AML either harboring genetic mutations, such as *FLT3-ITD*, *NUP98*-rearrangements, rare translocations, or without a molecular marker (Supplemental Figure 2D; Pearson correlation respectively $r=0.79$, 0.84 , 0.96 and 0.75 ; $p<0.05$).

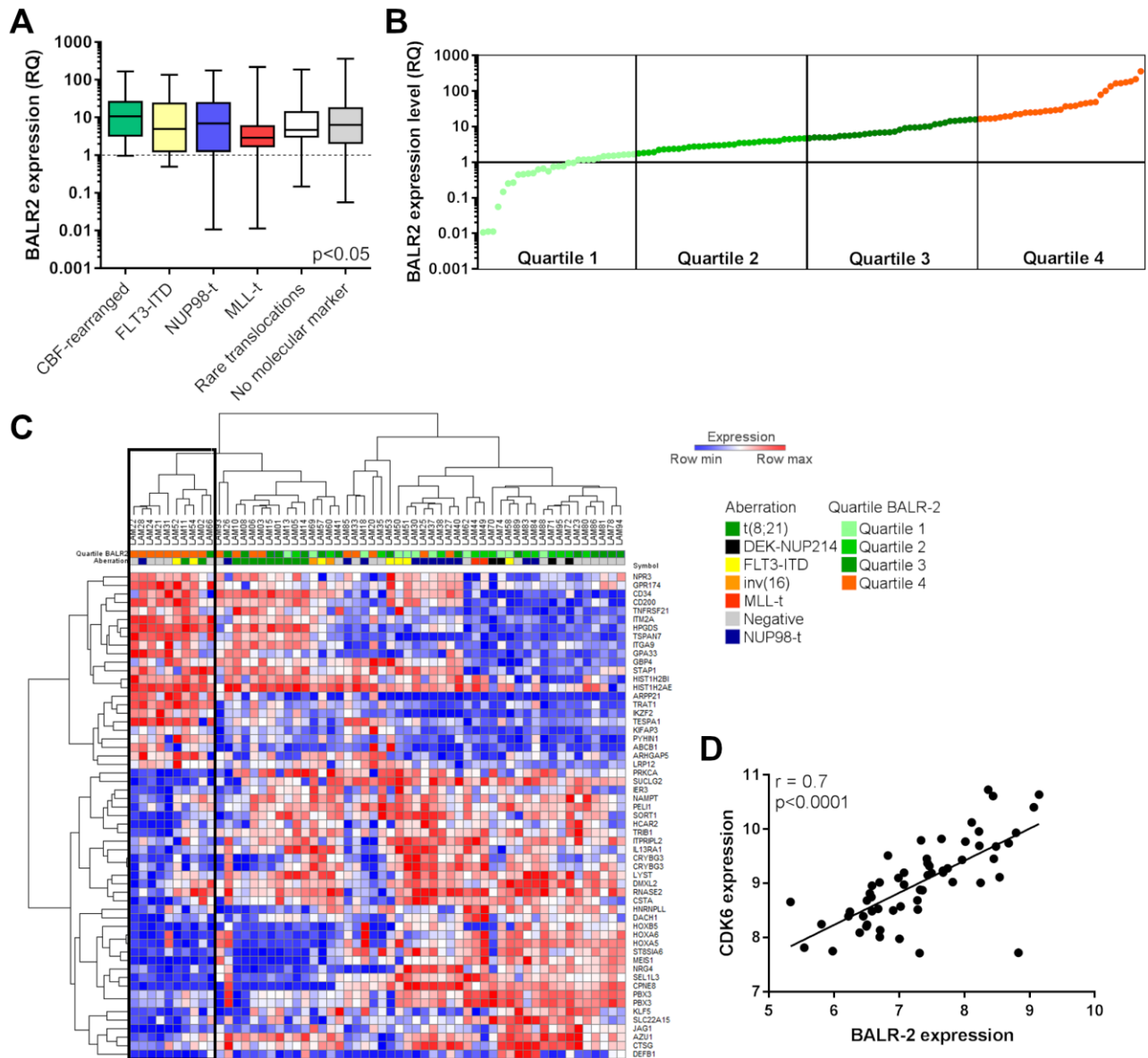


Figure 1. *BALR2* expression in AML pediatric bone marrow samples. (A) *BALR2* expression analyzed by RQ-PCR in bone marrow samples collected at diagnosis of 132 AML patients, including AML with core-binding factor aberrations (*CBF*), *FLT3-ITD*, *MLL* or *NUP*-translocations (*MLL-t*, *NUP-t*), rare translocations and negative for known recurrent genetic abnormalities (*No Molecular Marker*). RQ-PCR expression calculated with $2^{-\Delta\Delta Ct}$ of *BALR2* in AML patients compared to healthy bone marrow donors ($RQ=1$) (p -value <0.05 for all the subgroups). **(B)** Histogram of the quartiles subdivision of *BALR2* expression levels of the whole AML cohort. **(C)** Hierarchical clustering analyses of AML patients. High *BALR2* expression (Q4) patients clustered independently (black square; Pearson correlation distance, t -test, p -value <0.01 , $FC > 2$). Genetic AML subtypes and quartile distribution are indicated in the legend with color codes. **(D)** Correlation between *BALR2* and *CDK6* mRNA expressions (Pearson correlation, $r=0.7$, $p < 0.0001$) plotted in the scatter diagram and fitted in linear regression.

BALR2* controls the expression of its neighboring gene *CDK6

We hypothesized that *BALR2* might act *in cis* and coordinately regulates *CDK6* expression, supporting a functional and/or physical association. Indeed, bioinformatic analysis revealed that the two genes shared a common untranslated first exon being transcribed in opposite directions, as a putative bidirectional promoter would control their expression (Figure 2A). Additional *in silico* analyses identified this region as promoter in AML for enrichment in transcription factor binding sites (Supplemental Figure 2EF). For further corroborating the hypothesis of the common promoter for both *BALR2* and *CDK6*, we generated a dual luciferase reporter vector with one *luc2CP* Luciferase gene positioned at 5' and one positioned at 3' of the *BALR2/CDK6* predicted promoter. Results showed that dual vector increased luciferase up to 20% with respect to single luciferase vector, confirming this promoter region working bi-directionally. Then, stable cell lines silenced for *BALR2* were tested confirming the reduced luciferase activity of both constructs, this demonstrating that *BALR2* levels are crucial in controlling this promoter region (Figure 2B, *p-value<0.05). These findings spurred us to investigate the sub-cellular localization of *BALR2*²⁹. We performed RNA subcellular fractioning followed by RQ-PCR, finding that *BALR2* was localized mainly in the nucleus (Figure 2C), but also in the cytosolic fraction (Actin was used as cytosolic and U2sn for nuclear controls). To deconvolute the functional role of *BALR2*, we silenced *BALR2* in the SHI-1 AML cell line (documented to have high *BALR2* expression, comparable to that of the Q4-AML patients) both transiently and stably (namely *BALR2* KD). We found that *BALR2* KD cells reduced *CDK6* mRNA and protein expression (Figure 2D and Supplemental Figure 3AB, *p-value<0.05, **p-value<0.01), this finding being corroborated by a reduction of one of *CDK6* target, phospho-RB (at 24 hours, Supplemental Figure 3C). The observation of *CDK6* downregulation prompted us to interrogate cell cycle, given that *CDK6* is a cell-cycle checkpoint protein^{30,31}. Unexpectedly, *BALR2* silenced cells did not show cell-cycle abnormalities (Supplemental Figure 4A), and most of the genes involved in cell-cycle regulation were not aberrantly expressed with exception of *CDK6* (Supplemental Figure 4B, **p<0.01). We interrogated *CDK4*, the close homolog of *CDK6*, and found no change in its expression, supporting the idea that *BALR2* exerts control exclusively over its neighboring gene (Supplemental Figure 4C).

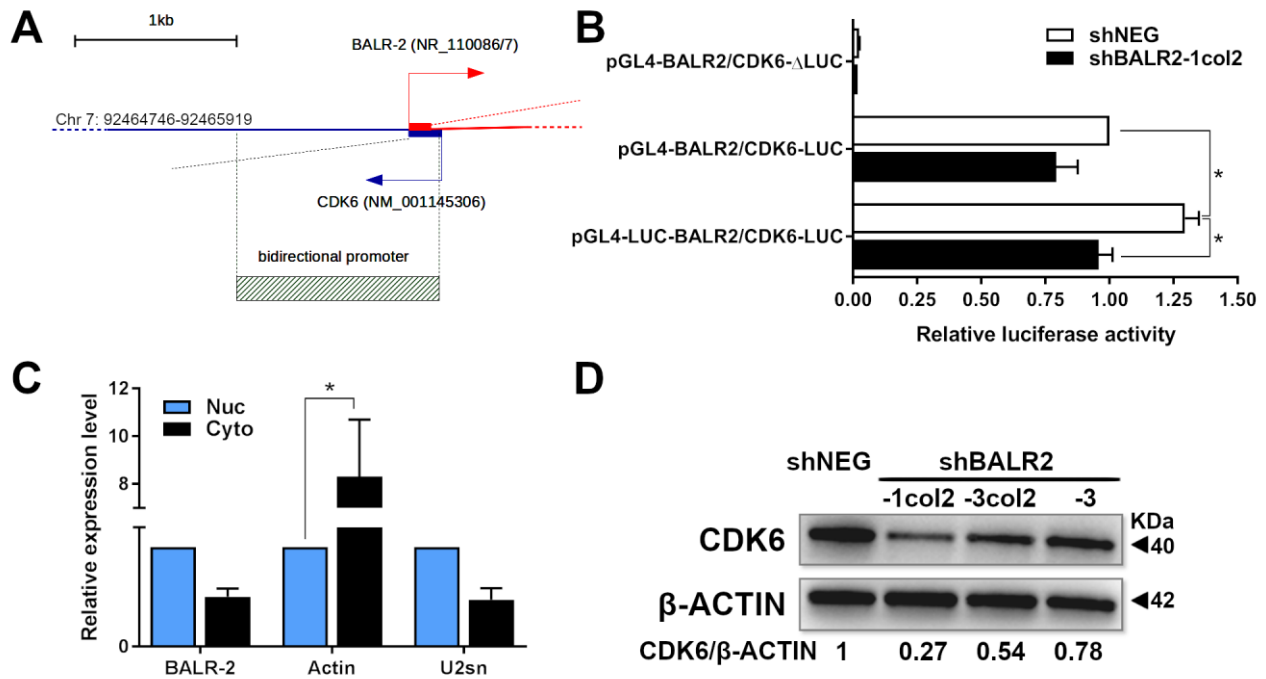


Figure 2. *BALR2-CDK6* interaction in AML cell. (A) Schematic view of the chromosomal position of *BALR2* (red) and adjacent *CDK6* (blue) on chromosome 7. The common region between *CDK6* and *BALR2* is highlighted by the overlapped red and blue sequences. (B) Relative single and dual luciferase activity of the reporter containing the promoter region of *BALR2/CDK6* in cells downregulated for *BALR2* compared to the control vector. Relative luciferase activity expressed by the ratio of firefly luciferase to Renilla luciferase. Data presented as mean±SEM from three independent experiments. *p-value<0.05. (C) RQ-PCR of *BALR2*, *Actin* and *U2sn* after RNA subcellular isolation from SHI-1 cell line. Nuclear (Nuc) and cytoplasmic (Cyto) fractions are shown. Data are presented as mean of three independent experiments ± SEM. *p-value<0.05. (D) Western blot after stable *BALR2* silencing in three different clones and two different sh-RNAs (namely 1 and 3). shBALR2-1col2 was selected as the most silenced colony and used for further experiments.

***BALR2* expression is associated with an immature myeloid phenotype**

Next, we looked beyond *CDK6*'s known role in the cell cycle, investigating a less known function involved in the control of hematopoietic myeloid differentiation process³². We investigated cell differentiation by monitoring *CD11b* expression, a marker of myeloid maturation, in *BALR2* KD cells, finding increased expression in comparison to the cells where *BALR2* and *CDK6* levels were higher. We documented that after decreasing *BALR2* expression, both stably and transiently, KD cells acquired *CD11b* expression (79.5% versus 55.2% respectively, Figure 3A, p<0.05, and Supplemental Figure 5AB). Functionally, *BALR2* KD cells showed a significantly increased phagocytic capability that was further augmented when cells were stimulated with GM-CSF (Figure 3BC and Supplemental Figure 5CD, p-value<0.05). Together, these data suggest that high *BALR2*

levels are associated with the maintenance of myeloid cells in an immature progenitor state without effects on cell viability (Supplemental Figure 5E). In line with these findings, *BALR2* KD cells showed a reduction of more than 30% in their colony-forming capacity, and an increase in PU1 protein, a transcription factor involved in early myeloid differentiation (Figure 3DE, p-value<0.05).

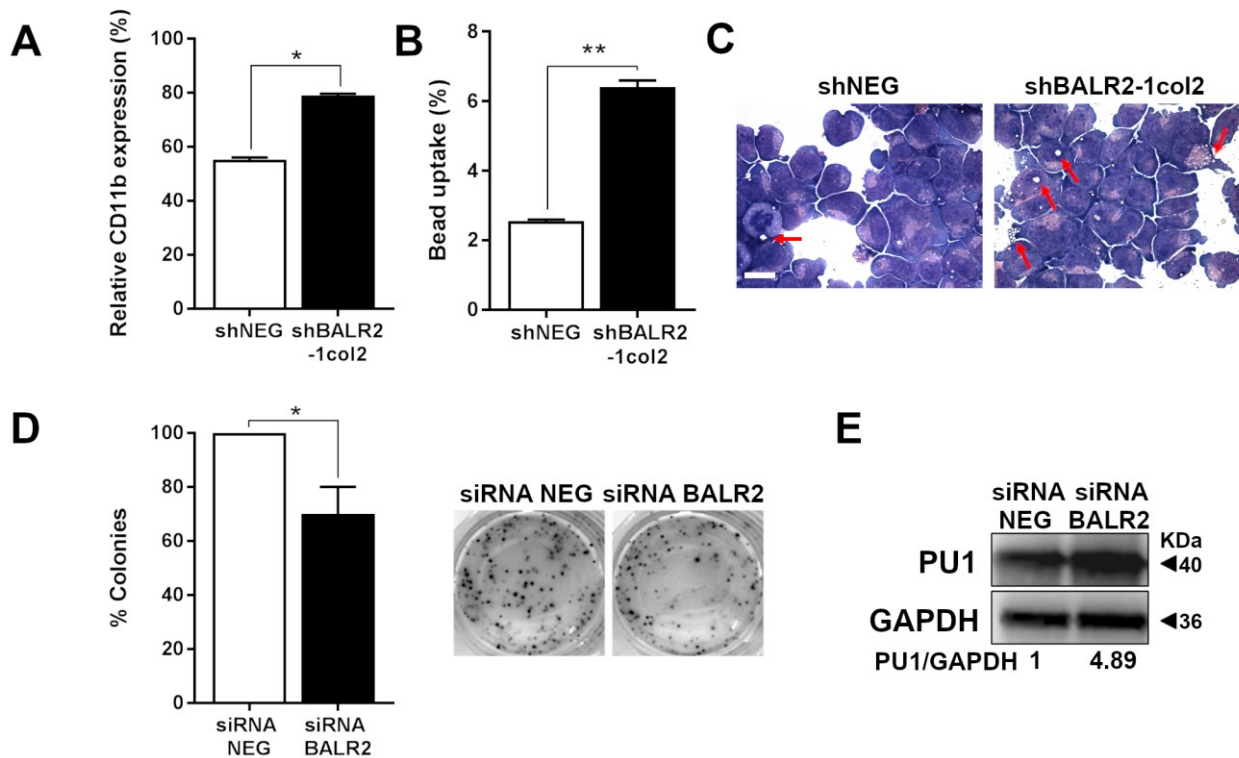


Figure 3. Myeloid maturation in *BALR2*-knockdown cells. (A) CD11b expression after *BALR2*-knockdown as compared to control cells (n=3, p<0.05). (B) Percentage of bead uptakes in phagocytosis assay (n=3, p<0.01) and (C) representative images of phagocytic cells with intracellular beads (magnification 40x, scale bar = 15µm). (D) Colony forming capability and (E) PU1 expression levels after *BALR2* silencing in SHI-1 cells. (n=3, *p-value<0.05). Data are presented as mean of three independent experiments ± SEM.

The CDK6 interaction with the Runt domain of the Runt-related transcription factor 1 (*RUNX1*) is a previously identified mechanism³² that controls genes necessary for the early differentiation steps towards mature blood cells. By proximity ligation assay, we found that *BALR2* expression levels influenced the CDK6-RUNX1 complex formation, showing a striking reduction of this interaction in *BALR2* KD cells (red spots in Figure 4A present only in the shNEG with high *BALR2* levels, and Supplemental Figure 6A shows similar results in the independent shBALR2-3col2 stable clone). Thus, we explored if this phenomenon of high CDK6 levels increasing its binding to *RUNX1* could

block its transcriptional program. We looked at expression of the 81 *RUNX1* target genes in *BALR2*-Q1-AML versus Q4-AML (deposited in ChEA database ³³ and annotated to myeloid cell differentiation by GO term 0030099). We found a significant deregulation of most of the *RUNX1* target genes in Q4-AML with respect to Q1-AML patients as shown by clustering, PCA and GSEA analyses (Figure 4BC, Supplemental Figure 6B and Supplemental Table 1C t-test $p < 0.05$).

***BALR2* correlates with healthy hematopoietic stem cell progenitors (HSCPs) differentiation**

We ranked the genes according to the top 1% *BALR2* and *CDK6* correlated probe values and obtained a signature of 337 transcripts used to perform an unsupervised clustering of 27 samples of human blood cells from healthy donors obtained from public dataset (GSE98633 ³⁴) dichotomized either into CD34+ or CD14+ groups. We found this 337 gene-signature perfectly distinguishing the two healthy hematopoietic pools (Figure 4D) with the non-linear dimensionality reduction by t-distributed stochastic neighbor embedding (t-SNE) analysis confirming a robust separation of the CD34+/CD14+ cells according to the *BALR2* quartiles (Figure 4E). Notably, the CD34+ cell expression profile was comparable to that of *BALR2* Q4-AML, whereas that of the mature CD14+ population with Q123-AML (Supplemental Figure 7A). To confirm that *BALR2* levels correlate with hematopoietic cell differentiation, we used CB samples and isolated the CD34+ HSPCs: we extracted total RNA finding a physiological higher expression of *BALR2* and *CDK6* in the more immature cell fraction CD34+ as seen *in silico* (Figure 4F). In order to capture the early modifications mediated by *BALR2* expression levels in HSPCs, we transduced CB-34+ cells with sh-*BALR2* constructs. We found reduced *CDK6* levels, which did not affect cell viability (Figure 4G), and loss of CD34 expression, which was retained in the shNEG control cells (Figure 4H, $p < 0.01$), supporting *BALR2* contribution toward an aberrant cell differentiation and malignant hematopoiesis.

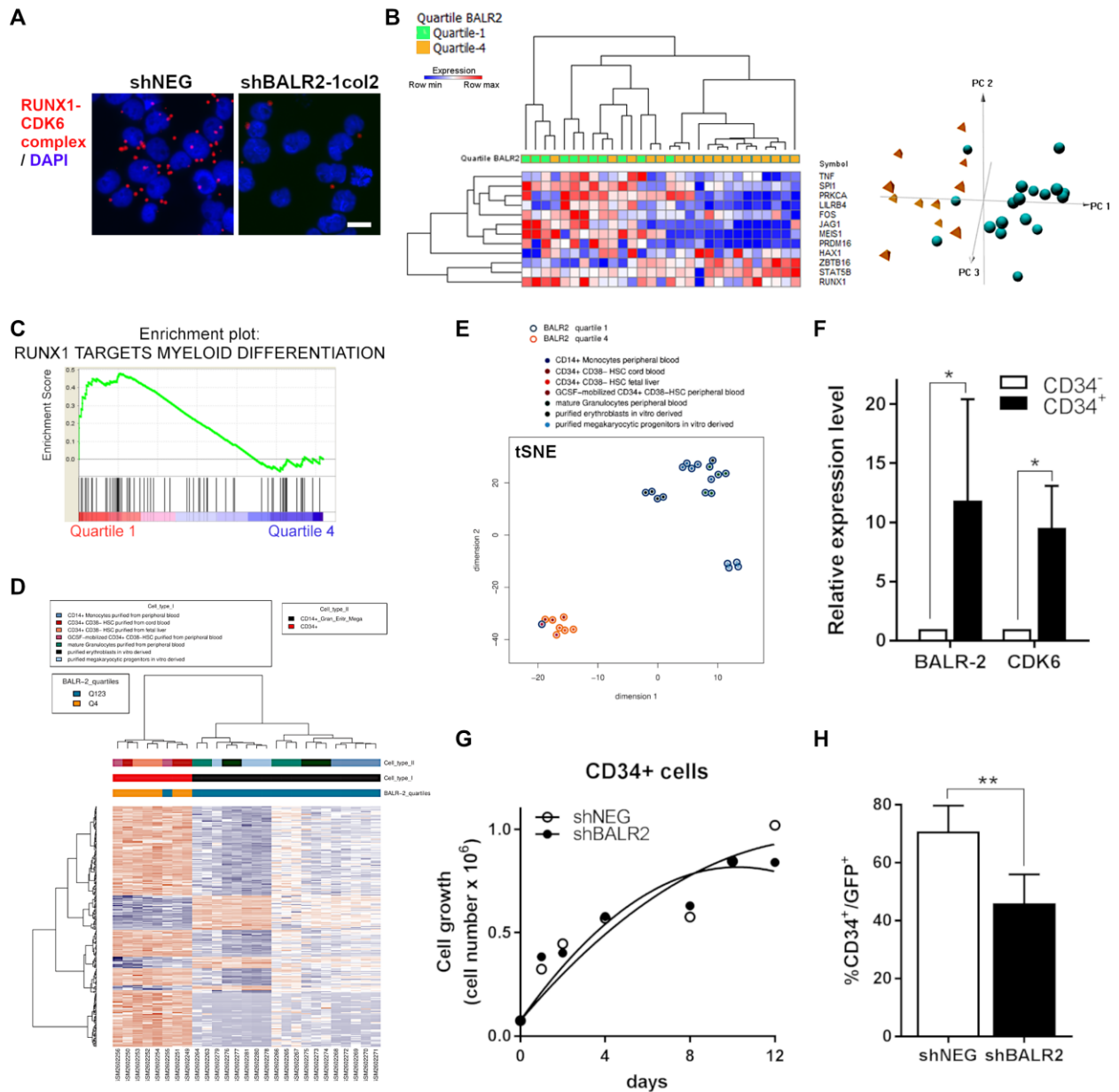


Figure 4. *BALR2/CDK6* controls hematopoietic differentiation process. (A) CDK6-RUNX1 complex (red dots) in Proximity Ligation Assay in SHI-1 cells knockdown for BALR2 expression. Nuclei were stained with DAPI (blue) (40x magnification, scale bar = 15µm). **(B)** Gene expression heatmap (upper panel, p-value<0.05) and Principal-Component Analysis (right panel) of significant RUNX1 target genes involved in myeloid cell differentiation in BALR2 Q1-AML versus Q4-AML (FDR q-value <0.25 and p-value <0.01). **(C)** Gene Set Enrichment Analysis (GSEA) confirmed the upregulation of RUNX1 target genes in Q1-AML versus Q4-AML patients. **(D)** Unsupervised hierarchical clustering of leukemia patients with the 337 BALR2-CDK6 signature. **(E)** t-SNE plot of the CD34⁺ and CD14⁺ cells from healthy donors clustered according to the expression values of the 337 BALR2-CDK6 signature. **(F)** BALR2 expression in CD34⁺ and CD34⁻ fractionated population (white bars are non-sorted cells, n=3). **(G)** Cell growth curve in shNEG and shBALR2-transduced CD34⁺ cells. **(H)** Decrease in CD34⁺ positive cell number upon BALR2 depletion (shBALR2 that are GFP⁺) by flow cytometry. (n=3, *p-value<0.05, **p-value<0.01).

***BALR2* controls mitochondrial biogenesis pathways in AML**

To further clarify these findings, we returned to interrogate gene ontology signatures (GO) of the AML (GSE75461) and of the genes of the previous found 337-gene-signature (the top 1% of genes correlated to *BALR2/CDK6*, see Figure 4D). This analysis revealed that overexpression of genes related to several mitochondria signatures strongly correlated with the Q4-AML and the 337 gene signature (Figure 5A FDR q -value <0.25 , $p<0.01$, Supplemental Figure 7B and Supplemental Table 2ABC). We investigated this feature by performing single-sample GSEA (ssGSEA) in patients, revealing that molecular signatures linked to mitochondrial biogenesis were increasingly enriched in patients whose blasts showed higher *BALR2* expression quartiles (Figure 5B * $p<0.05$, ** $p<0.01$, Supplemental Figure 7C and Supplemental Table 2D). This observation suggested aberrant mitochondrial synthesis in Q4-AML. We interrogated the biological meaning by re-annotating the significant mitochondrial GO-signature genes with DAVID and GenBank (Supplemental Table 3A) and selected 24 genes³⁵ that were significantly differentially expressed in immature CD34+ *versus* mature CD14+ healthy cells, and tested their expression in AML patients (Supplemental Table 3B). By unsupervised clustering analysis, we documented that both CD34+ HSCPs and Q4-AML have a unique mitochondrial signature expression portrait, whereas the mature CD14+ cells recapitulated the expression of the Q123-AML (Figure 5C). Dot plots of those genes known to regulate mitochondrial biogenesis, namely *TFAM*, *ACACA*, *PPARA* and *PPID* were confirmed to be highly expressed in Q4-AML with respect to Q123-AML (Figure 5D). Furthermore, in stable *BALR2* KD cells, we found a decrease of the main transcription factors *TFAM*, *NRF1* and *FIS1* involved in mitochondrial synthesis and dynamics (Figure 5E, $n=3$, p -value <0.05). Indeed, if *BALR2* expression alters the dynamics of mitochondria in AML cells, it could result in reprogramming blasts to meet the challenges of high energy demand, evade apoptosis promoting AML resistance^{36,37}.

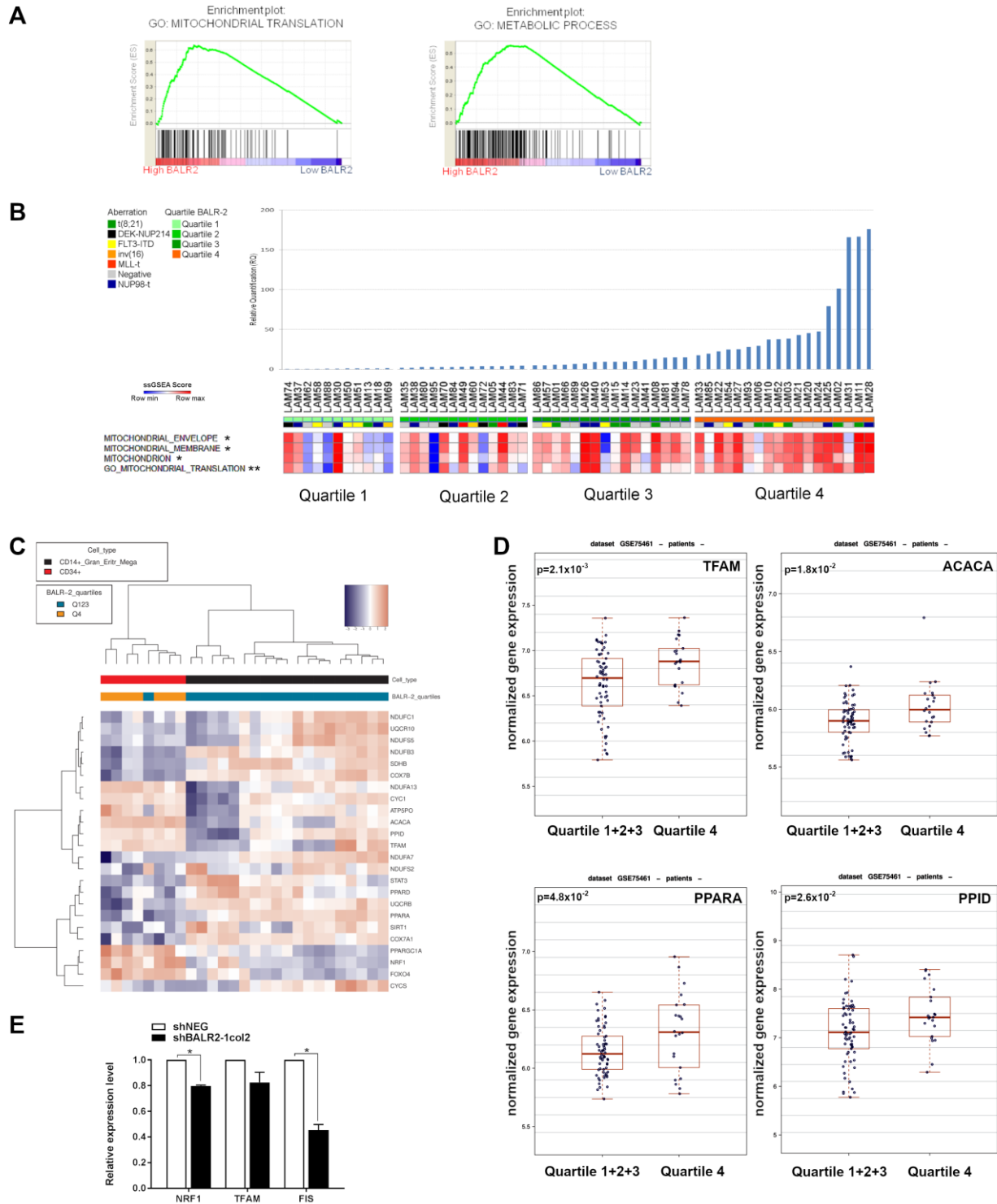


Figure 5. *BALR2* expression mark AML with peculiar mitochondriogenesis. (A) Significant Gene Set Enrichment Analysis (GSEA) in Q4-AML patients (FDR q-value <0.25 and p-value <0.01). **(B)** ssGSEA of AML according to *BALR2* expression (*p-value<0.05). **(C)** Unsupervised hierarchical clustering performed by using the 24 mitochondria genes significantly deregulated in healthy CD34+ and CD14+ cells (Supplemental Table 3B) correctly identified AML according to *BALR2* expression quartiles. **(D)** Box plots of main mitochondria biogenesis-genes in Q4-AML versus Q123-AML (*p-value<0.05, **p-value<0.01 significant by student's t-test). **(E)** *NRF1*, *TFAM* and *FIS1* gene expression measured in cell silenced for sh*BALR2* with respect to shRNA NEG (RQ=1) (n=3, *p-value<0.05).

In line with this biological finding, we observed that Q4-AML patients had a greater risk of not achieving complete remission (28% versus 12%, $p=0.03$, Table 1) when compared to children with Q123-AML. Although children with the highest *BALR2* expression were older (10.1 versus 7.4 years, $p=0.006$), they did not show any difference for all the other characteristics recorded at diagnosis, including white blood cell count, FAB morphological classification and genetic lesions. Notably, children with the highest *BALR2* expression ($n=32$) had a lower, although not statistically significant, 2-year EFS when compared to those assigned to the Q123-AML ($n=100$; 53% versus 62%, Supplemental Figure 8A $p=ns$, 8B).

Table 1. Clinical and biological features of AML patients.

BALR-2 RQ-exp	I+II+III quartile	IV quartile	#<i>p-value</i>
TOTAL n=132	100	32	
Gender (Female/Male)			<i>ns</i>
F	38 (38%)	21 (66%)	
M	62 (62%)	11 (34%)	
Age at diagnosis			<i>0.006</i>
<2 years	27 (27%)	1 (3%)	
2-10 years	36 (36%)	11 (34.5%)	
>10 years	37 (37%)	20 (62.5%)	
Mean	7.4	10.1	
Leucocyte count at diagnosis ($\times 10^9/l$)			<i>ns</i>
<10	29 (29%)	7 (21.9%)	
>10<99	47 (47%)	14 (43.8%)	
>100	16 (16%)	9 (28.1%)	
N/A	8 (8%)	2 (6.2%)	
Mean	49447	101279	
FAB subtype			<i>ns</i>
M0	10 (10%)	3 (9.4%)	
M1	11 (11%)	8 (25%)	
M2	17 (17%)	7 (21.9%)	
M4	13 (13%)	4 (12.5%)	
M5	27 (27%)	5 (15.6%)	
M6	1 (1%)	0	
M7	4 (4%)	3 (9.4%)	
Unclassified/not known	17 (17%)	2 (6.2%)	
Molecular Markers			<i>ns</i>

<i>t(8;21) or inv(16)</i>	13 (13 %)	7 (21.9%)	
<i>FLT3-ITD</i>	11 (11%)	4 (12.5%)	
<i>NUP98</i> -translocations	9 (9%)	6 (18.8%)	
<i>MLL</i> -translocations	33 (33%)	4 (12.5%)	
Rare translocations	8 (8%)	1 (3%)	
No Molecular Marker	26 (26%)	10 (31,3%)	
Cytogenetic data			<i>ns</i>
Complex karyotype	8 (8%)	4(12.5%)	
Monosomal karyotype	2 (2%)	1 (3%)	
Normal karyotype	65 (65%)	21 (65.7%)	
Unclassified/not known	25 (25%)	6 (18.8%)	
Remission			
YES	88 (88%)	23 (71.9%)	<i>0.03</i>
NO	12 (12%)	9 (28.1%)	
Relapse			
YES	25 (25%)	9 (28.1%)	<i>ns</i>
NO	75 (75%)	23 (71.9%)	

Legend: *ITD*: internal tandem duplication; # Chi-square test.

We next studied the effect of *BALR2* on mitochondrial mass, as suggested by their aberrant gene expression profile, to address this observed differences in treatment response. Consistently, we found a dramatic reduction in mitochondrial mass in *BALR2* KD cells, by measuring the area of mitochondria covered by the specific marker TOMM20 and by using an antibody targeting mitochondrial DNA³⁸ (Figure 6ABC and Supplemental Figure 9AB, $p < 0.0001$). We confirmed a disruption of mitochondrial functions by measuring the mitochondrial membrane potential ($\Delta\Psi$) in three AML cell lines with either high or low *BALR2* expression, finding a positive correlation between $\Delta\Psi$ and *BALR2* levels (Supplemental Figure 10A), as well as following *BALR2* silencing (Supplemental Figure 10BC). Next, in light with the working hypothesis of considering cell metabolism and mitochondria involved in cancer cell plasticity, we decided to target mitochondria by using, in our *BALR2*-model, TIGE, an antimicrobial agent known to inhibit mitochondrial protein translation and previously shown to have robust preclinical anti-leukemia activity both *in vitro* and *in vivo* against AML blasts³⁹. TIGE, when used either alone or combined with a currently employed cytotoxic agent, AraC, showed an inhibitory effect on cell proliferation, with significant increase in cytotoxic effects (Figure 6D, $*p < 0.05$, $***p < 0.001$), and $\Delta\Psi$ (Figure 6E, $*p < 0.05$, $**p < 0.01$). These effects were found to be further increased in *BALR2* KD cells, while the toxic

effect on healthy CD34⁺ cells was lower as previously reported^{39,40} (Supplemental Figure 10D, *p<0.05). *BALR2* KD cells when exposed to TIGE treatment recovered capacity of hematopoietic differentiation into more mature CD11b and CD14 expressing cells, with a potent differentiation shift toward more mature macrophage colony forming units (M-CFU) (Figure 6FG and Supplemental Figure 10E).

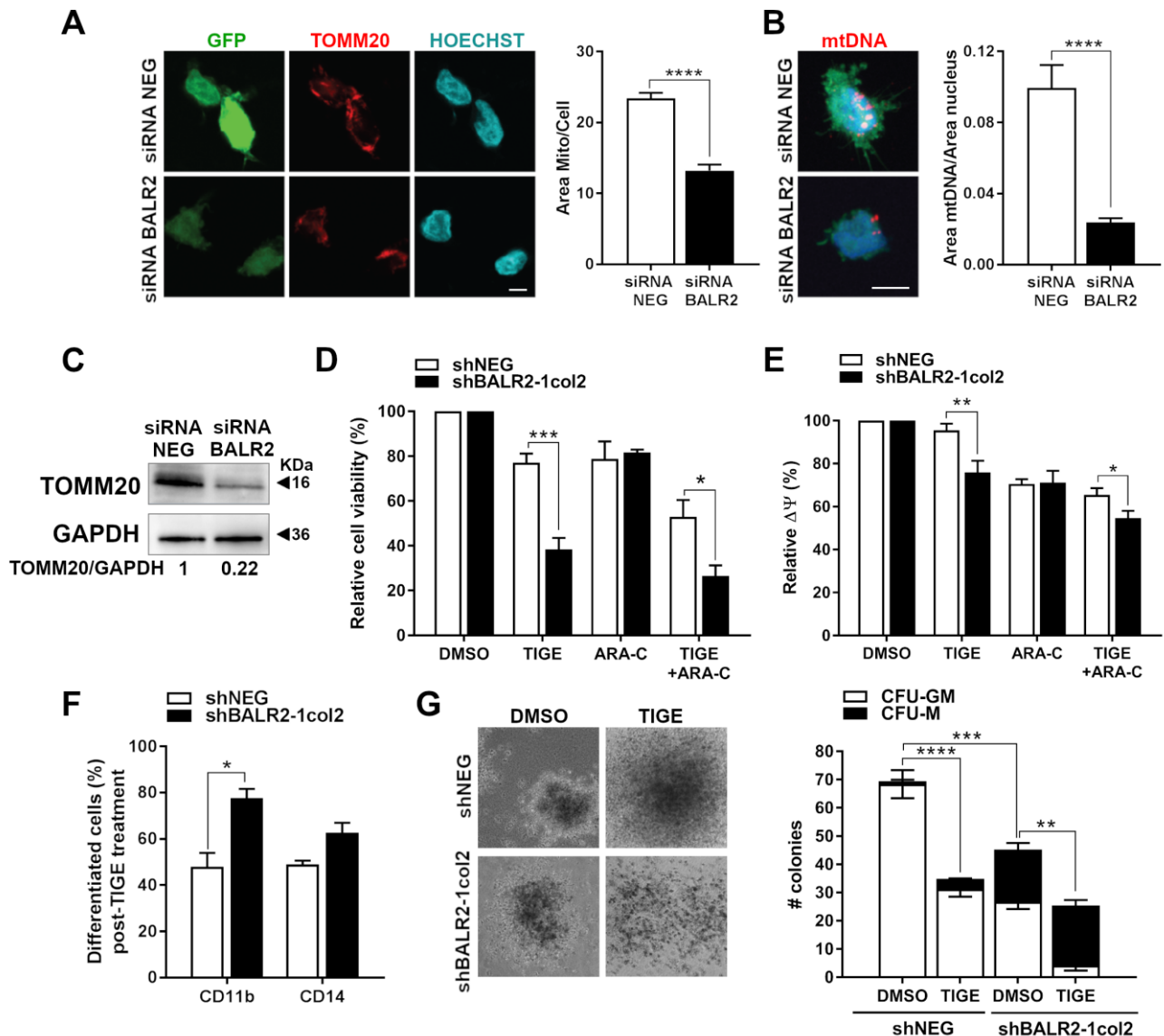


Figure 6. *BALR2* and mitochondrial mass. (A) Immunostaining of sh*BALR2*-transfected GFP⁺ (green) SHI-1 cells, stained for TOMM20 (red). Nuclei staining with Hoechst (blue) (40x magnification, scale bar = 10μm, left panel) and mitochondrial mass quantification by TOMM20 (covered area per cell, right panel, p<0.0001). (B) sh*BALR2*-transfected GFP⁺ (green) SHI-1 cells labeled for mtDNA (red) and nuclei staining with Hoechst (blue) (left panel) and mitochondrial mass quantification by mtDNA measurement (covered area per cell, right panel; 40x magnification, scale bar = 10μm, left panel p<0.001). (C) Immunoblotting of TOMM20 after *BALR2* knockdown. (D) Cell viability after 24-

hour treatment with TIGE and AraC determined with CellTiter-Glo (*p-value<0.05, **p-value<0.01; ***p-value<0.001). (E) Mitochondrial membrane potential (fluorescent TMRE probes in flow-cytometry) measured in shNEG and shBALR2-1col2 cells after DMSO, TIGE, AraC, TIGE+AraC treatments. (F) CD11b and CD14 expression during TIGE treatment in shBALR2 cells (*p-value<0.05). (G) Representative images and quantification of colonies formed after TIGE treatment and *BALR2* silencing in SHI-1 cells. Data are presented as mean of three independent experiments (n=3, **p-value<0.01; ***p-value<0.001; ****p-value<0.0001 by two-ways ANOVA).

These results point to a *BALR2* ability to switch the mitochondrial mass in AML, with important implications for mitochondria content and cell metabolism (Figure 7).

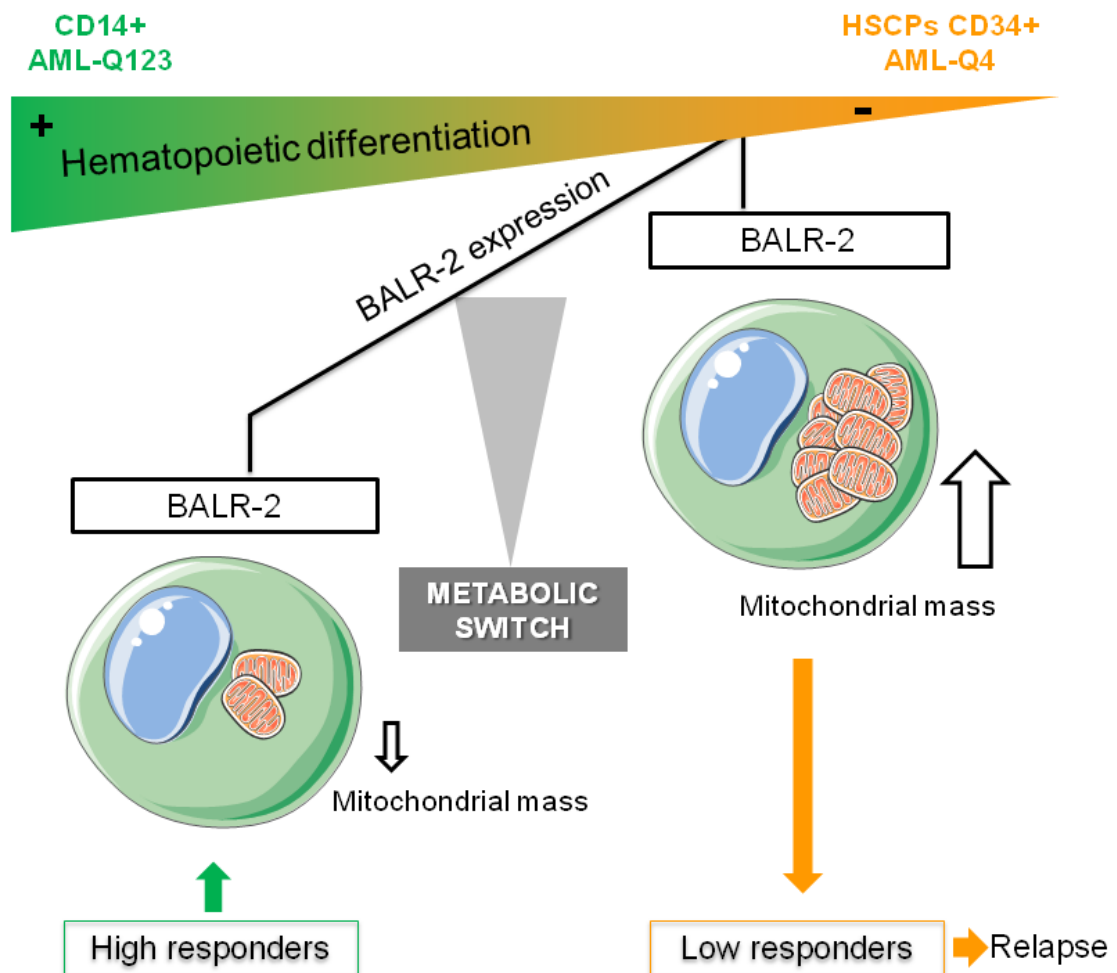


Figure 7. *BALR2* role in hematopoietic differentiation and response to therapy. As compared to Q123-AML patients, Q4-AML patients with high *BALR2* levels undergo to an arrest of the hematopoietic differentiation process, which is at least partly explained by a metabolic switch observed due to an increase in the mitochondrial mass. These features might be important elements responsible for both resistance to therapy and tumor relapse.

Discussion

Chemotherapy still dominates front-line therapy in most cancer clinical trials, but chemotherapy resistance and persistent disease after treatment discontinuation still result in relapse and poor outcome^{41, 2}. In most cases, relapse is preceded by MRD re-emergence as detected by molecular and flow-cytometry assays, but it can also occur without being preceded by MRD positivity^{4,9}. This finding indicates that current MRD monitoring of markers identified at diagnosis in part failed to identify poor-risk patients and to predict relapse⁴². Although cytogenetic and genetic aberrancies have long been used as prognostic indicators, their mechanistic role in conferring tumor resistance and tumor progression abilities, if any, are incompletely understood.

Our study was designed with the goal of discovering novel markers and pathways of resistance to treatment in AML. We previously reported that the non-coding transcriptome was able to cluster pediatric AML with the same accuracy as protein coding-genes, suggesting that, in addition to genetic alterations in protein-coding genes, aberrant expression of ncRNAs should be valorized in AML^{21,27,28,43}. Here, we explored non-genetic changes, and made an important advance in identifying the lncRNA *BALR2* as a robust novel marker associated with higher incidence of therapy resistance independent of other high risk factors in childhood AML. Clinically, *BALR2* expression in AML was heterogeneous and varied in correlation with *CDK6*, and the underlying mechanism involved *BALR2*-mediated regulation of a bi-directional promoter that regulates both *BALR2* and *CDK6* gene *in cis*⁴⁴. This finding, coherent with the small-RNAs capability to associate with components of regulatory systems to recruit chromatin modifiers or protein complexes to guide alternative genomic targets^{20,23}, defined a new *BALR2-CDK6* axis in AML. This sustained high expression of *CDK6* was revealed able to modulate its interaction with the Runt domain, mediating an inhibitory effects on several of the *RUNX1*-promoters³² and the block of hematopoietic differentiation, revealing an acquired non-canonical role of *CDK6* in AML³². Concordantly, reduced *BALR2-CDK6* expression in AML led to the emergence of more differentiated cells, as well as reduced clonogenic potential. We thus propose that the *BALR2* lncRNA plays a key control in the block of early hematopoietic differentiation that is thought to occur in leukemia^{34,45}.

To further investigate a role in myeloid differentiation, we evaluated whether *BALR2* could be involved in the healthy HSCPs differentiation program. We documented a common signature of co-expressed genes among highly expressing *BALR2-CDK6* AML blasts and the more undifferentiated healthy CD34+ HSCPs. Additionally, we described *BALR2* and *CDK6* being highly expressed in the CD34+ cell compartment in comparison to the more mature CD14+ cells,

demonstrating a skewed myeloid differentiation triggered by the single lncRNA *BALR2* in HSCPs. These results suggest a distinct role to *BALR2* in facilitating the switch of the myeloid stem cell differentiation process from physiological to aberrant, to initiate leukemogenesis. This observation paves the way for further investigations in modulating *BALR2* levels together with second events, such as chimeric transcripts resulting from translocations, for studying AML onset *in vivo* ^{46,47}.

Furthermore, in Q4-AML mitochondrial biogenesis gene signatures were highly expressed ^{35,48}, as well as in CD34+ HSCPs ^{39,49}. This similarity is likely connected with cancer's ability to reprogram cellular pathways working in macromolecular synthesis and energy production, with the goal of responding to a high demand of cells to divide or migrate, or survive under insults, as chemotherapy ⁵⁰. In fact, perturbed mitochondrial number and function have been associated to dysregulate cellular function, especially in relation to ROS tolerance, and genomic instability pathways ^{36,37}. We thus attribute to *BALR2* Q4-AML characteristics of lowered chemo-sensitivity due to their dysfunctional mitochondrial pathways. We confirmed *BALR2* levels strongly affecting AML mitochondrial dynamics in terms of a severe reduced mitochondrial mass. Thus, *BALR2* determines the mitochondrial cargo of cancer cells, implying a role for this lncRNA in determining AML chemotherapy susceptibility ⁴⁹. This hypothesis is supported by previous data indicating that the mitochondrial number and function are tightly regulated and coordinated to maintain the physiological cellular activity ^{39,49,51}, or to reduce sensitivity to drugs in cancer ^{50,52}. More recently, preclinical studies demonstrated the efficacy of IDH-targeted therapy, as well as Sirtuins deacetylases and BCL-2 inhibitors like Venetoclax, as novel therapeutic approaches aimed at triggering apoptosis of cancer cells, including AML ⁵²⁻⁵⁴. Thus, we tested whether chemotherapy-induced cytotoxicity and mitochondria targeting can synergistically promote killing of AML cell. Cell death and depolarization after the use of a mitochondria inhibitor, the tigecyclin, confirmed that viability of AML cells with high *BALR2* is largely influenced by mitochondrial content, and that in conditions where *BALR2* expression and mitochondria mass are reduced, tigecyclin can induce a potent effect promoting AML cell differentiation and death. Notably, the therapeutic potential of tigecyclin in eradicating leukemic stem cells (LSCs) has been already demonstrated in both acute and chronic leukemias ^{39,55}. Indeed, this drug inhibiting mitochondrial protein translation was shown to be able to destroy LSCs and cancer bulk ^{39,51} *in vitro* and *in vivo* when used either alone or combined in synergy with chemotherapy, these observations supporting the rationale for developing a similar therapeutic strategy in children with *BALR2* Q4-AML.

In summary, we propose high *BALR2* levels at diagnosis as a new molecular classifier of childhood AML patients, able to identify those cases with high mitochondrial mass for whom a mitochondrial targeting to enhance chemo-sensitivity might be considered. Furthermore, we think

that these results be supportive of a newly recognized mitochondrial priming in pediatric AML to be explored in the future for combining treatments where chemo and chemo-free therapies might be tested in patients with persistent MRD, and in all the categories unlikely to be cured by the standard chemotherapy alone.

References

1. Zwaan CM, Kolb E a., Reinhardt D, et al. Collaborative Efforts Driving Progress in Pediatric Acute Myeloid Leukemia. *J. Clin. Oncol.* 2015;33(27):2949–2962.
2. Pession A, Masetti R, Rizzari C, et al. Results of the AIEOP AML 2002/01 multicenter prospective trial for the treatment of children with acute myeloid leukemia. *Blood.* 2013;122(2):170–8.
3. Rubnitz JE, Inaba H, Dahl G, et al. Minimal residual disease-directed therapy for childhood acute myeloid leukaemia: results of the AML02 multicentre trial. *Lancet Oncol.* 2010;11(6):543–52.
4. Inaba H, Coustan-Smith E, Cao X, et al. Comparative analysis of different approaches to measure treatment response in acute myeloid leukemia. *J. Clin. Oncol.* 2012;30(29):3625–3632.
5. Bacher U, Dicker F, Haferlach C, et al. Quantification of rare NPM1 mutation subtypes by digital PCR. *Br. J. Haematol.* 2014;167(5):710–714.
6. Bolouri H, Farrar JE, Triche T, et al. The molecular landscape of pediatric acute myeloid leukemia reveals recurrent structural alterations and age-specific mutational interactions. *Nat. Med.* 2018;24(1):103–112.
7. Pigazzi M, Manara E, Buldini B, et al. Minimal residual disease monitored after induction therapy by rq-pcr can contribute to tailor treatment of patients with t(8;21) runx1-runx1t1 rearrangement. *Haematologica.* 2015;100(3):e99–e101.
8. Buldini B, Rizzati F, Masetti R, et al. Prognostic significance of flow-cytometry evaluation of minimal residual disease in children with acute myeloid leukaemia treated according to the AIEOP-AML 2002/01 study protocol. *Br. J. Haematol.* 2017;177(1):116–126.
9. M. Jongen-Lavrencic, T. Grob, D. Hanekamp, F.G. Kavelaars A al H, A. Zeilemaker, C.A.J. Erpelinck-Verschueren, P.L. Gradowska, R. Meijer JC, B.J. Biemond, C. Graux, M. van Marwijk Kooy, M.G. Manz, T. Pabst JRP, V. Havelange, G.J. Ossenkoppele, M.A. Sanders, G.J. Schuurhuis BL, Valk and PJM. Molecular Minimal Residual Disease in Acute Myeloid Leukemia. *N. Engl. J. Med.* 2018;378:1189–1199.
10. Schmitt AM, Chang HY. Long Noncoding RNAs in Cancer Pathways. *Cancer Cell.* 2016;29(4):452–463.
11. Fernando TR, Rodriguez-Malave NI, Waters E V, et al. LncRNA Expression Discriminates Karyotype and Predicts Survival in B-Lymphoblastic Leukemia. *Mol. Cancer Res.* 2015;13(5):839–851.
12. Garzon R, Volinia S, Papaioannou D, et al. Expression and prognostic impact of lncRNAs in acute myeloid leukemia. *Proc. Natl. Acad. Sci.* 2014;111(52):18679–18684.
13. Zampini M, Bisio V, Leszl A, et al. A three-miRNA-based expression signature at diagnosis can predict occurrence of relapse in children with t(8;21) *RUNX1* - *RUNX1T1* acute myeloid leukaemia. *Br. J. Haematol.* 2017;1–4.

14. Salmena L, Poliseno L, Tay Y, Kats L, Pandolfi PP. A ceRNA hypothesis: The rosetta stone of a hidden RNA language? *Cell*. 2011;146(3):353–358.
15. Bester AC, Lee JD, Chavez A, et al. An Integrated Genome-wide CRISPRa Approach to Functionalize lncRNAs in Drug Resistance. *Cell*. 2018;173(3):649-664.e20.
16. Pigazzi M, Manara E, Baron E, Basso G. MiR-34b targets cyclic AMP-responsive element binding protein in acute myeloid leukemia. *Cancer Res*. 2009;69:2471–2478.
17. Derrien T, Johnson R, Bussotti G, et al. The GENCODE v7 catalog of human long noncoding RNAs: Analysis of their gene structure, evolution, and expression. *Genome Res*. 2012;22(9):1775–1789.
18. Ulitsky I, Bartel DP. XlincRNAs: Genomics, evolution, and mechanisms. *Cell*. 2013;154(1):26.
19. Nagano T, Fraser P. No-nonsense functions for long noncoding RNAs. *Cell*. 2011;145(2):178–181.
20. Dykes IM, Emanuelli C. Transcriptional and Post-transcriptional Gene Regulation by Long Non-coding RNA. *Genomics, Proteomics Bioinforma*. 2017;15(3):177–186.
21. Deveson IW, Hardwick SA, Mercer TR, Mattick JS. The Dimensions, Dynamics, and Relevance of the Mammalian Noncoding Transcriptome. *Trends Genet*. 2017;33(7):464–478.
22. Sabin LR, Delás MJ, Hannon GJ. Dogma Derailed: The Many Influences of RNA on the Genome. *Mol. Cell*. 2013;49(5):783–794.
23. Kopp F, Mendell JT. Functional Classification and Experimental Dissection of Long Noncoding RNAs. *Cell*. 2018;172(3):393–407.
24. Quinn JJ, Zhang QC, Georgiev P, et al. Rapid evolutionary turnover underlies conserved lncRNA-genome interactions. *Genes Dev*. 2016;30(2):191–207.
25. Luo Y, Liang M, Yao W, et al. Functional role of lncRNA LOC101927497 in N-methyl-N'-nitro-N-nitrosoguanidine-induced malignantly transformed human gastric epithelial cells. *Life Sci*. 2018;193:93–103.
26. Manara E, Baron E, Tregnago C, et al. MLL-AF6 fusion oncogene sequesters AF6 into the nucleus to trigger RAS activation in myeloid leukemia. *Blood*. 2014;124(2):263–272.
27. Bisio V, Zampini M, Tregnago C, et al. NUP98-fusion transcripts characterize different biological entities within acute myeloid leukemia: a report from the AIEOP-AML group. *Leukemia*. 2017;31(4):974–977.
28. Zampini M, Tregnago C, Bisio V, et al. Epigenetic heterogeneity affects the risk of relapse in children with t(8;21)RUNX1-RUNX1T1-rearranged AML. *Leukemia*. 2018;32(5):1124–1134.
29. Albrecht AS, Ørom UA. Bidirectional expression of long ncRNA/protein-coding gene pairs in cancer. *Brief. Funct. Genomics*. 2016;15(3):167–173.
30. Laurenti E, Frelin C, Xie S, et al. CDK6 levels regulate quiescence exit in human hematopoietic stem cells. *Cell Stem Cell*. 2015;16(3):302–313.
31. Placke T, Faber K, Nonami A, et al. Requirement for CDK6 in MLL-rearranged acute

- myeloid leukemia. *Blood*. 2014;124(1):13–23.
32. Fujimoto T, Anderson K, Jacobsen SEW, Nishikawa SI, Nerlov C. Cdk6 blocks myeloid differentiation by interfering with Runx1 DNA binding and Runx1-C/EBP α interaction. *EMBO J*. 2007;26(9):2361–2370.
 33. Lachmann A, Xu H, Krishnan J, et al. ChEA: Transcription factor regulation inferred from integrating genome-wide ChIP-X experiments. *Bioinformatics*. 2010;26(19):2438–2444.
 34. Schwarzer A, Emmrich S, Schmidt F, et al. The non-coding RNA landscape of human hematopoiesis and leukemia. *Nat. Commun*. 2017;8(1):218.
 35. Ploumi C, Daskalaki I, Tavernarakis N. Mitochondrial biogenesis and clearance: a balancing act. *FEBS J*. 2017;284(2):183–195.
 36. Yoshida GJ. Metabolic reprogramming: the emerging concept and associated therapeutic strategies. *J. Exp. Clin. Cancer Res*. 2015;34(1):111.
 37. Roth KG, Mambetsariev I, Kulkarni P, Salgia R. The Mitochondrion as an Emerging Therapeutic Target in Cancer. *Trends Mol. Med*. 2019;
 38. Lazarou M, Sliter DA, Kane LA, et al. The ubiquitin kinase PINK1 recruits autophagy receptors to induce mitophagy. *Nature*. 2015;524(7565):309–314.
 39. Škrtić M, Sriskanthadevan S, Jhas B, et al. Inhibition of Mitochondrial Translation as a Therapeutic Strategy for Human Acute Myeloid Leukemia. *Cancer Cell*. 2011;20(5):674–688.
 40. Sarosiek KA, Letai A. Directly targeting the mitochondrial pathway of apoptosis for cancer therapy using BH3 mimetics - recent successes, current challenges and future promise. *FEBS J*. 2016;283(19):3523–3533.
 41. Ramos N, Mo C, Karp J, Hourigan C. Current Approaches in the Treatment of Relapsed and Refractory Acute Myeloid Leukemia. *J. Clin. Med*. 2015;4(4):665–695.
 42. McNeer NA, Philip J, Geiger H, et al. Genetic mechanisms of primary chemotherapy resistance in pediatric acute myeloid leukemia. *Leukemia*. 2019;
 43. Manara E, Basso G, Zampini M, et al. Characterization of children with FLT3ITD acute myeloid leukemia: a report from the AIEOP AML2002 study group. 2016;(January):1–8.
 44. Lai F, Orom UA, Cesaroni M, et al. Activating RNAs associate with Mediator to enhance chromatin architecture and transcription. *Nature*. 2013;494(7438):497–501.
 45. Corrà F, Agnoletto C, Minotti L, Baldassari F, Volinia S. The Network of Non-coding RNAs in Cancer Drug Resistance. *Front. Oncol*. 2018;8:327.
 46. Zorko NA, Bernot KM, Whitman SP, et al. Mll partial tandem duplication and Flt3 internal tandem duplication in a double knock-in mouse recapitulates features of counterpart human acute myeloid leukemias. *Blood*. 2012;120(5):1130–1136.
 47. Milne TA. Mouse models of MLL leukemia: recapitulating the human disease. *Blood*. 2017;129(16):2217–2223.
 48. Anderson GR, Wardell SE, Cakir M, et al. Dysregulation of mitochondrial dynamics proteins are a targetable feature of human tumors. *Nat. Commun*. 2018;9(1):1677.

49. Vo TT, Ryan J, Carrasco R, et al. Relative mitochondrial priming of myeloblasts and normal HSCs determines chemotherapeutic success in AML. *Cell*. 2012;151(2):344–355.
50. Soderquist RS, Crawford L, Liu E, et al. Systematic mapping of BCL-2 gene dependencies in cancer reveals molecular determinants of BH3 mimetic sensitivity. *Nat. Commun.* 2018;9(1):3513.
51. Kuntz EM, Baquero P, Michie AM, et al. Targeting mitochondrial oxidative phosphorylation eradicates therapy-resistant chronic myeloid leukemia stem cells. *Nat. Med.* 2017;23(10):1234–1240.
52. Chen X, Glytsou C, Zhou H, et al. Targeting mitochondrial structure sensitizes acute myeloid leukemia to Venetoclax treatment. *Cancer Discov.* 2019;CD-19-0117.
53. Waitkus MS, DiPlas BH, Yan H. Biological Role and Therapeutic Potential of IDH Mutations in Cancer. *Cancer Cell*. 2018;34(2):186–195.
54. Sarosiek KA, Ni Chonghaile T, Letai A. Mitochondria: gatekeepers of response to chemotherapy. *Trends Cell Biol.* 2013;23(12):612–9.
55. Kuntz EM, Baquero P, Michie AM, et al. Targeting mitochondrial oxidative phosphorylation eradicates therapy-resistant chronic myeloid leukemia stem cells. *Nat. Med.* 2017;23(10):1234–1240.

About the author

She achieved her Master Degree in Genetics and Molecular Biology at the University of Roma “Sapienza” in 2015. During her thesis she trained in the laboratory “iPS-Riprogrammazione cellulare” of Dr Jessica Rosati at Institute C.S.S. Mendel (Casa Sollievo e Sofferenza – Sezione Mendel, Roma, Italy). After graduation, she improved her research skills in the laboratory of Neuropathology of Dr. Paola Tonin at Azienda Ospedaliera Universitaria di Verona (Verona, Italy) obtaining a fellowship from Fondazione Telethon. In 2016, she decided to implement her scientific education starting a PhD program in the Pediatric Emato-oncology Unit – acute myeloid leukemia Laboratory of Dr. Martina Pigazzi (Istituto di Ricerca Pediatrica (IRP), Padova, Italy). During her PhD program she mainly focused her attention on the studying of the role played by the bone marrow niche components in leukemia, and at the development of a three dimensional (3D) culture system to mimic the leukemia bone marrow microenvironment. The ultimate goal of her project was to use the 3D model to perform more predictive *in vitro* drug screening to boost new front-line drugs into clinical trial in order to improve children outcome. Her research was presented as poster in national and international congress as ESH (European school of Hematology) and EHA (European Hematology Association).

Abstracts

G Borella, A Da Ros, E Porcù, C Tregnago, M Benetton, V Bisio, E Campodoni, S Panseri, M Sandri, M Montesi, S Cairo, F Locatelli, and M Pigazzi. Acute Myeloid Leukemia (AML) in a 3D Bone Marrow Niche Showed High Performance for *in Vitro* and *In Vivo* Drug Screenings. 61^o ASH Annual Meeting. Orlando (FL), December 7-10, 2019.

Borella G, Da Ros A, Porcù E, Tregnago C, Benetton M, Bisio V, Campodoni E, Panseri S, Sandri M, Montesi M, Cairo S, Locatelli F, Biffi A, Pigazzi M. AML blasts support a leukemia-permissive microenvironment revealing the stromal contribution eligible for innovative 3D targeting. Retreat IRP. Mogliano Veneto (TV), October 4-5, 2019.

Da Ros A, Porcù E, **Borella G**, Benetton M, Tregnago C, Bisio V, Michelotto B, Campodoni E, Panseri S, Sandri M, Montesi M, Buldini B, Cairo S, Biffi A, Pigazzi M. Establishment of Patient-

Derived Xenografts (PDXs) for the identification of new therapeutic strategies in pediatric cancer. Retreat IRP. Mogliano Veneto (TV), October 4-5, 2019.

Da Ros A, Porcù E, **Borella G**, Benetton M, Tregnago C, Cairo S, Michelotto B, Buldini B, Locatelli F, Pigazzi M. Sviluppo di modelli preclinici *in vivo* di Leucemia Acuta Mieloide pediatrica per lo screening di nuovi farmaci. XLIV Congresso Nazionale AIEOP. Catania, Italy. October 13-15, 2019.

G. Borella, V. Bisio, A. Da Ros, C. Tregnago, M. Benetton, E. Campodoni, S. Panseri, M. Sandri, M. Montesi, S. Cairo, F. Locatelli and M. Pigazzi. Development of innovative preclinical *in vitro* and *in vivo* tools for an effective therapeutic strategy in pediatric acute myeloid leukemia. 24th Congress of EHA. Amsterdam (Netherlands), June 13-16, 2019.

G. Borella, V. Bisio, A. Da Ros, C. Tregnago, M. Benetton, S. Panseri, M. Montesi, S. Cairo and M. Pigazzi. Development of innovative preclinical *in vitro* and *in vivo* tools for an effective therapeutic strategy in pediatric acute myeloid leukemia. 3rd Scientific Workshop on Tumor Microenvironment in the Hematological Malignancies and its Therapeutic Targeting. London (England), February 24-26, 2019.

Borella G, Bisio V, Da Ros A, Tregnago C, Benetton M, Scarparo P, Bresolin S, Rizzari C, Lo Nigro L, Fagioli F, Pession A, Buldini B, Locatelli F, Basso G, Pigazzi M. Sviluppo di un modello tridimensionale di leucemia mieloide acuta per eseguire screening di farmaci high throughput. V Workshop AIEOP... in Lab. Bologna, Italy. May 28-29, 2018.

Borella G and Bisio V, Da Ros A, Tregnago C, Benetton M, Basso G, Pigazzi M. Development of innovative preclinical *in vitro* and *in vivo* tools for an effective therapeutic strategy in pediatric acute myeloid leukemia. Retreat IRP. Preganziol (TV), April 6-7, 2018.

Abstracts - Secondary projects

Benetton M, Bisio V, Porcù E, Bordi M, Zanon C, **Borella G**, Da Ros A, Germano G, Manni S, Tregnago C, Campello S, Rao DS, Locatelli F, Pigazzi M. The long noncoding RNA BALR2 controls novel transcriptional circuits conferring chemotherapy resistance in pediatric acute myeloid leukemia. Retreat IRP. Mogliano Veneto (TV), October 4-5, 2019.

Tregnago C, Porcù E, Benetton M, **Borella G**, Da Ros A, Minuzzo S, Buldini B, Basso G, Locatelli F, Pigazzi M. Tioridazina: farmaco efficace e selettivo per la leucemia mieloide acuta con riarrangiamento t(6;11). XLIV Congresso Nazionale AIEOP. Catania, Italy. October 13-15, 2019.

Bisio V, Tregnago C, **Borella G**, Benetton M. Basso G, Pigazzi M. LncRNA BALR-2-CDK6 axis influences metabolic status and cell differentiation of acute myeloid leukemia. Retreat IRP. Preganziol (TV), April 6-7, 2018

Bisio V, Tregnago C, Zampini M, **Borella G**, Fernando T, Dinesh S R, Pession A, Locatelli F, Basso G and Pigazzi M. Long Non Coding RNA BALR2-CDK6 Axis Influences Cell Differentiation and Metabolic Status of Acute Myeloid Leukemia. 59° ASH Annual Meeting, Atlanta. December 9-12, 2017.

Publication

Zampini M, Tregnago C, Bisio V, Simula L, **Borella G**, Manara E, Zanon C, Zonta F, Serafin V, Accordi B, Campello S, Buldini B, Pession A, Locatelli F, Basso G, Pigazzi M. Epigenetic heterogeneity affects the risk of relapse in children with t(8;21)RUNX1-RUNX1T1-rearranged AML. *Leukemia*. **2018** May; 32(5):1124-1134.

Submitted manuscript

Bisio V, Benetton M, Porcù E, Bordi M, Zanon C, **Borella G**, Da Ros A, Germano G, Manni S, Tregnago C, Campello S, Rao DS, Locatelli F, Pigazzi M. The long noncoding RNA BALR2 controls strategic transcriptional circuits to confer chemotherapy resistance in acute leukemia. Submitted to *Blood*. **2019** September.

Manuscript in preparation

Borella G, Da Ros A, Porcù E, Tregnago C, Benetton M, Bisio V, Borile G, Campodoni E, Panseri S, Sandri M, Montesi M, Cairo S, Locatelli F, Biffi A, and Pigazzi M. Acute Myeloid Leukemia in a 3D bone marrow niche showed high performance for *in vitro* and *in vivo* drug screenings.

Congresses attended

- 24th Congress of EHA. Amsterdam (Netherlands), 13-16/6/2019;
- 3rd Scientific Workshop on Tumor Microenvironment in the Hematological Malignancies and its Therapeutic Targeting. London (England), 24-26/2/2019;
- Falcade XXVI° Winter Inter-Lab Meeting in Pediatric Hematology-Oncology. Falcade (BL) 15-16/3/2019;
- V WORKSHOP AIEOP.....in Lab. Bologna, 28-29/05/2018;
- Retreat IRP. Preganziol (TV), 6-7/04/2018;
- Falcade XXV° Winter Inter-Lab Meeting in Pediatric Hematology-Oncology. Falcade (BL) 2-3/03/2018.

Awards

- 24th Congress of EHA Travel Grant (**2019**);
- Best Presentation in “PhD student research project day medical and biomedical sciences (XXXII Cycle)” (**2018**).

